NASA Reference Publication 1376
Volume IV

Clouds and the Earth's Radiant Energy System (CERES) Algorithm Theoretical Basis Document

Volume IV—Determination of Surface and Atmosphere Fluxes and Temporally and Spatially Averaged Products (Subsystems 5–12)

CERES Science Team
Langley Research Center • Hampton, Virginia

National Aeronautics and Space Administration
Langley Research Center • Hampton, Virginia 23681-0001

December 1995

Available electronically at the following URL address: http://techreports.larc.nasa.gov/ltrs/ltrs.html

Printed copies available from the following:

NASA Center for AeroSpace Information
800 Elkridge Landing Road
Linthicum Heights, MD 21090-2934
(301) 621-0390

National Technical Information Service (NTIS)
5285 Port Royal Road
Springfield, VA 22161-2171
(703) 487-4650

Contents

Preface

The Release-1 CERES Algorithm Theoretical Basis Document (ATBD) is a compilation of the techniques and processes that constitute the prototype data analysis scheme for the Clouds and the Earth's Radiant Energy System (CERES), a key component of NASA's Mission to Planet Earth. The scientific bases for this project and the methodologies used in the data analysis system are also explained in the ATBD. The CERES ATBD comprises 11 subsystems of various sizes and complexities. The ATBD for each subsystem has been reviewed by three or four independently selected university, NASA, and NOAA scientists. In addition to the written reviews, each subsystem ATBD was reviewed during oral presentations given to a six-member scientific peer review panel at Goddard Space Flight Center during May 1994. Both sets of reviews, oral and written, determined that the CERES ATBD was sufficiently mature for use in providing archived Earth Observing System (EOS) data products. The CERES Science Team completed revisions of the ATBD to satisfy all reviewer comments. Because the Release-1 CERES ATBD will serve as the reference for all of the initial CERES data analysis algorithms and product generation, it is published here as a NASA Reference Publication.

Due to its extreme length, this NASA Reference Publication comprises four volumes that divide the CERES ATBD at natural break points between particular subsystems. These four volumes are

I: Overviews
  - CERES Algorithm Overview
  - Subsystem 0. CERES Data Processing System Objectives and Architecture

II: Geolocation, Calibration, and ERBE-Like Analyses
  - Subsystem 1.0. Instrument Geolocate and Calibrate Earth Radiances
  - Subsystem 2.0. ERBE-Like Inversion to Instantaneous TOA and Surface Fluxes
  - Subsystem 3.0. ERBE-Like Averaging to Monthly TOA

III: Cloud Analyses and Determination of Improved Top of Atmosphere Fluxes
  - Subsystem 4.0. Overview of Cloud Retrieval and Radiative Flux Inversion
  - Subsystem 4.1. Imager Clear-Sky Determination and Cloud Detection
  - Subsystem 4.2. Imager Cloud Height Determination
  - Subsystem 4.3. Cloud Optical Property Retrieval
  - Subsystem 4.4. Convolution of Imager Cloud Properties With CERES Footprint Point Spread Function
  - Subsystem 4.5. CERES Inversion to Instantaneous TOA Fluxes
  - Subsystem 4.6. Empirical Estimates of Shortwave and Longwave Surface Radiation Budget Involving CERES Measurements

IV: Determination of Surface and Atmosphere Fluxes and Temporally and Spatially Averaged Products
  - Subsystem 5.0. Compute Surface and Atmospheric Fluxes
  - Subsystem 6.0. Grid Single Satellite Fluxes and Clouds and Compute Spatial Averages
  - Subsystem 7.0. Time Interpolation and Synoptic Flux Computation for Single and Multiple Satellites
  - Subsystem 8.0. Monthly Regional, Zonal, and Global Radiation Fluxes and Cloud Properties
  - Subsystem 9.0. Grid TOA and Surface Fluxes for Instantaneous Surface Product
  - Subsystem 10.0. Monthly Regional TOA and Surface Radiation Budget
  - Subsystem 11.0. Update Clear Reflectance, Temperature History (CHR)
  - Subsystem 12.0. Regrid Humidity and Temperature Fields

The CERES Science Team serves as the editor for the entire document. A complete list of Science Team members is given below. Different groups of individuals prepared the various subsections that constitute the CERES ATBD. Thus, references to a particular subsection of the ATBD should specify the subsection number, authors, and page numbers. Questions regarding the content of a given subsection should be directed to the appropriate first or second author. No attempt was made to make the overall document stylistically consistent.

The CERES Science Team is an international group led by 2 principal investigators and 19 coinvestigators. The team members and their institutions are listed below.

CERES Science Team

Bruce A. Wielicki, Interdisciplinary Principal Investigator
Bruce R. Barkstrom, Instrument Principal Investigator

Atmospheric Sciences Division
NASA Langley Research Center
Hampton, Virginia 23681-0001

Coinvestigators

Bryan A. Baum
Atmospheric Sciences Division
NASA Langley Research Center
Hampton, Virginia 23681-0001

Maurice Blackmon
Climate Research Division
NOAA Research Laboratory
Boulder, Colorado 80303

Robert D. Cess
Institute for Terrestrial & Planetary Atmospheres
Marine Sciences Research Center
State University of New York
Stony Brook, New York 11794-5000

Thomas P. Charlock
Atmospheric Sciences Division
NASA Langley Research Division
Hampton, Virginia 23681-0001

James A. Coakley
Oregon State University
Department of Atmospheric Sciences
Corvallis, Oregon 97331-2209

Dominique A. Crommelynck
Institute Royal Meteorologique
B-1180 Bruxelles
Belgium

Richard N. Green
Atmospheric Sciences Division
NASA Langley Research Center
Hampton, Virginia 23681-0001

Robert Kandel
Laboratoire de Meteorologie Dynamique
Ecole Polytechnique
91128 Palaiseau
France

Michael D. King
Goddard Space Flight Center
Greenbelt, Maryland 20771

Robert B. Lee III
Atmospheric Sciences Division
NASA Langley Research Center
Hampton, Virginia 23681-0001

A. James Miller
NOAA/NWS
5200 Auth Road
Camp Springs, Maryland 20233

Patrick Minnis
Atmospheric Sciences Division
NASA Langley Research Center
Hampton, Virginia 23681-0001

Veerabhadran Ramanathan
Scripps Institution of Oceanography
University of California-San Diego
La Jolla, California 92093-0239

David R. Randall
Colorado State University
Department of Atmospheric Science
Foothills Campus, Laporte Avenue
Fort Collins, Colorado 80523

G. Louis Smith
Atmospheric Sciences Division
NASA Langley Research Center
Hampton, Virginia 23681-0001

Larry L. Stowe
NOAA/NWS
5200 Auth Road
Camp Springs, Maryland 20233

Ronald M. Welch
South Dakota School of Mines and Technology
Institute of Atmospheric Sciences
Rapid City, South Dakota 57701-3995

Nomenclature

Acronyms

ADEOS	Advanced Earth Observing System
ADM	Angular Distribution Model
AIRS	Atmospheric Infrared Sounder (EOS-AM)
AMSU	Advanced Microwave Sounding Unit (EOS-PM)
APD	Aerosol Profile Data
APID	Application Identifier
ARESE	ARM Enhanced Shortwave Experiment
ARM	Atmospheric Radiation Measurement
ASOS	Automated Surface Observing Sites
ASTER	Advanced Spaceborne Thermal Emission and Reflection Radiometer
ASTEX	Atlantic Stratocumulus Transition Experiment
ASTR	Atmospheric Structures
ATBD	Algorithm Theoretical Basis Document
AVG	Monthly Regional, Average Radiative Fluxes and Clouds (CERES Archival Data Product)
AVHRR	Advanced Very High Resolution Radiometer
BDS	Bidirectional Scan (CERES Archival Data Product)
BRIE	Best Regional Integral Estimate
BSRN	Baseline Surface Radiation Network
BTD	Brightness Temperature Difference(s)
CCD	Charge Coupled Device
CCSDS	Consultative Committee for Space Data Systems
CEPEX	Central Equatorial Pacific Experiment
CERES	Clouds and the Earth’s Radiant Energy System
CID	Cloud Imager Data
CLAVR	Clouds from AVHRR
CLS	Constrained Least Squares
COPRS	Cloud Optical Property Retrieval System
CPR	Cloud Profiling Radar
CRH	Clear Reflectance, Temperature History (CERES Archival Data Product)
CRS	Single Satellite CERES Footprint, Radiative Fluxes and Clouds (CERES Archival Data Product)
DAAC	Distributed Active Archive Center
DAC	Digital-Analog Converter
DB	Database
DFD	Data Flow Diagram
DLF	Downward Longwave Flux

DMSP	Defense Meteorological Satellite Program
EADM	ERBE-Like Albedo Directional Model (CERES Input Data Product)
ECA	Earth Central Angle
ECLIPS	Experimental Cloud Lidar Pilot Study
ECMWF	European Centre for Medium-Range Weather Forecasts
EDDB	ERBE-Like Daily Data Base (CERES Archival Data Product)
EID9	ERBE-Like Internal Data Product 9 (CERES Internal Data Product)
EOS	Earth Observing System
EOSDIS	Earth Observing System Data Information System
EOS-AM	EOS Morning Crossing Mission
EOS-PM	EOS Afternoon Crossing Mission
ENSO	El Niño/Southern Oscillation
ENVISAT	Environmental Satellite
EPHANC	Ephemeris and Ancillary (CERES Input Data Product)
ERB	Earth Radiation Budget
ERBE	Earth Radiation Budget Experiment
ERBS	Earth Radiation Budget Satellite
ESA	European Space Agency
ES4	ERBE-Like S4 Data Product (CERES Archival Data Product)
ES4G	ERBE-Like S4G Data Product (CERES Archival Data Product)
ES8	ERBE-Like S8 Data Product (CERES Archival Data Product)
ES9	ERBE-Like S9 Data Product (CERES Archival Data Product)
FLOP	Floating Point Operation
FIRE	First ISCCP Regional Experiment
FIRE II IFO	First ISCCP Regional Experiment II Intensive Field Observations
FOV	Field of View
FSW	Hourly Gridded Single Satellite Fluxes and Clouds (CERES Archival Data Product)
FTM	Functional Test Model
GAC	Global Area Coverage (AVHRR data mode)
GAP	Gridded Atmospheric Product (CERES Input Data Product)
GCIP	GEWEX Continental-Phase International Project
GCM	General Circulation Model
GEBA	Global Energy Balance Archive
GEO	ISSCP Radiances (CERES Input Data Product)
GEWEX	Global Energy and Water Cycle Experiment
GLAS	Geoscience Laser Altimetry System
GMS	Geostationary Meteorological Satellite
GOES	Geostationary Operational Environmental Satellite
HBTM	Hybrid Bispectral Threshold Method

HIRS	High-Resolution Infrared Radiation Sounder
HIS	High-Resolution Interferometer Sounder
ICM	Internal Calibration Module
ICRCCM	Intercomparison of Radiation Codes in Climate Models
ID	Identification
IEEE	Institute of Electrical and Electronics Engineers
IES	Instrument Earth Scans (CERES Internal Data Product)
IFO	Intensive Field Observation
INSAT	Indian Satellite
IOP	Intensive Observing Period
IR	Infrared
IRIS	Infrared Interferometer Spectrometer
ISCCP	International Satellite Cloud Climatology Project
ISS	Integrated Sounding System
IWP	Ice Water Path
LAC	Local Area Coverage (AVHRR data mode)
LaRC	Langley Research Center
LBC	Laser Beam Ceilometer
LBTM	Layer Bispectral Threshold Method
Lidar	Light Detection and Ranging
LITE	Lidar In-Space Technology Experiment
Lowtran 7	Low-Resolution Transmittance (Radiative Transfer Code)
LW	Longwave
LWP	Liquid Water Path
LWRE	Longwave Radiant Excitance
MAM	Mirror Attenuator Mosaic
MC	Mostly Cloudy
MCR	Microwave Cloud Radiometer
METEOSAT	Meteorological Operational Satellite (European)
METSAT	Meteorological Satellite
MFLOP	Million FLOP
MIMR	Multifrequency Imaging Microwave Radiometer
MISR	Multiangle Imaging Spectroradiometer
MLE	Maximum Likelihood Estimate
MOA	Meteorology Ozone and Aerosol
MODIS	Moderate-Resolution Imaging Spectroradiometer
MSMR	Multispectral, multiresolution
MTSA	Monthly Time and Space Averaging
MWH	Microwave Humidity

MWP	Microwave Water Path
NASA	National Aeronautics and Space Administration
NCAR	National Center for Atmospheric Research
NESDIS	National Environmental Satellite, Data, and Information Service
NIR	Near Infrared
NMC	National Meteorological Center
NOAA	National Oceanic and Atmospheric Administration
NWP	Numerical Weather Prediction
OLR	Outgoing Longwave Radiation
OPD	Ozone Profile Data (CERES Input Data Product)
OV	Overcast
PC	Partly Cloudy
POLDER	Polarization of Directionality of Earth's Reflectances
PRT	Platinum Resistance Thermometer
PSF	Point Spread Function
PW	Precipitable Water
RAPS	Rotating Azimuth Plane Scan
RPM	Radiance Pairs Method
RTM	Radiometer Test Model
SAB	Sorting by Angular Bins
SAGE	Stratospheric Aerosol and Gas Experiment
SARB	Surface and Atmospheric Radiation Budget Working Group
SDCD	Solar Distance Correction and Declination
SFC	Hourly Gridded Single Satellite TOA and Surface Fluxes (CERES Archival Data Product)
SHEBA	Surface Heat Budget in the Arctic
SPECTRE	Spectral Radiance Experiment
SRB	Surface Radiation Budget
SRBAVG	Surface Radiation Budget Average (CERES Archival Data Product)
SSF	Single Satellite CERES Footprint TOA and Surface Fluxes, Clouds
SSMI	Special Sensor Microwave Imager
SST	Sea Surface Temperature
SURFMAP	Surface Properties and Maps (CERES Input Product)
SW	Shortwave
SWICS	Shortwave Internal Calibration Source
SWRE	Shortwave Radiant Excitance
SYN	Synoptic Radiative Fluxes and Clouds (CERES Archival Data Product)
SZA	Solar Zenith Angle
THIR	Temperature/Humidity Infrared Radiometer (Nimbus)

TIROS	Television Infrared Observation Satellite
TISA	Time Interpolation and Spatial Averaging Working Group
TMI	TRMM Microwave Imager
TOA	Top of the Atmosphere
TOGA	Tropical Ocean Global Atmosphere
TOMS	Total Ozone Mapping Spectrometer
TOVS	TIROS Operational Vertical Sounder
TRMM	Tropical Rainfall Measuring Mission
TSA	Time-Space Averaging
UAV	Unmanned Aerospace Vehicle
UT	Universal Time
UTC	Universal Time Code
VAS	VISSR Atmospheric Sounder (GOES)
VIRS	Visible Infrared Scanner
VISSR	Visible and Infrared Spin Scan Radiometer
WCRP	World Climate Research Program
WG	Working Group
Win	Window
WN	Window
WMO	World Meteorological Organization
ZAVG	Monthly Zonal and Global Average Radiative Fluxes and Clouds (CERES Archival Data Product)

Symbols

A	atmospheric absorptance
$B_\lambda(T)$	Planck function
C	cloud fractional area coverage
CF_2Cl_2	dichlorofluorocarbon
$CFCl_3$	trichlorofluorocarbon
CH_4	methane
CO_2	carbon dioxide
D	total number of days in the month
D_e	cloud particle equivalent diameter (for ice clouds)
E_o	solar constant or solar irradiance
F	flux
f	fraction
G_a	atmospheric greenhouse effect
g	cloud asymmetry parameter
H_2O	water vapor

I	radiance
i	scene type
m_i	imaginary refractive index
$\hat{N}$	angular momentum vector
N_2O	nitrous oxide
O_3	ozone
P	point spread function
p	pressure
Q_a	absorption efficiency
Q_e	extinction efficiency
Q_s	scattering efficiency
R	anisotropic reflectance factor
r_E	radius of the Earth
r_e	effective cloud droplet radius (for water clouds)
r_h	column-averaged relative humidity
S_o	summed solar incident SW flux
S_o'	integrated solar incident SW flux
T	temperature
T_B	blackbody temperature
t	time or transmittance
W_{liq}	liquid water path
w	precipitable water
$\hat{x}_o$	satellite position at t_o
x, y, z	satellite position vector components
$\dot{x}, \dot{y}, \dot{z}$	satellite velocity vector components
z	altitude
z_{top}	altitude at top of atmosphere
α	albedo or cone angle
β	cross-scan angle
γ	Earth central angle
γ_{at}	along-track angle
γ_{ct}	cross-track angle
δ	along-scan angle
ε	emittance
Θ	colatitude of satellite
θ	viewing zenith angle
θ_o	solar zenith angle
λ	wavelength
μ	viewing zenith angle cosine

μ_o	solar zenith angle cosine
ν	wave number
ρ	bidirectional reflectance
τ	optical depth
$\tau_{aer}(p)$	spectral optical depth profiles of aerosols
$\tau_{H_2O\lambda}(p)$	spectral optical depth profiles of water vapor
$\tau_{O_3}(p)$	spectral optical depth profiles of ozone
Φ	longitude of satellite
ϕ	azimuth angle
$\tilde{\omega}_o$	single-scattering albedo

Subscripts:

c	cloud
cb	cloud base
ce	cloud effective
cld	cloud
cs	clear sky
ct	cloud top
ice	ice water
lc	lower cloud
liq	liquid water
s	surface
uc	upper cloud
λ	spectral wavelength

Units

AU	astronomical unit
cm	centimeter
cm-sec^{-1}	centimeter per second
count	count
day	day, Julian date
deg	degree
deg-sec^{-1}	degree per second
DU	Dobson unit
erg-sec^{-1}	erg per second
fraction	fraction (range of 0–1)
g	gram
g-cm^{-2}	gram per square centimeter
g-g^{-1}	gram per gram
g-m^{-2}	gram per square meter

h	hour
hPa	hectopascal
K	Kelvin
kg	kilogram
kg-m^{-2}	kilogram per square meter
km	kilometer
km-sec^{-1}	kilometer per second
m	meter
mm	millimeter
μm	micrometer, micron
N/A	not applicable, none, unitless, dimensionless
ohm-cm^{-1}	ohm per centimeter
percent	percent (range of 0–100)
rad	radian
rad-sec^{-1}	radian per second
sec	second
sr^{-1}	per steradian
W	watt
W-m^{-2}	watt per square meter
W-m^{-2}sr^{-1}	watt per square meter per steradian
W-m^{-2}sr^{-1}μm^{-1}	watt per square meter per steradian per micrometer

CERES Top Level Data Flow Diagram

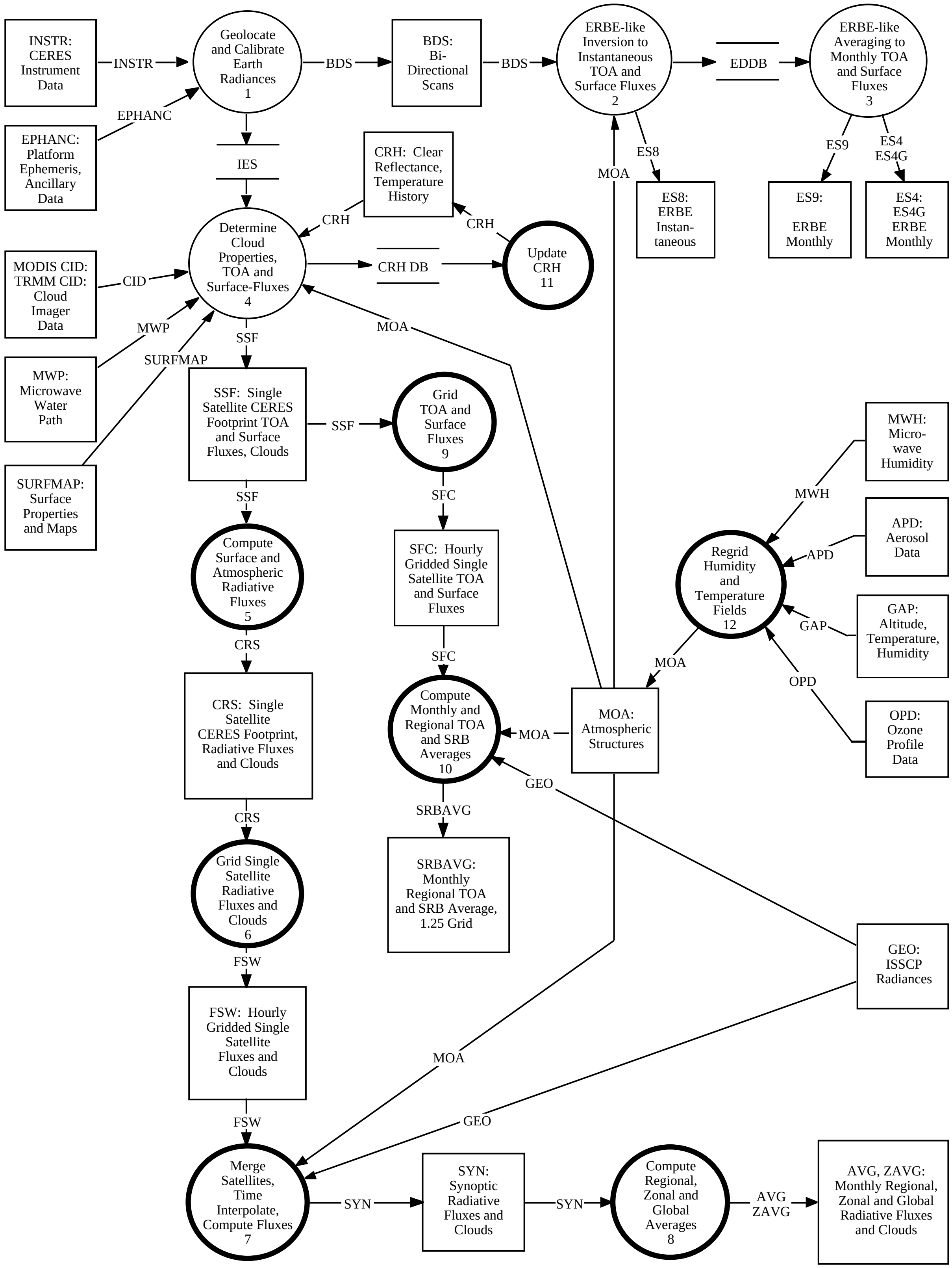

Clouds and the Earth's Radiant Energy System (CERES)

Algorithm Theoretical Basis Document

Compute Surface and Atmospheric Fluxes

(Subsystem 5.0)

Thomas P. Charlock[1]
David Rutan[2]
G. Louis Smith[1]
Fred G. Rose[2]
Timothy L. Alberta[2]
Nitchie Manalo-Smith[2]
Lisa H. Coleman[2]
David P. Kratz[1]
T. Dale Bess[1]
Kathryn A. Bush[3]

[1]NASA Langley Research Center, Hampton, Virginia 23681-0001
[2]Analytical Services & Materials, Inc., Hampton, Virginia 23666
[3]Science Applications International Corporation (SAIC), Hampton, Virginia 23666

Abstract

This document presents preliminary algorithms for the Clouds and the Earth's Radiant Energy System (CERES) retrieval of the vertical atmospheric profile of shortwave (SW, solar wavelengths) and longwave (LW, thermal infrared wavelengths) radiative fluxes: the surface and atmospheric radiation budget (SARB). The CERES effort to retrieve the SARB produces three sets of radiative fluxes as (a) the full vertical profile of fluxes in the atmosphere and at the surface, determined from radiative transfer calculations that match the simultaneously observed CERES top-of-the-atmosphere (TOA) fluxes, (b) an independent, parameterized set of radiative fluxes at the surface only, that are also simultaneous with the CERES TOA fluxes, and (c) the full vertical profile of fluxes in the atmosphere and at the surface as estimated for synoptic times (i.e., 3-hourly UTC). This document provides a brief scientific overview of all three sets of radiative fluxes, but its main purpose is to discuss the preliminary CERES SARB retrieval algorithms that will be used to obtain the first (a) of these three sets of radiative fluxes. The vertical profile of fluxes is calculated with satellite imager-retrieved clouds and meteorological data as inputs, and the input parameters are tuned to match the observed CERES broadband TOA fluxes. The initial, untuned radiative transfer calculations generally do not match the observed CERES TOA fluxes; the untuned fluxes at the surface and TOA are also archived for use in diagnostic studies of the radiative transfer techniques, the CERES cloud retrievals, and other parameters.

5.0. Compute Surface and Atmospheric Fluxes

5.1. Introduction

The SARB is the primary driver of the hydrological cycle and the general circulation of the atmosphere. Anthropogenically induced changes in radiatively active trace gases and aerosols will affect the SARB, and will therefore force a climatic response. There are, however, formidable challenges to developing accurate SARB records in CERES, or in the Earth Observing System (EOS) generally. While certain components of the SARB can now be determined accurately with existing data, other components, to be determined with certainty, must wait for the development of active remote sensing systems on satellites, such as cloud profiling radars (CPR). CERES will be a unique opportunity to expand the space-and-time domain wherein the SARB can be specified accurately. The CERES program will not only provide accurate TOA broadband fluxes and simultaneous cloud property retrievals, but will also be well suited to determine the effects of clouds on the various components of the SARB. The CERES SARB product will be an important tool for resolving the uncertainties in climate analysis and climate prediction that are associated with cloud-radiative and surface-albedo feedbacks.

The SARB algorithms in this document essentially complete the instantaneous satellite-based component of the CERES mission. Other CERES documents describe the more fundamental retrievals of TOA broadband radiative fluxes with the CERES instrument, the retrievals of cloud properties with the Advanced Very High Resolution Radiometer (AVHRR), High Resolution Infrared Sounder (HIRS/2), Visible Infrared Scanner (VIRS), and Moderate Resolution Imaging Spectroradiometer (MODIS) imaging instruments, and the preparation of meteorological and ancillary data that are used in both the cloud and SARB retrievals.

This document will discuss the retrieval of the SARB firstly from a theoretical standpoint. Then, we describe more concretely the pre-launch "Version 0" SARB retrieval that has been produced by the CERES team, using less than one orbit of AVHRR and Earth Radiation Budget Experiment (ERBE) data from October 1986; Version 0 was produced at National Aeronautics and Space Administration (NASA) Langley Research Center (LaRC) prior to March 1994. We further describe the more ambitious pre-launch "Release 1" retrieval, which employs both AVHRR and HIRS/2 for cloud retrievals and spans October 1986; Release 1 has not been fully programmed at this writing. The CERES Algorithm Theoretical Basis Documents (ATBD's), of which this document is a part (Subsystem 5), concentrate on a description of Release 1. Release 1 will be executed in 1995. Plans for the post-launch "Release 2" and "Release 3" are presented very roughly. Release 2 will be used by CERES for the Tropical Rainfall Measuring Mission (TRMM) launch in late 1997. Release 3, which will follow Release 2 by about 2 years, will use updated angular distribution models (ADM's) for TOA broadband fluxes. Version 0 and Releases 1–3 are summarized in Table 1.

Table 1. CERES Version 0 and Releases 1–3 for SARB Product

Name and date	Broadband	Imager	Vertical	Data
Version 0, Feb. 1994	ERBE	AVHRR	26 levels calculated	Oct. 1986 (one orbit only)
Release 1, 1995	ERBE	AVHRR and HIRS	4 levels for release	Oct. 1986 and Dec. 1986–Jan. 1987
Release 2, Postlaunch	CERES	VIRS and MODIS	TBD	TRMM and EOS
Release 3, Postlaunch	CERES with new ADM's	VIRS and MODIS	TBD	TRMM and EOS

5.2. Overview and Background Information

5.2.1. Experiment Objectives

A global record of the full SARB vertical profile is needed for diagnostic studies and the validation of climate models. Most general circulation models (GCMs) spend several tens of percent of their computational burden determining the SARB. Our techniques for the retrieval of SARB vertical profiles use radiative transfer codes (Harshvardhan et al. 1987; Wang et al. 1991; Chou 1992; Fu and Liou 1993) that have been built for GCM-type applications. We use the simple concept of tuning to achieve balance with broadband TOA observations. First, the SARB is calculated with standard meteorological data from National Meteorological Center (NMC) and satellite-retrieved cloud properties as input parameters; the cloud properties are produced by the CERES team with cloud imager data (see Subsystem 4 documents; AVHRR for Version 0, AVHRR and HIRS for Release 1, VIRS on the TRMM spacecraft, and MODIS on EOS). Second, the computed TOA fluxes are compared with observed broadband fluxes (ERBE radiometer for Version 0 and Release 1, CERES radiometer for TRMM and EOS polar orbiters). Then, in an iterative tuning process, the most uncertain and radiatively effective input parameters are adjusted to bring recalculated SARB to balance with the observed TOA broadband fluxes. The amount of tuning of the cloud parameters that is required to balance the broadband TOA observations is useful for evaluating the quality of the CERES products (see Subsystem 4 documents).

The SARB effort in CERES is directed at providing a set of through-the-atmosphere radiative fluxes that are applicable to large-scale general circulation and climate studies. Radiative fluxes also influence cloud processes at the microscale, but because we are working at the scale of CERES footprints (roughly 20 km and much larger than the cloud imager pixels), the CERES SARB will be too coarse for the study of very small cloud systems. SARB retrievals will provide energy fluxes that can be compared to GCM outputs directly, side-stepping the problem posed by different definitions of cloudiness in satellite retrievals and models. The CERES SARB products are anticipated to be useful for GCM validation because, as energy fluxes, they may be readily averaged in space and time. Other satellite-derived parameters (like cloud optical depth) relate to energy non-linearly and are thus more difficult to average and intercompare with GCM's.

We anticipate that the initial, untuned calculation (radiative transfer based on unadjusted input parameters) of SARB fluxes will be useful for diagnostic studies immediately after launch. The initial, untuned calculations will be compared with the first generation of CERES "ERBE-like" TOA fluxes (observed fluxes based on the old ERBE angular distribution models). Roughly a year after launch, new CERES ADMs will be produced with the CERES rotating axis scanner data, yielding a more accurate observed TOA record. CERES TOA observations account for three-dimensional effects empirically, and it will be interesting to compare them with the CERES SARB calculations. The CERES SARB calculations are based on the plane parallel assumption, as are the CERES cloud retrievals. The tuning that is required to bring the calculated plane parallel fluxes to a match with the CERES TOA observations will provide a diagnosis of the plane parallel assumption, which is widely used in models and retrievals.

For clear skies over oceans with TRMM (VIRS imager), we anticipate that early confidence could be placed on the tuned vertical profile of SARB fluxes that match the CERES TOA observations with the new ADMs. We could be confident of the tuned CERES SARB fluxes over clear-sky oceans and land in the EOS polar orbiter missions, as both new CERES ADMs and MODIS data (for aerosol retrieval over land) would both be available. Tuned SARB fluxes at the tropopause should also be reliable, even for total-sky conditions (i.e., above cloud tops), early in the EOS polar orbiter missions. A few years of post-launch study and validation will be needed before tuned SARB fluxes would be regarded as reliable below cloud tops.

The atmospheric portion of the SARB is calculated at many vertical levels (26 levels in the ERBE- and AVHRR-based exercise of Version 0 reported here). Formally, at the first SARB release 18 months after launch, however, only the fluxes at the tropopause, 500 hPa, TOA, and surface will be issued. Following validation of CERES cloud property products (Subsystem 4) and SARB fluxes (Subsystem 5), we anticipate that multiple levels of SARB fluxes will be issued 36 months after launch. As cloud overlap and cloud vertical thickness have substantial impacts, especially on the LW SARB, CERES validation activities will focus on cloud base height and cloud thickness, as well as on radiative fluxes.

Although much of CERES is oriented toward the tropospheric aspects of global change, the CERES SARB should also be useful for stratospheric studies. The 9.6 micrometer O_3 band is important for stratosphere-troposphere radiative exchange (Ramanathan and Dickinson 1979), because stratospheric O_3 absorbs upwelling photons from the warmer lower troposphere. CERES will determine the properties of the cloud tops, which are important in the modulation of the upwelling window flux and thus the stratospheric radiation balance. Because the tropopause is almost always above the cloud tops, the fluxes near the tropopause can be retrieved with more confidence than at lower levels. The radiative balance near the tropopause is vital because anthropogenic forcing has been calculated to heat the troposphere but cool the stratosphere (i.e., Intergovernmental Panel on Climate Change 1990). Raval and Ramanathan (1989) and Stephens and Greenwald (1991) have used ERBE and other data to quantitatively assess the clear-sky LW greenhouse effect of the integrated atmospheric column. The CERES SARB product will serve as the basis for a more highly resolved analysis.

5.2.2. Historical Perspective

The importance of the vertical profile of the atmospheric radiation budget was demonstrated with the development of the one-dimensional radiative-convective model (Manabe and Wetherald 1967). A change in the concentration of a infrared-active trace gas would change the model's temperature profile, but once in the new equilibrium state, the corresponding change to the broadband TOA planetary radiation budget could be very small or even vanish. The temperature profile would be maintained in the new equilibrium state by a significant vertical redistribution of energy fluxes *within* the atmosphere. Stephens and Webster (1984) further noted that clouds could play a vital role in such a process.

A three-dimensional model study by Hartmann et al. (1984) showed that the vertical distribution of atmospheric energy fluxes affects the primary modes of circulation, in addition to the temperature structure. The GCM results of Ting and Sardeshmukh (1993) indicate that a redistribution of vertical fluxes within the tropics would affect teleconnections to midlatitudes. The vertical energy fluxes are produced mainly by radiative (to be retrieved by CERES) and latent (to be retrieved using radar and other instruments on TRMM, i.e., Tao et al. 1993) processes. The full vertical profile of radiative flux divergence is needed to determine the effect of radiation on the generation of Available Potential Energy (APE; Lorenz 1955; Stuhlmann and Smith 1988a, b). Ramanathan et al. (1983) demonstrated the importance of the atmospheric LW budget in the simulation of the midlatitude jet in a GCM. The substantial effect of tropical cloud LW radiative forcing on atmospheric heating and circulation has been demonstrated with a GCM by Slingo and Slingo (1991); the accuracy of the LW forcing was found to be critical for computing impacts such as Amazon deforestation. The importance of radiation within the atmosphere for circulation has been demonstrated in other studies (e.g., Donner and Kuo 1984; Slingo and Slingo 1988; Randall et al. 1989).

London (1957) and Dopplick (1972) are classical, pre-satellite estimates of the SARB based on radiative transfer calculations with climatological data. The retrieval of radiative fluxes *at the surface* has been advanced by Darnell et al. (1992) and Pinker and Laszlo (1992a) using International Satellite Cloud Climatology Project (ISCCP) data (Schiffer and Rossow 1983; Rossow et al. 1991), as well as with HIRS/2 (Wu and Chang 1992), Nimbus 7 (Chertock et al. 1991; Charlock et al. 1990), GOES VISSR (Gautier and Frouin 1992), and ERBE (Cess et al. 1991; Li and Leighton 1993). The retrieval of surface LW fluxes has been developed at NASA LaRC by Darnell et al. (1992) and Gupta (1989). The World Climate Research Program (WCRP) Global Energy and Water Cycle Experiment (GEWEX; Chahine 1992) has established a formal project (Whitlock et al. 1994) that retrieves the global surface radiation budget (SRB), with the results archived at the NASA LaRC EOS DAAC (Distributed Active Archive Center). The GEWEX SRB *(surface only)* Project has used radiometric observations, compiled as the Global Energy Balance Archive (GEBA) by the Swiss Federal Institute (Ohmura and Gilgen 1993), for the validation of SW fluxes. The WCRP has organized a program of more precise surface observations, at a limited number of sites, in the Baseline Surface Radiation Network (BSRN). The development of these pioneering programs for surface fluxes provides the groundwork for the combined retrieval of surface and atmospheric flux profiles in CERES.

Calculations of clear-sky LW fluxes have been compared to broadband observations from aircraft for some time (Ellingson and Gille 1978). The recent Spectral Radiation Experiment (SPECTRE) activity (Ellingson et al. 1993), which provides an observational data base for clear-sky radiances, can be expected to hone more accurate codes for the calculation of LW and SW vertical flux profiles. Calculated cloudy-sky broadband fluxes are often compared to observations at selected vertical-levels in field campaigns (i.e., Stackhouse and Stephens 1991; Fu and Liou 1993). In an investigation of the energetics of small, cloud-scale systems (Churchill and Houze 1991), broadband flux profiles have been calculated with input data from aircraft and radar, and the calculated fluxes have been compared with observations (Churchill 1992). Field campaigns have not resolved the issue of the possible “anomalous” SW absorption by clouds, which has been reported for decades. Stephens and Tsay (1990) call for better measurements. Stephens and Tsay (1990) have examined hypotheses for the cause of anomalous absorption such as the presence of large droplets, cloud-absorbing aerosol, enhanced continuum absorption, and cloud inhomogeneities.

In applying satellite data to the global scale, we have about two decades of experience in the retrieval of temperature profiles and about one decade of experience in the retrieval of clouds. The large-scale, satellite-based retrieval of the full vertical profiles of radiative fluxes is a much newer activity. Stephens et al. (1994) use ERBE and Special Sensor Microwave/Imager (SSM/I) data to estimate the LW cooling of the full atmospheric column (rather than multi-layer profiles) over the oceans. Lee et al. (1993) describe an experimental program at National Atmospheric and Oceanic Administration

(NOAA) to retrieve the clear-sky LW heating rate for four atmospheric layers with HIRS/2 data; observed narrowband radiances are used in a statistical fit to detailed radiative transfer calculations.

Stuhlmann et al. (1993) used METEOSAT data to produce vertical profiles of both LW and SW fluxes. METEOSAT-derived cloud optical depth was used to determine the cloud ice water path (IWP) or liquid water path (LWP) following Rockel et al. (1991); water content is estimated using relations from Feigelson (1978) and Paltridge (1974); cloud geometric thickness was obtained from the ratio of water path to water content. Stuhlmann et al. (1993) then retrieved the flux profiles with delta-2-stream calculations based on the method of Schmetz (1984). For April 1985, the equator-to-pole temperature gradient over the METEOSAT region was found to be strengthened by the effects of net cloud-generated radiative heating.

Clear-sky and total-sky LW flux profiles have been computed (Charlock et al. 1993) with ISCCP data (Rossow et al. 1991) and the Harshvardhan et al. (1987) radiation code over the globe. The calculated outgoing longwave radiation (OLR) was compared (but not tuned) with ERBE, and the calculated surface downward longwave flux (DLF) was compared with a time-matched NMC Numerical Weather Prediction (NWP) simulation. Different cloud overlap assumptions produced very different vertical profiles of LW divergence. Despite the uncertainty caused by cloud overlap, it was possible to determine that LW divergence fluctuations damp temperature fluctuations in most of the troposphere but systematically enhance temperature fluctuations in a few regions.

5.2.3. Characteristics of EOS Data

CERES SARB retrievals will have several advantages over earlier SARB retrievals because of the improved characteristics of the EOS data that will be applied. Most importantly, CERES footprint-scale broadband TOA fluxes will be available as tie points for SARB calculations. The CERES broadband footprints will have a resolution twice that of ERBE (Barkstrom et al. 1989). Data from the CERES rotating axis scanner will permit the development of improved angular and directional models, reducing the error in the broadband albedo especially.

The scene identification for the CERES angular and directional models will, unlike ERBE (Wielicki and Green 1989), include the use of high-resolution cloud imager data for each footprint, which will increase the accuracy of the CERES broadband TOA fluxes and SARB calculations. CERES will distinguish clear scenes more reliably than ERBE because of both the application of cloud imager data and the higher spatial resolution of the CERES broadband sensor. CERES cloud retrievals on the TRMM mission will use the VIRS imager. Unlike AVHRR, VIRS has a 1.60 micrometer channel, which will be useful for identifying the phase of particles (liquid water or ice) in cloud tops. The phase of the cloud particles can have a dramatic impact on the cloud optical properties and the effect of the cloud on the radiation budget (Liou 1992). Knowledge of the particle phase permits a more accurate retrieval of cloud height and optical depth (Minnis et al. 1993a, b). The Minnis et al. (1993a, b) Layer Bispectral Threshold Method (LBTM) technique has been somewhat successful with estimations of cloud geometric thickness, a parameter that significantly influences the LW SARB. On the EOS AM and PM spacecraft, CERES will use the MODIS cloud imager. MODIS has a higher spatial resolution than VIRS or present cloud imagers, and the spectral coverage of the MODIS channels is more suited to cloud retrieval than AVHRR and HIRS/2. Wielicki and Parker (1992) have noted the increased accuracy in the retrieval of cloud area that is obtained with higher spatial resolution. Because of the low TRMM orbital altitude, VIRS will have a substantially higher resolution than AVHRR.

In addition to instrumentation, other aspects of the EOS data stream are also expected to increase the accuracy of the CERES cloud retrieval. NMC operational temperature and humidity profiles are available for cloud vertical placement; NMC profiles are used for SARB calculations, too. ISCCP (Rossow et al. 1991) was restricted to approximately daily Tiros Operational Vertical Sounder (TOVS) soundings, while Nimbus 7 cloud retrievals (Stowe et al. 1988) were based on climatological temperature lapse rates. We anticipate that, in the CERES time frame, the NMC humidity profiles will benefit from microwave-based retrievals on the Defense Meteorological Satellite Program (DMSP), TRMM, and EOS.

Information on aerosol optical loading will be available for CERES SARB calculations. On TRMM, CERES will retrieve aerosols with the VIRS sensor. On EOS, aerosol retrievals will be produced by the MODIS and Multi-angle Imaging Spectro-Radiometer (MISR) teams.

5.3. Algorithm Description

5.3.1. Theoretical Description

5.3.1.1. Radiative transfer codes. CERES presently uses several broadband radiative transfer codes. To date, two distinct SARB retrieval algorithms have been developed with these codes. It is anticipated that by launch, an improved version of one of these SARB retrieval algorithms, using a SW and a LW radiative transfer code, will be selected. All broadband radiative transfer codes (as distinguished from the SARB retrieval algorithms that employ them) in use at the present time were developed outside of NASA LaRC and have been generously provided to CERES by Drs. Ming-Dah Chou, Qiang Fu, Harshvardhan, Kuo-Nan Liou, and Wei-Chyung Wang. The radiation codes determine tropospheric and stratospheric broadband fluxes fairly efficiently and have been tested in the International Comparison of Radiation Codes in Climate Models (ICRCCM; Ellingson and Fouquart 1990). The Chou (1992), Fu and Liou (1993), Harshvardhan et al. (1987), and Wang et al. (1991) codes all use the plane-parallel assumption. Because of computational resources, we do not use narrowband or line-by-line radiative transfer codes for global processing.

Harshvardhan et al. (1987) developed a fast broadband code for GCM application. We use the Harshvardhan et al. (1987) LW code, which accounts for absorption and emission using methods by Chou (1984) for water vapor, by Chou and Peng (1983) for carbon dioxide, and by Rodgers (1968) for ozone. This code treats clouds as black bodies.

The minor species methane (CH_4), nitrous oxide (N_2O), dichlorofluorocarbon (CF_2Cl_2), and trichlorofluorocarbon ($CFCl_3$) reduce the clear-sky OLR by 5–8 W/m^2. Wang et al. (1991) have included these species in a fast GCM-type parameterization that we employ. This code is partly based on the Wang and Shi (1988) parameterization for total-band absorptance in a homogeneous layer. Clouds are treated as black bodies.

We use the Chou (1992) code for SW calculations in conjuction with the LW codes of Harshvardhan et al. (1987) and Wang et al (1991). This combination is referred to as HCW (as Harshvardhan, Chou, and Wang; see Table 2). HCW uses the Harshvardhan et al. (1987) fluxes for LW fluxes in the atmosphere, but at the TOA (where we attempt to balance with ERBE), HCW employs a small adjustment from the Wang et al. (1991) code to account for CH_4, N_2O, $CFCl_2$ and $CFCl_3$. For HCW, the effective OLR forcing of CH_4, N_2O, and CFC’s has been parameterized with a temperature dependent fit to fluxes calculated with the Wang et al. (1991) code.

The Chou (1992) code uses the Liou et al. (1988) delta-4-stream treatment of clouds and aerosols. Clear and scattering layers are composited with the two-stream adding method. The effects of H_2O, O_3, CO_2, O_2, and Rayleigh scattering are included. In a clear atmosphere, near-infrared absorption by water vapor is computed with a broadband technique; in an atmosphere with scattering by clouds or aerosols, water vapor absorption is computed with the k-distribution method.

Another code in use is the Fu and Liou (1993) code, which uses the delta-4-stream approximation (Liou et al. 1988). In Table 2 and throughout this document, the SARB retrieval algorithm that uses this code is referred to as FL. In the Fu and Liou (1993) code, numerical solutions for large optical depths are enabled by use of the scaling technique of Stamnes and Conklin (1984); results have been checked

Table 2. Radiative Transfer for Two SARB Retrieval Algorithms, HCW and FL

Algorithm	Longwave	Shortwave
HCW	Harshvardhan et al. (1987) minor adjustment with Wang et al. (1991) emissivity type codes	Chou (1992) delta-4-stream broadband clear sky aerosols included
FL	Fu and Liou (1993) includes scattering correlated k	Fu and Liou (1993) delta-4-stream correlated k

with the “exact” adding technique of Liou (1992). The Fu and Liou (1993) code accounts for the scattering of both LW and SW radiation, as do earlier studies by Stackhouse and Stephens (1991) and Ritter and Geleyn (1992). The correlated-k-distribution method for gaseous absorption is employed. Ice particles are modeled as randomly oriented hexagonal crystals. The effects of H_2O, O_3, CO_2, O_2, and Rayleigh scattering are included in the SW, and H_2O, CO_2, O_3, CH_4 and N_2O are included in the LW.

The HCW and FL algorithms are used to generate tuned vertical profiles of LW and SW fluxes in the atmosphere, at the TOA and at the surface. CERES also applies more specialized, faster parameterizations to produce fluxes at the surface only. The CERES surface-only parameterizations, which are described in other documents, apply algorithms based on Li et al. (1993), Gupta et al. (1992), and the activities of Inamdar and Ramanathan (1994).

5.3.1.2. Illustrations of LW profiles and TOA fluxes. Here, we provide a few examples of the SARB and its sensitivity to the TOA flux that CERES will determine from broadband ERBE-like measurements and other data.

In figure 1(a–d), the Wang et al. (1991) code has been used to compute the broadband LW fluxes for a climatological midlatitude summer condition. For clear skies (Fig. 1(a)), the LW cooling rate (K/day) is shown in solid. The dashed profile (Fig. 1(a)) shows the LW cooling rate for the same atmospheric sounding, but with an increase of 2 K in the surface temperature. By increasing the temperature of the surface (skin only) by 2 K, the cooling rate in the lowest 100 hPa has been reduced by about 25%; the clear-sky OLR has increased by 1.8 W/m^2 (note “1.8” in upper right portion of Fig. 1(a)); the downward longwave flux (DLF) has not changed (“0.0” indicated in lower right portion of Figure 1(a)). In a SARB retrieval for CERES, an initial temperature and humidity profile from NMC is used to compute the LW cooling rate profile indicated in solid in Figure 1(a). If the computed clear-sky OLR is 1.8 W/m^2 less than the broadband CERES observation, one tuning option would be an increase in the surface skin temperature by 2 K. The dashed line in Figure 1(a) shows the resulting, hypothetically tuned, clear-sky cooling rate profile.

Tuning can also be done by adjusting the temperature, cloud, and humidity profiles within the atmosphere. In Figure 1(b) (upper right), we have applied a 2-K increase, to the atmospheric layer only, between 900 and 1000 hPa. The dashed line (Fig. 1(b)) indicates that the 900–1000 hPa LW cooling rate has increased from 2.2 K/day to 3.4 K/day. The OLR has increased by only 0.7 W/m^2, but the DLF has increased by 14.2 W/m^2.

Figures 1(c–d) show how important clouds are for the LW SARB. In Figure 1(c), the dashed line shows the dramatically increased cooling rate for a midlatitude summer atmosphere with a black cloud added to the layer 900–1000 hPa. The low cloud increases the DLF by 62.2 W/m^2 but decreases the OLR by only 4.2 W/m^2 (Fig. 1(c)). In Figure 1(d), the black cloud has been moved to the layer between 300 and 350 hPa. For the high black cloud, the LW cooling rate increases slightly at the cloud layer, but

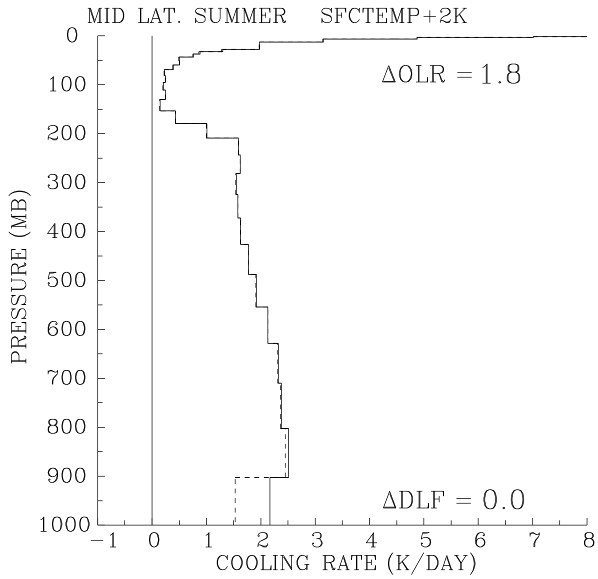

(a) Surface temperature increased by 2 K.

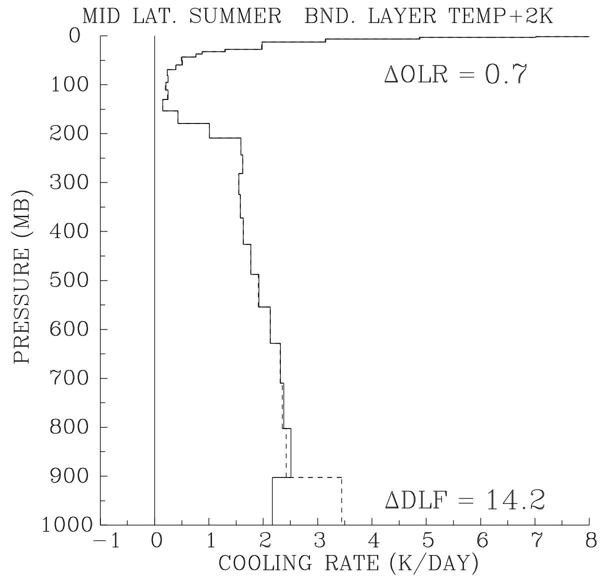

(b) Temperature in layer at 950 hPa increased by 2 K.

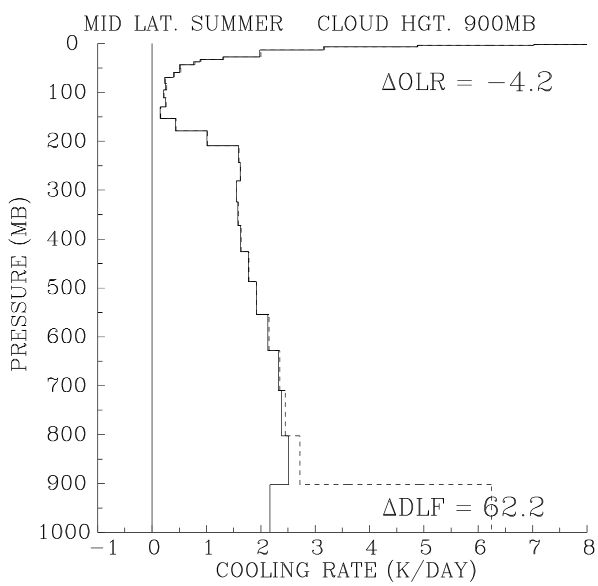

(c) Cloud placed in layer with top at 900 hPa.

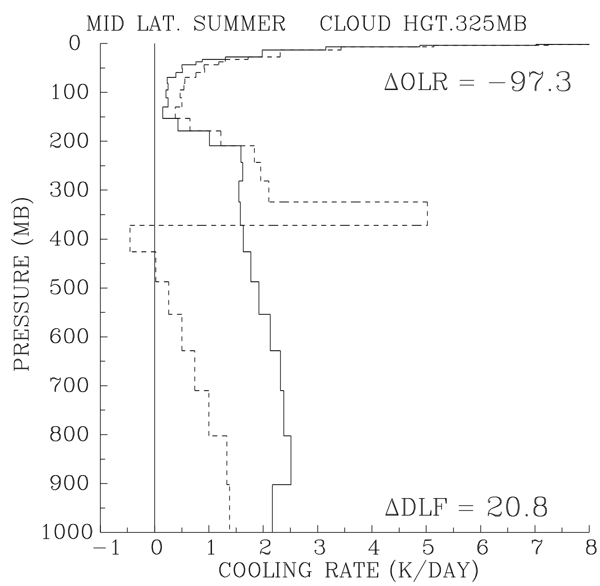

(d) Cloud placed in layer with top at 325 hPa.

Figure 1. Broadband LW cooling rates (K/day) for midlatitude summer climatological (solid) and perturbed atmospheres. Change in OLR (as perturbed OLR minus climatological OLR) in upper right of each panel in W/m^2; change in DLF in lower right of each panel in W/m^2.

it significantly decreases below the cloud, while the OLR falls by 97.3 W/m^2 and the DLF increases by 20.8 W/m^2 (Fig. 1(d)).

The impact of changes in the humidity profile to the LW SARB is shown in Figures 2(a–c). Note that the solid lines in Figures 2(a–b) use the same climatological midlatitude summer profile as the solid lines in Figures 1(a–d). By increasing the humidity between 700–800 hPa by 25%, the cooling rate is increased in that layer and decreased in the layer below; the OLR drops by only 1.6 W/m^2, and the DLF

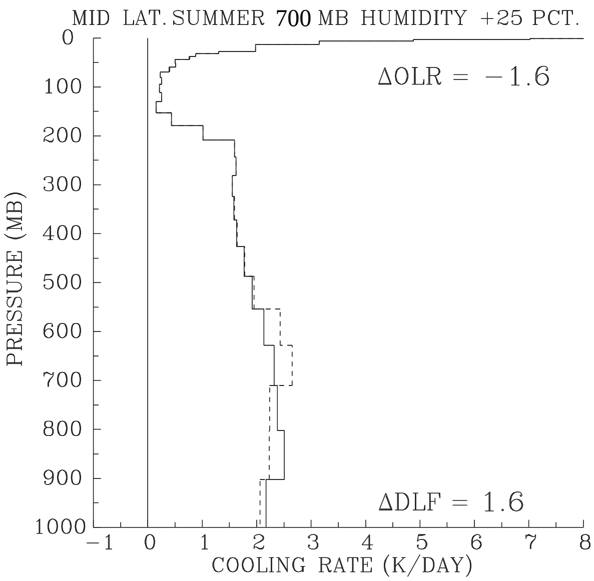

(a) Midlatitude summer, an increase in humidity of layer at 700 hPa by 25%.

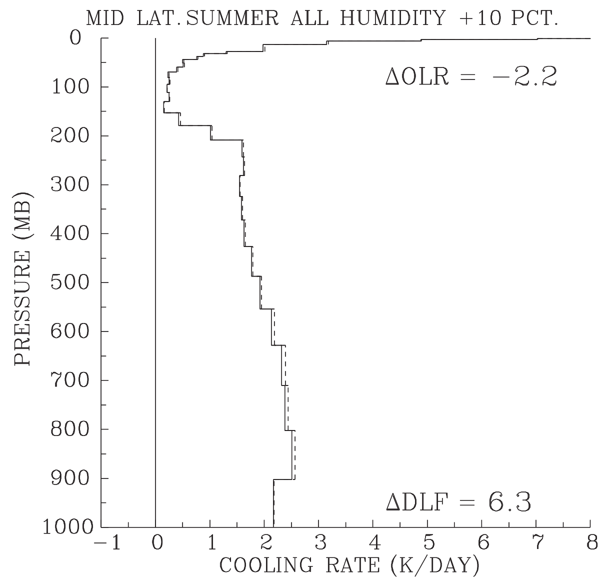

(b) Midlatitude summer, an increase in humidity of all layers by 10%.

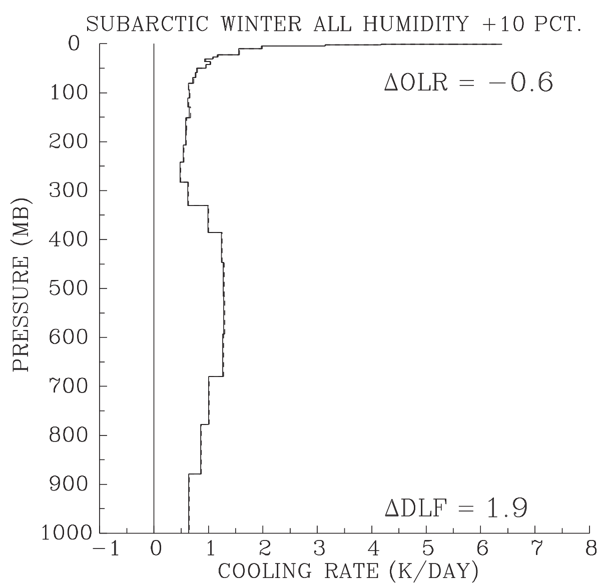

(c) Subarctic winter, an increase in humidity of all layers by 10%.

Figure 2. Broadband LW cooling rates (K/day) for climatological (dashed) and perturbed (solid) atmospheres. Change in OLR (as perturbed OLR minus climatological OLR) in upper right of each panel W/m^2; change in DLF in lower right of each panel in W/m^2.

increases by 1.6 W/m^2 (Fig. 2(a)). In Figure 2(b), the humidity has been increased by 10% at all levels, giving a larger drop in the OLR (2.2 W/m^2) and a larger increase in the DLF (6.3 W/m^2), but the impact on the cooling rate at any individual level is small. The same 10% increase in humidity has been applied to a subarctic winter profile in Figure 2(c) (note change of scale), and the impact is much smaller because in a colder atmosphere, a given increase in relative humidity translates to a smaller increase in absolute humidity and optical depth.

The impact of clouds on the LW SARB, coupled with uncertainties in retrieving the geometric thickness of clouds with a passive satellite observation, poses a formidable obstacle to CERES. We have attempted to assess the consequences of such uncertainties with ISCCP C1 data, using in this case the Wang et al. (1991) LW code. ISCCP C1 bins retrieved clouds into one of seven fixed vertical layers. In each of the 280-km by 280-km equivalent area gridboxes used by ISCCP, we have calculated the LW SARB every 3 hours for October 1986. The cloud forcing (i.e., Charlock and Ramanathan 1985) of the LW cooling rate profile is negative in our assumed, 50-hPa thick, cloud-free boundary layer from pole to pole in Figure 3(a). The monthly and zonally averaged cloud forcing exceeds 1 K/day in portions of the extratropics. ISCCP does not provide information on cloud overlap. For Figure 3(a), we have used non-overlapping “thick” clouds, which are idealized in Figure 4(a). A “thick” cloud fully occupies one of the seven fixed vertical layers (50–180 hPa, 180–310 hPa, 310–440 hPa, 440–560 hPa, 560–680 hPa, 680–800 hPa, and 800–950 hPa). In Figure 3(b), the difference of the cooling rate for nonoverlapping thick clouds (idealized in Fig. 4(a)) and randomly overlapping thick clouds (idealized in Fig. 4(b)) is substantial, exceeding the mean cloud forcing in some areas. In Figure 3(c), the difference of two non-overlapping cloud-forced cooling rates are again compared, but here the difference is for thick clouds (Fig. 4(a)) and “thin” clouds (Fig. 4(c)); for the “thin” clouds, the cloud pressure thickness has been reduced by 50%. The effect of maximum overlap (idealized in Fig. 4(d)) is even more substantial as shown in Figure 3(d), which gives the difference in the cloud-forced cooling rate for non-overlapping thick and maximum overlapping thick clouds.

Despite the uncertainty in the LW cloud forcing to the SARB (Fig. 4(a)) that is induced by overlap (Figs. 4(b) and 4(d)) and geometric thickness (Fig. 4(c)) at some levels, we note a broad region, centered around 700 hPa, where the integrated lower tropospheric cooling rate is not strongly sensitive to cloud overlap or thickness. Improved estimates of cloud overlap and thickness will be provided by the CERES Cloud Working Group.

The LW SARB calculations in Figures 1, 2, and 3 have assumed that the LW radiation from a cloud is black. The Fu and Liou (1993) code accounts for LW scattering and nonblack absorption and emission by clouds, and we now use that code to illustrate the importance, in certain cases, of those effects. Figure 5(a) shows cloud forcing to DLF (CFdlf) and cloud forcing to OLR (CFolr) for a cloud located 800–850 hPa, as a function of the natural logarithm of the cloud liquid water content (LWC in g/m^3). A code that does not explicitly account for nonblack clouds would commonly treat a nonblack cloud as an effective area fraction of a black cloud. The effective fraction (EF) can be determined from TOA fluxes as

$$\mathrm{EF} = \frac{\mathrm{CFolr(cloud)}}{\mathrm{CFolr(optically\ thick\ cloud)}}$$

The EF would then be used to determine the cloud’s impact on the LW SARB by treating any cloud forcing as an EF of the cloud forcing for an optically thick cloud. Figure 5(b) repeats the CFdlf from Figure 5(a), but it also shows an estimated CFdlf based on the EF above. In some cases, the estimated CFdlf errs by 5 W/m^2. This error in the estimated CFdlf suggests that, in some cases, one must explicitly account for LW scattering by clouds to provide an accurate determination of the LW surface budget.

5.3.1.2. SW issues. The SW heating of the atmosphere, like the LW cooling, is sensitive to variations in humidity and cloud opacity. In the SW, however, clouds primarily scatter radiation (rather than absorb), and their impact on the SW surface budget is not as strongly dependent on cloud altitude as is the LW. Li et al. (1993) have noted that, for a given solar zenith angle (SZA), there is an approximately linear relationship between the SW reflected flux at the TOA and the SW net (absorbed) flux at the surface. Such a relationship permits the ready estimation of surface fluxes from CERES and ERBE TOA observations. The Li et al. (1993) algorithm is used in another component of the CERES processing stream for the determination of SW “surface net only” fluxes.

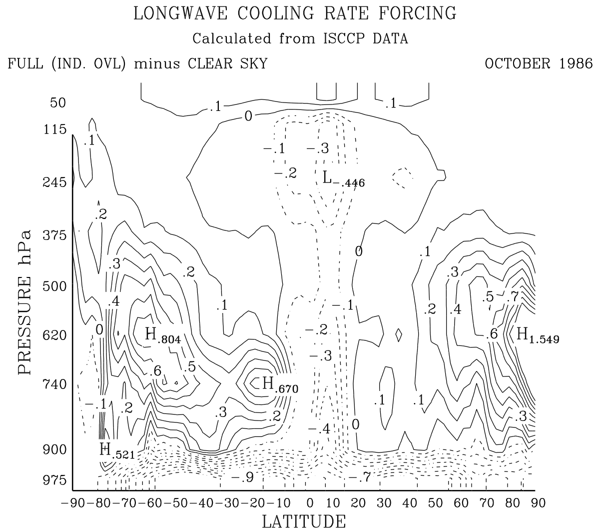

(a) Nonoverlapping thick clouds.

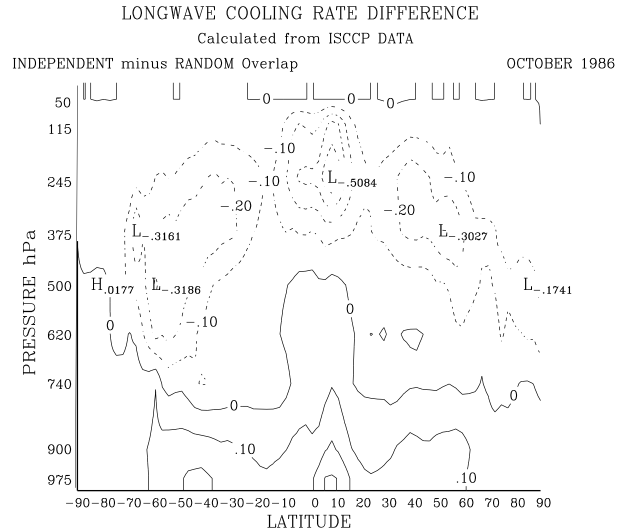

(b) Difference of nonoverlapping thick clouds minus randomly overlapping thick clouds.

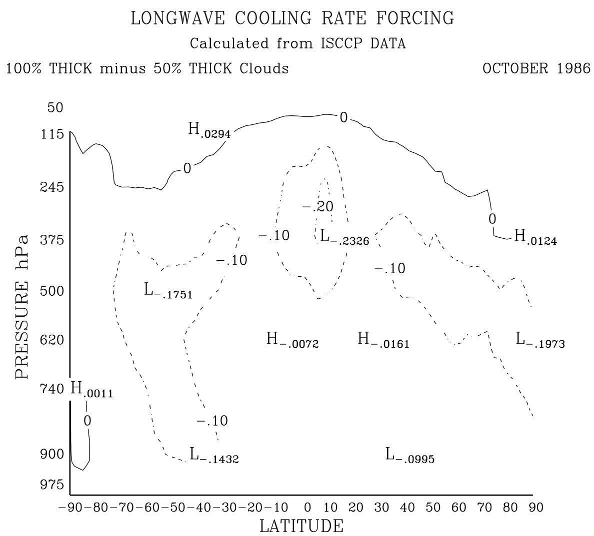

(c) Difference of geometrically thick clouds minus thin clouds.

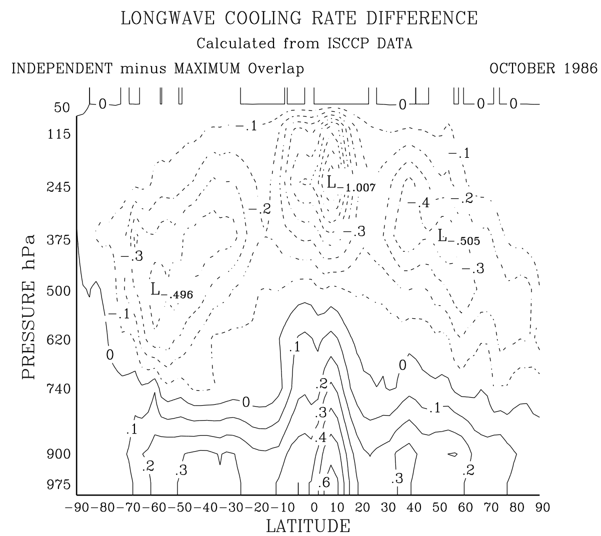

(d) Difference of nonoverlapping thick clouds minus maximum overlap thick clouds.

Figure 3. Zonal average of cloud forcing of LW cooling rate (K/day). Contour interval = 0.1°/day.

Here, we have calculated the reflected TOA and net surface fluxes with the Fu and Liou (1993) code in order to illustrate the Li et al. (1993) relationship. The thin solid lines in Figure 6 have each been calculated for fixed solar zenith angles using various optical depths for a cloud at 800 hPa, and they are quite linear. The linearity is somewhat surprising, but it is not universal. The thick lines of Figure 6 show the same relationship for two fixed solar zenith angles, but with a cloud at 200 hPa. The relationship for 200 hPa is again approximately linear. We note that it is important, however, to distinguish the case with a low cloud (800 hPa) and a high cloud (200 hPa). Cloud altitude must be accounted for, to place the SW heating at the right vertical level in the atmosphere. The different slopes of the thin (800-hPa cloud) and thick (200-hPa cloud) lines also show that cloud altitude must be taken into account, in order to improve the estimate of SW surface fluxes as well.

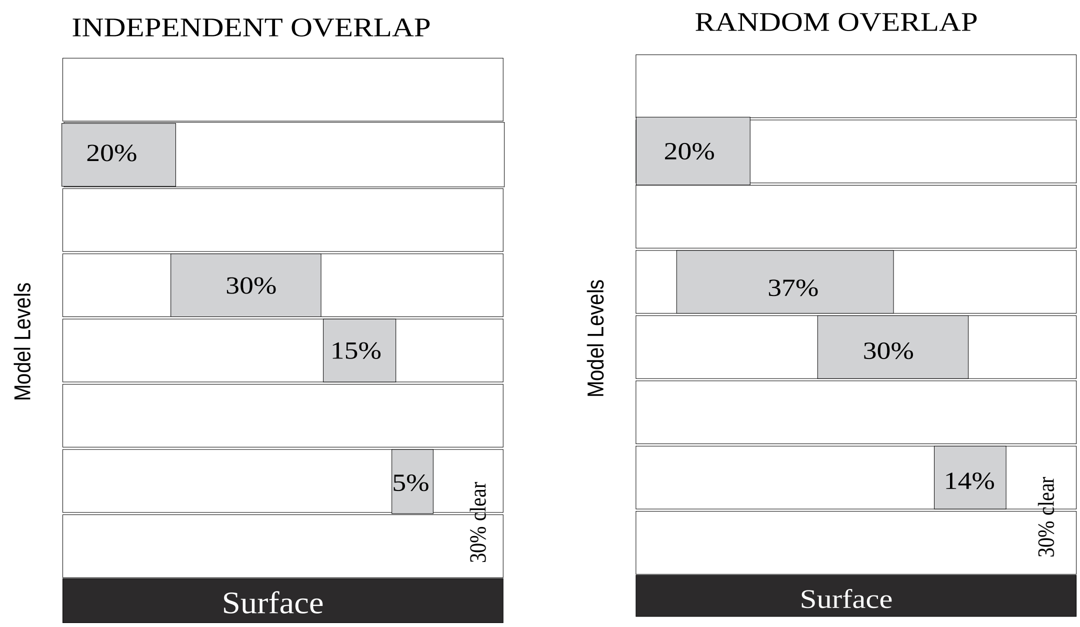

(a) Nonoverlapping (independent) thick clouds.

(b) Randomly overlapped thick clouds.

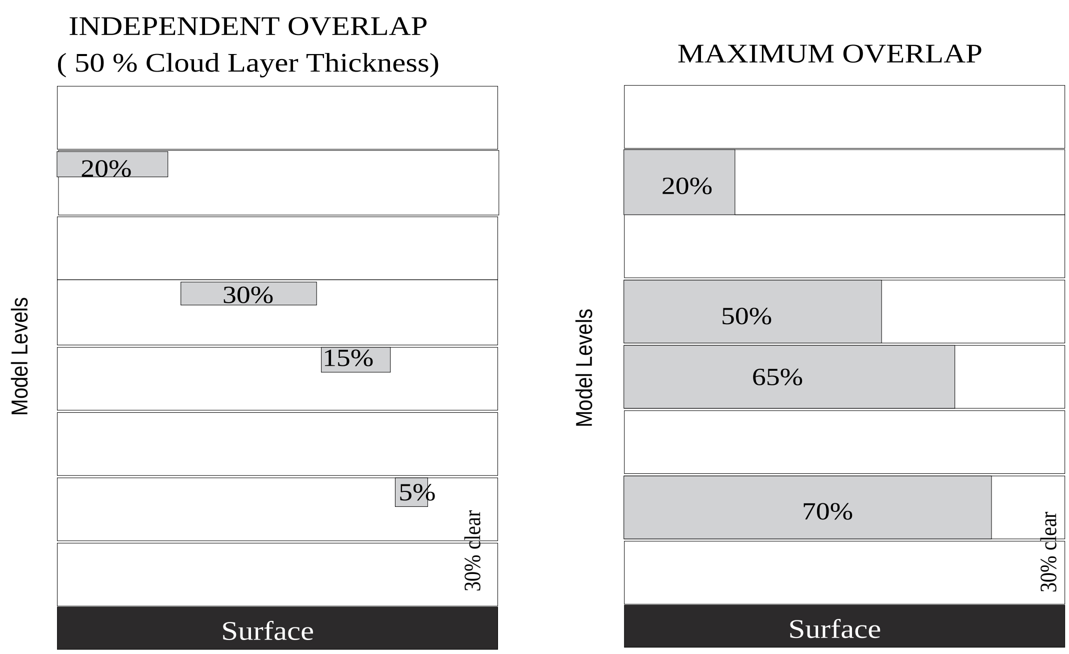

(c) Nonoverlapping thin clouds.

(d) Maximum overlap thick clouds.

Figure 4. Idealization of overlap schemes applied to ISCCP cloud data for calculations of LW cooling rate. Cloud fraction viewed from space is the same in all cases.

Ramaswamy and Freidenreich (1992) have studied the effect of the spectral overlap of absorption by water vapor and water droplets on the SW SARB. Most broadband codes are not adequate in their treatments of the spectral overlap, which is influenced by the distribution of water vapor above and within clouds. The corresponding errors in cloud-induced SW atmospheric heating can exceed 35%.

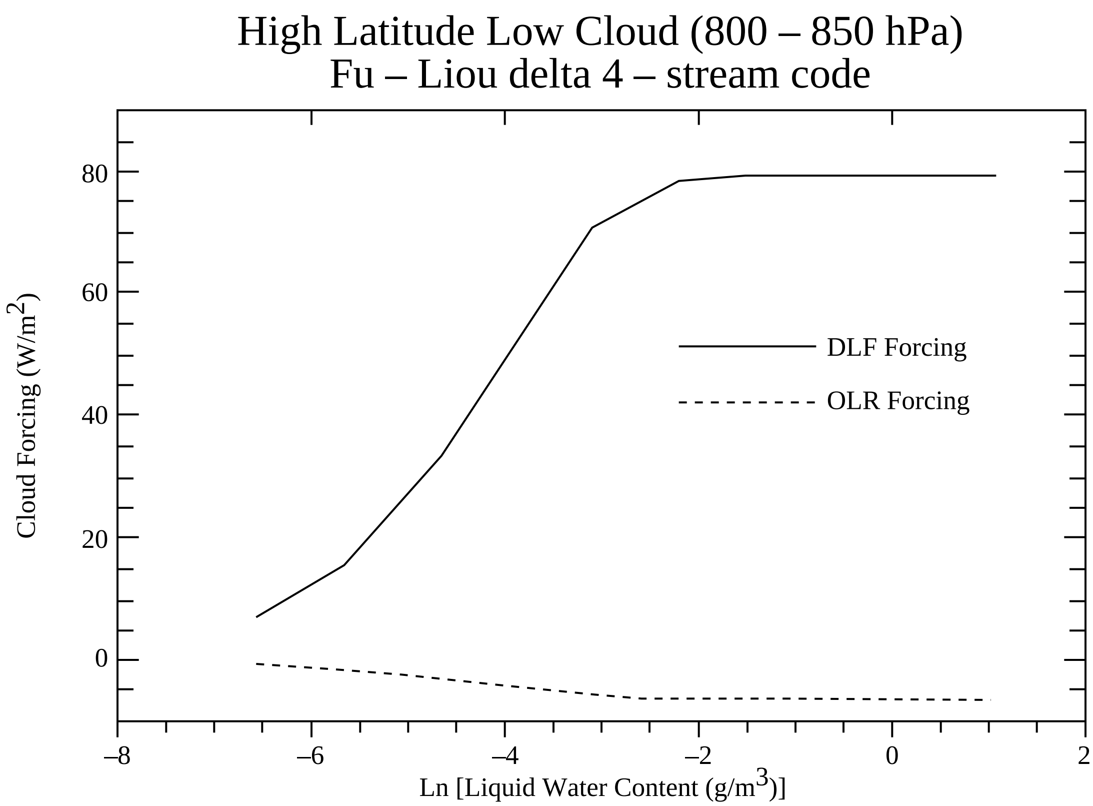

(a) Directly computed OLR and DLF cloud forcing.

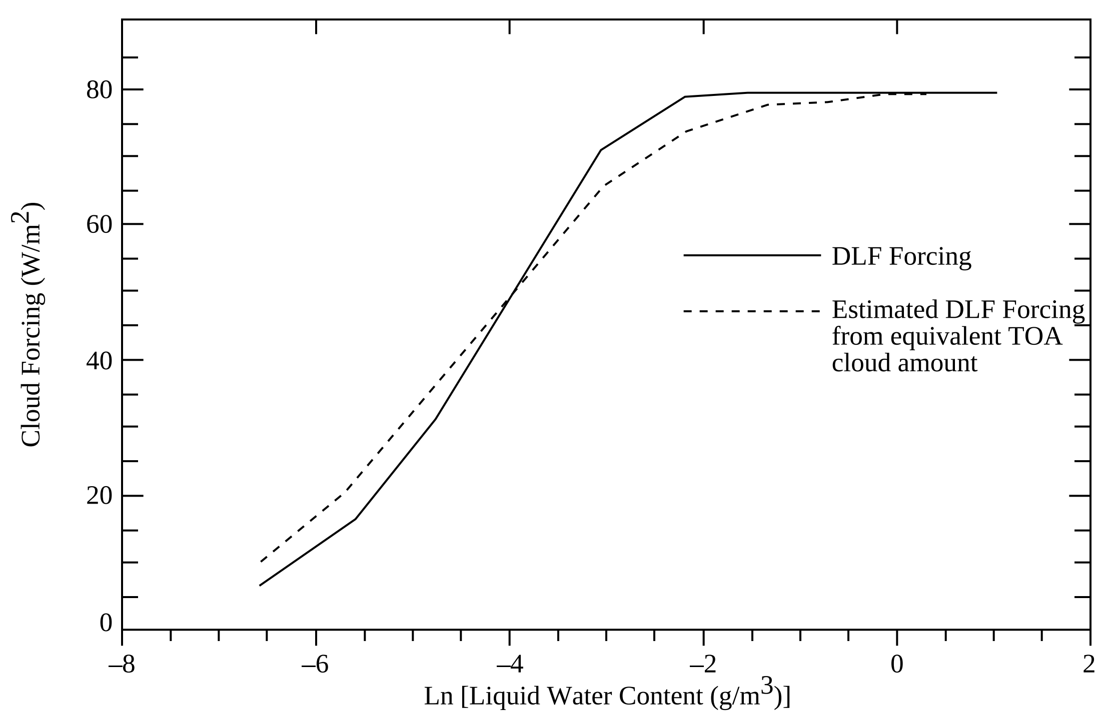

(b) Estimated DLF cloud forcing from equivalent TOA cloud amount.

Figure 5. LW cloud forcing (W/m^2) to OLR (TOA) and DLF (surface) as a function of cloud liquid water content.

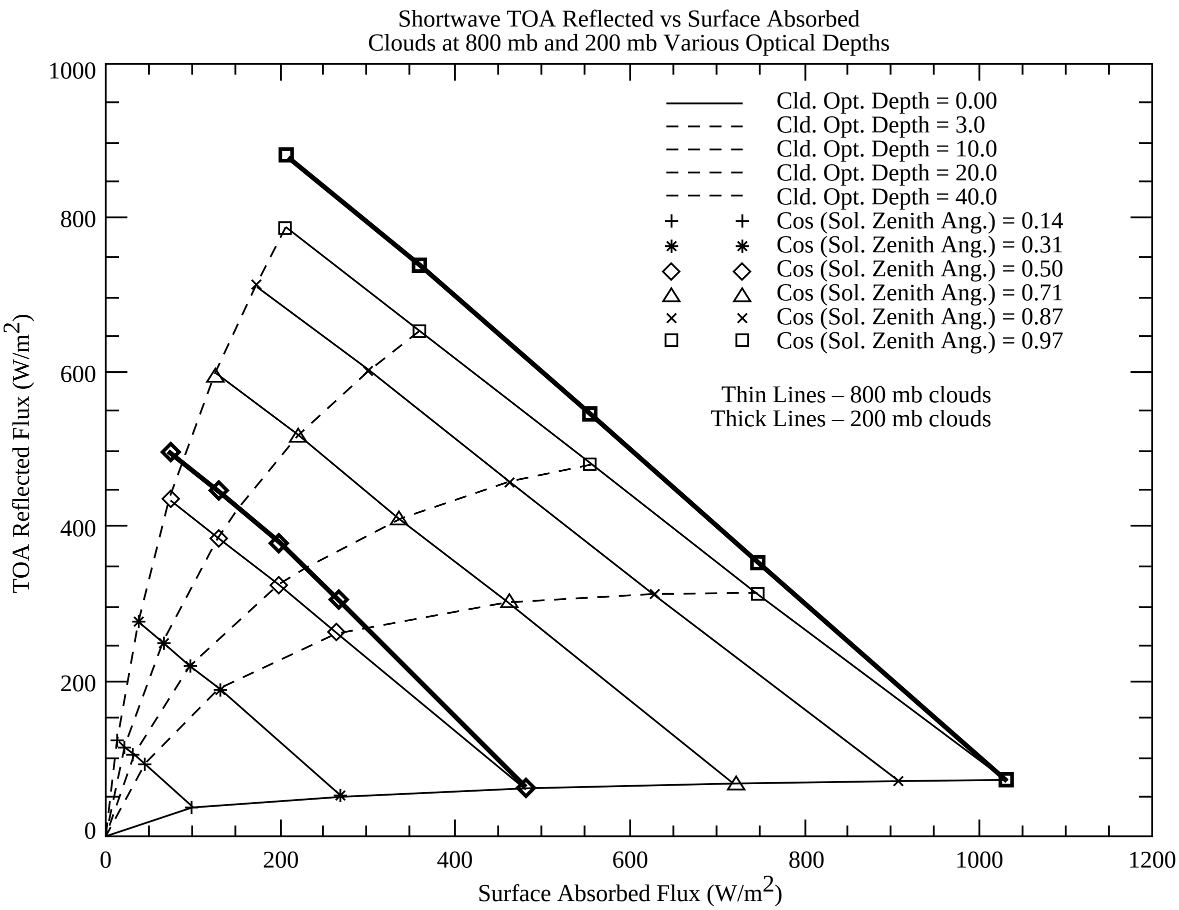

Figure 6. Computed SW reflected flux at TOA and SW surface absorbed (net) flux. Lines sloping downward to right are calculated for constant solar zenith angle with varying cloud optical depth. Thin lines for cloud at 800 hPa. Thick lines for cloud at 200 hPa.

The essence of the problem is the lack of effective spectral resolution for cloud single scattering albedo in the broadband radiative transfer codes. Ramaswamy and Fredericton (1992) have developed a parameterization that partly accounts for the spectral overlap. CERES has begun a collaboration with Drs. Liou and Fu at the University of Utah, where an effort will be made to improve the treatment of this effect for both liquid and ice cloud particles.

5.3.2. Algorithm Exercise With October 1986 Data

CERES has begun a global exercise with AVHRR, ERBE, and NMC data from October 1986. The algorithms that are described in this document have been applied in the exercise. To date, one orbit of ERBE instantaneous flux data has been processed and denoted as Version 0 (Table 1). In each ERBE footprint, the CERES Cloud Team (see Subsystem 4) used 8×8 “pixels” of AVHRR GAC data and the Minnis et al. (1993a, b) LBTM to retrieve cloud fractional area, SW optical depth, LW emittance, and cloud particle phase. The CERES SARB Team broadband radiative transfer calculations were made at 26 vertical levels using the Harshvardhan et al. (1987), Wang et al. (1991), Chou (1992), and Fu and Liou (1993) codes. The HCW and FL tuning algorithms were applied to produce adjustments to surface skin temperature, humidity, aerosol, surface albedo, and cloud properties, in order to produce a vertical profile of flux that balances the ERBE SW and LW at the TOA. A summary of the parameter adjustments in the HCW and FL retrieval algorithms is given in Table 3. The parameter adjustments for SARB retrieval algorithms will be different for the actual CERES launch in the late 1990s. We

Table 3. Adjustable Parameters in Current HCW and FL Algorithms

Algorithm	Clear-sky LW	Clear-sky SW	Total-sky LW & SW
HCW	PW & skin temp.	Surface albedo aerosol	LW tuned first: cloud area, then height & emissivity if needed SW tuned only cloud optical depth
FL	PW & skin temp.	Surface albedo	Cloud area fixed Cloud LWP and height tuned simultaneously in LW & SW

anticipate that our current Lagrange multiplier technique, described in the next section, for the simultaneous tuning of precipitable water (PW) and surface skin temperature in the clear-sky LW case, will be extended to the clear-sky SW and the total-sky LW and SW.

The adjustable parameters listed in Table 3 are products of the SARB tuning calculations in the Version 0 phase of the CERES activity; additional parameters will be adjusted in Releases 1 and 2. For the clear-sky conditions, the SARB tuning adjusts the surface skin temperature and the PW; during the day, the surface albedo and/or aerosol optical depth are tuned. Total-sky tuning will adjust the cloud area, the cloud temperature (height), the SW optical depth, and LW emissivity; the SW optical depth is not retrieved or adjusted at night.

The vertical structure used for SARB calculations in Version 0 and Release 1 are shown in Figure 7. Two 10-hPa thick layers are always placed above the surface. Over mountainous regions, some of the lower of the 50-hPa thick layers are eliminated. In Version 0, the clouds occupy fixed, discrete altitudes; cloud tops and bottoms coincide exactly with the tops and bottoms of the discrete levels. In Release 1, the cloud tops and bottoms can be placed at arbitrary levels.

5.3.3. Clear-Sky LW Algorithm

Clear-sky OLR calculations, based on operational temperature and humidity profiles, compare well with ERBE over the oceans for a monthly average (Slingo and Webb 1992; Kiehl and Briegleb 1992). We iteratively tune two parameters, the surface skin temperature (T) and the precipitable water (PW), to bring the calculated flux for each clear-sky footprint to a match with the instantaneous ERBE OLR observation. We have not adjusted the atmospheric temperature from NMC because we regard the atmospheric temperature profile to be much more accurate than the humidity profile. The surface skin temperature is notably difficult to sense reliably, especially over land. The tuning equation is

$$D(F) = D(T) \times dF/dT + D(W) \times dF/dW \tag{1}$$

where

F = clear-sky OLR
T = surface skin temperature
W = ln(PW)
PW = precipitable water

D(F) = F(observed) − F(calculated)	Known
D(T) = T(adjusted) − T(input)	Unknown
D(W) = W(adjusted) − W(input)	Unknown

The derivatives dF/dT and dF/dW are obtained from a table of radiative transfer calculations; the present table was developed with the Harshvardhan et al. (1987) code and April 1989 ISCCP/TOVS

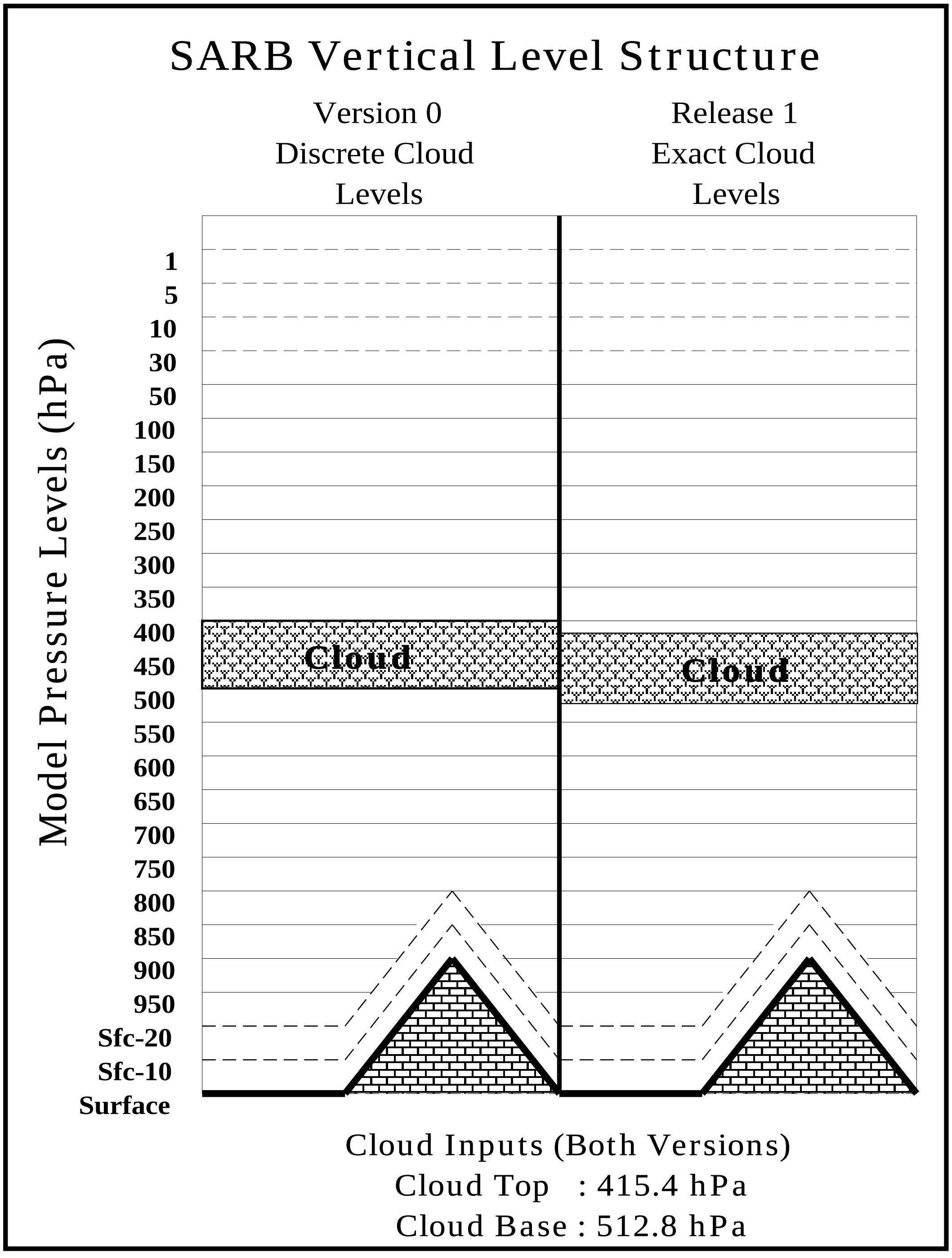

Figure 7. Idealization of atmospheric vertical structure for SARB calculations in Version 0 and Release 1.

vertical profiles. The tuning routine for (1) above must determine the adjustments D(T) and D(W) that cause the difference D(F) to vanish. A Lagrange multiplier solution is used:

$$D(T) = f[D(F), dF/dT, dF/dW, S(T), S(W)]$$

$$D(W) = g[D(F), dF/dT, dF/dW, S(T), S(W)]$$

S(T) and S(W) are the expected errors for the input sounding. Over the sea, we set S(T) = 1 K (i.e., the expected error in SST) and S(W) = 0.15. Over the land, S(T) = 5 K, reflecting the much larger probable error in the retrieval of land skin temperature (i.e., Sellers and Hall 1992). Donner (1988) has used concepts analogous to those above, for the initialization of convection in a NWP model.

Results from independent retrievals of the clear-sky LW SARB using the HCW and FL algorithms (see Tables 2 and 3) and ERBE data are shown in Figure 8. For both HCW and FL, only small adjustments to T and PW were needed to balance the observed OLR and provide a tuned LW profile; this situation is typical for a clear-sky ocean case. There are, however, more substantial differences between the HCW and FL profiles because of differences in the Harshvardhan et al. (1987), Wang et al. (1991), and Fu and Liou (1993) codes as we have applied them. Such differences will ultimately be resolved through activities like SPECTRE (Ellingson et al. 1993) and the Atmospheric Radiation Measurement (ARM; Stokes and Schwartz 1994) program.

Figure 9 shows, for a single orbit, the ERBE-footprint scale differences of clear-sky OLR observations and the initial (untuned) calculations for the HCW algorithm. For the few clear-sky ocean cases in this sample, the differences between the ERBE observations and HCW calculations are small. With the FL algorithm over roughly 1/4 orbit in the Western Pacific (not shown), the mean ERBE minus FL clear-sky ocean difference was -4.4 W/m^2. These small successes were anticipated by earlier comparisons for clear-sky ocean conditions by Slingo and Webb (1992) and Kiehl and Briegleb (1992). For the land cases, Figure 9 indicates much larger differences between the observed and HCW-calculated OLR. There are also much larger differences, over land, for untuned and HCW-tuned surface skin temperatures with the Lagrange multiplier (Fig. 10). In Figure 11, the differences between the untuned and HCW-tuned PW approaches a magnitude of 1 cm in very few cases.

5.3.4. Clear-sky SW Algorithm

For the footprints that are identified as clear-sky, we tune to the ERBE TOA by adjusting the surface albedo and/or the aerosol optical depth with HCW (Table 2), which uses Chou (1992) in the SW. With the Chou (1992) code, we specify the initial aerosol optical depth, asymmetry parameter, and single scattering albedo from a geographically dependent World Meteorological Organization (WMO) climatology as used by Darnell et al. (1992). In HCW, the aerosol is included only below 500 hPa, where it is distributed with a scale height of 3 km. Some of the initial surface albedo values for HCW are obtained from the SRB Project (Whitlock et al. 1994; Staylor algorithm); over land, this valuse is based on monthly averaged clear-sky ERBE results; for clear skies over the sea, it is essentially a catalogued result from Briegleb et al. (1986). For clear skies over land, the surface albedo is set from the Li and Garand (1993) algorithm applied at individual ERBE footprints. Over land, when we lack a match between ERBE and our HCW calculations with the clear-sky Chou (1992) code, we tune the surface albedo. An example of HCW untuned (initial) and tuned (adjusted) heating rates over land is shown in Figure 12(a); the aerosol optical depth is fixed at 0.25, and the broadband surface albedo is tuned. Over the sea, the aerosol optical depth is tuned. In Figure 12(b), the optical depth of the maritime aerosol has increased from 0.100 to 0.258 because of tuning. The tuning of land surface albedo in Figure 12(a) affected the TOA and surface budgets substantially. The tuning of maritime aerosol in Figure 12(b) produces a significant change in the radiative heating profile in the atmosphere, as well as at the TOA and surface.

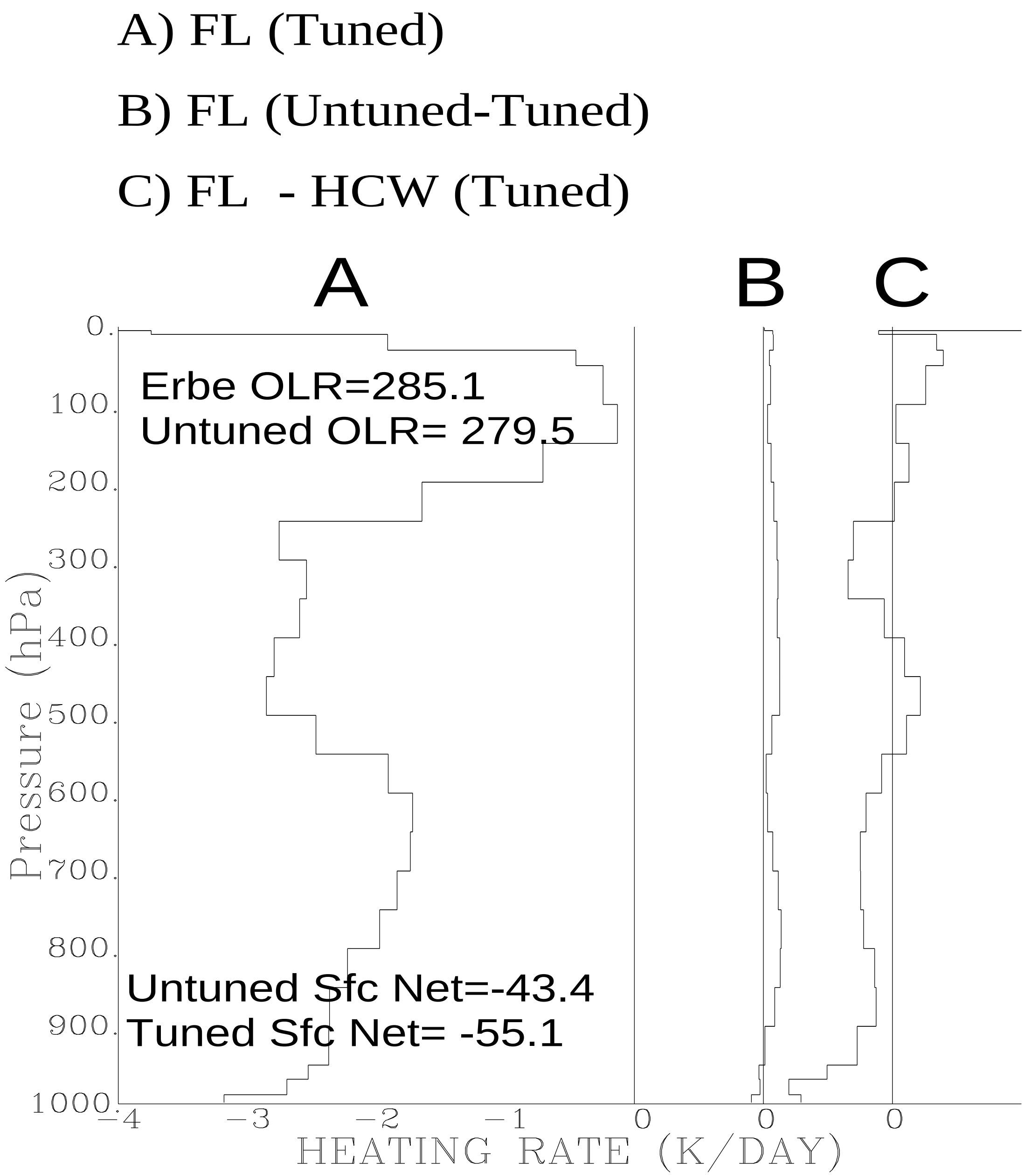

Figure 8. Retrievals of LW heating rate (K/day) for a clear-sky ERBE footprint with FL and HCW tuning algorithms. Line A for FL (tuned). Line B for FL (untuned minus tuned). Line C for FL minus HCW (tuned).

Clear-sky SW tuning with the FL algorithm (Tables 1 and 2) is analogous. The FL algorithm does not yet include aerosols, however. All the clear-sky SW tuning with the FL algorithm is presently based on adjustments to surface albedo only. All initial surface albedo values in FL are presently taken from the SRB Project monthly average (Staylor algorithm).

In Version 0, we have not yet conducted an integrated LW and SW clear-sky test with the HCW and FL algorithms, wherein the PW adjustments produced by the clear-sky LW tuning are used to calculate SW atmospheric heating. During the actual CERES TRMM mission, aerosol retrievals based on the VIRS cloud imager will be available for SARB calculations. During the CERES EOS AM mission, aerosol information from MODIS will be available.

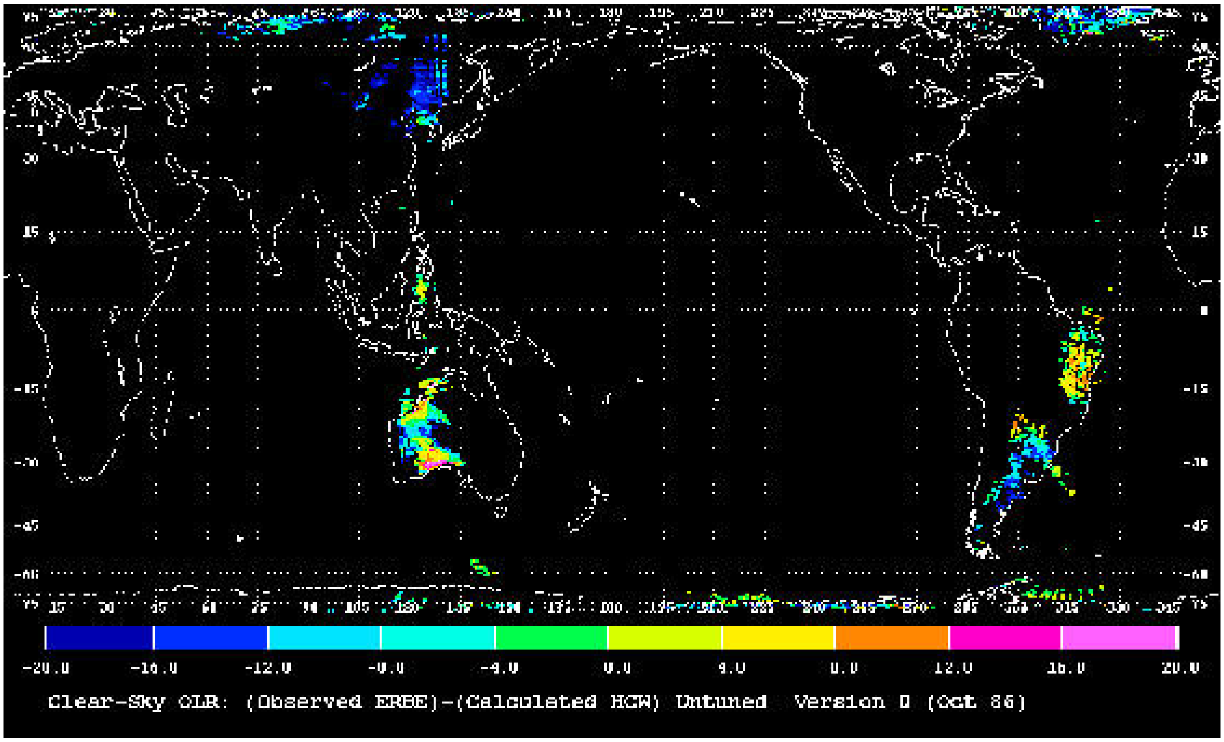

Figure 9. Difference of footprint scale clear-sky OLR in W/m^2 as (observed ERBE) minus (calculated but untuned HCW). Version 0. Clear-sky footprints from one orbit (October 1986).

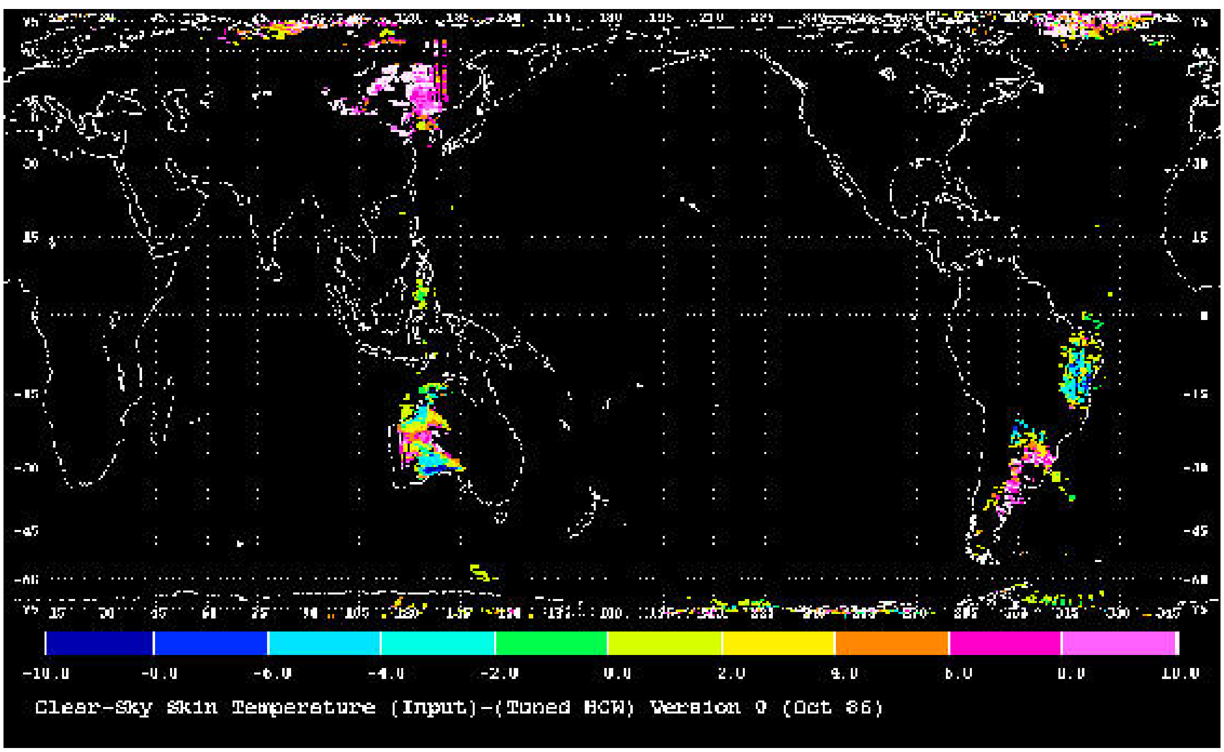

Figure 10. Difference of clear-sky surface skin temperature in K as (input) minus (tuned HCW). Version 0. Clear-sky footprint from one orbit (October 1986 data).

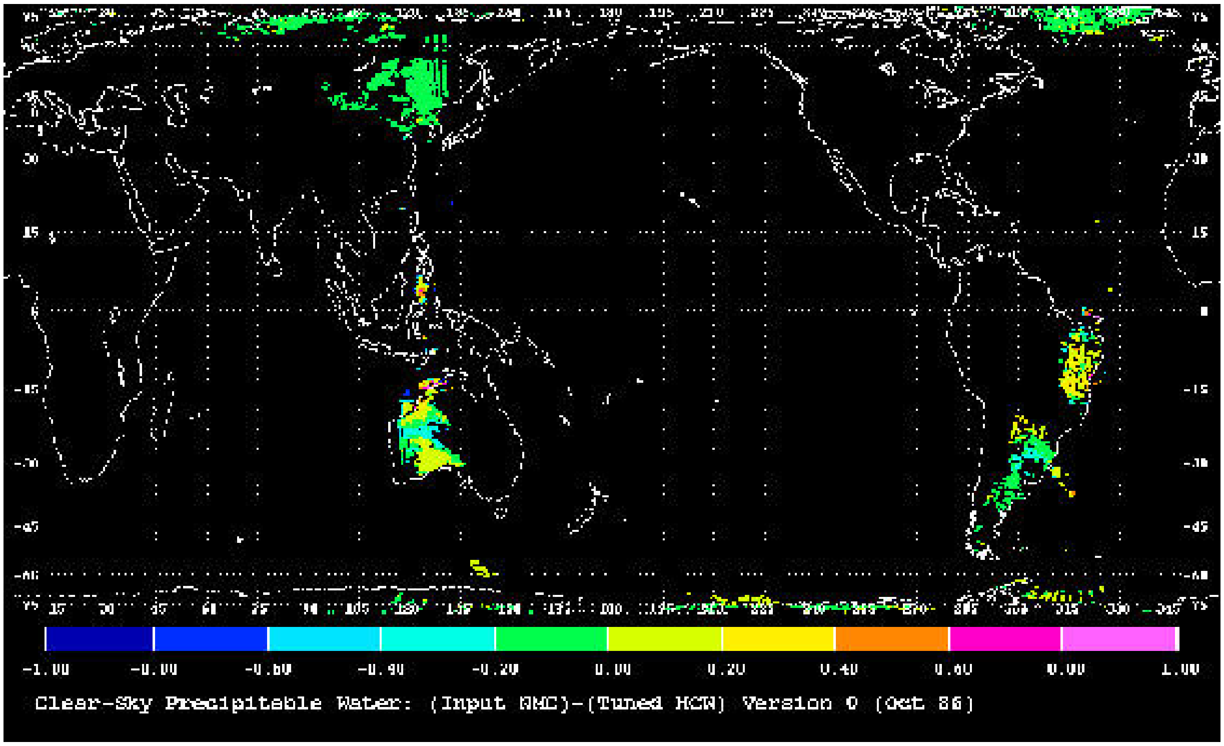

Figure 11. Difference of clear-sky surface precipitable water in cm as (NMC input) minus (tuned HCW). Version 0. Clear-sky footprints from one orbit (October 1986 data).

5.3.5. Total-Sky LW and SW Algorithms

For cloudy skies, we again use two independent SARB retrieval algorithms, HCW and FL, which use plane-parallel radiative transfer. In Version 0, the basic input for both HCW and FL is the modified Minnis et al. (1993a, b) Layer Bi-spectral Threshold Method (LBTM) cloud retrieval algorithm, as described in Subsystem 4 documents. LBTM delivers the fraction of cloudiness, the mean SW optical depth, the mean infrared (IR) emissivity, the mean height, the mean radiating temperature, the estimated geometric thickness, and other cloud parameters, for up to three distinct cloud cases within each ERBE footprint. The three distinct cloud cases in LBTM are low, middle, and high. LBTM in Version 0 assumes that clouds do not overlap (i.e., the independent clouds of Fig. 4(a)) and that cloud droplet sizes are fixed. For the clear-sky fraction and the cloudy-sky fraction of a partly cloudy ERBE footprint, HCW and FL both initially calculate the LW and SW SARB with fixed (unadjusted) LBTM input parameters. These calculations are used to apportion the observed ERBE fluxes to the clear and cloudy components of the footprint. Subsequent iterative tuning of cloud parameters by HCW and FL is based upon the apportioned ERBE fluxes, which are treated as constants. In the clear-sky portion of a partly cloudy ERBE footprint, HCW and FL use completely unadjusted input parameters. There is no tuning for PW, surface skin temperature, surface albedo, or aerosol optical depth with a partly cloudy or cloudy ERBE footprint.

For preliminary data (1/4 orbit with approximately 15000 ERBE footprints in the Western Pacific, from the coast of China to the southern tip of Australia), we find a large scatter of differences between ERBE and the initial (untuned) HCW calculations (Fig. 13). HCW treats clouds as black bodies in the LW; the effective area of a nonblack cloud is reduced as an area equivalent fraction of a black cloud. In the SW, HCW uses the Chou (1992) code, which is based on two-stream adding with delta-4-stream for aerosol and clouds. As expected, cloudy footprints have larger differences (ERBE-HCW) than clear footprints.

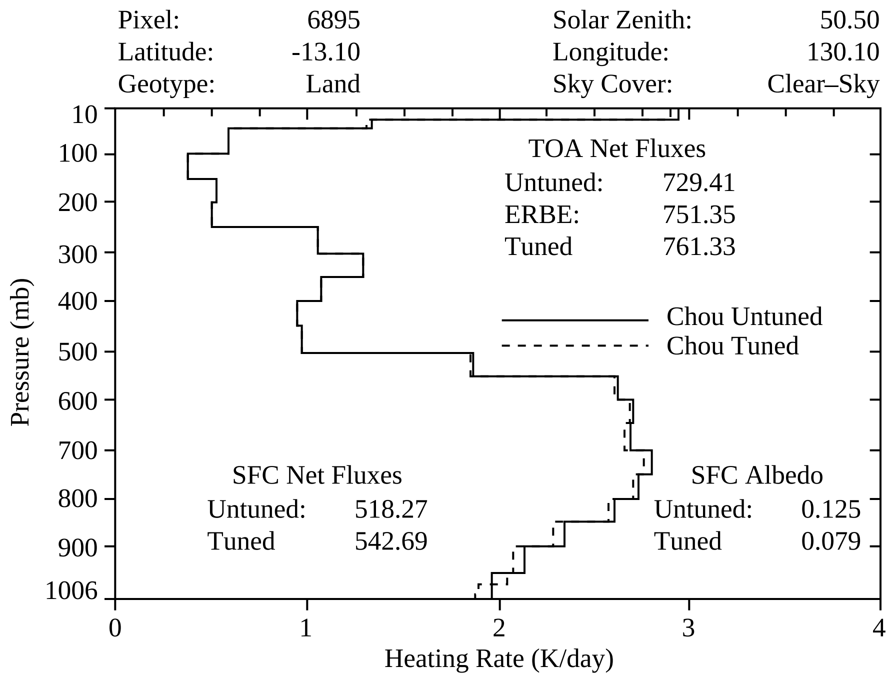

(a) Tuning of surface albedo over land.

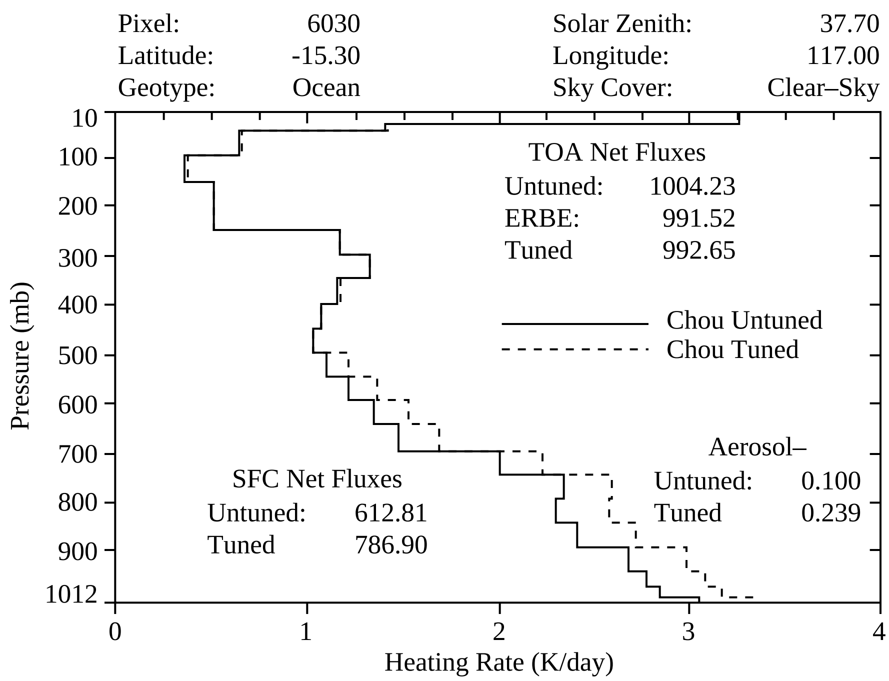

(b) Tuning of aerosol over sea.

Figure 12. SW net fluxes at TOA and SW heating rates over individual footprints. Solid lines show untuned (initial) HCW calculations. Dashed lines show tuned HCW result.

For the total-sky condition in Figure 13(a), the mean difference (ERBE-HCW) in the *reflected* SW flux (vertical axis) is −7.83 W/m^2, and the mean difference in OLR (horizontal axis) is −1.77 W/m^2. The relatively close agreement of the averages of the HCW fluxes with ERBE may be unfortunate at this stage, at least for the reflected SW flux. Radiative transfer calculations have been done at the ERBE-footprint scale, using mean LBTM cloud optical depths from up to 8×8 AVHRR GAC "pixels." In Version 0, there are at most four idealized atmospheres used by HCW and FL for the SARB calculations in each ERBE footprint: the atmospheres for clear skies, low clouds, middle clouds, and high clouds. More properly, the radiative transfer calculations should be done at the scale of AVHRR GAC (and then even nudging further, to account for inhomogeneity within the smaller AVHRR GAC). When such independent pixel (AVHRR GAC) calculations are done, we expect that the SW reflectivity will increase, causing the ERBE-HCW SW flux differences to fall further below the present −7.83 W/m^2.

The negative slope of Figure 13(a) is consistent in that, if one changed the retrieved cloud properties (area or optical depth) to cause HCW to more closely match ERBE SW, one would also produce a closer match to ERBE LW. This phenomenon suggests that the HCW TOA broadband calculations may be useful for adjusting the LBTM cloud retrievals at the scale of the ERBE footprints. Such adjustments could reduce the large root mean square (RMS) error shown in Figure 13(a). If the RMS error is a result

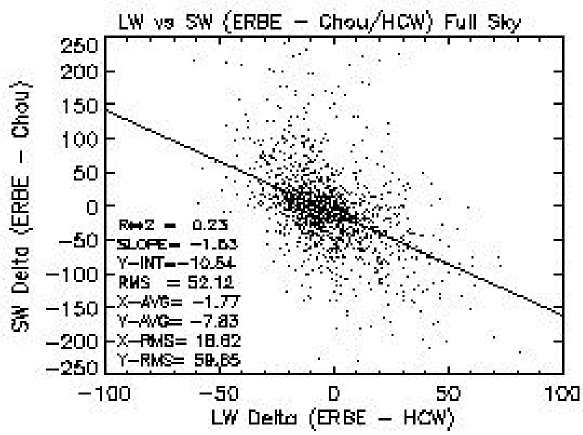

(a) All 15 000 footprints with various sky conditions.

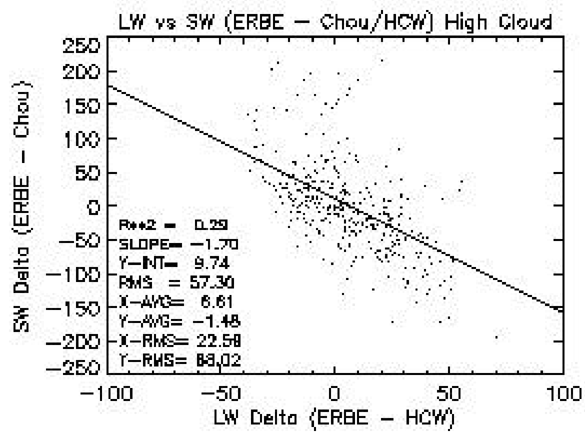

(b) Subset with high clouds.

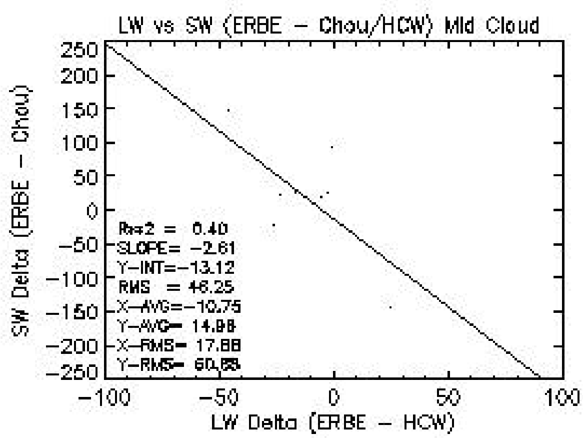

(c) Subset with middle clouds.

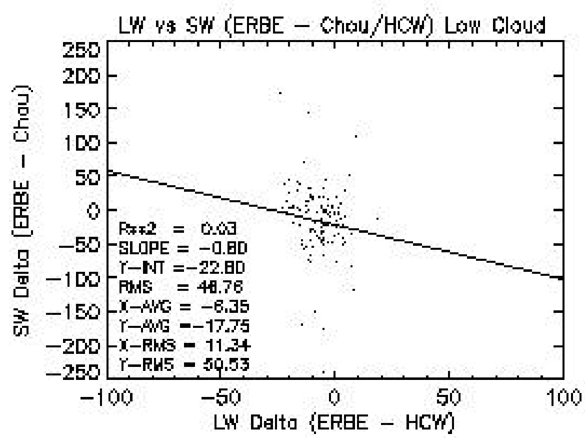

(d) Subset with low clouds.

Figure 13. Scatter plots of differences of ERBE observations and initial (untuned) HCW calculations for 15 000 footprints over western Pacific Ocean and Australia. Difference of reflected SW (as ERBE minus HCW) on vertical axis and difference of (emitted) OLR as (ERBE minus HCW).

of (a) errors in the input LBTM or NMC data and/or (b) the limitations of the radiative transfer codes used to calculate the TOA fluxes, adjustments to LBTM would then be justified. A negative slope is again obtained for high clouds (Fig. 13(b)), middle clouds (Fig. 13(c)), and low clouds (Fig. 13(d)). The HCW TOA broadband calculations thus suggest consistent LW and SW adjustments to cloud area, for various cloud types.

Angular and directional modeling (ADM) effects account for most of the RMS error in Figure 13(a). As expected for instantaneous, footprint-scale angular and directional effects, the RMS error in SW (59.85 W/m^2) is much larger than LW (18.62 W/m^2). A large RMS error in SW is not surprising in this comparison of ERBE, which implicitly accounts for three-dimensional effects using a small number of assumed ADM's, versus HCW, which uses plane parallel radiative transfer. The LBTM cloud retrievals serve as HCW input data, and LBTM uses the plane parallel assumption, too. We also note that the present few ERBE ADM's, which do not account for the optical depth dependence of anisotropy and other factors, may also contribute to the RMS error; in such cases, the LBTM- and NMC-based TOA flux calculations may be useful for diagnosing problems in the ADM's. In the actual CERES experiment, a considerable ADM advance is anticipated. The rotating axis scanner will be used to develop a large number of accurate ADM's.

After the initial calculations, HCW tunes the cloud parameters in the LW, and then passes the adjusted LBTM cloud parameters to the SW (Table 3). In the LW, cloud area is tuned first; cloud height and emissivity are tuned if the cloud area adjustment cannot balance the apportioned ERBE OLR. SW cloud optical depth is tuned in HCW with the Chou (1992) code. For HCW, all clouds in the Chou (1992) SW code are regarded to be composed of liquid droplets. The tuning of cloud effective IR emissivity in the LW is independent of the cloud optical depth tuning in the SW. The present, simple HCW algorithm thus does not produce a tuned cloud field that is microphysically consistent in the LW and SW.

Figure 14 shows, for one orbit (85000 ERBE footprints) of a total-sky condition, the differences of the ERBE OLR and the HCW calculations with the initial LBTM and NMC data. For the total-sky condition (Fig. 14), the OLR differences are much larger than for clear skies (Fig. 9). The data to the east of 220 W were obtained at night. The nighttime ERBE minus HCW OLR differences are consistent with the interpretation that LBTM needs slightly more cloud area (or higher clouds). During the day, there are large positive and negative OLR differences with initial data. By tuning the LBTM cloud and NMC meteorological inputs with the HCW algorithm, we cause the difference of calculated and observed OLR to vanish. The tuning affects the radiation at all levels and not just the OLR. Figure 15 shows the difference of the untuned and tuned total-sky DLF. Most of the adjustments to DLF were produced by cloud tuning, but humidity adjustments are also substantial over a smaller number of clear-sky ERBE footprints.

The Fu and Liou (1993) code includes explicit parameterizations for both liquid and solid phase cloud particles that we employ. FL (Table 2) uses the Fu and Liou (1993) delta-4-stream code for SW and LW. As with the HCW algorithm (Figs. 13(a–d)), the slopes of the ERBE minus FL initial differences (Figs. 16(a–d)) indicate that adjustments to cloud area or optical depth would generally bring both LW and SW consistently into agreement with the ensemble mean ERBE minus FL differences for the 15,000 footprints. In the FL retrieval scheme, both the tuning algorithm and the radiative transfer differ from the HCW scheme, however (Tables 1 and 2). In cloudy-sky condition, FL tunes SW and LW simultaneously, unlike the sequential tuning for clear-skies. FL treats the retrieved LBTM cloud area as a constant, but it adjusts the cloud water path and cloud height simultaneously with coupled LW and SW equations:

$$D(F) = D(L) \times dF/dL + D(H) \times dF/dH \tag{2a}$$

$$D(R) = D(L) \times dR/dL + D(H) \times dR/dH \tag{2b}$$

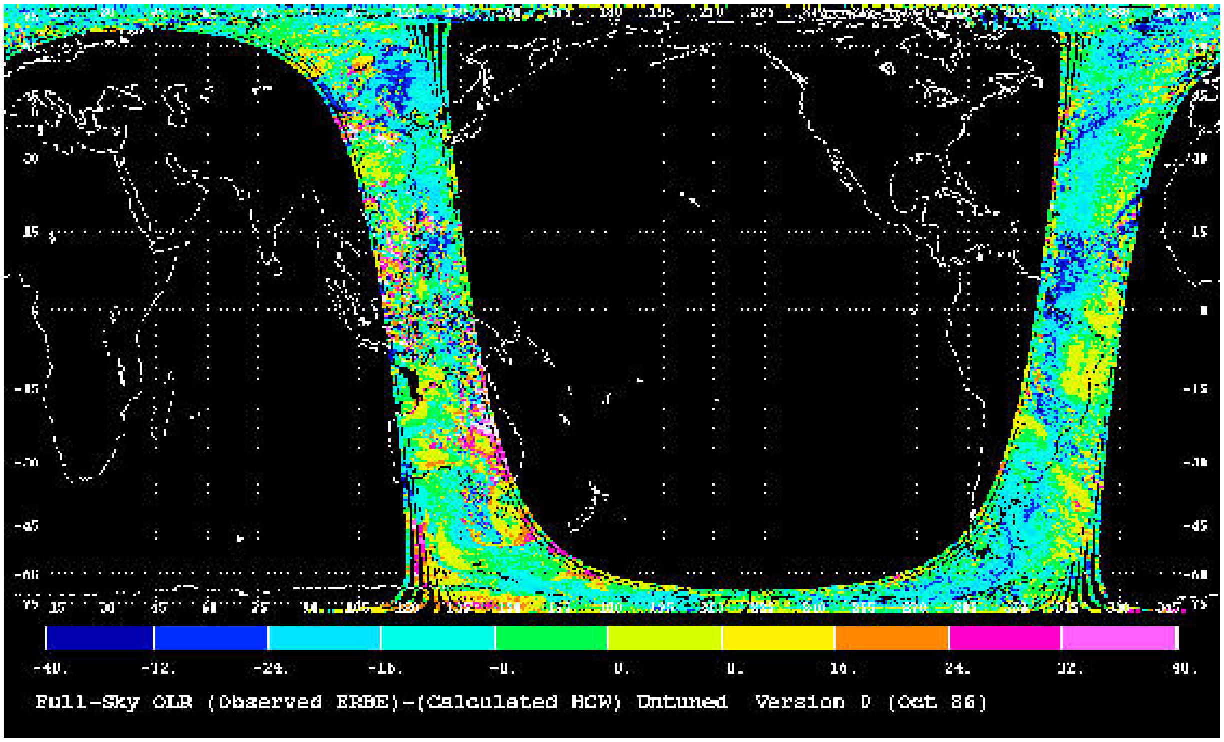

Figure 14. Difference of footprint scale total sky OLR in W/m^2 as (observed ERBE) minus (calculated but untuned HCW). Version 0. Approximately 85 000 footprints comprise this single orbit (October 1986 data). Figure 9 contains clear-sky footprints of Figure 14.

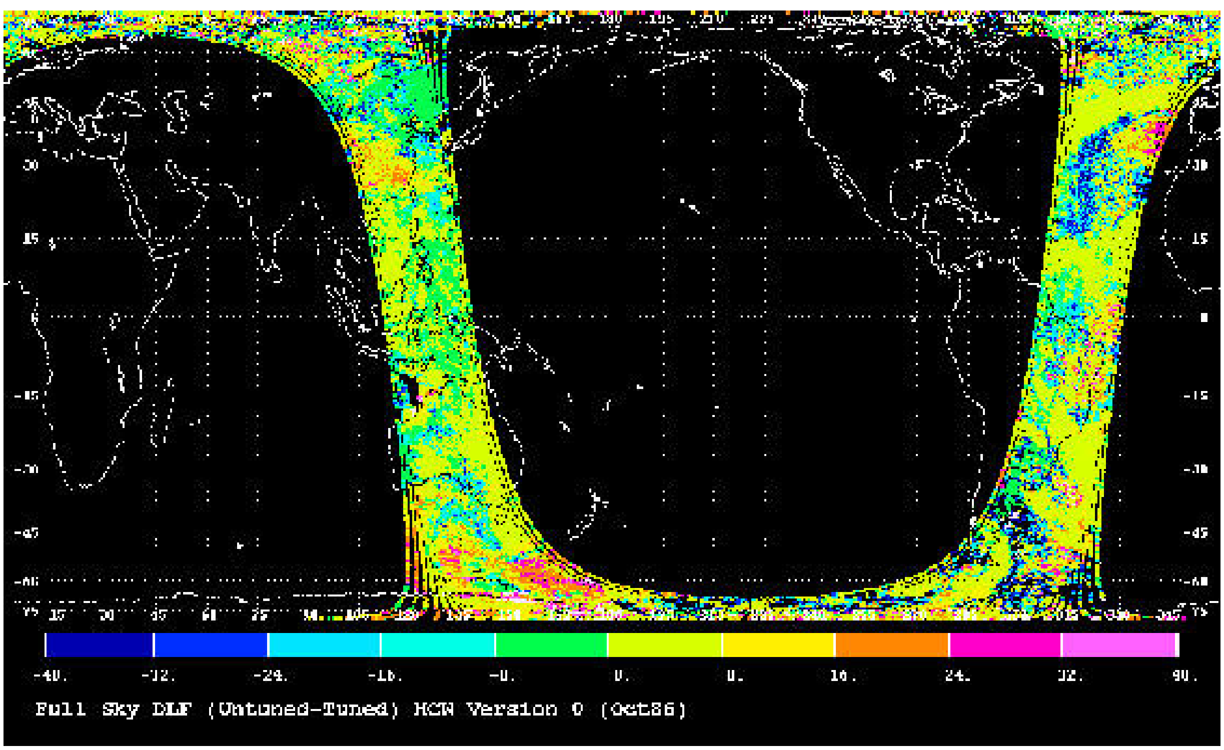

Figure 15. Difference of total-sky surface DLF as (untuned HCW) minus (tuned HCW) for footprints of Figure 14.

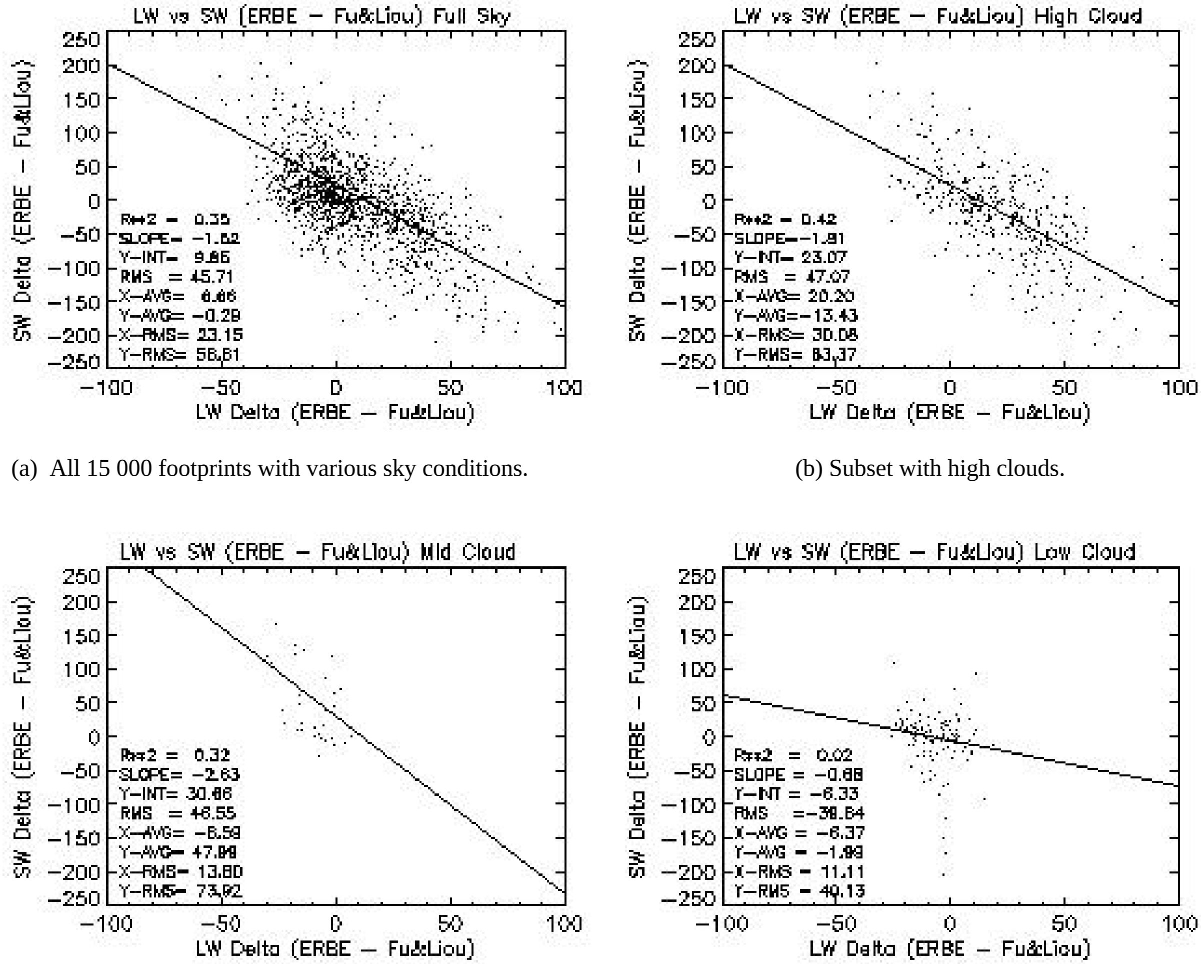

(a) All 15 000 footprints with various sky conditions.

(b) Subset with high clouds.

(c) Subset with middle clouds.

(d) Subset with low clouds.

Figure 16. Scatter plots of differences of ERBE observations and initial (untuned) FL calculations for 15 000 footprints over western Pacific Ocean and Australia. Difference of reflected SW (as ERBE minus FL) on vertical axis and difference of (emitted) OLR (as ERBE minus FL) on horizontal axis.

where

F = cloudy-sky OLR
R = cloudy-sky reflected TOA SW
L = cloud LWP or IWP
H = cloud top height

D(F) = F(observed OLR) − F(calculated OLR)	*Known*
D(R) = R(observed TOA SW) − R(calculated TOA SW)	*Known*
D(L) = L(adjusted LWP) − L(initial LWP)	*Unknown*
D(H) = H(adjusted cld. ht.) − H(initial cld. ht.)	*Unknown*

dF/dL, dF/dH, dR/dL, dR/dH calculated partial derivatives

Unlike HCW, the FL algorithm does produce cloud tuning that is consistent in the LW and SW. Note also the impact of a cloud height adjustment by FL on the vertical profile in Figure 17; tuning has produced a large change in the radiation budget at the TOA and in the lower troposphere. To date, rapid tuning (to within a few W/m^2) with FL is produced for only about 50% of the ERBE footprints. In contrast, the HCW algorithm tunes more quickly to within 1 W/m^2 for most ERBE footprints. At night, FL assumes that clouds are optically thick and tuning provides an adjustment to cloud height only.

Because of the difficulties of determining the geometric thickness of clouds (locating cloud base, as well as cloud top) with passive satellite remote sensing, we anticipate substantial uncertainties in the SARB that CERES determines below cloud tops. By adding passive microwave to CERES, some advances can be expected. Cloud LWP can be retrieved with microwave data, and the LWP can in turn be used to estimate the cloud geometric thickness. CERES plans to buttress VIRS- and MODIS-based cloud retrievals with microwave information from TRMM and Multifrequency Imaging Microwave Radiometer (MIMR). Even without such microwave sensing, there are good prospects for producing a reliable vertical profile of the radiation budget *above* the cloud tops. Figure 18 gives an example of the significant impact of tropospheric clouds on the LW budget at 30–50 hPa in the stratosphere. Because radiative relaxation times are small in the stratosphere (Ramanathan 1987), the small radiative perturbations that are induced by tropospheric clouds can have a large impact on the equilibrium stratospheric temperature. The radiation budget near the tropopause has received relatively little attention in global satellite-based retrieval programs to date, but the budget in the upper troposphere and lower stratosphere is an important forcing of the climate. The radiation budget in the vicinity of the tropopause will be a key CERES product. Figure 18 suggests that the detailed cloud property retrievals that CERES provides, in addition to the broadband TOA fluxes, will be essential in determining the space and time variability of the stratospheric radiation budget.

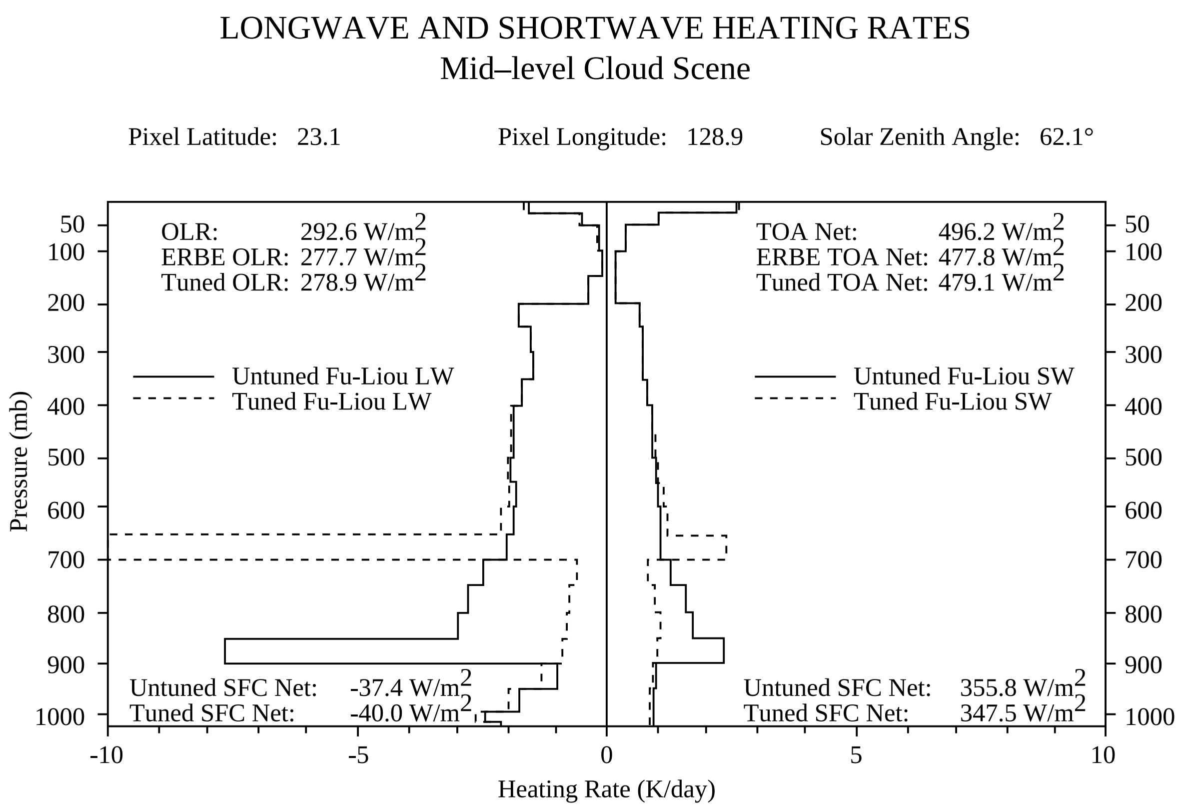

Figure 17. For LW and SW, fluxes at the TOA (as untuned FL, ERBE observations, and tuned FL), fluxes at surface (as untuned FL and tuned FL), and heating rates (untuned are solid and tuned are dashed). One ERBE footprint containing low clouds.

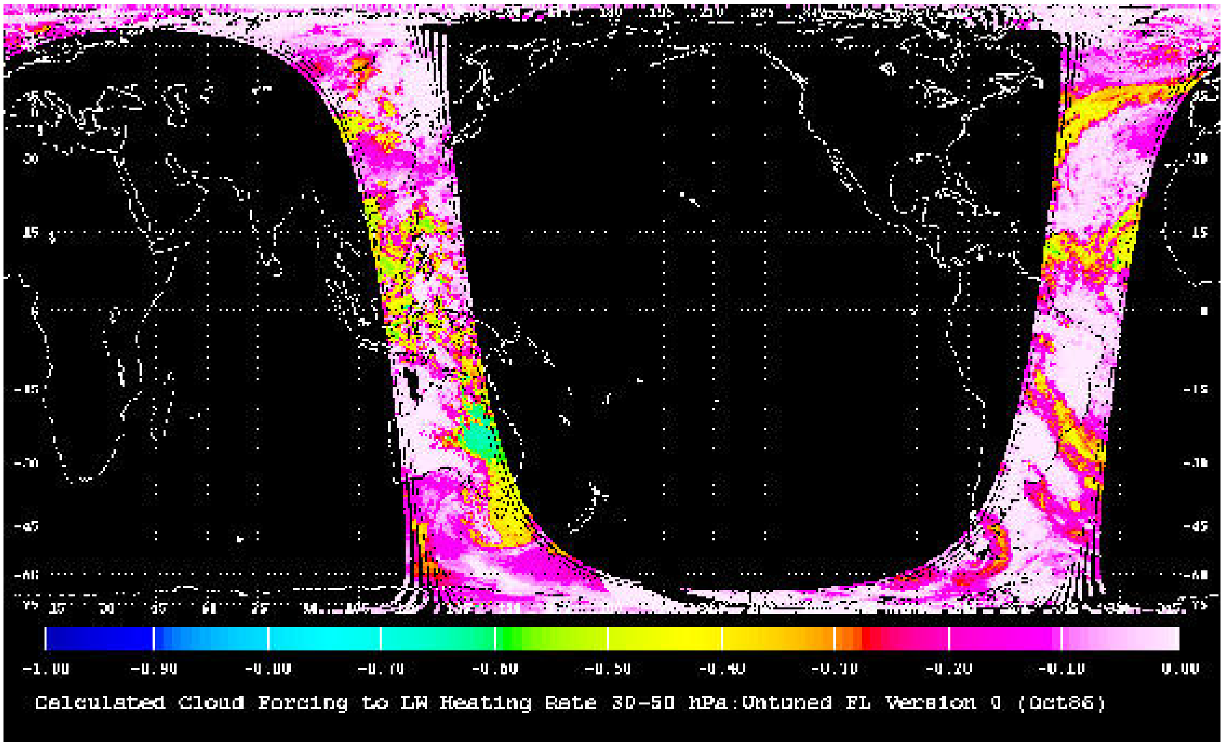

Figure 18. LW cloud forcing to heating rate (K/day) in 30:50 hPa layer for untuned FL. Footprints as Figure 14.

5.4. Algorithm Application

5.4.1. Algorithm Modifications for Release 1

The FL and HCW retrieval algorithms, described above in the completed Version 0, are different in Release 1. Release 1 covers the full month of October 1986 and December 1986–January 1987 at the ERBE footprint scale and is planned for issue in late 1995.

In Release 1, the HCW algorithm is processed “unofficially” for diagnostic purposes, and the FL algorithm provides the “official” SARB result. The HCW algorithm in Release 1 uses the Wang et al. (1991) algorithm exclusively for LW calculations. A modification of the Wang et al. (1991) code made at NASA LaRC permits the input of sounding data at the end points of model layers. The vertical grid of Release 1 permits the input of cloud top and cloud bottom information at any vertical level, rather than at the fixed levels set in Version 0 (Fig. 7).

For Release 1, the spectrally flat broadband surface albedo of Version 0 is modified to include spectral dependence following Briegleb et al. (1986) and Pinker and Laszlo (1992a). The FL algorithm includes aerosols in Release 1; work is in progress at the University of Utah to incorporate aerosols in the Fu and Liou (1993) code. In Virginia, Dr. David Kratz has developed the correlated-k’s for the five channels of AVHRR for use in the Fu and Liou (1993) code, permitting the Release 1 FL algorithm to generate an AVHRR flux product, as well as the broadband SARB. Release 1 extracts and adjusts narrowband information from the Chou (1992) and Fu and Liou codes (1993) and estimates the surface downwelling photosynthetically active radiation (PAR; i.e., Pinker and Laszlo 1992b) and the surface SW direct-to-diffuse ratio (Pinker and Laszlo 1992a).

One distinction between the SARB retrievals in Version 0 and Release 1 is the application of Lagrange multipliers to tuning for cloudy skies with FL for SW and LW. In Version 0 with the HCW and FL algorithms, Lagrange multiplier adjustments D(T) and D(W) are applied in Equation (1) to tune the surface skin temperature and the natural logarithm of the PW for the clear-sky OLR. A new FL formulation for cloudy skies is used in Release 1 because of the deficiencies in the FL and HCW retrieval algorithms for cloudy skies in Version 0. In Version 0, we have noted that FL tuning for cloudy skies, which does not adjust cloud area, works for only 50% of the cases. In Version 0, the HCW tuning does not tune to a consistent LW emissivity and SW optical depth, because SW and LW tuning is independent in HCW. The new Release 1 SARB algorithm modifies FL for cloudy skies as follows. We have not yet tested the new algorithm with satellite data.

Similar to the LW and SW Equations (2a–b) in terms of cloud L (LWP or IWP), we include a third variable, cloud area A:

$$D(F) = D(L) \times dF/dL + D(H) \times dF/dH + D(A) \times dF/dA \tag{3a}$$

$$D(R) = D(L) \times dR/dL + D(H) \times dR/dH + D(A) \times dR/dA \tag{3b}$$

where

F = cloudy-sky OLR
R = cloudy-sky reflected TOA SW
L = cloud LWP or IWP
H = cloud top height
A = cloud area

D(F) = F(observed OLR) − F(calculated OLR)	*Known*
D(R) = R(observed TOA SW) − R(calculated TOA SW)	*Known*
D(L) = L(adjusted LWP) − L(initial LWP)	*Unknown*
D(H) = H(adjusted cld. ht.) − H(initial cld. ht.)	*Unknown*
D(A) = A(adjusted cld. area) − A(initial cld. area)	*Unknown*

The proposed solution assumes a normal distribution P for D(L), D(H), D(A) as

$$P[D(H),D(L),D(A)] = 1/[2.*pi*S(H)*S(L)*S(A)]*exp(-Z)$$

where S(H), S(L), and S(A) are the expected errors in cloud height H, cloud L (LWP or IWP), and cloud area A, and

$$\begin{aligned} Z = {} & [D(H)/S(H)]^2 + [D(L)/S(L)]^2 + [D(A)/S(A)]^2 \\ & - 2 \times r(L,H) \times [D(L) \times D(H)]/[(S(L) \times S(H)] \\ & - 2 \times r(L,A) \times [D(L) \times D(A)]/[(S(L) \times S(A)] \\ & - 2 \times r(H,A) \times [D(H) \times D(A)]/[S(H) \times S(A)] \end{aligned}$$

where

r(L,H) = correlation between D(L) and D(H)
r(L,A) = correlation between D(L) and D(A)
r(H,A) = correlation between D(H) and D(A)

To maximize the probability that the three errors satisfy Equations (3a) and (3b), it is necessary to minimize Z constrained by (3a) and (3b). The method of Lagrange multipliers provides

$$G[D(H),D(L),D(A),lam1,lam2] = Z + lam1 \times (Eqn\ 3a) + lam2 \times (Eqn\ 3b)$$

Partial derivatives of G with respect to D(H), D(L), D(A), lam1, and lam2 provides five equations with five unknowns. The solution provides the D(H), D(L), and D(A), which are the needed adjustments to cloud height H, the cloud L (LWP or IWP), and cloud area A. We presently assume that the correlations r(L,H), r(L,A), and r(H,A) are zero; similar assumptions were made for the clear-sky LW solution of Equation (1)

Cloud height H is an analog of cloud temperature through the meteorological sounding. A solution for H with the FL retrieval algorithm for the SARB thus yields the cloud radiating temperature. As noted in the cloud property retrieval documents (Subsystem 4 in the CERES package), Release 1 provides a retrieval of cloud particle size. When combined with LWP or IWP, for which the FL algorithm tunes, the input cloud partical size can then be matched to provide the cloud SW optical depth or IR emissivity. The SARB tuning process for Release 1 retrieves a new LWP (or IWP) and a new SW optical depth and IR emissivity for the clouds; these are used to generate adjustments to LWP, SW optical depth, and IR emissivity from the Subsystem 4 cloud-imager based retrievals.

5.4.2. Execution of Release 1

5.4.2.1. Input data. The CERES calculation of the SARB in Release 1 uses the CERES cloud imager data (Subsystem 4.4), which is based mostly on AVHRR and HIRS, and the atmospheric sounding data (Subsystem 12), which is based mostly on 6-hourly NMC Reanalysis.

The sounding data are similar to those used above in Version 0. In Release 1, the sounding profiles are interpolated to 38 vertical levels, for every 1.25-deg equal-area region, to the nearest hour of the satellite overpass. The change to 38 levels for the sounding input is provided at the 26 levels of Figure 7, and also at the midpoints of some of the 50-hPa-thick layers of Figure 7 (Appendix B of Subsystem 12 and Appendix A of this Subsystem 5). The ozone profile is based on a climatological data and the SBUV record from NMC. We distribute the total column aerosol using a scale height of 3 km, but unlike Version 0, Release 1 permits aerosols throughout the troposphere and stratosphere.

The clear-sky LW and SW calculations for the SARB are initialized with data from Release 1. The land skin temperature is a product of the CERES Release 1 cloud retrieval (if the skies are truly clear) or from the 3-hourly ISCCP C1 Clear-Sky Composite. For an initial skin temperature over the oceans, Release 1 uses the sea surface temperature (SST) from NMC. As in Version 0, the initial surface albedo is set from the monthly average SRB Project result (Whitlock et al. 1994), and for clear-sky land we use an instantaneous albedo based on the Li and Garand (1993) algorithm.

The major change in the input for Release 1 SARB calculations are to the cloud retrievals as documented in Subsystem 4. In the Version 0 calculations described earlier, the LBTM cloud retrievals have no overlap within *cloud imager pixels*, and cloud conditions were grouped within each *ERBE footprint* as clear, low cloud, middle cloud, and high cloud (or a combination of clear, low, middle, and high, but with no overlap). Release 1 permits one of four cloud cases within a single *cloud imager pixel* as (a) clear, (b) cloud in first layer, (c) cloud in a second layer, or (d) overlap of cloudiness in the first and second layers. Each Release 1 cloud imager pixel is flagged as (a), (b), (c), or (d). Each of the up to two cloud layers in Release 1 pixels are grouped as high, upper middle, lower middle, or low. Release 1 cloud retrievals are then binned into the *ERBE footprints.* In the ERBE footprints, Release 1 permits up to 11 cloud conditions as permutations of high, upper middle, lower middle, and low, with the constraint that none of the 11 cloud conditions can have more than 2 overlapping cloud layers. A Release 1 ERBE footprint can be, for example, 10% clear, 10% high cloud, 10% low cloud, 10% overlap of high and low, 10% upper middle, and 50% overlap of high and upper middle. A Release 1 ERBE footprint *cannot* have 10% clear, 10% high, 10% low, 10% upper middle, and 60% overlap of high, upper middle, and low; the condition of 60% overlap of high, upper middle, and low would violate “cloud conditions cannot have more than two overlapping layers.”

Release 1 will specify the cloud heights (temperature) of the cloud layers and also provide the spatial standard deviations of the cloud heights (temperatures) for the cloud layers. For each of the high, upper middle, lower middle, or low clouds retrieved (Subsystem 4 and the Appendix A of this document), we have the mean and spatial standard deviation of the AVHRR radiance (0.6, 3.7, 11.0 micrometers), SW optical depth, IR emissivity, LWP, IWP, pressure of top, effective pressure, effective temperature, effective height, estimated pressure of bottom, water particle radius, and ice particle radius. Release 1 also provides the cloud phase (water or ice), the cloud aspect ratio, and the SW optical depth in 13 percentiles. Release 1 assumes that an overlapped cloud consists of two layers, with each overlapped layer having the same physical properties (excepting area) as the nonoverlapped portions.

The mean cloud areas, tops, and bottoms of the high, upper middle, lower middle, and low clouds are inserted directly into SARB calculations. Although cloud SW optical depth is available in Release 1, the SARB calculations do not use cloud optical depth directly in the FL algorithm. For daylight conditions, cloud microphysical properties for FL algorithm LW and SW calculations are determined from the cloud LWP (IWP) and the cloud partical radius as retrieved by the cloud imager. Cloud-imager based retrievals of microphysics are much less reliable at night. At night, we use the cloud particle size and the IR emittance as inputs; a set of off-line calculations, based on runs with the Fu and Liou (1993) code, provide a mapping of the cloud-particle size and IR emittance into LWP (IWP), which is used in subsequent FL calculations.

5.4.2.2. Initial calculations for SARB. Release 1 proceeds as Version 0, performing initial calculations of the SARB with FL and HCW algorithms. In Version 0, we used up to four conditions (clear, low cloud, middle cloud, and high cloud), which permitted up to four SARB calculations within each ERBE footprint. In Release 1, we have up to 11 cloud conditions (clear and permutations of cloud as high, upper middle, lower middle, and low cloud, with aforementioned overlap permitted). The TOA and surface fluxes are calculated for up to 11 cloud conditions in each ERBE footprint. Release 1 uses the mean cloud optical properties of each of the conditions for SARB calculations (see Appendix A). The spatial standard deviations of the cloud properties are not used for formal Release 1 SARB calculations.

The TOA and surface fluxes in the initial calculations are formally archived in Release 1 (see Appendix B), as they are useful diagnostics for the broadband radiative transfer calculations (the calculated SARB), the cloud retrievals, and the observed TOA fluxes. Release 1 formally archives the initially calculated TOA and surface fluxes for (1) the theoretical clear-sky condition in the footprint (archived even if the footprint is overcast) and (2) the total-sky condition. Release 1 does not formally archive the *initially* calculated fluxes within the atmosphere or the partitioned fluxes, at any level, for the first cloud, second cloud, and overlapped cloud which may be in the footprint; such items are archived only informally “off-line.” Release 1 calculates fluxes in the AVHRR channels, but these are again not part of the formal archive.

5.4.2.3. Tuned SARB. After calculating the initial SARB with the Release 1 input data, the observed ERBE TOA flux in the footprint is apportioned, as in Version 0. A single ERBE footprint consists of up to 11 conditions (clear and permutations of cloud with overlap). The apportionment determines the fractions of the TOA ERBE footprint flux that are assigned to each of the conditions. From the *calculated* TOA flux for each of the 11 conditions, the *input* areas of the 11 conditions within the footprint, and the *calculated* TOA flux for the entire ERBE footprint, we determine the fractional apportionment of the TOA flux to each of the 11 conditions. The fractional apportionment is then fixed, and we use it to apportion the *observed* TOA flux among the 11 conditions for subsequent tuning.

In Release 1, the surface skin temperature, the PW, the surface albedo (land) and the aerosol optical depth (sea) are tuned for only ERBE footprints that are completely clear. If a portion of the footprint is cloudy, these parameters are fixed to the input values, and tuning proceeds for cloud properties only. A clear footprint is tuned in the LW with the Lagrange multiplier technique, as in Version 0. This procedure produces LW fluxes at all levels, but Release 1 formally archives the tuned fluxes at only four levels: the surface, 500 hPa, the tropopause, and the TOA (Appendix B). For SW clear-sky footprints, we adjust the surface albedo over land the aerosol optical depth over the sea to balance with the observed ERBE fluxes. This procedure yields SW fluxes at all levels, and they are archived at only four levels. For a completely clear footprint, Release 1 archives the adjusted PW, the adjusted skin temperature, the adjusted aerosol optical depth, and the adjusted surface albedo (Appendix B). Estimates for the PAR and the surface SW flux direct/diffuse ratio are archived for all sunlit footprints in Release 1.

If the ERBE footprint contains clouds, the clear-sky inputs to the SARB calculations are frozen and SARB tuning proceeds for the cloud variables only. The apportioned ERBE fluxes are used for tuning during daylight with Equations (3a) and (3b). The crucial item in the tuning with (3a) and (3b) is the selection of S(H), S(L), and S(A), which are the expected errors in cloud height H, cloud water path L (LWP or IWP), and cloud area A. If a parameter is assigned a large expected error, the adjustment of that parameter in the tuning process tends to increase. We currently assume 1 km for S(H) and 10% for S(A). S(L) is not yet determined, but will be weighted by the natural logarithm of LWP/IWP and the cosine of the SZA. Careful examination of the results of Release 1 will be needed to make more sound estimates of S(H), S(L), and S(A). Equation (3b) cannot be used at night, for which we use an alternate formulation with different S(H), S(L), and S(A).

The cloudy-sky tuning for the SARB yields SW and LW fluxes at all 26 levels of Figure 7. In Release 1, the tuned fluxes at the surface, 500 hPa, tropopause, and TOA are formally archived (in addition to the untuned, initially calculated fluxes at those four levels and ERBE-observed TOA fluxes). The formal archive contains fluxes at the four levels for the total-sky and the clear-sky conditions; the clear-sky condition is always calculated and archived, regardless of the presence of clouds. The SARB tuning also changes the cloud height H, L (LWP or IWP), and cloud area A, which were originally retrieved with the imager; for an output, we also record consistent values of cloud SW optical depth and IR emittance (from L and cloud imager droplet size); these cloud variables are archived for low, lower middle, upper middle, and high clouds. The tuned cloud area A includes an adjustment, if needed, to the fraction of overlapped cloud.

5.5. Strategic Concerns

5.5.1. Input Data

Release 1, although a formidable effort that covers the globe for a full month, is limited. Calculations of the SARB are performed at the fairly large scale of an ERBE footprint using spatially averaged properties of clouds for 11 or fewer idealized atmospheric profiles. The smaller cloud imager pixels have inhomogeneities that generate errors when one attempts (as in Subsystem 4) to retrieve cloud physical and optical properties from pixel-scale data (Wielicki and Parker 1992). It is anticipated that successive generations of CERES cloud retrievals will improve through intercomparison with data from field campaigns such as the First ISCCP Regional Experiment (FIRE). Because of the large impact of ice crystal characteristics on cloud optical properties (Liou 1992), improved retrievals of cloud ice are eagerly awaited. Takano and Liou (1994) have developed a new Monte Carlo/geometric ray-tracing method for calculating the scattering from ice crystals; this approach can be expected to advance both the remote sensing of ice clouds (i.e., Minnis et al. 1993a, b) and the effect of ice clouds on broadband fluxes (Fu and Liou 1993).

There are considerable uncertainties relating to the properties of the surface, aerosols, and meteorological data. As noted earlier, aerosol absorption is one possible source of the (possibly) anomalous absorption by clouds (Stephens and Tsay 1990). Whereas we tune for aerosols over the sea, aerosols are fixed over the land because of the larger and more uncertain surface albedo. Any optical property that Release 1 infers about the surface is tied to the limitations of the input aerosol data. We await MODIS aerosol retrievals for aerosol optical depths over land. CERES will provide an independent aerosol retrieval with VIRS on TRMM.

Over land, the input surface albedo for clear skies from ERBE and the Li and Garand (1993) algorithm is straightforward, but essentially unvalidated. For cloudy skies, we use the SRB Project surface albedo, which is uniform through the month. Lacking a time history of retrieved albedos for cloudy skies, we have assumed an albedo and tuned the resulting error into the cloud properties. Some of the problems relating to the SW optical properties of the surface could be resolved with a time-history study, wherein a surface albedo record would be developed and successively honed with repeated passes. Release 1 does not use spatial interpolation/adjustment from neighboring clear-sky footprints as a source of information on the optical properties of cloud-covered surfaces. This approach is proposed for Release 2. When we attempt to partition the SW surface fluxes into upwelling and downwelling components, we are affected by our lack of information on the surface bidirectional reflectance function (BDRF). Some advances can be expected in this arena as the GEWEX SRB Project advances. CERES has planned a series of helicopter flights over the ARM site in Oklahoma, which will scan in four SW channels and one LW channel, to determine the BDRF and directional dependence of the emission.

There are corresponding problems with the surface with the LW. Sellers and Hall (1992) noted the strong directional dependence of LW emission from the surface itself, which suggests that a tuning at one satellite angle may not be representative of the hemispherically integrated flux. Simply stated, the effect is produced by a vegetation canopy, which commonly has a vertical temperature gradient; by observing at different viewing angles, one sees different parts of the canopy, which have different temperatures. Further, we have to date assumed that the surface emissivity is unity, which again will generate an error in the surface flux (Wan and Dozier 1989; Prata 1993). MODIS will retrieve the surface emissivity, but some care will be needed in such a retrieval because of the aforementioned directional dependence. In analyzing the LW flux and directional radiance data from the forthcoming CERES helicopter measurements over ARM, we will experiment with the retrieval of surface temperature and emissivity. Surface emissivity can fall well below 0.90 over some dry, unvegetated soils (Salisbury and D’Aria, 1992). For a fixed atmospheric sounding and a fixed value for the clear-sky OLR, there is a corresponding theoretical family of surface skin temperatures and surface broadband LW emissivities; the surface net LW flux is not uniquely determined. With the Fu and Liou (1993) code and a fixed midlatitude sounding, a clear-sky OLR of 280 W/m^2 is consistent with both case A (skin temperature of 291 K; emissivity 1.00) and case B (skin temperature 296 K; emissivity 0.85); the surface net LW in cases A and B differ by 12 W/m^2. There are prospects for reducing this uncertainty by analyzing multiple channels (i.e., broadband LW and AVHRR window channels, which are both observed and simulated in Release 1).

The NMC data for atmospheric temperature is generally regarded as accurate to within 1 or 2 K. Under most circumstances, other parameters will induce larger errors. Uncertainties in water vapor are known to have a great impact on fluxes; GEWEX (Chahine 1992) has been organized partly because of these uncertainties. Our tuning of PW to match TOA broadband fluxes is a small step forward. Microwave water vapor data for the actual CERES mission and tuning to narrowband (in addition to broadband) would yield further advances. The development of correlated-k’s for use in the AVHRR channels with the Fu and Liou (1993) code will permit the testing of this concept before launch. The CERES/ARM/GEWEX exercise (see Fig. 19 and following section) will investigate sounding input issues intensively over the ARM site in Oklahoma. The ARM program includes special radiosonde launches, a nearby network of National Weather Service (NWS) remote profilers, and on-site microwave and Raman lidar retrievals of water vapor. Through GCIP, NWS mesoscale Eta model outputs with hundreds of parameters at nested points around the ARM site are archived hourly (July–August 1994 and indefinitely after April 1995); these include analyses from the Eta Data and Assimilation System (EDAS).

The accuracy of the input sounding data will have an obvious impact on the CERES retrievals of fluxes near the tropopause. For the October 1986 exercise, NMC provided to CERES a special high-altitude temperature product (above the usual standard levels). The Total Ozone Mapping Spectrometer

(TOMS) will be the primary source for column-integrated O_3 during later periods of CERES algorithm development. We consult with researchers at NASA LaRC who are involved with the Stratospheric Aerosol and Gas Experiment (SAGE) and the Solar Backscattered Ultraviolet (SBUV); SAGE and SBUV provide information on the vertical distribution of O_3. Release 1 Data Product Tables indicate that CERES will provide radiative fluxes “at the tropopause.” One strategic concern is the selection of the exact level for archiving the fluxes near the tropopause. A time series of fluxes at a fixed pressure altitude in the upper troposphere may be more meaningful than the flux at the tropopause itself. We plan to select the level (1) as we compare our calculated fluxes with ARM observed fluxes in prelaunch exercises (see the next section 5.5.2) and (2) as guided by an examination of the flux profiles in the Atmospheric Model Intercomparison Project (AMIP) GCM simulations (Gates 1992).

We will compare our Release 1 results with more temporally extensive efforts like ISCCP and the GEWEX SRB Project. The CERES retrievals of clouds and fluxes are quite different than in ISCCP and the SRB Project, and it will be scientifically interesting to analyze the cloud-to-flux correlations in these other global retrievals.

5.5.2. Inhomogeneities and 3-D Effects

Release 1 SARB calculations do not account for the differences in cloud optical depth between the groups of cloud imager pixels. We simply average them over the ERBE footprint to the mean properties of high, upper middle, lower middle, and low clouds, thereby introducing a systematic error. We further assume that the world is plane parallel, both with regard to the CERES cloud retrievals used as inputs and the broadband radiative transfer codes used to calculate the SARB itself. Three-dimensional calculations by Schmetz (1984) suggest that under some circumstances, three-dimensional effects may be accounted for in the SW with minor adjustments to plane-parallel calculations. Heidinger and Cox (1994) have reported some success in accounting for finite (three-dimensional) cloud effects on surface DLF.

We regard cloud inhomogeneity and finite geometry as the most formidable barriers to our effort to retrieve the radiative flux divergence in the troposphere. Some advance is expected through CERES participation in the ARM program. ARM makes continuous measurements of radiative fluxes at a battery of sites in Oklahoma (Stokes and Schwartz 1994). During some of the ARM Intensive Observing Periods (IOP), atmospheric radiative fluxes are measured by Unmanned Aerospace Vehicles (UAV). CERES has an agreement with ARM and GEWEX to foster the development of satellite-based retrievals of the SARB in the atmospheric sciences community. A component of the CERES SARB group, which has formal “Adjunct Science Team” status in ARM, now accesses (1) formatted versions of the GOES-based cloud retrievals with the Minnis et al. (1993a, b) LBTM technique over the ARM site, (2) sounding and other data needed to calculate the SARB with such satellite data, and (3) the ARM fluxes needed to validate retrievals of the SARB. The formatted set, 1-2-3 above, are made available to the GEWEX community electronically by CERES investigators researching the SARB. CERES will furnish some of these provisional, experimental SARB retrievals to ARM.

The initial CERES approach to the April 1994 ARM IOP data set is shown in Figure 19. In daylight, Minnis et al. (1993a, b) LBTM cloud retrievals have been provided every 30 minutes. A run of the Fu and Liou (1993) code for DLF with LBTM clouds and interpolated NMC radiosonde data over the ARM Central Facility gridbox is shown in Figure 20, with the ARM pyrgeometer observations. For overcast conditions, the computed and observed DLF are different, probably because the satellite cannot estimate the cloud geometric thickness very well; in clear conditions, the computed and observed DLF match; the largest discrepancies are in the overcast to clear transition, where the grid of 0.3×0.3 degree computations and single-point pyrgeometer observations are not mutually representative. There will be opportunity, in the April 1994 dataset and in other IOP’s, to address the finite cloud and inhomogeneous cloud issues (i.e., lower right of Fig. 19) with a time series of expanding ARM surface observations (i.e., upper left of Fig. 19) and UAV vertical profiles of fluxes. Our early goal is partly empirical: a

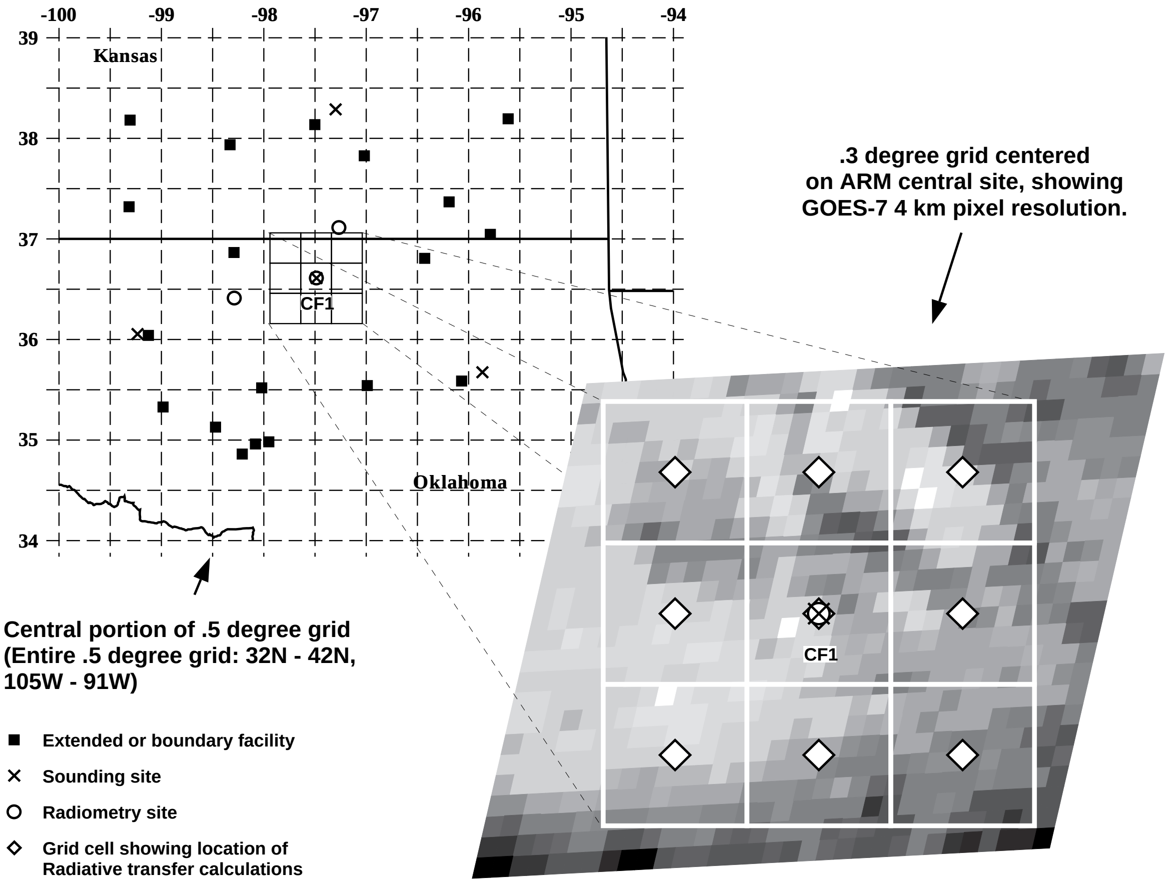

Figure 19. Domain of preliminary CERES/ARM/GEWEX test of satellite-based retrievals of radiative flux with April 1994 data.

determination of the error in satellite-based, plane-parallel SARB calculations in various space-time domains. We will use grid-averaged calculations (Fig. 20) for a start and also investigate independent-pixel calculations.

In validating our results, we will rely upon time series of radiometric measurements at the ARM sites. In Oklahoma, ARM will eventually have 20 radiometric sites. The spatial representedness of the ARM Central Facility will be determined with the 1995 CERES helicopter program. Measurements of vertical flux profiles with UAV data will be limited; studies of the space/time characteristics of both the observed surface and satellite TOA radiometric records will be used to estimate the sampling errors in UAV data. The widely dispersed, SW and LW BSRN radiometers will generate another database for CERES validation at about 30 locations worldwide.

The “finite” cloud effect of uncertainty in satellite-observed cloud geometric thickness has an enormous impact on assessments of the LW SARB especially. A satellite-borne CPR would be needed to provide a reliable global survey of cloud geometric thickness. The present Automated Surface Observing Sites (ASOS), which have been deployed with laser beam ceilometers (LBC) at hundreds of locations in the US, providing hourly cloud bases below 4 km, will yield a more accurate climatology of cloud base heights. When combined with satellite data in the GEWEX Continental-Phase International Project (GCIP; World Climate Research Program 1992) and enhanced surface radiometric observations, a sound test of satellite-based retrievals of the SARB and cloud base heights would be possible.

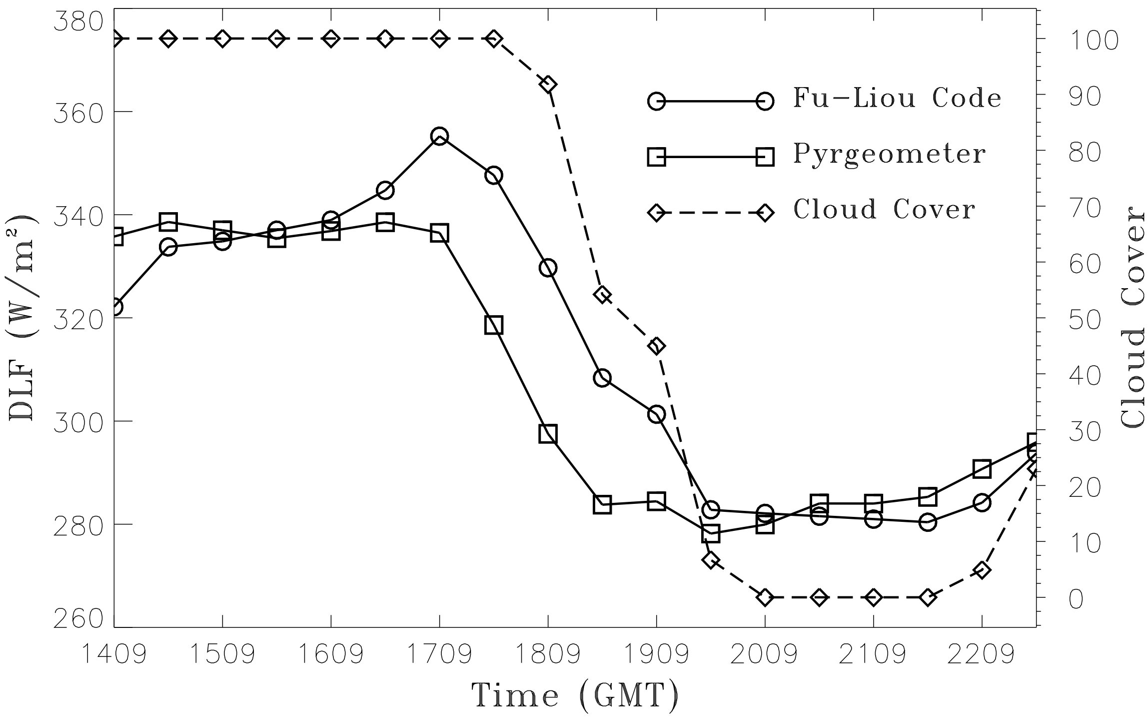

Figure 20. Time series over ARM Central Facility from 1409 UTC (0809 L) to 2239 UTC (1639 L) April 28, 1994: CERES calculations of surface DLF using interpolated NMC soundings and GOES-7 cloud retrievals (Fu-Liou code), ARM observed DLF (pyrgeometer, and GOES-7 cloud retrievals from Minnis et al. (1993) LBTM (cloud cover).

5.6. Data Processing Requirements

The computational burden of detailed radiative transfer codes has traditionally been heavy. To offset this problem codes that had been designed for GCM-type applications were chosen as they were created with efficiency in mind. All are currently being run on either SPARC-2 or SPARC-10 workstations which when dedicated to a single code can run up to 95% efficiency. Again, the various codes being used currently for the SARB calculations are the Harshvardhan et al. (1987) and Wang et al. (1991) codes for LW calculations with the Chou (1992) code for SW (HCW); and the Fu and Liou (1993) code for both LW and SW calculations (FL). Added to the radiative transfer is of course, the desire to use the meteorological data as input, and then to adjust (tune) several variables to bring the model TOA fluxes in line with the CERES measurements. Using a data set of LBTM analyzed AVHRR pixels collocated within ERBE footprints, a single orbit of data is used to develop and test software designed to match model results based on the AVHRR cloud analysis with the ERBE TOA fluxes. Currently cloud top height, cloud optical depth, and cloud area are being tuned for the total-sky footprints, surface temperature, and precipitable water for the clear-sky longwave footprints and surface albedo over land and aerosol optical depth over ocean are tuned for clear-sky shortwave footprints. The tuning of clear-sky footprints is typically very efficient, taking only one to two iterations of the tuning algorithms to match TOA ERBE fluxes. Of course each iteration is dominated by the radiative transfer calculation which will have to be made each time a tuning parameter is adjusted.

Computational burden, in seconds of computer time (sct), of both the tuning algorithms and radiative transfer codes with 30 layers is as follows on SPARC-10 computers:

Longwave	
HCW:	1000 iterations - 34sct
FL(LW):	1000 iterations - 330sct

Shortwave
Chou: 1000 iterations - 165sct
FL(SW) 1000 iterations - 395sct

Hence, at 61 footprints per second, assuming 40% clear-sky footprints (fp), the total computational burden due to SARB per day would be:

Full sky Clear sky

$$(Nsct/it) \times (10it/fp) \times (5570400fp/day) \times 0.60 + (Nsct/it) \times (2it/fp) \times (5570400fp/day) \times 0.40$$

with SW being divided by two for daytime-only calculations. For the various codes then:

Longwave
HCW: 1,287,876.5 sct/day (or at 95% efficiency ≈ 15.7 days real time per day of data)
FL(LW): 1.25e + 7 sct/day (or at 95% efficiency ≈ 152 days real time per day of data)

Shortwave
Chou: 3.13e + 6 sct/day (or at 95% efficiency ≈ 38.1 days real time per day of data)
FL(SW): 7.50e + 6 sct/day (or at 95% efficiency ≈ 91.2 days real time per day of data)

Though seemingly exorbitant, the use of an SGI parallel processor estimated to be 40 times faster than a SPARC-10 would make the HCW and Chou codes accessible to real-time processing of the SARB codes.

5.7. References

Barkstrom, B.; Harrison, E.; Smith, G.; Kibler, J.; and Green, R. 1989: Earth Radiation Budget Experiment (ERBE) Archival and April 1985 Results. *Bull. American Meteorol. Soc.*, vol. 70, pp. 1254–1262.

Briegleb, B. P.; Ramanathan, V.; Harrison, E.; and Minnis, P. 1986: Comparison of Regional Clear-Sky Albedos Inferred From Satellite Observations and Model Computations. *J. Climat. & Appl. Meteorol.*, vol. 25, pp. 214–226.

Cess, Robert D.; Jiang, Feng; Dutton, Ellsworth G.; and Deluisi, John J. 1991: Determining Surface Solar Absorption From Broadband Satellite Measurements for Clear Skies—Comparison With Surface Measurements. *J. Climat.*, vol. 4, pp. 236–247.

Chahine, M. T. 1992: The Hydrological Cycle and Its Influence on Climate. *Nature*, vol. 359, no. 6394, pp. 373–379.

Charlock, T. P.; and Ramanathan, V. 1985: The Albedo Field and Cloud Radiative Forcing Produced by a General Circulation Model With Internally Generated Cloud Optics. *J. Atmos. Sci.*, vol. 42, pp. 1408–1429.

Charlock, Thomas P.; Smith, G. L.; and Rose, Fred G. 1990: A Satellite Retrieval of the Shortwave Heating of the Atmosphere and the Surface—Relationship to the General Circulation, Interannual Climate Variability, and the Cryosphere. *Seventh Conference on Atmospheric Radiation*, American Meteorol. Soc., pp. 137–140.

Charlock, T.; Rose, F.; Yang, S.-K.; Alberta, T.; and Smith, G. 1993: An Observational Study of the Interaction of Clouds, Radiation, and the General Circulation. *Proceedings of IRS '92—Current Problems in Atmospheric Radiation*, A. Deepak Publ., pp. 151–154.

Chertock, Beth; Frouin, Robert; and Somerville, Richard C. J. 1991: Global Monitoring of Net Solar Irradiance at the Ocean Surface—Climatological Variability and the 1982–1983 El Nino. *J. Climat.*, vol. 4, pp. 639–650.

Chou, M.-D. 1984: Broadband Water Vapor Transmission Functions for Atmospheric IR Flux Computations. *J. Atmos. Sci.*, vol. 41, pp. 1775–1778.

Chou, Ming-Dah 1992: A Solar Radiation Model for Use in Climate Studies. *J. Atmos. Sci.*, vol. 49, no. 9, pp. 762–772.

Chou, M.-D.; and Peng, L. 1983: A Parameterization of the Absorption in the 15 Micron CO_2 Spectral Region With Application to Climate Sensitivity Studies. *J. Atmos. Sci.*, vol. 40, pp. 2183–2192.

Churchill, Dean D. 1992: Vertical Retrieval of Solar and Infrared Irradiances in the Stratiform Regions of EMEX Cloud Clusters. *J. Appl. Meteorol.*, vol. 31, no. 11, pp. 1229–1247.

Churchill, Dean D.; and Houze, Robert A., Jr. 1991: Effects of Radiation and Turbulence on the Diabatic Heating and Water Budget of the Stratiform Region of a Tropical Cloud Cluster. *J. Atmos. Sci.*, vol. 48, pp. 903–922.

Darnell, Wayne L.; Staylor, W. F.; Gupta, Shashi K.; Ritchey, Nancy A.; and Wilber, Anne C. 1992: Seasonal Variation of Surface Radiation Budget Derived From International Satellite Cloud Climatology Project C1 Data. *J. Geophys. Res*., vol. 97, no. D14, pp. 15741–15760.

Donner, Leo J. 1988: An Initialization for Cumulus Convection in Numerical Weather Prediction Models. *Mon. Weather Rev*., vol. 116, pp. 377–385.

Donner, L. J.; and Kuo, H.-L. 1984: Radiative Forcing of Stationary Planetary Waves. *J. Atmos. Sci.*, vol. 41, pp. 2849–2868.

Dopplick, T. G. 1972: Radiative Heating of the Global Atmosphere. *J. Atmos. Sci*., vol. 29, pp. 1278–1294.

Ellingson, R.; and Fouquart, Y. 1990: Radiation and Climate. Intercomparison of Radiation Codes in Climate Models (ICRCCM), World Climate Research Programme-39, p. 38.

Ellingson, R. G.; and Gille, J. C. 1978: An Infrared Radiative Transfer Model. I—Model Description and Comparison of Observations With Calculations. *J. Atmos. Sci.*, vol. 35, pp. 523–545.

Ellingson, R.; Wiscombe, W.; DeLuisi, J.; Kunde, V.; Melfi, H.; Murcray, D.; and Smith, W. 1993: The Spectral Radiation Experiment (SPECTRE)—Clear-Sky Observations and Their use in ICRC-CM and ITRA. *Proceedings of IRS '92—Current Problems in Atmospheric Radiation*, A. Deepak Publ., pp. 451–453.

Feigelson, E. M. 1978: Preliminary Radiation Model of a Cloudy Atmosphere. I—Structure of Clouds and Solar Radiation. *Beitraege zur Physik der Atmosphaere*, vol. 51, no. 3, pp. 203–229.

Fu, Quiang; and Liou, K. N. 1993: Parameterization of the Radiative Properties of Cirrus Clouds. *J. Atmos. Sci.*, vol. 50, no. 13, pp. 2008–2025.

Gates, W. 1992: AMIP—The Atmospheric Model Intercomparison Project. *Bull. American Meterol. Soc*., vol. 73, pp. 1962–1970.

Gautier, Catherine; and Frouin, Robert 1992: Net Surface Solar Irradiance Variability in the Central Equatorial Pacific During 1982–1985. *J. Climat.*, vol. 5, pp. 30–55.

Gupta, Shashi K. 1989: A Parameterization for Longwave Surface Radiation From Sun-Synchronous Satellite Data. *J. Climat*., vol. 2, pp. 305–320.

Gupta, Shashi K.; Darnell, Wayne L.; Wilber, Anne C. 1992: A Parameterization for Longwave Surface Radiation From Satellite Data—Recent Improvements. *J. Appl. Meteorol.*, vol. 31, no. 12, pp. 1361–1367.

Harshvardhan; Davies, Roger; Randall, David A.; and Corsetti, Thomas G. 1987: A Fast Radiation Parameterization for Atmospheric Circulation Models. *J. Geophys. Res.*, vol. 92, pp. 1009–1016.

Hartmann, D. L.; Hendon, H. H.; and Houze, R. A., Jr. 1984: Some Implications of the Mesoscale Circulations in Tropical Cloud Clusters for Large-Scale Dynamics and Climate. *J. Atmos. Sci.*, vol. 41, pp. 113–121.

Heidinger, A.; and Cox, S. 1994: Radiative Surface Forcing of Boundary Layer Clouds. *Eighth Conference on Atmospheric Radiation*, pp. 246–248.

Houghton, J. T.; Jenkins, G. J.; and Ephraums, J. J., eds. 1990: *Climate Change—The IPCC Scientific Assessment*. Cambridge Univ. Press.

Inamdar, A. K.; and Ramanathan, V. 1994: Physics of Greenhouse Effect and Convection in Warm Oceans. *J. Climat.*, vol. 7, no. 5, pp. 715–731.

Kiehl, J. T.; and Briegleb, B. P. 1992: Comparison of the Observed and Calculated Clear Sky Greenhouse Effect—Implications for Climate Studies. *J. Geophys. Res.*, vol. 97, no. D9, pp. 10,037–10,049.

Lee, H.-T.; Ellingson, R.; and Yanuk, D. 1993: Estimation of Longwave Radiation Budget Parameters With HIRS Radiances. *Proceedings of IRS '92—Current Problems in Atmospheric Radiation*, A. Deepak Publ., pp. 224–226.

Li, Z.; and Garand, L. 1993: Estimation of Surface Albedo From Space—A Parameterization for Global Application. Submitted to *J. Geophys. Res.*

Li, Zhanqing; and Leighton, H. G. 1993: Global Climatologies of Solar Radiation Budgets at the Surface and in the Atmosphere From 5 Years of ERBE Data. *J. Geophys. Res.*, vol. 98, no. D3, pp. 4919–4930.

Li, Zhanqing; Leighton, H. G.; Masuda, Kazuhiko; and Takashima, Tsutomu 1993: Estimation of SW Flux Absorbed at the Surface From TOA Reflected Flux. *J. Climat.*, vol. 6, no. 2, pp. 317–330.

Liou, Kuo-Nan. 1992: Radiation and Cloud Processes in the Atmosphere—Theory, Observation and Modeling. *Oxford Univ. Press*.

Liou, Kuo-Nan; Fu, Qiang; and Ackerman, Thomas P. 1988: A Simple Formulation of the Delta-Four-Stream Approximation for Radiative Transfer Parameterizations. *J. Atmos. Sci.*, vol. 45, pp. 1940–1947.

London, Julius 1957: *Study of the Atmospheric Heat Balance.* New York Univ. Press, p. 99.

Lorenz, E. 1955: Available Potential Energy and the Maintenance of the General Circulation. *Tellus,* vol. 7, pp. 157–167.

Manabe, S.; and Wetherald, R. 1967: Thermal Equilibrium of the Atmosphere With a Given Distribution of Relative Humidity. *J. Atmos. Sci.*, vol. 24, pp. 241–259.

Minnis, Patrick; Liou, Kuo-Nan; and Takano, Yoshihide 1993a: Inference of Cirrus Cloud Properties Using Satellite-Observed Visible and Infrared Radiances. I—Parameterization of Radiance Fields. *J. Atmos. Sci*., vol. 50, no. 9, pp. 1279–1304.

Minnis, Patrick; Heck, Patrick W.; and Young, David F. 1993b: Inference of Cirrus Cloud Properties Using Satellite-Observed Visible and Infrared Radiances. II—Verification of Theoretical Cirrus Radiative Properties. *J. Atmos. Sci*., vol. 50, no. 9, pp. 1305–1322.

Ohmura, A.; and Gilgen, H. 1993: Re-Evaluation of the Global Energy Balance. *Geophys. Monogr. 75,* IUGG Vol. 15, pp. 93–110.

Paltridge, G. W. 1974: Atmospheric Radiation and the Gross Character of Stratiform Cloud. *J. Atmos. Sci.*, vol. 31, pp. 244–250.

Pinker, R. T.; and Laszlo, I. 1992a: Modeling Surface Solar Irradiance for Satellite Applications on a Global Scale. *J. Appl. Meteorol.*, vol. 31, pp. 194–211.

Pinker, R. T.; and Laszlo, I. 1992b: Global Distribution of Photosynthetically Active Radiation as Observed From Satellites. *J. Climat.*, vol. 5, pp. 56–65.

Prata, A. J. 1993: Land Surface Temperatures Derived From the Advanced Very High Resolution Radiometer and the Along-Track Scanning Radiometer: I—Theory. J. Geophys. Res., vol. 98, pp. 16689–16702.

Ramanathan, V. 1987: Atmospheric General Circulation and Its Low Frequency Variance—Radiative Influences. *International Symposium—Collection of Papers,* Meteorol. Soc. of Japan, pp. 151–175.

Ramanathan, V. and Dickinson, R. E. 1979: The Role of Stratospheric Ozone in the Zonal and Seasonal Radiative Energy Balance of the Earth-Troposphere System. *J. Atmos. Sci*., vol. 36, pp. 1084–1104.

Ramanathan, V.; Blackmon, M. L.; Pitcher, E. J.; and Malone, R. C. 1983: The Response of a Spectral General Circulation Model to Refinements in Radiative Processes. *J. Atmos. Sci.,* vol. 40, pp. 605–630.

Ramaswamy, V.; and Freidenreich, S. M. 1992: A Study of Broadband Parameterizations of the Solar Radiative Interactions With Water Vapor and Water Drops. *J. Geophys. Res.*, vol. 97, no. D11, pp. 11,487–11,512.

Randall, David A.; Harshvardhan; Dazlich, Donald A.; and Corsetti, Thomas G. 1989: Interactions Among Radiation, Convection, and Large-Scale Dynamics in a General Circulation Model. *J. Atmos. Sci.*, vol. 46, pp. 1943–1970.

Raval, A.; and Ramanathan, V. 1989: Observational Determination of the Greenhouse Effect. *Nature*, vol. 342, pp. 758–761.

Ritter, Bodo; and Geleyn, Jean-Francois 1992: A Comprehensive Radiation Scheme for Numerical Weather Prediction Models With Potential Applications in Climate Simulations. *Mon. Weather Rev.*, vol. 120, pp. 303–325.

Rockel, B.; Raschke, E.; and Weyres, B. 1991: A Parameterization of Broad Band Radiative Transfer Properties of Water, Ice, and Mixed Clouds. *Beitraege zur Physik der Atmosphaere,* vol. 64, pp. 1–12.

Rodgers, C. 1968: Some Extension and Applications of the New Random Model for Molecular Band Transmission. *Q. J. R. Meteorol. Soc.*, vol. 94, pp. 99–102.

Rossow, William B.; Garder, Leonid C.; Lu, Pei-Jane; and Walker, Alison 1992: International Satellite Cloud Climatology Project (ISCCP): Documentation of Cloud Data. World Meteorological Organization.

Salisbury, John W.; and D'Aria, Dana M. 1992: Emissivity of Terrestrial Materials in the 8–14 Microns Atmospheric Window. *Remote Sens. Environ*., vol. 42, no. 2, pp. 83–106.

Schiffer, R. A.; and Rossow, W. B. 1985: ISCCP Global Radiance Data Set—A New Resource for Climate Research. *Bull. American Meteorol. Soc*., vol. 66, pp. 1498–1505.

Schmetz, J. 1984: On the Parameterization of the Radiative Properties of Broken Clouds. *Tellus,* vol. 36A, pp. 417–432.

Sellers, P. J.; and Hall, F. G. 1992: FIFE in 1992—Results, Scientific Gains, and Future Research Directions. *J. Geophys. Res.*, vol. 97, no. D17, pp. 19091–19109.

Slingo, A.; and Slingo, J. M. 1988: The Response of a General Circulation Model to Cloud Longwave Radiative Forcing. I—Introduction and Initial Experiments. *Q. J. R. Meteorol. Soc.,* vol. 114, pp. 1027–1062.

Slingo, J. M.; and Slingo, A. 1991: The Response of a General Circulation Model to Cloud Longwave Radiative Forcing. II—Further Studies. *Q. J. R. Meteorol. Soc.,* vol. 117, pp. 333–364.

Slingo, A.; and Webb, M. J. 1992: Simulation of Clear-Sky Outgoing Longwave Radiation Over the Oceans Using Operational Analyses. *Q. J. R. Meteorol. Soc*., vol. 118, no. 508, pp. 1117–1144.

Stackhouse, Paul W., Jr.; and Stephens, Graeme L. 1991: A Theoretical and Observational Study of the Radiative Properties of Cirrus—Results From FIRE 1986. *J. Atmos. Sci.,* vol. 48, pp. 2044–2059.

Stamnes, K.; and Conklin, P. 1984: A New Multi-Layer Discrete Ordinate Approach to Radiative Transfer in Vertically Inhomogeneous Atmospheres. *J. Quant. Spectrosc. & Radiat. Trans.,* vol. 31, pp. 273–282.

Stephens, Graeme L.; and Greenwald, Thomas J. 1991: The Earth's Radiation Budget and Its Relation to Atmospheric Hydrology. I—Observations of the Clear Sky Greenhouse Effect. *J. Geophys. Res.*, vol. 96, pp. 15311–15325.

Stephens, Graeme L.; Slingo, Anthony; Webb, Mark J.; Minnett, Peter J.; Daum, Peter H.; Kleinman, Lawrence; Wittmeyer, Ian; and Randall, David A. 1994: Observations of the Earth's Radiation Budget in Relation to Atmospheric Hydrology. IV—Atmospheric Column Radiative Cooling Over the World's Ocean. *J. Geophys. Res.*, vol. 99, no. D9, pp. 18585–18604.

Stephens, Graeme L.; and Tsay, Si-Chee 1990: On the Cloud Absorption Anomaly. *Q. J. R. Meteorol. Soc.*, vol. 116, pp. 671–704.

Stephens, G. L.; and Webster, P. J. 1984: Cloud Decoupling of the Surface and Planetary Radiative Budgets. *J. Atmos. Sci.*, vol. 41, pp. 681–686.

Stokes, G.; and Schwartz, S. 1994: The Atmospheric Radiation Measurement (ARM) Program—Programmatic Background and Design of the Cloud and Radiation Testbed. *Bull. American Meteorol. Soc.,* vol. 75, p. 1201.

Stowe, L. L.; Wellemeyer, C. G.; Yeh, H. Y. M.; Eck, T. F.; Hwang, P. H.; and Kyle, H. L. 1988: Nimbus-7 Global Cloud Climatology. I—Algorithms and Validation. *J. Climat.,* vol. 1, pp. 445–470.

Stuhlmann, R.; Raschke, E.; and Schmid, U. 1993: Cloud Generated Radiative Heating From METEOSAT Data. *Proceedings of IRS '92—Current Problems in Atmospheric Radiation,* A. Deepak Publ., pp. 69–75.

Stuhlmann, R.; and Smith, G. L. 1988a: A Study of Cloud-Generated Radiative Heating and Its Generation of Available Potential Energy. I—Theoretical Background. *J. Atmos. Sci*., vol. 45, pp. 3911–3927.

Stuhlmann, R.; and Smith, G. L. 1988b: A Study of Cloud-Generated Radiative Heating and Its Generation of Available Potential Energy. II—Results for a Climatological Zonal Mean January. *J. Atmos. Sci*., vol. 45, pp. 3928–3943.

Takano, Y.; and Liou, K.-N. 1994: Light Scattering by Irregularly Shaped Ice Crystals—Climatic Implications. *Eighth Conference on Atmospheric Radiation*, pp. 440–442.

Tao, W.-K.; Simpson, J.; Sui, C.-H.; Ferrier, B.; Lang, S.; Scala, J.; Chou, M.-D.; and Pickering, K. 1993: Heating, Moisture, and Water Budgets of Tropical and Midlatitude Squall Lines—Comparisons and Sensitivity to Longwave Radiation. *J. Atmos. Sci.,* vol. 50, no. 5, pp. 673–690.

Ting, Mingfang; and Sardeshmukh, Prashant D. 1993: Factors Determining the Extratropical Response to Equatorial Diabatic Heating Anomalies. *J. Atmos. Sci.,* vol. 50, no. 6, pp. 907–918.

Wan, Zhengming; and Dozier, Jeff 1989: Land-Surface Temperature Measurement From Space—Physical Principles and Inverse Modeling. *IEEE Trans. Geosci. & Remote Sens.*, vol. 27, pp. 268–278.

Wang, Wei-Chyung; and Shi, Guang-Yu 1988: Total Band Absorptance and K-Distribution Function for Atmospheric Gases. *J. Quant. Spectrosc. & Radiat. Transf.*, vol. 39, pp. 387–397.

Wang, Wei-Chyung; Shi, Guang-Yu; and Kiehl, Jeffrey T. 1991: Incorporation of the Thermal Radiative Effect of CH_4, N_20, CH_2Cl_2, and $CFCl_3$ into the National Center for Atmospheric Research Community Climate Model. *J. Geophys. Res.*, vol. 96, pp. 9097–9103.

Wielicki, Bruce A.; and Green, Richard N. 1989: Cloud Identification for ERBE Radiative Flux Retrieval. *J. Appl. Meteorol.*, vol. 28, pp. 1133–1146.

Wielicki, Bruce A.; and Parker, Lindsay 1992: On the Determination of Cloud Cover From Satellite Sensors—The Effect of Sensor Spatial Resolution. *J. Geophys. Res.*, vol. 97, no. D12, pp. 12799–12823.

Whitlock, C.; Charlock, T.; Staylor, W.; Pinker, R.; Laszlo, I.; Ohmura, A.; Gilgen, H.; DiPasquale, R.; LeCroy, S. R.; and Ritchey, N. 1994: First Global WCRP Surface Radiation Budget Data Set. *Submitted to BAMS.*

World Climate Research Program (WCRP) 1992: Scientific Plan for the GEWEX Continental Scale International Project (GCIP). WCRP-67 WMO/TD-No. 461.

Wu, Man L. C.; and Chang, Lang-Ping 1992: Longwave Radiation Budget Parameters Computed From ISCCP and HIRS2/ MSU Products. *J. Geophys. Res.*, vol. 97, no. D9, pp. 10083–10101.

Appendix A

Input Data Products

Compute Surface and Atmospheric Radiative Fluxes (Subsystem 5.0)

This appendix describes the data products produced by the algorithms in this subsystem. Table A-1 below summarizes these products, listing the CERES and EOSDIS product codes or abbreviations, a short product name, the product type, the production frequency, and volume estimates for each individual product as well as a complete data month of production. The product types are defined as follows:

Archival products:	Assumed to be permanently stored by EOSDIS
Internal products:	Temporary storage by EOSDIS (days to years)
Ancillary products:	Non-CERES data needed to interpret measurements

The following pages describe each product. An introductory page provides an overall description of the product and specifies the temporal and spatial coverage. The table which follows the introductory page briefly describes every parameter which is contained in the product. Each product may be thought of as metadata followed by data records. The metadata (or header data) is not well-defined yet and is included mainly as a placeholder. The description of parameters which are present in each data record includes parameter number (a unique number for each distinct parameter), units, dynamic range, the number of elements per record, an estimate of the number of bits required to represent each parameter, and an element number (a unique number for each instance of every parameter). A summary at the bottom of each table shows the current estimated sizes of metadata, each data record, and the total data product. A more detailed description of each data product will be contained in a user's guide to be published before the first CERES launch.

Table A-1. Output Products Summary

Product code						Monthly
CERES	EOSDIS	Name	Type	Frequency	Size,MB	size, MB
SSF	CER11	Single satellite footprint, and surface flux, clouds	archival	1/hour	154.0	114576

Single Satellite Footprint, TOA and Sfc Flux, Clouds (SSF)

The single satellite flux and cloud swaths (SSF) is produced from the cloud identification, inversion, and surface processing for CERES. Each SSF covers a single hour swath from a single CERES instrument mounted on one satellite. The product has a product header and multiple records of approximately 125 parameters or 315 elements for each pixel.

The major categories of data output on the SSF are

- CERES footprint geometry and CERES viewing angles
- CERES footprint radiance and flux (TOA and Surface)
- CERES footprint cloud statistics and imager viewing angles
- CERES footprint clear area statistics
- CERES footprint cloudy area statistics for each of four cloud height categories
    - Visible optical depth (mean and standard deviation)
    - Infrared emissivity (mean and standard deviation)
    - Liquid water path (mean and standard deviation)
    - Ice water path (mean and standard deviation)
    - Cloud top pressure (mean and standard deviation)
    - Cloud effective pressure (mean and standard deviation)
    - Cloud effective temperature (mean and standard deviation)

Cloud effective height (mean and standard deviation)
Cloud bottom pressure (mean and standard deviation)
Water particle radius (mean and standard deviation)
Ice particle radius (mean and standard deviation)
Particle phase (mean and standard deviation)
Vertical aspect ratio (mean and standard deviation)
Visible optical depth/IR emissivity (13 percentiles)

CERES footprint cloud overlap conditions (11 conditions)

The SSF is an archival product that will be run daily in validation mode starting with the TRMM launch until sufficient data have been collected and analyzed to produce a production quality set of CERES angular distribution models (ADM). It is estimated that at TRMM launch plus 18 months, the SSF product will be produced on a routine basis and will be archived within EOSDIS for distribution. The inversion process will be rerun starting from the TRMM launch and a new SSF produced, in which case, only the TOA fluxes and surface parameters will be replaced in the inversion rerun process. If the cloud algorithms are rerun, the SSF product itself will be input into the cloud identification process in order to retrieve the CERES radiance and location data input data needed.

Level: 2
Type: Archival
Frequency: 1/hour

Time Interval Covered
File: 1 hour
Record: 1/100 second

Portion of Globe Covered
File: Satellite swath
Record: One footprint

Portion of Atmosphere Covered
File: Surface to TOA

Table A-2. Single Satellite Footprint, TOA and Sfc Flux, Clouds (SSF)

Description	Parameter Number	Units	Range	Elements/ Record	Bits/ Elem	Elem Num
SSF						
SSF_Header						
Julian Day at Hour Start		day	2449353..2458500	1	32	
Julian Time at Hour Start		day	0..1	1	32	
Character name of satellite		N/A		1	16	
Number of orbits		N/A	TBD	1	16	
Name of high resolution imager instrument		N/A	N/A	1	16	
Number of footprints in IES product		count	1..245475	1	32	
Number of imager channels used		N/A	1 .. 11	1	16	
WavLen_Array is Array[11] of:						
Central wavelengths of imager channels		µm	0.4 .. 15.0	11	16	
SSF_Record is Array[245475] of:						
SSF_Footprints						
Footprint_Geometry						
Time_and_Position						
Time of observation	1	day	0..1	1	32	1
Earth-Sun distance	2	AU	0.98 .. 1.02	1	16	2
Radius of satellite from center of Earth at observation	3	km	6000..8000	1	32	3
Colatitude of satellite at observation	4	deg	0..180	1	16	4
Longitude of satellite at observation	5	deg	0..360	1	16	5
Colatitude of Sun at observation	6	deg	0..180	1	16	6
Longitude of Sun at observation	7	deg	0..360	1	16	7
Colatitude of CERES FOV at TOA	8	deg	0..180	1	16	8
Longitude of CERES FOV at TOA	9	deg	0..360	1	16	9
Colatitude of CERES FOV at surface	10	deg	0..180	1	16	10
Longitude of CERES FOV at surface	11	deg	0..360	1	16	11
Scan sample number	12	N/A	1..660	1	16	12
Cone angle of CERES FOV at satellite	13	deg	0..180	1	16	13
Clock angle of CERES FOV at satellite wrt inertial velocity	14	deg	0..180	1	16	14
Rate of change of cone angle	15	deg sec^{-1}	-100..100	1	16	15
Rate of change of clock angle	16	deg sec^{-1}	-10..10	1	16	16
Along-track angle of CERES FOV at TOA	17	deg	0..360	1	16	17
Cross-track angle of CERES FOV at TOA	18	deg	-90..90	1	16	18
X component of satellite inertial velocity	19	km sec^{-1}	-10..10	1	16	19
Y component of satellite inertial velocity	20	km sec^{-1}	-10..10	1	16	20
Z component of satellite inertial velocity	21	km sec^{-1}	-10..10	1	16	21
CERES_Viewing_Angles						
CERES viewing zenith at TOA	22	deg	0..90	1	16	22
CERES solar zenith at TOA	23	deg	0..180	1	16	23
CERES relative azimuth at TOA	24	deg	0..360	1	16	24
CERES viewing azimuth at TOA wrt North	25	deg	0..360	1	16	25
Surface_Map_Parameters						
Mean altitude of surface above sea level	26	km	-12 .. 10	1	16	26
LandTyps is Array[10] of:						
Area fraction of land types in percent	27	N/A	0 .. 100	10	16	27
SeaTyps is Array[3] of:						
Area fraction of sea types in percent	28	N/A	0 .. 100	3	16	37
Scene_Type						
CERES clear sky or full sky indicator	29	N/A	N/A	1	16	40
CERES scene type for Inversion process	30	N/A	0 .. 200	1	16	41
Footprint_Radiation						
CERES_Filtered_Radiances						
CERES total filtered radiance, upwards	31	$W\text{-}m^{-2}\ sr^{-1}$	0..700	1	16	42
CERES shortwave filtered radiance, upwards	32	$W\text{-}m^{-2}\ sr^{-1}$	-10..510	1	16	43

Table A-2. Continued

Description	Parameter Number	Units	Range	Elements/ Record	Bits/ Elem	Elem Num
CERES window filtered radiance, upwards	33	W-m^{-2} sr^{-1}	0..50	1	16	44
Quality flag for total radiance value	34	N/A	N/A	1	16	45
Quality flag for SW radiance value	35	N/A	N/A	1	16	46
Quality flag for window radiance value	36	N/A	N/A	1	16	47
CERES_Unfiltered_Radiances						
CERES shortwave radiance, upwards	37	W-m^{-2}sr^{-1}	-10..510	1	16	48
CERES longwave radiance, upwards	38	W-m^{-2}sr^{-1}	0..200	1	16	49
CERES window radiance, upwards	39	W-m^{-2}sr^{-1}	0..50	1	16	50
TOA_and_Surface_Flux						
CERES shortwave flux at TOA, upwards	40	W-m^{-2}	0..1400	1	16	51
CERES longwave flux at TOA, upwards	41	W-m^{-2}	0..500	1	16	52
CERES window flux at TOA, upwards	42	W-m^{-2}	10..400	1	16	53
CERES shortwave flux at surface, downwards	43	W-m^{-2}	0..1400	1	16	54
CERES longwave flux at surface, downwards	44	W-m^{-2}	0..500	1	16	55
CERES net shortwave flux at surface	45	W-m^{-2}	0..1400	1	16	56
CERES net longwave flux at surface	46	W-m^{-2}	0..500	1	16	57
CERES surface emissivity	47	N/A	0..1	1	16	58
Photosynthetically active radiation at surface	48	W-m^{-2}	0..780	1	16	59
Direct/Diffuse ratio at the surface	49	TBD	0..30	1	16	60
Full_Footprint_Area						
Mean imager viewing zenith over CERES FOV	50	deg	0 .. 90	1	16	61
Mean imager relative aziumth angle over CERES FOV	51	deg	0 .. 360	1	16	62
Number of cloud height categories	52	N/A	-1 .. 4	1	16	63
Number of imager pixels in CERES FOV	53	N/A	0 .. 9000	1	16	64
BDRF_Image is Array[11] of:						
Bidirectional reflectance or brightness temperature	54	TBD	TBD	11	16	65
Precipitable water	55	cm	0.001 .. 8	1	16	76
5th percentile of 0.6 µm imager radiances over CERES FOV	56	W-m^{-2}sr^{-1}µm^{-1}	TBD	1	16	77
Mean of 0.6 µm imager radiances over CERES FOV	57	W-m^{-2}sr^{-1}µm^{-1}	TBD	1	16	78
95th percentile of 0.6 µm imager radiances over CERES FOV	58	W-m^{-2}sr^{-1}µm^{-1}	TBD	1	16	79
5th percentile of 3.7 µm imager radiances over CERES FOV	59	W-m^{-2}sr^{-1}µm^{-1}	TBD	1	16	80
Mean of the 3.7 µm imager radiances over CERES FOV	60	W-m^{-2}sr^{-1}µm^{-1}	TBD	1	16	81
95th percentile of 3.7 µm imager radiances over CERES FOV	61	W-m^{-2}sr^{-1}µm^{-1}	TBD	1	16	82
5th percentile of 11 µm imager radiances over CERES FOV	62	W-m^{-2}sr^{-1}µm^{-1}	TBD	1	16	83
Mean of the 11 µm imager radiances over CERES FOV	63	W-m^{-2}sr^{-1}µm^{-1}	TBD	1	16	84
95th percentile of 11 µm imager radiances over CERES FOV	64	W-m^{-2}sr^{-1}µm^{-1}	TBD	1	16	85
Notes on general procedures	65	N/A	TBD	1	16	86
Texture algorithm flag	66	N/A	TBD	1	16	87
Multi-level cloud algorithm flag	67	N/A	TBD	1	16	88
Spatial coherence algorithm flag	68	N/A	TBD	1	16	89
Infrared sounder algorithm flag	69	N/A	TBD	1	16	90
Threshhold algorithm flag	70	N/A	TBD	1	16	91
Visible optical depth algorithm flag	71	N/A	TBD	1	16	92
Infrared emissivity algorithm flag	72	N/A	TBD	1	16	93
Cloud particle size algorithm flag	73	N/A	TBD	1	16	94
Cloud water path algorithm flag	74	N/A	TBD	1	16	95
Clear_Footprint_Area						
Mean of 0.6 µm imager radiances over clear area	75	W-m^{-2}sr^{-1}µm^{-1}	TBD	1	16	96
Stddev of the 0.6 µm imager radiances over clear area	76	W-m^{-2}sr^{-1}µm^{-1}	TBD	1	16	97
Mean of the 3.7 µm imager radiances over clear area	77	W-m^{-2}sr^{-1}µm^{-1}	TBD	1	16	98
Stddev of 3.7 µm imager radiances over clear area	78	W-m^{-2}sr^{-1}µm^{-1}	TBD	1	16	99
Mean of the 11 µm imager radiances over clear area	79	W-m^{-2}sr^{-1}µm^{-1}	TBD	1	16	100
Stddev of the 11 µm imager radiances over clear area	80	W-m^{-2}sr^{-1}µm^{-1}	TBD	1	16	101
Stratospheric aerosol visible optical depth in clear area	81	N/A	0 .. 0.5	1	16	102

Table A-2. Concluded

Description	Parameter Number	Units	Range	Elements/ Record	Bits/ Elem	Elem Num
Stratospheric aerosol effective radius in clear area	82	μm	0 .. 10	1	16	103
Total aerosol visible optical depth in clear area	83	N/A	0 .. 2	1	16	104
Total aerosol effective radius in clear area	84	μm	0 .. 20	1	16	105
Cloudy_Footprint_Area is Array[4] of:						
Cloud_Cat_Arrays						
Number of imager pixels for cloud category	85	N/A	0 .. 9000	4	16	106
Number of overcast pixels for cloud category	86	N/A	0 .. 9000	4	16	110
Cloud category weighted area fraction	87	N/A	0 .. 1	4	16	114
Cloud category weighted overcast fraction	88	N/A	0 .. 1	4	16	118
Cloud category weighted broken fraction	89	N/A	0 .. 1	4	16	122
Mean of 0.6μm imager radiances for cloud category	90	$W\text{-}m^{-2}sr^{-1}\mu m^{-1}$	TBD	4	16	126
Stddev of 0.6μm imager radiance for cloud category	91	$W\text{-}m^{-2}sr^{-1}\mu m^{-1}$	TBD	4	16	130
Mean of 3.7μm imager radiances for cloud category	92	$W\text{-}m^{-2}sr^{-1}\mu m^{-1}$	TBD	4	16	134
Stddev of 3.7μm imager radiances for cloud category	93	$W\text{-}m^{-2}sr^{-1}\mu m^{-1}$	TBD	4	16	138
Mean of 11μm imager radiances for cloud category	94	$W\text{-}m^{-2}sr^{-1}\mu m^{-1}$	TBD	4	16	142
Stddev of 11μm imager radiances for cloud category	95	$W\text{-}m^{-2}sr^{-1}\mu m^{-1}$	TBD	4	16	146
Mean cloud visible optical depth for cloud category	96	N/A	0 .. 400	4	16	150
Stddev of visible optical depth for cloud category	97	N/A	TBD	4	16	154
Mean cloud infrared emissivity for cloud category	98	N/A	0 .. 1	4	16	158
Stddev of cloud infrared emissivity for cloud category	99	N/A	TBD	4	16	162
Mean liquid water path for cloud category	100	kg m^{-2}	TBD	4	16	166
Stddev of liquid water path for cloud category	101	kg m^{-2}	TBD	4	16	170
Mean ice water path for cloud category	102	kg m^{-2}	TBD	4	16	174
Stdev of ice water path for cloud category	103	kg m^{-2}	TBD	4	16	178
Mean cloud top pressure for cloud category	104	hPa	0 .. 1100	4	16	182
Stddev of cloud top pressure for cloud category	105	hPa	TBD	4	16	186
Mean cloud effective pressure for cloud category	106	hPa	0 .. 1100	4	16	190
Stddev of cloud effective pressure for cloud category	107	hPa	TBD	4	16	194
Mean cloud effective temperature for cloud category	108	K	100 .. 350	4	16	198
Stddev of cloud effective temperature for cloud category	109	K	TBD	4	16	202
Mean cloud effective height for cloud category	110	km	0 .. 20	4	16	206
Stddev of cloud effective height for cloud category	111	km	TBD	4	16	210
Mean cloud bottom pressure for cloud category	112	hPa	0 .. 1100	4	16	214
Stddev of cloud bottom pressure for cloud category	113	hPa	TBD	4	16	218
Mean water particle radius for cloud category	114	TBD	TBD	4	16	222
Stddev of water particle radius for cloud category	115	TBD	TBD	4	16	226
Mean ice particle radius for cloud category	116	TBD	TBD	4	16	230
Stddev of ice particle radius for cloud category	117	TBD	TBD	4	16	234
Mean cloud particle phase for cloud category	118	N/A	0 .. 1	4	16	238
Stddev of cloud particle phase for cloud category	119	N/A	0 .. 1	4	16	242
Mean vertical aspect ratio for cloud category	120	N/A	0 .. 1	4	16	246
Stddev of vertical aspect ratio for cloud category	121	N/A	TBD	4	16	250
Optical_Depth_Percentile is Array[13] of:						
Percentiles of visible optical depth/IR emissivity for cloud category	122	N/A	TBD	52	16	254
Overlap_Footprint_Area is Array[11] of:						
Overlap_Conditions						
Number of imager pixels for overlap condition	123	N/A	0 .. 9000	11	16	306
Overlap condition weighted area fraction	124	N/A	0 .. 1	11	16	317

Total Meta Bits/File:	336
Total Data Bits/Record:	5264
Total Records/File:	245475
Total Data Bits/File:	1292180400
Total Bits/File :	1292180736

Appendix B

Output Data Products

Compute Surface and Atmospheric Radiative Fluxes (Subsystem 5.0)

This appendix describes the data products which are produced by the algorithms in this subsystem. Table B-1 below summarizes these products, listing the CERES and EOSDIS product codes or abbreviations, a short product name, the product type, the production frequency, and volume estimates for each individual product as well as a complete data month of production. The product types are defined as follows:

Archival products: Assumed to be permanently stored by EOSDIS
Internal products: Temporary storage by EOSDIS (days to years)

The following pages describe each product. An introductory page provides an overall description of the product and specifies the temporal and spatial coverage. The table which follows the introductory page briefly describes every parameter which is contained in the product. Each product may be thought of as metadata followed by data records. The metadata (or header data) is not well-defined yet and is included mainly as a placeholder. The description of parameters which are present in each data record includes parameter number (a unique number for each distinct parameter), units, dynamic range, the number of elements per record, an estimate of the number of bits required to represent each parameter, and an element number (a unique number for each instance of every parameter). A summary at the bottom of each table shows the current estimated sizes for metadata, each data record, and the total data product. A more detailed description of each data product will be contained in a user's guide to be published before the first CERES launch.

Table B-1. Output Products Summary

Product code		Name	Type	Frequency	Size,MB	Monthly size, MB
CERES	EOSDIS					
CRS	CER04	Single satellite CERES footprint, radiative fluxes and clouds	archival	1/hour	220.5	164052

Single Satellite CERES Footprint, Radiative Fluxes and Clouds (CRS)

The CERES archival product, cloud radiative swath (CRS), is produced by the CERES compute surface and Atmospheric Radiative Fluxes Subsystem. Each CRS file contains longwave and shortwave radiative fluxes for the surface, internal atmosphere and TOA for each CERES footprint. The CRS contains data for 1 hour, or one satellite swath (8–12 percent of the Earth), from one satellite. In addition to being an archival product, the CRS is used by the CERES subsystem, Grid Single Satellite Radiative Fluxes and Clouds.

For each CERES footprint, the CRS contains

- Time and location data
- CERES observed TOA data
- Full footprint data
- Full footprint algorithm flags
- Footprint clear-sky properties
- Cloud category properties for up to four (low, lower middle, upper middle and high) cloud layers

- Overlap data for eleven (clear, low (L), lower middle (LM), upper middle (UM), high (H), H/UM, H/LM, H/L, UM/LM, UM/L, LM/L) cloud overlap conditions
- Atmospheric flux profile for both clear-sky and total-sky at the surface, 500 hPa, the tropopause and the TOA
- Flux adjustments (tuned-untuned) for clear-sky and total-sky at the surface and TOA
- Surface-only data
- Adjustment parameters for clear-sky (note that these are for both clear-sky and total-sky footprints)
- Adjustment parameters for L, LM, UM, and H cloud layers

Level: 2
Type: Archival
Frequency: 1/ hour

Portion of Globe Covered
File: Satellite swath
Record: 1 CERES footprint

Time Interval Covered
File: 1 hour
Record: Instantaneous

Portion of Atmosphere Covered
File: Surface, internal and TOA

Table B-2. Single Satellite CERES Footprint, Radiative Fluxes and Clouds (CRS)

Description	Parameter Number	Units	Range	Elements/ Record	Bits/ Elem	Elem Num
Meta Data						
CRS File Header		N/A		1	320	
Time and Location Data						
Julian day	1	day	2449353..2458500	1	32	1
Julian time	2	day	0..1	1	32	2
Earth-Sun distance	3	AU	0.98..1.02	1	32	3
Sun colatitude	4	deg	0..180	1	32	4
Sun longitude	5	deg	0..360	1	32	5
Pixel colatitude, TOA	6	deg	0..180	1	32	6
Pixel longitude, TOA	7	deg	0..360	1	32	7
Pixel colatitude, surface	8	deg	0..180	1	32	8
Pixel longitude, surface	9	deg	0..360	1	32	9
Spacecraft colatitude, nadir	10	deg	0..180	1	32	10
Spacecraft longitude, nadir	11	deg	0..360	1	32	11
Spacecraft inertial velocity vector (X, Y, Z)	12	km sec^{-1}	-10..10	3	32	12
Satellite radius	13	km	6500..8000	1	16	15
Along-track angle	14	deg	0..360	1	16	16
Cross-track angle	15	deg	-90..90	1	16	17
Cone angle	16	deg	0..90	1	16	18
Clock angle	17	deg	0..360	1	16	19
Cone rate	18	deg sec^{-1}	-100..100	1	16	20
Clock rate	19	deg sec^{-1}	-8..8	1	16	21
Scan sample number	20	N/A	1..660	1	16	22
Surface altitude	21	km	-12..10	1	16	23
Surface land area	22	percent	0..100	10	16	24
Surface sea area	23	percent	0..100	3	16	34
Flag, clear-sky or total-sky	24	N/A	0..1	1	16	37
Scene type	25	N/A	0..200	1	16	38
Satellite viewing zenith angle, TOA	26	deg	0..90	1	16	39
Solar zenith angle, TOA	27	deg	0..180	1	16	40
Relative azimuth angle, TOA	28	deg	0..180	1	16	41
Satellite viewing azimuth at TOA wrt North	29	deg	0..360	1	16	42
CERES Observed TOA Data						
CERES TOT radiance, TOA, filtered	30	$W\text{-}m^{-2}sr^{-1}$	0..700	1	16	43
CERES SW radiance, TOA, filtered	31	$W\text{-}m^{-2}sr^{-1}$	-10..510	1	16	44
CERES LW WN radiance, TOA, filtered	32	$W\text{-}m^{-2}sr^{-1}$	0..50	1	16	45
CERES TOT radiance, TOA, unfiltered	33	$W\text{-}m^{-2}sr^{-1}$	0..700	1	16	46
CERES SW radiance, TOA, unfiltered	34	$W\text{-}m^{-2}sr^{-1}$	-10..510	1	16	47
CERES LW WN radiance, TOA, unfiltered	35	$W\text{-}m^{-2}sr^{-1}$	0..50	1	16	48
Flag, TOT radiance quality	36	N/A	TBD	1	16	49
Flag, SW radiance quality	37	N/A	TBD	1	16	50
Flag, LW WN radiance quality	38	N/A	TBD	1	16	51
CERES SW flux, TOA	39	$W\text{-}m^{-2}$	0..1400	1	16	52
CERES LW flux, TOA	40	$W\text{-}m^{-2}$	0..500	1	16	53
CERES LW WN flux, TOA	41	$W\text{-}m^{-2}$	10..400	1	16	54
Full Footprint Data						
Imager identification code	42	N/A	TBD	1	16	55
Number of imager pixels	43	N/A	0..9000	1	16	56
Number cloud height catagories	44	N/A	-1..4	1	16	57
Imager radiance, 0.6µm channel, 5th percentile	45	$W\text{-}m^{-2}sr^{-1}\mu m^{-1}$	TBD	1	16	58
Imager radiance, 0.6µm channel, mean	46	$W\text{-}m^{-2}sr^{-1}\mu m^{-1}$	TBD	1	16	59
Imager radiance, 0.6µm channel, 95th percentile	47	$W\text{-}m^{-2}sr^{-1}\mu m^{-1}$	TBD	1	16	60
Imager radiance, 3.7µm channel, 5th percentile	48	$W\text{-}m^{-2}sr^{-1}\mu m^{-1}$	TBD	1	16	61
Imager radiance, 3.7µm channel, mean	49	$W\text{-}m^{-2}sr^{-1}\mu m^{-1}$	TBD	1	16	62
Imager radiance, 3.7µm channel, 95th percentile	50	$W\text{-}m^{-2}sr^{-1}\mu m^{-1}$	TBD	1	16	63
Imager radiance, 11.0µm channel, 5th percentile	51	$W\text{-}m^{-2}sr^{-1}\mu m^{-1}$	TBD	1	16	64
Imager radiance, 11.0µm channel, mean	52	$W\text{-}m^{-2}sr^{-1}\mu m^{-1}$	TBD	1	16	65
Imager radiance, 11.0µm channel, 95th percentile	53	$W\text{-}m^{-2}sr^{-1}\mu m^{-1}$	TBD	1	16	66
Bidirectional reflectance	54	TBD	TBD	11	16	67
Imager mean viewing zenith angle, TOA	55	deg	0..90	1	16	78
Imager mean relative azimuth angle, TOA	56	deg	0..360	1	16	79
Precipitable water	57	cm	0.001..8.000	1	16	80

Table B-2. Continued

Description	Parameter Number	Units	Range	Elements/ Record	Bits/ Elem	Elem Num
Full Footprint Algorithm Flags						
Notes on general procedures	58	N/A	TBD	1	16	81
Texture algorithm flag	59	N/A	TBD	1	16	82
Multi-layer cloud algorithm flag	60	N/A	TBD	1	16	83
Spatial coherence algorithm flag	61	N/A	TBD	1	16	84
IR sounder algorithm flag	62	N/A	TBD	1	16	85
Threshhold algorithm flag	63	N/A	TBD	1	16	86
Visible optical depth algorithm flag	64	N/A	TBD	1	16	87
IR emissivity algorithm flag	65	N/A	TBD	1	16	88
Cloud particle size algorithm flag	66	N/A	TBD	1	16	89
Cloud water path algorithm flag	67	N/A	TBD	1	16	90
Footprint Clear Sky Properties						
Imager radiance, 0.6µm channel, mean	68	$W\text{-}m^{-2}sr^{-1}\mu m^{-1}$	TBD	1	16	91
Imager radiance, 0.6µm channel, std	69	$W\text{-}m^{-2}sr^{-1}\mu m^{-1}$	TBD	1	16	92
Imager radiance, 3.7µm channel, mean	70	$W\text{-}m^{-2}sr^{-1}\mu m^{-1}$	TBD	1	16	93
Imager radiance, 3.7µm channel, std	71	$W\text{-}m^{-2}sr^{-1}\mu m^{-1}$	TBD	1	16	94
Imager radiance, 11.0µm channel, mean	72	$W\text{-}m^{-2}sr^{-1}\mu m^{-1}$	TBD	1	16	95
Imager radiance, 11.0µm channel, std	73	$W\text{-}m^{-2}sr^{-1}\mu m^{-1}$	TBD	1	16	96
Stratospheric aerosol, optical depth	74	N/A	0.0..0.5	1	16	97
Stratospheric aerosol effective radius	75	µm	0..10	1	16	98
Total aerosol, optical depth	76	N/A	0.0..2.0	1	16	99
Total aerosol effective radius	77	µm	0..20	1	16	100
Cloud Properties for 4 Cloud Layers						
(Cloud layers are low, lower middle, upper middle and high)						
Number imager pixels	78	N/A	0..9000	4	16	101
Cloud layer index	79	N/A	1..11	4	16	105
Overcast cloud area fraction	80	N/A	0..1	4	16	109
Total cloud area fraction	81	N/A	0..1	4	16	113
Broken cloud area fraction	82	N/A	0..1	4	16	117
Imager radiance, 0.6µm channel, mean	83	$W\text{-}m^{-2}sr^{-1}\mu m^{-1}$	TBD	4	16	121
Imager radiance, 0.6µm channel, std	84	$W\text{-}m^{-2}sr^{-1}\mu m^{-1}$	TBD	4	16	125
Imager radiance, 3.7µm channel, mean	85	$W\text{-}m^{-2}sr^{-1}\mu m^{-1}$	TBD	4	16	129
Imager radiance, 3.7µm channel, std	86	$W\text{-}m^{-2}sr^{-1}\mu m^{-1}$	TBD	4	16	133
Imager radiance, 11.0µm channel, mean	87	$W\text{-}m^{-2}sr^{-1}\mu m^{-1}$	TBD	4	16	137
Imager radiance, 11.0µm channel, std	88	$W\text{-}m^{-2}sr^{-1}\mu m^{-1}$	TBD	4	16	141
Visible optical depth, mean	89	N/A	0..400	4	16	145
Visible optical depth, std	90	N/A	TBD	4	16	149
IR emissivity, mean	91	N/A	0..1	4	16	153
IR emissivity, std	92	N/A	0..1	4	16	157
Cloud liquid water path, mean	93	$g\ m^{-2}$	0.001..10.000	4	16	161
Cloud liquid water path, std	94	$g\ m^{-2}$	TBD	4	16	165
Cloud ice water path, mean	95	$g\ m^{-2}$	0.001..10.000	4	16	169
Cloud ice water path, std	96	$g\ m^{-2}$	TBD	4	16	173
Cloud top pressure, mean	97	hPa	0..1100	4	16	177
Cloud top pressure, std	98	hPa	TBD	4	16	181
Cloud effective pressure, mean	99	hPa	0..1100	4	16	185
Cloud effective pressure, std	100	hPa	TBD	4	16	189
Cloud effective temperature, mean	101	K	100..350	4	16	193
Cloud effective temperature, std	102	K	TBD	4	16	197
Cloud effective height, mean	103	km	0..20	4	16	201
Cloud effective height, std	104	km	TBD	4	16	205
Cloud bottom pressure, mean	105	hPa	0..1100	4	16	209
Cloud bottom pressure, std	106	hPa	TBD	4	16	213
Cloud water particle radius, mean	107	µm	0..200	4	16	217
Cloud water particle radius, std	108	µm	TBD	4	16	221
Cloud ice particle radius, mean	109	µm	0..200	4	16	225
Cloud ice particle radius, std	110	µm	TBD	4	16	229
Cloud particle phase, mean	111	N/A	0..1	4	16	233
Cloud aspect ratio, mean	112	N/A	0..1	4	16	237
Cloud aspect ratio, std	113	N/A	0..1	4	16	241
Visible optical depth/IR emissivity, 13 percentiles	114	N/A	0..400	52	16	245

Table B-2. Concluded

Description	Parameter Number	Units	Range	Elements/ Record	Bits/ Elem	Elem Num
Overlap Footprint Data for 11 Cloud Overlap Conditions						
(Overlap conditions are clear, low (L), lower middle (LM), upper middle (UM), high (H), H/UM, H/LM, H/L, UM/LM, UM/L, and LM/L)						
Number overlap pixels	115	N/A	0..9000	11	16	297
Total cloud area fraction	116	N/A	0..1	11	16	308
Atmospheric Flux Profile for Clear-sky and Total-sky						
(Atmospheric layers in profile are surface, 500 hPa, tropopause and TOA)						
Number atmospheric layers	117	N/A	0..4	1	16	319
Layer pressures	118	hPa	0..1100	4	16	320
SW upwards, atmospheric layer, tuned	119	$W\text{-}m^{-2}$	0..1400	8	16	324
SW downwards, atmospheric layer, tuned	120	$W\text{-}m^{-2}$	0..1400	8	16	332
LW upwards, atmospheric layer, tuned	121	$W\text{-}m^{-2}$	0..500	8	16	340
LW downwards, atmospheric layer, tuned	122	$W\text{-}m^{-2}$	0..500	8	16	348
Flux Adjustments (Tuned - Untuned) for Clear-sky and Total-sky at Surface and TOA						
SW upwards, atmospheric layer, delta	123	$W\text{-}m^{-2}$	0..1400	4	16	356
SW downwards, atmospheric layer, delta	124	$W\text{-}m^{-2}$	0..1400	4	16	360
LW upwards, atmospheric layer, delta	125	$W\text{-}m^{-2}$	0..500	4	16	364
LW downwards, atmospheric layer, delta	126	$W\text{-}m^{-2}$	0..500	4	16	368
Surface-only Data						
Photosynthetically active radiation	127	$W\text{-}m^{-2}$	0..780	1	16	372
Direct/diffuse ratio	128	N/A	0..30	1	16	373
Adjustment Parameters for Clear Skies						
Adjusted precipitable water, delta	129	cm	0.001..8.000	1	16	374
Adjusted surface albedo, delta	130	N/A	0..1	1	16	375
Adjusted aerosol optical depth, delta	131	N/A	0.0..2.0	1	16	376
Adjusted skin temperature, delta	132	K	TBD	1	16	377
Adjustment Parameters for L, LM, UM and H Cloud Layers						
Adjusted mean visible optical depth, delta	133	N/A	0..400	4	16	378
Adjusted std visible optical depth	134	N/A	TBD	4	16	382
Adjusted mean cloud fractional area, delta	135	N/A	0..1	4	16	386
Adjusted std cloud fractional area	136	N/A	TBD	4	16	390
Adjusted mean IR emissivity, delta	137	N/A	0..1	4	16	394
Adjusted std mean IR emissivity	138	N/A	TBD	4	16	398
Adjusted mean cloud effective temperature, delta	139	K	0..250	4	16	402
Adjusted std cloud effective temperature	140	K	TBD	4	16	406
Adjusted optical depth/IR emissivity freq dist, delta	141	N/A	0..400	52	16	410

Total Meta Bits/File:	320
Total Data Bits/Record:	7536
Total Records/File:	245475
Total Data Bits/File:	1849899600
Total Bits/FIle:	1849899920

Clouds and the Earth's Radiant Energy System (CERES)

Algorithm Theoretical Basis Document

Grid Single Satellite Fluxes and Clouds and Compute Spatial Averages

(Subsystem 6.0)

G. Louis Smith[1]
Kathryn A. Bush[2]
Rajeeb Hazra[3]
Natividad Manalo-Smith[4]
Frank E. Martino III[2]
David Rutan[4]

[1]Atmospheric Sciences Division, NASA Langley Research Center, Hampton, Virginia 23681-0001
[2]Science Applications International Corporation (SAIC), Hampton, Virginia 23666
[3]Oregon State University, Corvallis, Oregon
[4]Analytical Services & Materials, Inc., Hampton, Virginia 23666

Abstract

This subsystem, Hourly Grided Single Satellite Radiative Fluxes and Clouds (FSW) provides the transformation from instrument-referenced data to Earth-referenced data. In this subsystem, a CERES footprint is assigned to the appropriate region of a 1.25° equal-area grid. Fluxes and cloud properties are spatially averaged over each region on an hourly basis. After passing through this subsystem, the CERES data lose their traceability to specific CERES measurements.

FSW uses the CRS archival product for input (see Appendix A). FSW also uses the internal grid definition REGIONS as input.

The FSW subsystem outputs the FSW archival data product, which includes radiative fluxes at TOA, surface and atmospheric levels for clear sky and total sky conditions, cloud overlap conditions, cloud category properties, column-averaged cloud properties, angular model scene classes, surface-only data, and adjustment parameters (see Appendix B).

The gridding and spatial averaging subsystem performs two major functions. The first is to assign CERES footprints to the proper gridded regions. This assignment is based on the colatitude and longitude of the CERES footprint field of view at the top of the atmosphere. The second major process is to perform spatial averaging of the various radiative fluxes and cloud properties over each region for the time of observation.

6.0. Grid Single Satellite Fluxes and Clouds and Compute Spatial Averages

6.1. Introduction

In order to make the CERES data more useful to researchers, the measured fields are presented in an Earth-based coordinate system. A quasi-equal area grid is defined consisting of regions that are 1.25° in latitude and nearly the same geometric extent in longitude. Average values of the different parameters are computed over each region at the time of observation. Only CERES data obtained when the instrument is operating in the cross-track scan mode will be used in computing regional averages.

The equal-area grid was selected for the CERES grid system because in an equal-angle grid system, such as was used for ERBE, grid elements near the poles are extremely small. For example, a 1.25° × 1.25° grid element between 87.5°N and 88.75°S will be 111 km along the west and east sides, 1.9 km across the northern side and 3.8 km across the southern boundary. Thus, even at nadir, the CERES footprint would overlap several regions due to the convergence of the lines of longitude at the poles. The equal area grid system reduces the distortion of the grid elements at high latitudes. These elements are of only approximately equal area, as there must be an integral number of them in a latitude band.

Means of basic physical quantities in a region are computed as arithmetic averages of the quantities in those CERES footprints whose centers are within the region. It is also necessary to compute regional values for other quantities which have been computed for individual CERES footprints, such as variances and probability distributions.

The CERES footprints are 25 km in diameter near nadir, so that there are more footprints on the boundary of a region than inside the region. Moreover, as CERES scans away from nadir, the footprints grow such that they are not small compared to the size of the region, and the distance between footprints in the scan direction increases. If the footprints are large compared to the region, as illustrated in

Figure 1, overlap of the footprints with each other and with the boundaries of the region complicates the problem of computing regional averages. The selection of particular footprints to use at the boundaries of the region and the correlation of values of overlapping footprints needs to be considered. Because of these problems, improved techniques for computing regional averages have been developed (Hazra et al., 1992, 1993). At present, error studies are underway to define the degree of improvement which these methods provide.

6.2. Algorithm Description

Two basic functions are performed in the FSW and SFC subsystems. The first is the gridding function, in which individual CERES footprints are assigned to the appropriate region or grid box. The second is the averaging function, in which spatial averages of time and geometry data, radiative flux data, cloud overlap conditions, cloud category properties, column-averaged cloud properties, and angular model scene classes are computed. The data flow diagram (see Fig. 2 in CERES Overview) illustrates these functions. The algorithms used to perform these functions are described below.

6.2.1. Gridding Algorithm

The grid system is an equal area grid of 1.25° quasi-squares in latitudinal rings or zones. Each 1.25° square is known as a region. There are 144 zones, which are numbered consecutively starting with 1 at the South Pole (Green, 1995). The regions in each zone are numbered consecutively starting at the Greenwich meridian, and progressing eastward. The number of the first region of the *M*th latitude zone will be NZONE(*M*). The *M*th zone will contain NZONE(*M* + 1) − NZONE(*M*) regions. The regions in zone *M* will be DLONG(*M*) degrees wide. DLONG and NZONE arrays will define the grid system. The width of each region in a zone is

$$\mathrm{DLONG}(M) = 360/(\mathrm{NZONE}(M+1) - \mathrm{NZONE}(M)) \tag{6-1}$$

The position COLAT and ALONG for each CERES footprint is computed by Subsystem 1 based on the optical axis position displaced by an angle due to the time response of the detector and electronic filter. The region number is then computed by making distinctions between the colatitude and longitude. First we count the number of zones from the south pole to the point, so that the zone number *M* is determined by:

$$M = 1 + \mathrm{INT}((180 - \mathrm{COLAT})/1.25) \tag{6-2}$$

Next we count the number of regions from the Greenwich meridian to the point and add the number of the first region of the zone. The region number NREGION for a CERES footprint is computed as:

$$\mathrm{NREGION} = \mathrm{NZONE}(M) + \mathrm{INT}(\mathrm{ALONG}/\mathrm{DLONG}(M)) \tag{6-3}$$

6.2.2. Spatial Averaging Algorithms

6.2.2.1. Time and geometry data. Instead of spatially averaging time and location data over a region, time and location data are determined using the concept of a “key” footprint. The time of interest is the “over-flight” time, which is taken as the time corresponding to the “key” footprint assigned to a region. The determination of the key footprint depends upon the scan mode in operation when the CERES data were obtained. During cross-track operation, the region is scanned in an orderly manner. The set of all footprints in region NREGION is denoted as S(NREGION). The KEY footprint is that footprint whose axis is closest to the centroid of the region. The centroid of the region is calculated using an isosceles trapezoid approximation. Given the centroid of the region, the KEY footprint is determined by finding the footprint in S(NREGION) for which

$$(\mathrm{ALAT} - \mathrm{ALATCNR})^{**}2 + ((\mathrm{ALONG} - \mathrm{ALONGCT})^{*}\sin(\mathrm{COLAT}))^{**}2 \tag{6-4}$$

is a minimum, where ALAT and ALONG are the colatitude and longitude of a footprint, ALATCNR and ALONGCT are the latitude and longitude of the centroid of the region, and COLAT is the colatitude of the footprint.

The KEY footprints are used to identify the Julian date and time, Sun longitude and colatitude, solar zenith angle, spacecraft viewing zenith angle, spacecraft viewing azimuth angle, spacecraft relative azimuth viewing angle, and insolation for each region.

6.2.2.2. Spatial averaging algorithm. Means: The regional average of a quantity x is computed from its measurements x_i as

$$x_{\text{mean}} = \left(\sum_{i \in S} x_i\right) \Big/ N_S$$

where N_S is the number of footprints included in the set S for which the average is being computed. This technique was used for ERBE and for many other satellite processing systems. Given one or more observations in a region, one can compute a regional average with no difficulty. Without such measurements, one does not wish to attempt the computation. This algorithm will be applied to fluxes at the top of the atmosphere, surface and at intermediate layers in the atmosphere.

For averaging microphysical properties of clouds, it is necessary to account for the amount of clouds for which a number applies, e.g. in computing the average optical depth for clouds over a region, the average applies only to that part of the region which has clouds. A region may contain no clouds, one cloud or many clouds. It follows that for regional averages of cloud microphysical properties, a weighting by the fraction f_i of cloud in the footprint is included:

$$\tilde{x} = \frac{\sum_i f_i x}{\sum_i f_i}$$

The direct/diffuse ratio r is computed for each CERES footprint for the downward shortwave flux at the surface. The regional average direct/diffuse ratio is computed on a flux-weighted basis, so that the regional average ratio applies to the regional average values of direct, diffuse and total downward shortwave flux. The equation for the regional average direct/diffuse ratio (see Appendix C.1) is:

$$\tilde{r} = \left(\sum_i \frac{r_i F_i}{(1 + r_i)}\right) \Big/ \left(\sum_i \frac{F_i}{(1 + r_i)}\right)$$

Variances: There are two cases of computing variances. For the first case, there will be one measurement of a quantity for each CERES footprint. The variance of this quantity over the region will be given by

$$s^2 = (N - 1)^{-1} \left[\sum_{i=1}^{N} x_i^2 - N x_{\text{mean}}{}^2\right]$$

For the second case, variances will be computed in Subsystem 4 for cloud microphysical properties from MODIS pixels over each CERES footprint weighted by the CERES point spread function as

$$s^2 = \frac{\sum_i w_i (x_i - \hat{x})^2}{\sum_i w_i}$$

It can be shown (see Appendix C.2) that s^2 is related to the variance of the quantity σ^2 by

$$E[s^2] = \sigma^2 F(\alpha)$$

The parenthetical expression of the right-hand side will be a function of the view zenith angle α, which will vary slowly over a given region. Also, the number of MODIS pixels within a CERES footprint will be nearly the same for all footprints within a region. Thus, we can simply average the footprint variances to produce a regional average variance. Because the statistic thus computed is a function of view zenith angle α, its values should not be compared across a satellite measurement swath except as a measure of the variation of the bracket term.

<u>Optical Depth and Infrared Emissivity Histograms</u>: For each CERES footprint, Subsystem 4 will form a histogram of visible optical depths during the day and infrared emissivities during the night. For compactness, these histograms will be defined in terms of arrays of optical depths and emissivities corresponding to percentiles. In the present subsystem it is necessary to reconstruct the histograms from the percentiles, and from them form regional mean histograms for each cloud height class.

A set of percentile values $\{p_k\}$ is defined for $k \in [1, 13]$. For a given cloud altitude class the set of optical depths $\{x_{ki}\}$ corresponding to these percentiles is computed by Subsystem 4 for each CERES footprint i. In order to spatially average the histograms over a region, we first reconstruct the histogram on a fine optical depth grid consisting of a set of points $\{z_j\}$ for $j \in [1, 50]$. For optical depth computations, these points will not be evenly distributed. The reconstructed histograms $\{p_{ji}\}$ are then averaged over all footprints i within the region, weighted by the fractional cloud area f_i, to produce the regional mean histogram $\{P_j\}$:

$$P_j = P(z_j) = \frac{\sum_i f_i p_i(z_j)}{\sum_i f_i}$$

From these $\{z_j, P_j\}$ pairs, the x_k values corresponding to the selected percentile values of the regional average optical depth can then be computed by interpolation. In producing this regional mean histogram, the optical depth grid $\{z_j\}$ is accepted as sufficient so that there is no loss of accuracy due to interpolation errors. Thus, the grid will be somewhat smaller than the accuracy of the optical depth computation. The infrared emissivity histograms will be computed in the same manner. The interpolation points will differ between optical depth and infrared emissivity because the range of optical depths is [0, 50] and the range of infrared emissivity is [0, 1.].

6.3. Procedural Considerations

6.3.1. Routine Operations Expectations

The gridding and spatial averaging functions are performed on an hourly basis. The input CRS archival data product is an hourly product. The output FSW archival data product is a monthly product. Intermediate FSW-hour data products need to be stored in a data repository until an entire month of data is available to produce an FSW product to be passed on to the next processing subsystem. We expect that the logistics for this will be worked out cooperatively by the CERES Data Management Team, the CERES Science Team, and EOSDIS.

6.3.2. Exception Handling Strategy: Missing Data, Invalid Data

All invalid data are expected to have been eliminated from the input data products by the time FSW processing takes place. Routine limit checks will be made to make sure that data are within reasonable limits. Data that are outside these limits will be excluded from further processing, and a diagnostic report will be issued. These data will also be noted on the quality control (QC) reports generated by the subsystem.

6.3.3. Routine Diagnostics and Quality Control Expectations

Routine diagnostics will include a quality control report for each hourly FSW-hour data product. These reports will include information such as:

- The number of input records processed and the number of output records written
- The number of regions into which data were placed
- The number of CERES footprints of data placed into each region
- Per region, the minimum, maximum, mean, and standard deviation of selected parameters
- Missing data

As the definition of the FSW data product matures, this list will be expanded.

6.3.4. Storage Estimate (MB)

We estimate the size of each FSW-hour hourly product to be 4.2 MB (see Appendix B). As the definition of the FSW data product matures, this size estimate may change. There will be 24 FSW-hour data products per day, and 744 per month. This latter number is based on an average of 31 days per month. Thus, we anticipate a monthly size of 3226 MB. Since the next step in the CERES data processing system operates on a month of data, FSW will require at least 3226 MB of storage space.

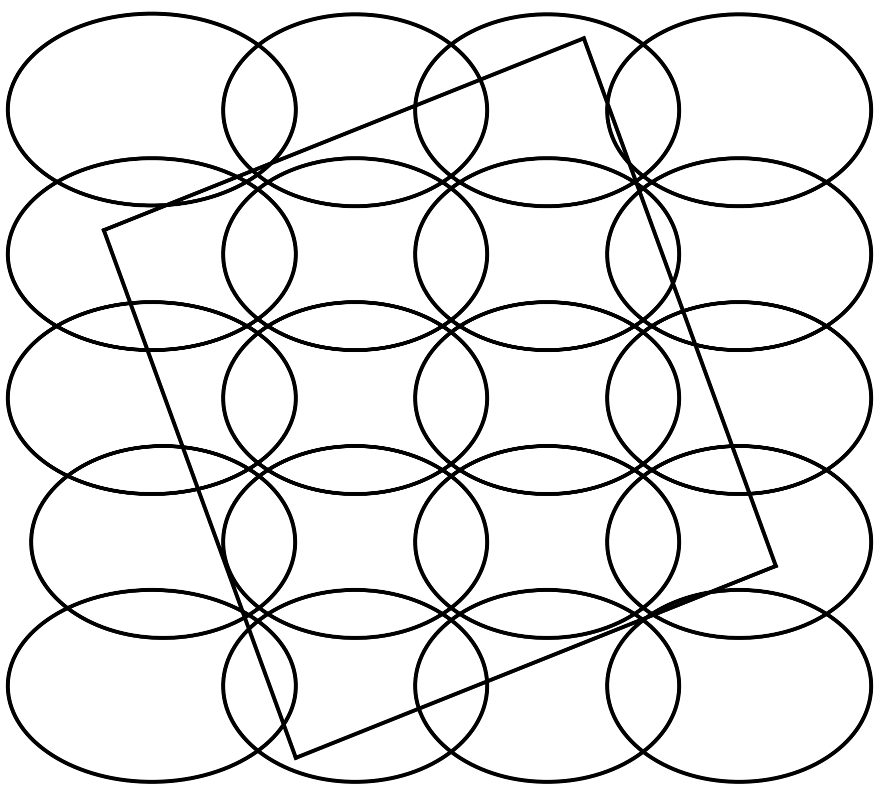

Figure 1. Area coverage by scan modes showing cross-track scan.

Appendix A

Input Data Products

Grid Single Satellite Radiative Fluxes and Clouds (Subsystem 6.0)

This appendix describes the data products which are produced by the algorithms in this subsystem. Table A-1 below summarizes these products, listing the CERES and EOSDIS product codes or abbreviations, a short product name, the product type, the production frequency, and volume estimates for each individual product as well as a complete data month of production. The product types are defined as follows:

Archival products:	Assumed to be permanently stored by EOSDIS
Internal products:	Temporary storage by EOSDIS (days to years)
Ancillary products:	Non-CERES data needed to interpret measurements

The following pages describe each product. An introductory page provides an overall description of the product and specifies the temporal and spatial coverage. The table which follows the introductory page briefly describes every parameter which is contained in the product. Each product may be thought of as metadata followed by data records. The metadata (or header data) is not well-defined yet and is included mainly as a placeholder. The description of parameters which are present in each data record includes parameter number (a unique number for each distinct parameter), units, dynamic range, the number of elements per record, an estimate of the number of bits required to represent each parameter, and an element number (a unique number for each instance of every parameter). A summary at the bottom of each table shows the current estimated sizes for metadata, each data record, and the total data product. A more detailed description of each data product will be contained in a user's guide to be published before the first CERES launch.

Table A-1. Input Products Summary

Product code		Name	Type	Frequency	Size, MB	Monthly size, MB
CERES	EOSDIS					
CRS	CER04	Single satellite CERES footprint, radiative fluxes and clouds	archival	1/hour	220.5	164052

Single Satellite CERES Footprint, Radiative Fluxes and Clouds (CRS)

The CERES archival product, cloud radiative swath (CRS), is produced by the CERES compute surface and Atmospheric Radiative Fluxes Subsystem. Each CRS file contains longwave and shortwave radiative fluxes for the surface, internal atmosphere and TOA for each CERES footprint. The CRS contains data for one hour, or one satellite swath (8-12 percent of the Earth), from one satellite. In addition to being an archival product, the CRS is used by the CERES subsystem, Grid Single Satellite Radiative Fluxes and Clouds.

For each CERES footprint, the CRS contains

- Time and location data
- CERES observed TOA data
- Full footprint data
- Full footprint algorithm flags
- Footprint clear-sky properties
- Cloud category properties for up to four (low, lower middle, upper middle and high) cloud layers

- Overlap data for eleven (clear, low (L), lower middle (LM), upper middle (UM), high (H), H/UM, H/LM, H/L, UM/LM, UM/L, LM/L) cloud overlap conditions
- Atmospheric flux profile for both clear-sky and total-sky at the surface, 500 hPa, the tropopause and the TOA
- Flux adjustments (tuned-untuned) for clear-sky and total-sky at the surface and TOA
- Surface-only data
- Adjustment parameters for clear-sky (note that these are for both clear-sky and total-sky footprints)
- Adjustment parameters for L, LM, UM, and H cloud layers

Level: 2
Type: Archival
Frequency: 1/ hour

Time Interval Covered
File: 1 hour
Record: Instantaneous

Portion of Globe Covered
File: Satellite swath
Record: 1 CERES footprint

Portion of Atmosphere Covered
File: Surface, internal and TOA

Table A-2. Single Satellite CERES Footprint, Radiative Fluxes and Clouds (CRS)

Description	Parameter Number	Units	Range	Elements/ Record	Bits/ Elem	Elem Num
Meta Data						
CRS File Header		N/A		1	320	
Time and Location Data						
Julian day	1	day	2449353..2458500	1	32	1
Julian time	2	day	0..1	1	32	2
Earth-Sun distance	3	AU	0.98..1.02	1	32	3
Sun colatitude	4	deg	0..180	1	32	4
Sun longitude	5	deg	0..360	1	32	5
Pixel colatitude, TOA	6	deg	0..180	1	32	6
Pixel longitude, TOA	7	deg	0..360	1	32	7
Pixel colatitude, surface	8	deg	0..180	1	32	8
Pixel longitude, surface	9	deg	0..360	1	32	9
Spacecraft colatitude, nadir	10	deg	0..180	1	32	10
Spacecraft longitude, nadir	11	deg	0..360	1	32	11
Spacecraft inertial velocity vector (X, Y, Z)	12	km sec^{-1}	-10..10	3	32	12
Satellite radius	13	km	6500..8000	1	16	15
Along-track angle	14	deg	0..360	1	16	16
Cross-track angle	15	deg	-90..90	1	16	17
Cone angle	16	deg	0..90	1	16	18
Clock angle	17	deg	0..360	1	16	19
Cone rate	18	deg sec^{-1}	-100..100	1	16	20
Clock rate	19	deg sec^{-1}	-8..8	1	16	21
Scan sample number	20	N/A	1..660	1	16	22
Surface altitude	21	km	-12..10	1	16	23
Surface land area	22	percent	0..100	10	16	24
Surface sea area	23	percent	0..100	3	16	34
Flag, clear-sky or total-sky	24	N/A	0..1	1	16	37
Scene type	25	N/A	0..200	1	16	38
Satellite viewing zenith angle, TOA	26	deg	0..90	1	16	39
Solar zenith angle, TOA	27	deg	0..180	1	16	40
Relative azimuth angle, TOA	28	deg	0..180	1	16	41
Satellite viewing azimuth at TOA wrt North	29	deg	0..360	1	16	42
CERES Observed TOA Data						
CERES TOT radiance, TOA, filtered	30	$W\text{-}m^{-2}sr^{-1}$	0..700	1	16	43
CERES SW radiance, TOA, filtered	31	$W\text{-}m^{-2}sr^{-1}$	-10..510	1	16	44
CERES LW WN radiance, TOA, filtered	32	$W\text{-}m^{-2}sr^{-1}$	0..50	1	16	45
CERES TOT radiance, TOA, unfiltered	33	$W\text{-}m^{-2}sr^{-1}$	0..700	1	16	46
CERES SW radiance, TOA, unfiltered	34	$W\text{-}m^{-2}sr^{-1}$	-10..510	1	16	47
CERES LW WN radiance, TOA, unfiltered	35	$W\text{-}m^{-2}sr^{-1}$	0..50	1	16	48
Flag, TOT radiance quality	36	N/A	TBD	1	16	49
Flag, SW radiance quality	37	N/A	TBD	1	16	50
Flag, LW WN radiance quality	38	N/A	TBD	1	16	51

Table A-2. Continued

Description	Parameter Number	Units	Range	Elements/ Record	Bits/ Elem	Elem Num
CERES SW flux, TOA	39	W-m^{-2}	0..1400	1	16	52
CERES LW flux, TOA	40	W-m^{-2}	0..500	1	16	53
CERES LW WN flux, TOA	41	W-m^{-2}	10..400	1	16	54
Full Footprint Data						
Imager identification code	42	N/A	TBD	1	16	55
Number of imager pixels	43	N/A	0..9000	1	16	56
Number cloud height catagories	44	N/A	-1..4	1	16	57
Imager radiance, 0.6µm channel, 5th percentile	45	W-m^{-2}sr^{-1}µm^{-1}	TBD	1	16	58
Imager radiance, 0.6µm channel, mean	46	W-m^{-2}sr^{-1}µm^{-1}	TBD	1	16	59
Imager radiance, 0.6µm channel, 95th percentile	47	W-m^{-2}sr^{-1}µm^{-1}	TBD	1	16	60
Imager radiance, 3.7µm channel, 5th percentile	48	W-m^{-2}sr^{-1}µm^{-1}	TBD	1	16	61
Imager radiance, 3.7µm channel, mean	49	W-m^{-2}sr^{-1}µm^{-1}	TBD	1	16	62
Imager radiance, 3.7µm channel, 95th percentile	50	W-m^{-2}sr^{-1}µm^{-1}	TBD	1	16	63
Imager radiance, 11.0µm channel, 5th percentile	51	W-m^{-2}sr^{-1}µm^{-1}	TBD	1	16	64
Imager radiance, 11.0µm channel, mean	52	W-m^{-2}sr^{-1}µm^{-1}	TBD	1	16	65
Imager radiance, 11.0µm channel, 95th percentile	53	W-m^{-2}sr^{-1}µm^{-1}	TBD	1	16	66
Bidirectional reflectance	54	TBD	TBD	11	16	67
Imager mean viewing zenith angle, TOA	55	deg	0..90	1	16	78
Imager mean relative azimuth angle, TOA	56	deg	0..360	1	16	79
Precipitable water	57	cm	0.001..8.000	1	16	80
Full Footprint Algorithm Flags						
Notes on general procedures	58	N/A	TBD	1	16	81
Texture algorithm flag	59	N/A	TBD	1	16	82
Multi-layer cloud algorithm flag	60	N/A	TBD	1	16	83
Spatial coherence algorithm flag	61	N/A	TBD	1	16	84
IR sounder algorithm flag	62	N/A	TBD	1	16	85
Threshhold algorithm flag	63	N/A	TBD	1	16	86
Visible optical depth algorithm flag	64	N/A	TBD	1	16	87
IR emissivity algorithm flag	65	N/A	TBD	1	16	88
Cloud particle size algorithm flag	66	N/A	TBD	1	16	89
Cloud water path algorithm flag	67	N/A	TBD	1	16	90
Footprint Clear Sky Properties						
Imager radiance, 0.6µm channel, mean	68	W-m^{-2}sr^{-1}µm^{-1}	TBD	1	16	91
Imager radiance, 0.6µm channel, std	69	W-m^{-2}sr^{-1}µm^{-1}	TBD	1	16	92
Imager radiance, 3.7µm channel, mean	70	W-m^{-2}sr^{-1}µm^{-1}	TBD	1	16	93
Imager radiance, 3.7µm channel, std	71	W-m^{-2}sr^{-1}µm^{-1}	TBD	1	16	94
Imager radiance, 11.0µm channel, mean	72	W-m^{-2}sr^{-1}µm^{-1}	TBD	1	16	95
Imager radiance, 11.0µm channel, std	73	W-m^{-2}sr^{-1}µm^{-1}	TBD	1	16	96
Stratospheric aerosol, optical depth	74	N/A	0.0..0.5	1	16	97
Stratospheric aerosol effective radius	75	µm	0..10	1	16	98
Total aerosol, optical depth	76	N/A	0.0..2.0	1	16	99
Total aerosol effective radius	77	µm	0..20	1	16	100
Cloud Properties for 4 Cloud Layers						
(Cloud layers are low, lower middle, upper middle and high)						
Number imager pixels	78	N/A	0..9000	4	16	101
Cloud layer index	79	N/A	1..11	4	16	105
Overcast cloud area fraction	80	N/A	0..1	4	16	109
Total cloud area fraction	81	N/A	0..1	4	16	113
Broken cloud area fraction	82	N/A	0..1	4	16	117
Imager radiance, 0.6µm channel, mean	83	W-m^{-2}sr^{-1}µm^{-1}	TBD	4	16	121
Imager radiance, 0.6µm channel, std	84	W-m^{-2}sr^{-1}µm^{-1}	TBD	4	16	125
Imager radiance, 3.7µm channel, mean	85	W-m^{-2}sr^{-1}µm^{-1}	TBD	4	16	129
Imager radiance, 3.7µm channel, std	86	W-m^{-2}sr^{-1}µm^{-1}	TBD	4	16	133
Imager radiance, 11.0µm channel, mean	87	W-m^{-2}sr^{-1}µm^{-1}	TBD	4	16	137
Imager radiance, 11.0µm channel, std	88	W-m^{-2}sr^{-1}µm^{-1}	TBD	4	16	141
Visible optical depth, mean	89	N/A	0..400	4	16	145
Visible optical depth, std	90	N/A	TBD	4	16	149
IR emissivity, mean	91	N/A	0..1	4	16	153
IR emissivity, std	92	N/A	0..1	4	16	157
Cloud liquid water path, mean	93	g m^{-2}	0.001..10.000	4	16	161
Cloud liquid water path, std	94	g m^{-2}	TBD	4	16	165
Cloud ice water path, mean	95	g m^{-2}	0.001..10.000	4	16	169
Cloud ice water path, std	96	g m^{-2}	TBD	4	16	173
Cloud top pressure, mean	97	hPa	0..1100	4	16	177

Table A-2. Concluded

Description	Parameter Number	Units	Range	Elements/ Record	Bits/ Elem	Elem Num
Cloud top pressure, std	98	hPa	TBD	4	16	181
Cloud effective pressure, mean	99	hPa	0..1100	4	16	185
Cloud effective pressure, std	100	hPa	TBD	4	16	189
Cloud effective temperature, mean	101	K	100..350	4	16	193
Cloud effective temperature, std	102	K	TBD	4	16	197
Cloud effective height, mean	103	km	0..20	4	16	201
Cloud effective height, std	104	km	TBD	4	16	205
Cloud bottom pressure, mean	105	hPa	0..1100	4	16	209
Cloud bottom pressure, std	106	hPa	TBD	4	16	213
Cloud water particle radius, mean	107	µm	0..200	4	16	217
Cloud water particle radius, std	108	µm	TBD	4	16	221
Cloud ice particle radius, mean	109	µm	0..200	4	16	225
Cloud ice particle radius, std	110	µm	TBD	4	16	229
Cloud particle phase, mean	111	N/A	0..1	4	16	233
Cloud aspect ratio, mean	112	N/A	0..1	4	16	237
Cloud aspect ratio, std	113	N/A	0..1	4	16	241
Visible optical depth/IR emissivity, 13 percentiles	114	N/A	0..400	52	16	245
Overlap Footprint Data for 11 Cloud Overlap Conditions						
(Overlap conditions are clear, low (L), lower middle (LM), upper middle (UM), high (H), H/UM, H/LM, H/L, UM/LM, UM/L, and LM/L)						
Number overlap pixels	115	N/A	0..9000	11	16	297
Total cloud area fraction	116	N/A	0..1	11	16	308
Atmospheric Flux Profile for Clear-sky and Total-sky						
(Atmospheric layers in profile are surface, 500 hPa, tropopause and TOA)						
Number atmospheric layers	117	N/A	0..4	1	16	319
Layer pressures	118	hPa	0..1100	4	16	320
SW upwards, atmospheric layer, tuned	119	$W\text{-}m^{-2}$	0..1400	8	16	324
SW downwards, atmospheric layer, tuned	120	$W\text{-}m^{-2}$	0..1400	8	16	332
LW upwards, atmospheric layer, tuned	121	$W\text{-}m^{-2}$	0..500	8	16	340
LW downwards, atmospheric layer, tuned	122	$W\text{-}m^{-2}$	0..500	8	16	348
Flux Adjustments (Tuned - Untuned) for Clear-sky and Total-sky at Surface and TOA						
SW upwards, atmospheric layer, delta	123	$W\text{-}m^{-2}$	0..1400	4	16	356
SW downwards, atmospheric layer, delta	124	$W\text{-}m^{-2}$	0..1400	4	16	360
LW upwards, atmospheric layer, delta	125	$W\text{-}m^{-2}$	0..500	4	16	364
LW downwards, atmospheric layer, delta	126	$W\text{-}m^{-2}$	0..500	4	16	368
Surface-only Data						
Photosynthetically active radiation	127	$W\text{-}m^{-2}$	0..780	1	16	372
Direct/diffuse ratio	128	N/A	0..30	1	16	373
Adjustment Parameters for Clear Skies						
Adjusted precipitable water, delta	129	cm	0.001..8.000	1	16	374
Adjusted surface albedo, delta	130	N/A	0..1	1	16	375
Adjusted aerosol optical depth, delta	131	N/A	0.0..2.0	1	16	376
Adjusted skin temperature, delta	132	K	TBD	1	16	377
Adjustment Parameters for L, LM, UM and H Cloud Layers						
Adjusted mean visible optical depth, delta	133	N/A	0..400	4	16	378
Adjusted std visible optical depth	134	N/A	TBD	4	16	382
Adjusted mean cloud fractional area, delta	135	N/A	0..1	4	16	386
Adjusted std cloud fractional area	136	N/A	TBD	4	16	390
Adjusted mean IR emissivity, delta	137	N/A	0..1	4	16	394
Adjusted std mean IR emissivity	138	N/A	TBD	4	16	398
Adjusted mean cloud effective temperature, delta	139	K	0..250	4	16	402
Adjusted std cloud effective temperature	140	K	TBD	4	16	406
Adjusted optical depth/IR emissivity freq dist, delta	141	N/A	0..400	52	16	410
Total Meta Bits/File:	320					
Total Data Bits/Record:	7536					
Total Records/File:	245475					
Total Data Bits/File:	1849899600					
Total Bits/FIle:	1849899920					

Appendix B

Output Data Products

Grid Single Satellite Radiative Fluxes and Clouds (Subsystem 6.0)

This appendix describes the data products which are produced by the algorithms in this subsystem. Table B-1 below summarizes these products, listing the CERES and EOSDIS product codes or abbreviations, a short product name, the product type, the production frequency, and volume estimates for each individual product as well as a complete data month of production. The product types are defined as follows:

Archival products: Assumed to be permanently stored by EOSDIS
Internal products: Temporary storage by EOSDIS (days to years)

The following pages describe each product. An introductory page provides an overall description of the product and specifies the temporal and spatial coverage. The table which follows the introductory page briefly describes every parameter which is contained in the product. Each product may be thought of as metadata followed by data records. The metadata (or header data) is not well-defined yet and is included mainly as a placeholder. The description of parameters which are present in each data record includes parameter number (a unique number for each distinct parameter), units, dynamic range, the number of elements per record, an estimate of the number of bits required to represent each parameter, and an element number (a unique number for each instance of every parameter). A summary at the bottom of each table shows the current estimated sizes for metadata, each data record, and the total data product. A more detailed description of each data product will be contained in a user's guide to be published before the first CERES launch.

Table B-1. Output Products Summary

Product code		Name	Type	Frequency	Size, MB	Monthly size, MB
CERES	EOSDIS					
FSW	CER05	Hourly gridded single satellite fluxes and clouds	archival	1/hour	4.2	3105

Hourly Gridded Single Satellite Fluxes and Clouds (FSW)

The hourly gridded single satellite gluxes and clouds (FSW) archival data product contains hourly single satellite flux and cloud parameters averaged over 1.25° regions. Input to the FSW subsystem is the single satellite CERES footprint, radiative fluxes and clouds (CRS) archival data product. Each FSW covers a single hour swath from a single CERES instrument mounted on one satellite. The product has a product header and multiple records. Each record contains spatially averaged data for an individual region.

The major categories of data output on the FSW are

- Region data
- Total sky radiative fluxes at TOA, surface, and atmospheric levels
- Clear sky radiative fluxes at TOA, surface, and atmospheric levels
- Cloud overlap conditions
- Cloud category properties
- Column-averaged cloud properties
- Angular model scene classes
- Surface only data
- Adjustment parameters

FSW is an archival product generated on an hourly basis. Initially at the launch of the TRMM spacecraft, this product will be produced in validation mode once every 3 months, or for 4 data months a year. During the first 18 months after the launch of TRMM, the CERES Science Team will derive a production quality set of angular distribution models, which are needed to produce the shortwave (SW) and longwave (LW) instantaneous fluxes. Eighteen months after the launch of TRMM, this product will be archived and will contain SW and LW fluxes at the tropopause and at the 500 hPa pressure level, in addition to fluxes at TOA and at the surface. Thirty-six months after the launch of TRMM, this archived product will contain SW and LW fluxes at 26 standard pressure levels.

Level: 3
Type: Archival
Frequency: 1/hour

Portion of Globe Covered
File: Gridded satellite swath
Record: 1.25-degree equal-area regions

Time Interval Covered
File: Hour
Record: N/A

Portion of Atmosphere Covered
File: TOA, surface and atmospheric pressure levels

Table B-2. Hourly Gridded Single Satellite Fluxes and Clouds (FSW)

Description	Parameter Number	Units	Range	Elements/ Record	Bits/ Elem	Elem Num
FSW						
FSW_File_Header						
CERES data product code		N/A	N/A	1	16	
Spacecraft name		N/A	N/A	1	16	
CERES instrument identification code		N/A	N/A	1	16	
Julian Day		Day	2449353 .. 2458500	1	32	
Hour of the day for the FSW product		Hours	1 .. 24	1	16	
Number of regions (records) in the product		N/A	1 .. 2500	1	16	
FSW_Region_Data						
Region number	1	N/A	1 .. 26542	1	16	1
Number of CERES footprints in the region	2	N/A	1 .. 40	1	16	2
Julian Time	3	Day	0.0 .. 1.0	1	32	3
Hour box number for the region	4	N/A	1 .. 744	1	16	4
Precipitable water	5	cm	0.001 .. 8.000	1	16	5
Mean of land type percentage	6	Percent	0.0 .. 100.0	10	16	6
Mean of sea type percentage	7	Percent	0.0 .. 100.0	3	16	16
Mean Sun colatitude	8	Degrees	0.0 .. 180.0	1	16	19
Mean Sun longitude	9	Degrees	0.0 .. 360.0	1	16	20
Mean relative azimuth angle at TOA	10	Degrees	0.0 .. 360.0	1	16	21
Mean cosine of solar zenith angle at TOA	11	N/A	0.0 .. 1.0	1	16	22
Mean spacecraft zenith angle	12	Degrees	0.0 .. 90.0	1	16	23
FSW_Radiative_Flux_Data						
Total_Sky_TOA_Flux_Statistics						
Mean, st dev, and num obs of SW upward flux at TOA	13	$W\text{-}m^{-2}$	0.0 .. 1400.0	3	16	24
Mean, st dev, and num obs of LW upward flux at TOA	14	$W\text{-}m^{-2}$	100.0 .. 500.0	3	16	27
Mean, st dev, and num obs of LW window upward flux at TOA	15	$W\text{-}m^{-2}$	0.0 .. 800.0	3	16	30
Mean, st dev, and num obs of observed - untuned SARB SW flux at TOA	16	$W\text{-}m^{-2}$	0.0 .. 1400.0	3	16	33
Mean, st dev, and num obs of observed - tuned SARB SW flux at TOA	17	$W\text{-}m^{-2}$	0.0 .. 1400.0	3	16	36
Mean, st dev, and num obs of observed - untuned SARB LW flux at TOA	18	$W\text{-}m^{-2}$	0.0 .. 500.0	3	16	39
Mean, st dev, and num obs of observed - tuned SARB LW flux at TOA	19	$W\text{-}m^{-2}$	0.0 .. 500.0	3	16	42
Total_Sky_Surface_Flux_Statistics						
Mean, st dev, and num obs of tuned SW downward sfc flux	20	$W\text{-}m^{-2}$	0.0 .. 1400.0	3	16	45
Mean, st dev, and num obs of tuned SW upward sfc flux	21	$W\text{-}m^{-2}$	0.0 .. 1400.0	3	16	48
Mean, st dev, and num obs of tuned LW downward sfc flux	22	$W\text{-}m^{-2}$	100.0 .. 500.0	3	16	51
Mean, st dev, and num obs of tuned LW upward sfc flux	23	$W\text{-}m^{-2}$	100.0 .. 500.0	3	16	54
Mean, st dev, and num obs of tuned - untuned SW downward sfc flux	24	$W\text{-}m^{-2}$	0.0 .. 1400.0	3	16	57
Mean, st dev, and num obs of tuned - untuned SW upward sfc flux	25	$W\text{-}m^{-2}$	0.0 .. 1400.0	3	16	60

Table B-2. Continued

Description	Parameter Number	Units	Range	Elements/ Record	Bits/ Elem	Elem Num
Mean, std, and num obs of tuned - untuned LW downward sfc flux	26	$W\text{-}m^{-2}$	0.0 .. 500.0	3	16	63
Mean, st dev, and num obs of tuned - untuned LW upward sfc flux	27	$W\text{-}m^{-2}$	0.0 .. 500.0	3	16	66
Total_Sky_Atmospheric_Flux_Statistics						
(Atmospheric levels are tropopause and 500 hPa)						
Mean, st dev, and num obs of tuned SW downward flux at atm levels	28	$W\text{-}m^{-2}$	0.0 .. 1400.0	6	16	69
Mean, st dev, and num obs of tuned SW upward flux at atm levels	29	$W\text{-}m^{-2}$	0.0 .. 1400.0	6	16	75
Mean, st dev, and num obs of tuned LW downward flux at atm levels	30	$W\text{-}m^{-2}$	100.0 .. 500.0	6	16	81
Mean, st dev, and num obs of tuned LW upward flux at atm levels	31	$W\text{-}m^{-2}$	100.0 .. 500.0	6	16	87
FSW_Clear_Sky_Fluxes						
Clear_Sky_TOA_Flux_Statistics						
Mean, st dev, and num obs of SW upward flux at TOA	32	$W\text{-}m^{-2}$	0.0 .. 1400.0	3	16	93
Mean, st dev, and num obs of LW upward flux at TOA	33	$W\text{-}m^{-2}$	100.0 .. 500.0	3	16	96
Mean, st dev, and num obs of LW window upward flux at TOA	34	$W\text{-}m^{-2}$	0.0 .. 800.0	3	16	99
Mean, st dev, and num obs of observed - untuned SARB SW flux at TOA	35	$W\text{-}m^{-2}$	0.0 .. 1400.0	3	16	102
Mean, st dev, and num obs of observed - tuned SARB SW flux at TOA	36	$W\text{-}m^{-2}$	0.0 .. 1400.0	3	16	105
Mean, st dev, and num obs of observed - untuned SARB LW flux at TOA	37	$W\text{-}m^{-2}$	0.0 .. 500.0	3	16	108
Mean, st dev, and num obs of observed - tuned SARB LW flux at TOA	38	$W\text{-}m^{-2}$	0.0 .. 500.0	3	16	111
Clear_Sky_Surface_Flux_Statistics						
Mean, st dev, and num obs of tuned SW downward sfc flux	39	$W\text{-}m^{-2}$	0.0 .. 1400.0	3	16	114
Mean, st dev, and num obs of tuned SW upward sfc flux	40	$W\text{-}m^{-2}$	0.0 .. 1400.0	3	16	117
Mean, st dev, and num obs of tuned LW downward sfc flux	41	$W\text{-}m^{-2}$	100.0 .. 500.0	3	16	120
Mean, st dev, and num obs of tuned LW upward sfc flux	42	$W\text{-}m^{-2}$	100.0 .. 500.0	3	16	123
Mean, st dev, and num obs of tuned - untuned SW downward sfc flux	43	$W\text{-}m^{-2}$	0.0 .. 1400.0	3	16	126
Mean, st dev, and num obs of tuned - untuned SW upward sfc flux	44	$W\text{-}m^{-2}$	100.0 .. 500.0	3	16	132
Mean, st dev, and num obs of tuned - untuned LW upward sfc flux	46	$W\text{-}m^{-2}$	100.0 .. 500.0	3	16	135
Clear_Sky_Atmospheric_Flux_Statistics						
(Atmospheric levels are tropopause and 500 hPa)						
Mean, st dev, and num obs of tuned SW upward flux at atm levels	47	$W\text{-}m^{-2}$	0.0 .. 1400.0	6	16	138
Mean, st dev, and num obs of tuned SW downward flux at atm levels	48	$W\text{-}m^{-2}$	0.0 .. 1400.0	6	16	144
Mean, st dev, and num obs of tuned LW upward fluxes at atm levels	49	$W\text{-}m^{-2}$	100.0 .. 500.0	6	16	150
Mean, st dev, and num obs of tuned LW downward flux at atm levels	50	$W\text{-}m^{-2}$	100.0 .. 500.0	6	16	156
FSW_Cloud_Data						
FSW_Cloud_Overlap_Conditions is Array[11] of:						
(Cloud overlap conditions are clear, low (L), lower middle (LM), upper middle (UM), high (H), H/UM, H/LM, H/L, UM/LM, and Lm/L)						
Fractional area for each of 11 conditions	51	Fraction	0.0 .. 1.0	11	16	162
FSW_Cloud_Category_Properties						
(Cloud categories are High, Uppler Middle, Lower Middle, and Low)						
Number of cloud categories with data	52	N/A	0 .. 4	1	16	173
FSW_Cloud_Properties						
Cloud Area Fractions for overcast, broken, and total clouds	53	Fraction	0.0 .. 1.0	12	16	174
Mean, st dev, and num obs of effective pressure	54	hPa	0.0 .. 1100.0	12	16	186
Mean, st dev, and num obs of effective temperature	55	K	100.0 .. 350.0	12	16	198
Mean, st dev, and num obs of effective altitude	56	km	0.0 .. 20.0	12	16	210
Mean, st dev, and num obs of cloud top pressure	57	hPa	0.0 .. 1100.0	12	16	222
Mean, st dev, and num obs of cloud bottom pressure	58	hPa	0.0 .. 1100.0	12	16	234
Mean, st dev, and num obs of particle phase	59	Fraction	0.0 .. 1.0	12	16	246
Mean, st dev, and num obs of liquid water path	60	$g\ m^{-2}$	0.01 .. 1000.0	12	16	258
Mean, st dev, and num obs of ice water path	61	$g\ m^{-2}$	0.01 .. 1000.0	12	16	270
Mean, st dev, and num obs of liquid particle radius	62	µm	0.0 .. 1000.0	12	16	282
Mean, st dev, and num obs of ice particle radius	63	µm	0.0 .. 100.0	12	16	294
Mean, st dev, and num obs of visible optical depth	64	Dimensionless	0.0 .. 50.0	12	16	306
Mean, st dev, and num obs of infrared emissivity	65	Dimensionless	0.0 .. 2.0	12	16	318
Mean, st dev, and num obs of vertical aspect ratio	66	Dimensionless	TBD	12	16	330
Mean, st dev, and num obs of adj. infrared emissivity	67	Dimensionless	0.0 .. 2.0	12	16	342
Mean, st dev, and num obs of adj. fractional area	68	Fraction	0.0 .. 1.0	12	16	354

Table B-2. Concluded

Description	Parameter Number	Units	Range	Elements/ Record	Bits/ Elem	Elem Num
Mean, st dev, and num obs of adj. effective temperature	69	K	0.0 .. 250.0	12	16	366
Mean, st dev, and num obs of adj. visible optical depth	70	Dimensionless	0.0 .. 400.0	12	16	378
Visible Opt Depth (day) / Infrared Emissivity (night) percentiles	71	Dimensionless	0.0 .. 50.0	52	16	390
FSW_Weighted_Column_Average_Cloud_Properties is Array[5] of:						
(Cloud weightings are SW, LW TOA, LW Surface,						
liquid water path, and ice water path)						
FSW_Cloud_Properties						
Cloud Area Fractions for overcast, broken, and total clouds	72	Fraction	0.0 .. 1.0	15	16	442
Mean, st dev, and num obs of effective pressure	73	hPa	0.0 .. 1100.0	15	16	457
Mean, st dev, and num obs of effective temperature	74	K	100.0 .. 350.0	15	16	472
Mean, st dev, and num obs of effective altitude	75	km	0.0 .. 20.0	15	16	487
Mean, st dev, and num obs of cloud top pressure	76	hPa	0.0 .. 1100.0	15	16	502
Mean, st dev, and num obs of cloud bottom pressure	77	hPa	0.0 .. 1100.0	15	16	517
Mean, st dev, and num obs of particle phase	78	Fraction	0.0 .. 1.0	15	16	532
Mean, st dev, and num obs of liquid water path	79	g m^{-2}	0.01 .. 1000.0	15	16	547
Mean, st dev, and num obs of ice water path	80	g m^{-2}	0.01 .. 1000.0	15	16	562
Mean, st dev, and num obs of liquid particle radius	81	µm	0.0 .. 1000.0	15	16	577
Mean, st dev, and num obs of ice particle radius	82	µm	0.0 .. 100.0	15	16	592
Mean, st dev, and num obs of visible optical depth	83	Dimensionless	0.0 .. 50.0	15	16	607
Mean, st dev, and num obs of infrared emissivity	84	Dimensionless	0.0 .. 2.0	15	16	622
Mean, st dev, and num obs of vertical aspect ratio	85	Dimensionless	TBD	15	16	637
Mean, st dev, and num obs of adj. infrared emissivity	86	Dimensionless	0.0 .. 2.0	15	16	652
Mean, st dev, and num obs of adj. fractional area	87	Fraction	0.0 .. 1.0	15	16	667
Mean, st dev, and num obs of adj. effective temperature	88	K	0.0 .. 250.0	15	16	682
Mean, st dev, and num obs of adj. visible optical depth	89	Dimensionless	0.0 .. 400.0	15	16	697
Visible Opt Depth (day) / Infrared Emissivity (night) percentiles	90	Dimensionless	0.0 .. 50.0	65	16	712
Angular_Model_Scene_Type_Parameters						
Fractional area coverage	91	Fraction	0.0 .. 1.0	12	16	777
Mean and standard deviation of albedo	92	Dimensionless	0.0 .. 1.0	24	16	789
Mean and standard deviation of incident solar flux	93	W-h m^{-2}	TBD	24	16	813
Mean and standard deviation of LW flux	94	W-m^{-2}	0.0 .. 400.0	24	16	837
FSW_Surface_Only_Data						
Photosynthetically active radiation	95	W-m^{-2}	0.0 .. 780.0	1	16	861
Direct/Diffuse Ratio	96	N/A	0.0 .. 30.0	1	16	862
FSW_Adjustment_Parameter_Statistics						
Mean and std dev of adjusted precipitable water for clear skies	97	cm	0.001 .. 8.000	2	16	863
Mean and st dev of adjusted precipitable water for total skies	98	cm	0.001 .. 8.000	2	16	865
Mean and standard deviation of adjusted surface albedo	99	Dimensionless	0.0 .. 1.0	2	16	867
Mean and standard deviation of adjusted aerosol optical depth	100	Dimensionless	0.0 .. 2.0	2	16	869
Mean and std dev of adjusted skin temp. for clear skies	101	K	TBD	2	16	871
Mean and std of skin temp. adjustment for total skies	102	K	TBD	2	16	873
Total Meta Bits/File:	112					
Total Data Bits/Record:	14000					
Total Records/File:	2500					
Total Data Bits/File:	35000000					
Total Bits/File:	35000112					

Appendix C

Theoretical Notes

This appendix gives the derivation of equation for regional average of direct/diffuse ratio used in this subsystem.

C.1. Direct/Diffuse Averaging

At the surface, we have footprint values of the downward shortwave flux F_i and the direct/diffuse ratio r_i. It is required to form the average direct/diffuse ratio $\tilde{r}$ such that the average direct flux and average diffuse flux can be computed from this average ratio $\tilde{r}$ and the average flux $\tilde{F}$. By definition,

$$\text{Direct flux}i/\text{diffuse flux}i = r_i$$

We note that

$$\text{Direct flux} + \text{diffuse flux} = \text{Total flux}$$

It follows that for each CERES footprint

$$\text{Diffuse flux } i = F_i/(1 + r_i)$$

$$\text{Diffuse flux } i = r_i F_i/(1 + r_i)$$

The average direct flux is $\sum_i \frac{r_i F_i}{(1 + r_i)}$ and the average diffuse flux is $\sum_i \frac{F_i}{(1 + r_i)}$. The regional average direct/diffuse ratio is thus computed

$$\tilde{r} = \left(\sum_i \frac{r_i F_i}{(1 + r_i)}\right)\left(\sum_i \frac{F_i}{(1 + r_i)}\right)$$

The regional mean direct and diffuse components of downward shortwave radiation are given in terms of this mean ratio and the regional mean downward shortwave flux $\tilde{F}$ as

$$\text{Regional mean direct flux} = \tilde{r}\tilde{F}/(1 + \tilde{r})$$

$$\text{Regional mean diffuse flux} = \tilde{F}/(1 + \tilde{r})$$

C.2. Notes on Point Spread Function Weighted Statistics

The statistics

$$\hat{x} = \frac{\sum_i w_i x_i}{\sum_i w_i}$$

and

$$s^2 = \frac{\sum_i w_i (x_i - \hat{x})^2}{\sum_i w_i}$$

are to be computed for each CERES footprint, in which the x_i are computed from MODIS measurements and the w_i are the point spread function values at the MODIS measurement point (see section 4.4).

These statistics have the following properties:

I. $\hat{x}$ is an unbiased estimator of the mean of the x_i values.

II. The variance of $\hat{x}$ about the population mean is

$$\left(\sum_i w_i\right)^{-2} \sigma^2 \sum_i \sum_j w_i w_j \rho_{ij}$$

If the x_i are uncorrelated and the weights are 1, the sample mean variance reduces to $\frac{\sigma^2}{n}$.

III. The expected value of the s^2 statistic is $E[s^2] = \sigma^2\left[1 - \left(\sum_i w_i\right)^{-2} \sigma^2 \sum_i \sum_j w_i w_j \rho_{ij}\right]$. If the x_i are uncorrelated and the weights are 1, this expression reduces to the familiar expression for the sample variance: $E[s^2] = \sigma^2\left[\frac{n-1}{n}\right]$

We need to consider how we want to average the $\hat{x}$ and s over a region. If the correlations are included, the summations will be functions of the crosstrack scan angle α and may be computed once as a table look-up *if we assume we know the spatial correlation* $\rho_{ij.}$ Thus, we tabulate

$$F(\alpha) = \left[1 - \left(\left(\sum_i w_i\right)^{-2} \sigma^2 \sum_i \sum_j w_i w_j \rho_{ij}\right)\right]$$

whence we compute the unbiased estimate of the sample variance $\hat{\sigma}^2 = s^2 F^{-1}(\alpha)$. This quantity can then be spatially averaged. The problem is in the assumption of the correlation structure. When we examine the effects of this approximation, we have to ask, "What is the use of the variance once we have it?" Without an understanding of this, we have no way to assess this approximation or an alternative. If $F(\alpha)$ varies slowly with nadir angle, we then can average the CERES footprint s^2 values over a region to obtain an average s^2 value. However, it would be a gross approximation to compare the s^2 values for a region near nadir with those near the limb.

Clouds and the Earth's Radiant Energy System (CERES)

Algorithm Theoretical Basis Document

Time Interpolation and Synoptic Flux Computation for Single and Multiple Satellites

(Subsystem 7.0)

David F. Young[1]
Edwin F. Harrison[2]
Bruce A. Wielicki[2]
Patrick Minnis[2]
Gary G. Gibson[1]
Bruce R. Barkstrom[2]
Thomas P. Charlock[2]
David R. Doelling[1]
Alvin J. Miller[3]
Olivia C. Smith[4]
Joseph C. Stassi[4]

[1]Lockheed Engineering & Sciences Company, Hampton, Virginia 23666
[2]Atmospheric Sciences Division, NASA Langley Research Center, Hampton, Virginia 23681-0001
[3]Climate Analysis Center, Room 805, NOAA/NWS, Washington, DC 20233
[4]Science Applications International Corporation (SAIC), Hampton, Virginia 23666

CERES Top Level Data Flow Diagram

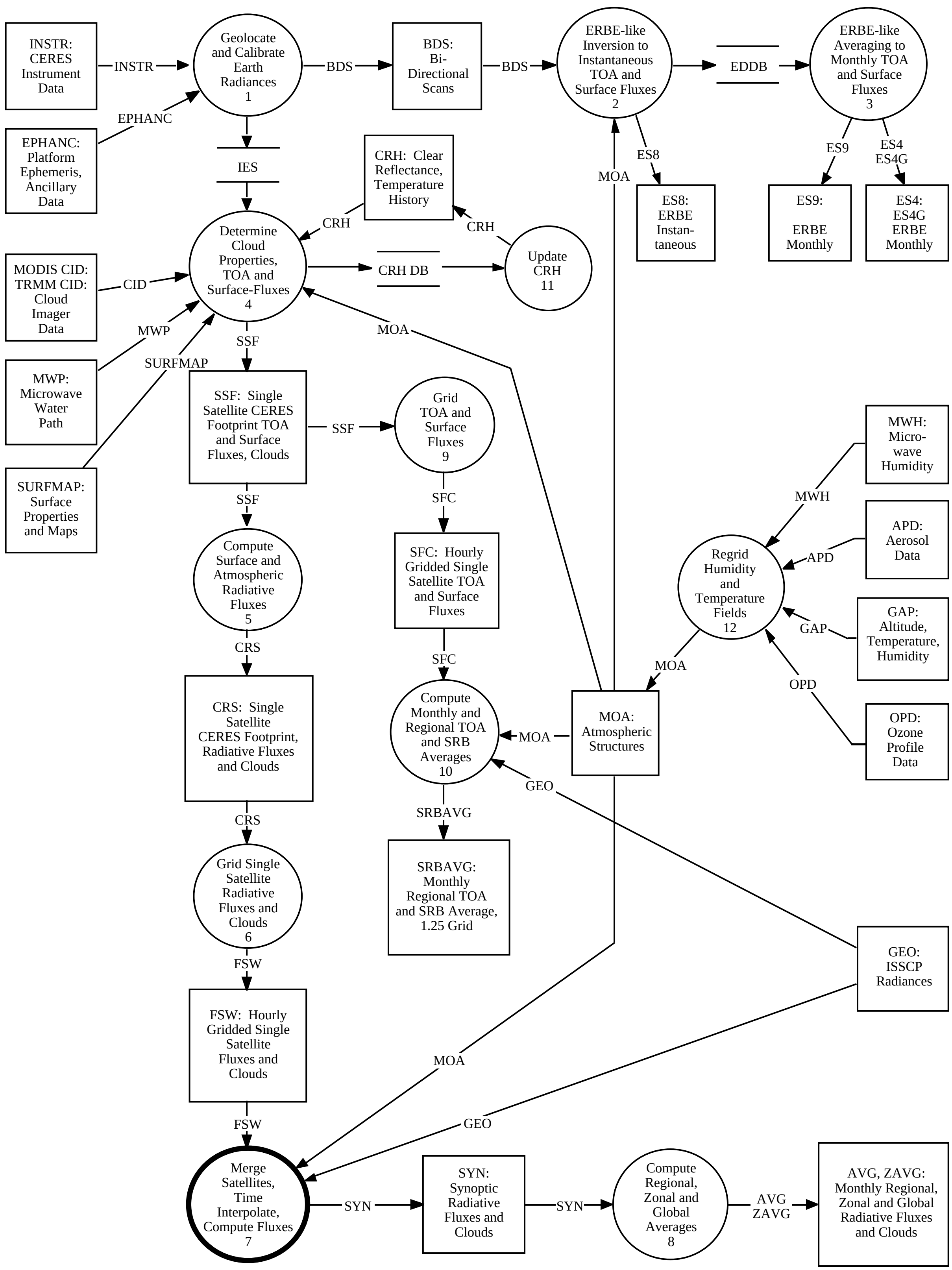

Abstract

The Clouds and the Earth's Radiant Energy System (CERES) Data Management System temporally interpolates CERES data in order to produce global, synoptic maps of top-of-atmosphere (TOA) fluxes and cloud properties on a 1.25° equal-area grid. These interpolated data are used as input and boundary conditions to the calculation of synoptic maps of the vertical structure of atmospheric and surface flux.

The chief input to the time interpolation process is the gridded shortwave (SW) and longwave (LW) TOA clear-sky and total-sky fluxes and cloud information provided by the FSW data product (see appendix A). These data contain spatial averages of one hour of CERES measurements on a 1.25° equal-area grid.

This process produces global maps of TOA total-sky LW and SW flux, TOA clear-sky LW and SW flux, TOA window radiances, and cloud properties at 0, 3, 6, ..., 21 GMT for each day of the month. Radiative fluxes at various levels in the atmosphere are then calculated using these data. The final data product contains synoptic maps of the above parameters plus radiative fluxes at four atmospheric levels (see appendix B).

The steps in producing synoptic maps are

1. *Merge gridded cloud and radiation data from multiple satellites*
2. *Regionally and temporally sort and merge ancillary geostationary data used in the interpolation of TOA fluxes*
3. *Interpolate cloud properties from the CERES times of observation to the synoptic times*
4. *Interpolate CERES TOA LW and SW fluxes to synoptic times using geostationary data to assist in modeling meteorological variations between times of observations*
5. *Use time-interpolated cloud properties to calculate radiative flux profiles as in subsystem 5, which are constrained by the synoptic TOA flux estimates*

7.0. Time Interpolation and Synoptic Flux Computation for Single and Multiple Satellites

7.1. Time Interpolation for Producing Synoptic Maps

7.1.1. Introduction

The CERES experiment (Wielicki and Barkstrom 1991) will produce a data set of highly accurate measurements of the incoming and outgoing energy in the Earth's climate system. As with any satellite experiment, the data will not be uniformly distributed in time and space. Instead, data will be arranged in patterns determined by the orbital characteristics of the satellites that are carrying the instruments. However, many researchers prefer data sets that are both global and ordered uniformly in time.

In order to provide such a product for potential data users, CERES will develop global synoptic maps of TOA fluxes and cloud properties as well as the vertical structure of atmospheric radiative fluxes. These maps will be produced for each day of data in 3-hourly intervals at 0, 3, 6, ..., 21 GMT.

Producing data sets for synoptic times ensures consistency with ground truth meteorological observations from weather station observations and radiosondes as well as with geostationary satellites which provide images at synoptic hours. The use of such data is valuable for CERES validation and for science studies using CERES radiation parameters. Also, calculating the atmospheric radiative fluxes at only the synoptic times minimizes the considerable computational resources required for this product. The production of a CERES synoptic data product is important for several reasons: (1) synoptic views provide a basis for studying the life cycle of cloud systems (Desbois et al. 1989; Garand 1988) and understanding the associated atmospheric meteorology, (2) synoptic views are very useful in validating the CERES data processing, particularly of time interpolation, and (3) the synoptic data product provides a regular data structure which simplifies the design of algorithms and operation of the data processing system. In addition to providing a fundamental tool for understanding the organization of cloud systems, synoptic views of cloud and radiation fields provide a major tool for diagnostic work on operational weather forecasting and general circulation models because the analysis fields are produced at synoptic times. Data that have been independently interpreted to such standard times provide stronger tests of the validity of the processes parameterized in the models than do monthly average data. The synoptic fields of radiation and clouds should be particularly valuable in developing and understanding of the role of clouds in the generation and dissipation of available potential energy, since the calculation of this quantity requires integration over approximately horizontal layers within the atmosphere.

For each CERES footprint, information is provided on up to four cloud pressure categories (for a detailed description, see section 4.4.). This cloud information is then used along with ancillary atmospheric sounding data to derive a radiative profile for each footprint consistent with the observed CERES TOA fluxes (subsystem 5). The cloud and radiative parameters are then spatially averaged onto the CERES 1.25° equal-area grid (subsystem 6). The data must then be temporally interpolated to produce synoptic images. It has been recognized that because of the highly nonlinear quality of the radiative fields, it would be difficult to retain internally consistent radiation fields while interpolating to times without measurements. In order to circumvent this problem, only the TOA total-sky and clear-sky SW and LW fluxes, the window channel radiance, and cloud properties will be interpolated to the synoptic times. The radiative profile will then be recalculated using the TISA-produced fields as constraints (section 7.2.). Monthly means can then be produced by averaging the synoptic fields (subsystem 8).

Time averaging techniques used in previous Earth radiation budget (ERB) satellite experiments such as the Earth Radiation Budget Experiment (ERBE) (Barkstrom 1984; Barkstrom and Smith 1986) concentrated on the combination of measurements and modeling of TOA SW and LW fluxes (Brooks et al. 1986). The CERES time-space averaging algorithm emphasizes and builds upon this strength. The temporal interpolation techniques will produce accurate estimates of TOA flux at the synoptic times; the TOA data are then used as the primary constraint to the radiation field calculations. Estimates of the cloud properties at synoptic times will also be provided for use in radiative transfer calculations. Cloud optical and physical parameters are adjusted during the Surface and Atmospheric Radiation Budget (SARB) calculations to better match the TOA flux constraint.

7.1.2. Algorithm Description

7.1.2.1. Time interpolation philosophy. The ERBE time interpolation method produced the most accurate estimates of monthly mean TOA LW and SW flux currently available (Harrison et al. 1990; Barkstrom et al. 1990). However, numerous simulations by the ERBE Science Team have shown that the ERBE time interpolation technique does not produce daily means and estimates of diurnal variability to the same degree of accuracy. This deficiency could introduce significant errors when producing synoptic maps of TOA flux. The primary difficulties in producing accurate measures on a shorter time scale involve limited temporal sampling and the lack of knowledge of variations in meteorology between measurements.

The problems of limited sampling must be addressed by the time interpolation process. The most severe effects of sparse sampling in the ERBE experiment occurred in the calculation of clear-sky fluxes. Much of this problem arose from the coarseness of the ERBE cloud identification process which systematically underestimated clear-sky occurrence. The improved cloud products for CERES will help alleviate this sampling problem since clear-sky identification will be performed with much greater accuracy. However, during periods when only one CERES instrument is flying, data sparseness can affect even the total-sky flux interpolations.

Of course, the temporal sampling can be improved through the use of multiple CERES instruments aboard different spacecraft. An ideal ERB mission would account for diurnal variability by employing a large fleet of satellites to make measurements at all times of day over all regions. In practice, however, only a limited number of satellites (1–3) are flown and the unsampled hours are filled in with diurnal models or data from other sources. The first CERES mission in 1997 will involve a single satellite (Tropical Rainfall Measuring Mission, TRMM) in 35° inclined orbit providing sampling only twice a day between about 45°N and 45°S. With the 1998 launch of the Earth Observing System (EOS)-AM platform in a Sun-synchronous orbit with an equatorial crossing local time of 1030, the diurnal sampling will increase to 4 times per day. In the year 2000, the EOS-PM platform will be launched into a Sun-synchronous orbit with an equatorial crossing time of 1330. CERES will then have 6 samples per day, assuming EOS-AM and TRMM are operating or their follow-on spacecraft with CERES instruments are launched. Simulation studies using hourly Geostationary Operational Environmental Satellite (GOES) data indicate that the ERBE time-space averaging algorithm gives regional monthly mean temporal sampling errors that are significantly reduced as more satellites are added. For example, the temporal sampling errors in SW flux are reduced from 9 W-m^{-2} for TRMM alone to 4 W-m^{-2} for TRMM plus EOS-AM, and down to 2 W-m^{-2} for TRMM plus EOS-AM and EOS-PM. Since satellites can fail prematurely, it is useful to provide a strategy to reduce time sampling errors, especially for the single satellite case. The CERES strategy is to incorporate 3-hourly geostationary radiance data to account for diurnal cycles which are insufficiently sampled by CERES. The key to this strategy is to use the geostationary data to assist in determining the shape of the diurnal cycle, but use the CERES observations as the absolute reference to anchor the more poorly calibrated geostationary data. One advantage of this method is that it produces 3-hourly synoptic radiation fields for use in testing global models, and for improved examination of the diurnal cycles of clouds and radiation.

CERES can indeed make significant improvements to the ERBE time interpolation process by using ancillary data to provide additional information concerning meteorological changes occurring between CERES measurements. The ERBE Science Team explicitly excluded the use of ancillary data in order to produce a self-contained and relatively straightforward climate data set specifically geared toward accurate measures of monthly mean TOA fluxes. The goals of CERES are more ambitious than ERBE. In addition to the products delivered by the ERBE experiment, CERES also provides extensive analyses of cloud properties as well as surface and atmospheric radiation parameters. In order to calculate these parameters, it is necessary to use ancillary data such as moderate resolution imaging spectroradiometer (MODIS) or Visible Infrared Scanner (VIRS) radiance data, atmospheric structure data, and constantly updated background surface data (see subsystem 4).

In order to meet the CERES goal of improved temporal averaging, numerous simulations were performed to explore techniques of incorporating additional data sources into the time averaging process. Since the main requirement of such data is to have enhanced temporal resolution, an obvious candidate data source is geostationary and polar-orbiting satellite radiance measurements. Geostationary data from such satellites as GOES, METEOSAT, INSAT, and GMS provide measurements of narrowband visible and infrared radiances for much of the globe (~50°N to 50°S) at a temporal resolution as fine as every hour. The polar-orbiting satellites provide much less temporal information, but are useful for providing information at higher latitudes.

Because of the excellent temporal resolution of geostationary data, many attempts have been made to derive broadband radiation budget parameters from these narrowband measurements (Minnis et al. 1991; Briegleb and Ramanathan 1982; Doelling et al. 1990). Generally, these studies have demonstrated that the narrowband measurements are insufficient for radiation budget calculations since they miss valuable spectral information contained in broadband observations. Minnis et al. (1991) showed that the LW narrowband-broadband relation varied significantly in time and space even when water vapor, surface type, and cloud data were considered. Figure 7.1-1 shows regional means and standard deviations of the differences between ERBE measured LW fluxes and broadband fluxes derived from GOES narrowband measurements using a global correlation that includes an atmospheric water vapor term. The overall relative error of the correlation is ~11 W-m^{-2} and mean biases greater than 15 W-m^{-2} are evident in many regions. Regressions performed on a region-by-region basis can reduce the relative error to 7.7 W-m^{-2}, and essentially eliminate the mean bias. However, these regional correlations require frequent updating to account for changes in calibration and seasonal variations in the narrowband-broadband relation. Thus, narrowband data should be used in climate studies only if the narrowband-broadband relationship is continually calibrated using coincident measurements with a broadband instrument such as CERES.

While narrowband measurements cannot be used directly for radiative studies, these data contain valuable information that can be used with a broadband monitoring satellite system such as CERES. In particular, these measurements provide a glimpse at the variations in meteorology occurring between the times of CERES observations. Several simulations have demonstrated that judicious use of geostationary data can enhance the accuracy of time interpolation of broadband observations. The techniques that produce the most accurate averages are described below.

For release 1, cloud conditions are assumed to vary linearly with time when producing input to the synoptic radiative transfer calculations. Since only radiances and no cloud information are provided by the narrowband data at synoptic times, all cloud information will necessarily be derived solely from the CERES analysis of MODIS or VIRS observations. Since this approach will, at times, produce cloud conditions that are inconsistent with the interpolated TOA fluxes, these cloud properties will be adjusted during the atmospheric flux calculations to obtain agreement between the interpolated and calculated TOA fluxes. In this way, monthly means can be computed from the synoptic grids of radiatively balanced data.

7.1.2.2. Organizing and merging spatially gridded observations. The first step in the time interpolation process is to accumulate and organize the observed CERES data. The primary input to the computation of synoptic maps is the gridded CERES SW and LW TOA fluxes and cloud information provided by the FSW data product. This input consists of regionally and temporally sorted averages of CERES measurements for each observed region of the 1.25° equal-area grid (see appendix A). As with the ERBE-like monthly time-space averaging product (see subsystem 3), one month of data will be processed together. In addition, each region will be analyzed independently of all others.

At this point in the processing, data from instruments on different satellites are combined. Whenever multiple-satellite data are available, measurements from all sampled hour boxes are used in the averaging process and the number of input files increases proportionally. When data exist for a given hour and region from more than one satellite, the data are linearly averaged.

The process of sorting and merging these data is very similar to that used in the processing of the ERBE-like data. The major difference is that the CERES grid contains approximately four times as many regions as used by ERBE. Fortunately, only a small number of the parameters from the FSW files need to be retained in this step. The relevant parameters from FSW which are used in the averaging process are the total-sky LW and SW TOA fluxes, the clear-sky TOA LW and SW fluxes, and the CERES-derived cloud information.

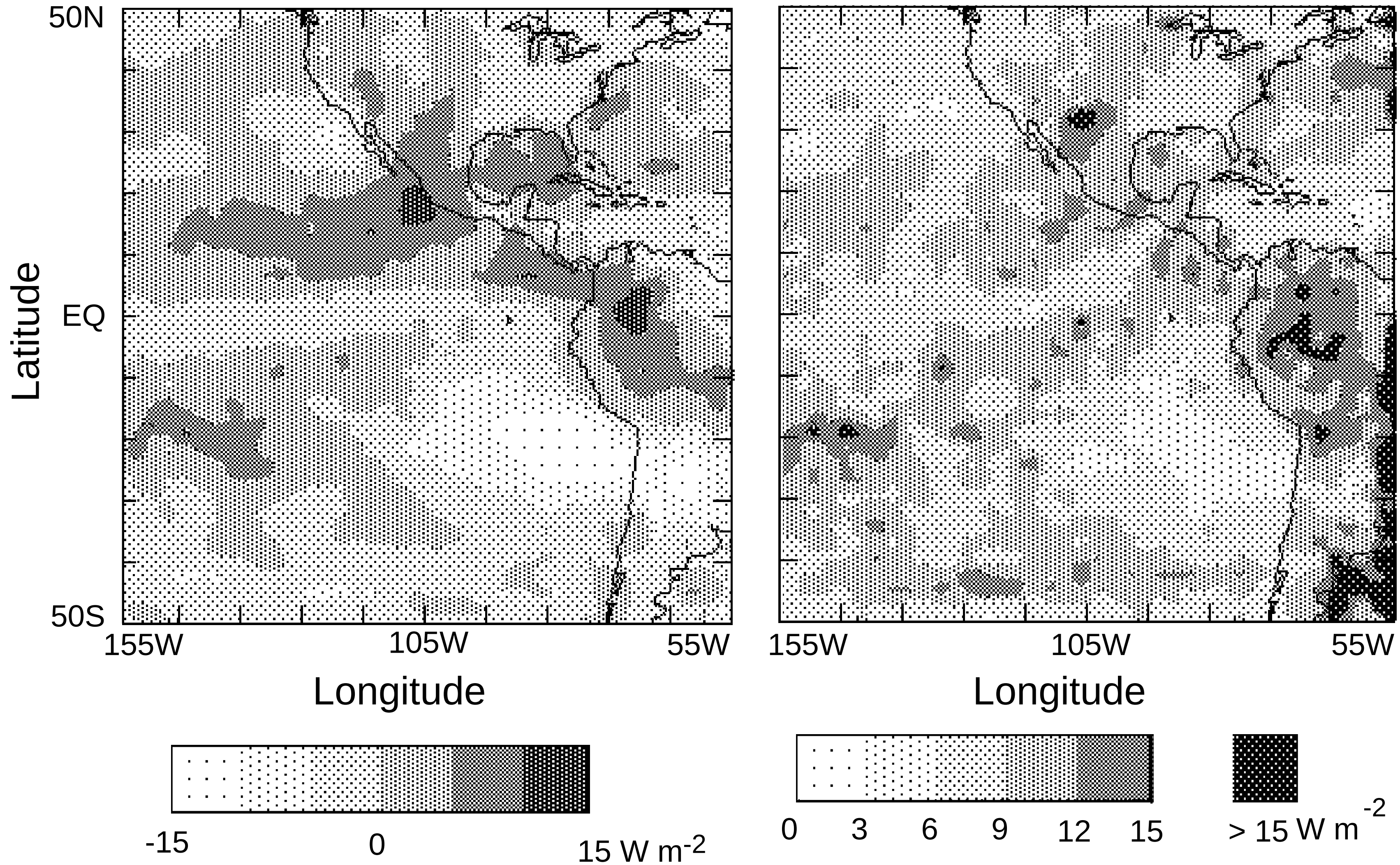

(a) Means.

(b) Standard deviations.

Figure 7.1-1. Regional means and standard deviations of the differences between ERBE broadband LW fluxes and inferred broadband fluxes derived from GOES narrowband IR radiances.

7.1.2.3. Regridding of geostationary data. The next step in the time interpolation process is the organization of the geostationary data. The most likely data source for the geostationary data will be the International Satellite Cloud Climatology Project (ISCCP) B3 or DX data. These data are provided at 3-hourly intervals at 0, 3, 6, ..., 21 GMT. The data are a subset of the complete, high resolution geostationary data. The complete data set has been subsampled at a spatial resolution of ~30 km. Only calibrated radiance values from the visible and infrared window channels are included in this data set. One advantage to the B3 or DX data sets over the ISCCP gridded products (such as the C1) is that the data can be sorted and averaged onto the CERES 1.25° equal-area grid. Additionally, the gridded ISCCP SW products are restricted to times with solar zenith angle less than 72.5°, while the B3 product includes the data at higher angles. This will provide better temporal sampling which is very important for the time interpolation of SW flux.

7.1.2.4. Time interpolation of cloud properties. CERES will advance the understanding of the Earth's radiation budget through a more detailed description of the effects of clouds. Extensive information concerning the physical and radiative properties of clouds is provided with each CERES footprint. After the CERES footprints are sorted and averaged onto the CERES 1.25° equal-area grid, these cloud data will be binned and stored in four separate data structures. These data structures, which are discussed in detail in section 4.4. and subsystem 6, are reviewed here for clarity since each is necessary as input for different aspects of time interpolation.

The cloud imager data have been sorted primarily as a function of cloud-top pressure. Four main pressure categories have been identified for use throughout the CERES Data Management System: low ($P > 700$ hPa), lower middle ($700 \text{ hPa} > P > 500$ hPa), upper middle ($500 \text{ hPa} > P > 300$ hPa), and high ($P < 300$ hPa). The vertical spacing of these categories (~3 km) allows the assumption that the cloud properties of these four categories can be spatially and temporally averaged independently. From these four categories, 11 cloud conditions are possible: clear, the four categories occurring as single layer clouds, and the six possible two-layer conditions (high over low, etc.).

The first cloud data structure, denoted as cloud overlap conditions, is simply a vector of frequency of occurrence for each of the 11 possible cloud conditions.

The second data structure is cloud category properties, which contains the means and standard deviations of each of the cloud properties detailed in table 4.4-3 for each of the four cloud pressure categories.

The third data structure is column-averaged cloud properties. These data are averaged using five different weighting schemes that reflect the needs of different potential users of CERES data. Separate statistics using different averaging schemes are to be compiled for two main groups of users. The first group of users is the atmospheric radiation community. These researchers are interested in studying the effects of changes in cloud radiative forcing. In order to conserve radiative properties during the averaging process, parameters saved for this group should be weighted by their effect on cloud radiative forcing. The second group of CERES users is the atmospheric dynamics community. These researchers are interested in cloud generation/dissipation parameterizations to be used in general circulation models. In contrast with the averaging used to preserve radiative features, average properties to be used by this group of researchers should be weighted by the liquid or ice water volume in a region. The details of the five weighting schemes are described in subsystem 6.

The fourth cloud data structure is the angular model scene class. This structure is analogous to the scene fraction and albedo arrays provided for each hour box in the ERBE-like processing. Scene fraction, mean albedo, mean LW flux, and mean incident solar flux are provided for each angular distribution model (ADM) class. For release 1, the ADM classes are limited to the twelve ERBE scene types (Suttles et al. 1988 and 1989). For later releases, new ADM's will be developed as discussed in section 4.5.

The interpolation of these cloud data to synoptic times is performed using three main assumptions:

1. The properties of the four cloud pressure categories can be interpolated independently
2. Cloud properties for each region will be interpolated independently from surrounding regions
3. Variations in cloud properties between CERES observation times will be modeled as linear

The linear variation assumption is applied in one of two ways, depending on the cloud conditions of the two points between which the interpolation is performed. If a nonzero cloud amount exists for a given cloud pressure category at both times, then the means and standard deviations of all cloud properties are linearly interpolated with respect to time. This case is illustrated in figure 7.1-2a. The sole exception to this is the visible optical depth, which is recalculated from the interpolated values of liquid (or ice) water path and particle size using the relationships described in subsystem 4. If, however, only one of the two observation times contains a nonzero cloud amount for the cloud category, then only cloud amount is linearly interpolated. As shown in figure 7.1-2b, the remaining properties are assumed to be constant throughout the time period, but the cloud simply reduces in area coverage as if it were advecting out of the region.

The averaging techniques are performed on each of the four cloud data structures. The first two structures, the cloud overlap conditions and the cloud category properties, are used as initial conditions of the radiative transfer calculations. The fourth structure is used in the TOA SW flux interpolation process to provide information for the selection of ADM's used with broadband fluxes derived from geostationary narrowband SW data. The column-averaged data are not used in the production of the synoptic radiative fields, but are passed along to produce monthly mean information concerning the cloud conditions associated with the radiation budget.

7.1.2.5. Time interpolation of total-sky TOA LW flux. The TOA LW flux is interpolated to the synoptic times in one of two ways. The first, termed method 1, is identical to the technique used in the ERBE-like processing. This technique, which uses a combination of linear interpolation and idealized diurnal models, is described in subsystem 3. An example of results using this method are given in Harrison et al. (1988).

The chief improvement proposed for method 2 is the inclusion of narrowband geostationary and polar-orbiting satellite-derived information. Instead of the combination of linear interpolation and idealized half-sine curves used by the ERBE-like technique to fit the observations, method 2 uses narrowband data to provide a more accurate picture of the shape of the curve that is fit to the observations.

For release 1, method 2 is used whenever possible. However, geostationary data are not available for all latitudes, and occasional gaps can occur in the data record (such as the unavailability of INSAT data). Whenever narrowband data are not available or are inadequate, the TOA fluxes are derived using method 1.

Narrowband radiances are transformed into broadband fluxes using the regression techniques developed by Minnis et al. (1991). The regression is derived from coincident calibrated geostationary and CERES measurements and ancillary relative humidity data available from the ASTR atmospheric data set. The form of the regression is:

$$F_{bb} = a_0 + a_1 F_{nb} + a_2 F_{nb}^2 + a_3 F_{nb} \ln(rh) \tag{7.1-1}$$

where F_{bb} is the LW broadband flux, F_{nb} is the narrowband flux, rh is the column-averaged relative humidity, and a_i are the derived coefficients. The LW narrowband radiance is converted to narrowband flux by:

$$F_{nb} = \frac{6.18 I_{nb}}{\gamma(\theta)} \tag{7.1-2}$$

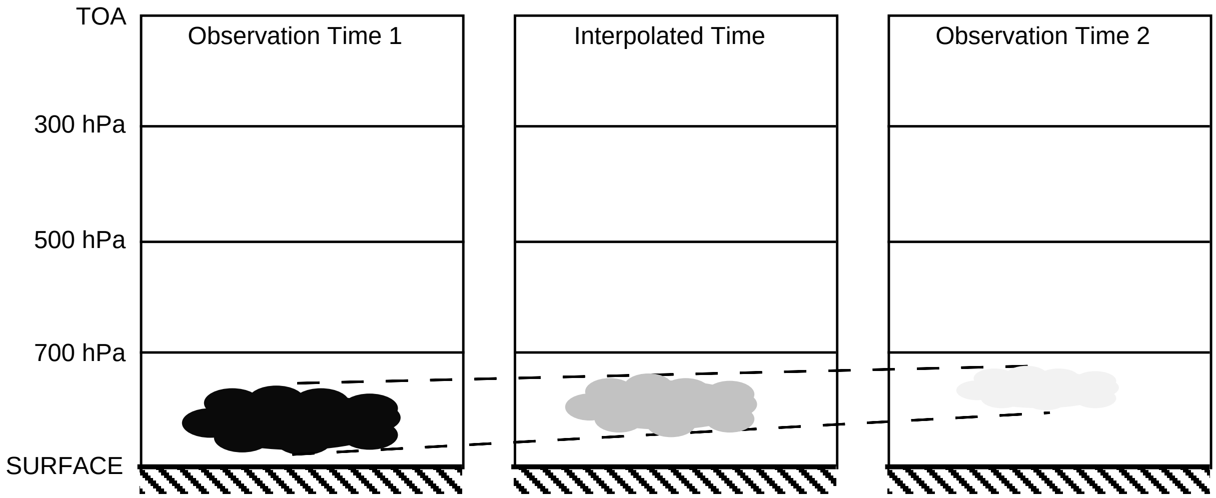

(a) Cloud properties are linearly interpolated between two cloud observation times.

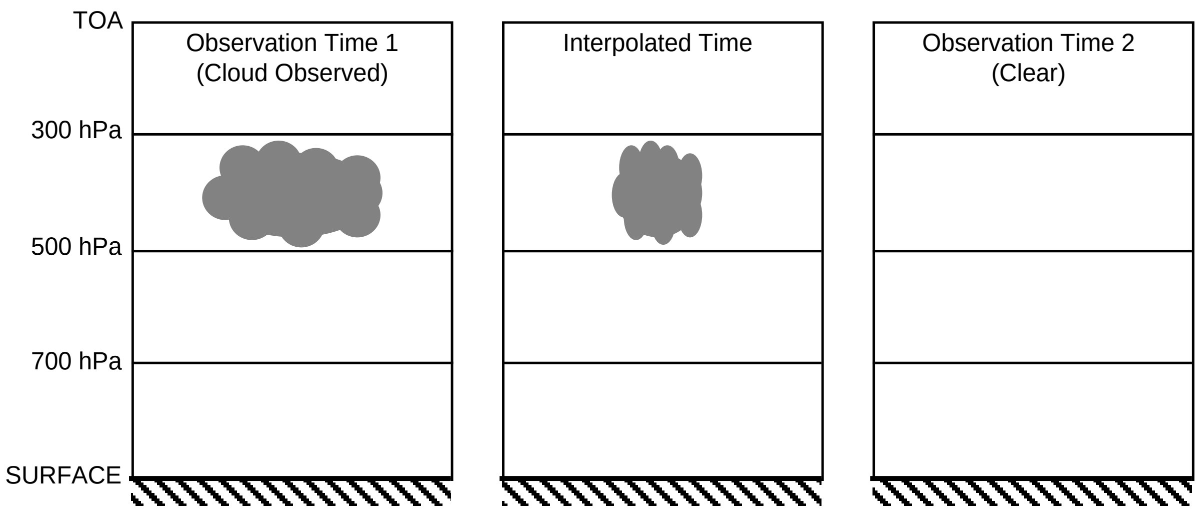

(b) All properties except cloud amount are assumed constant between cloud observation time 1 and clear observation time 2.

Figure 7.1-2. Temporal interpolation of cloud properties.

where I_{nb} is the LW narrowband radiance, $\gamma(\theta)$ is the longwave limb-darkening function at viewing zenith angle θ, and 6.18 represents the product of the limb darkening function integrated over an entire hemisphere and the narrowband spectral interval (Minnis et al. 1991).

As discussed above, Minnis et al. demonstrated that there is significant variability in the narrowband-broadband relationship both regionally and temporally. In order to account for temporal variability, the regressions are rederived each month using global data. Separate correlations are performed for ocean and land regions. Since the derivation of separate regressions for each CERES region for each month of data may not be feasible, another technique is required to account for regional variations in the correlation. Once a complete time series of simulated broadband measurements is constructed for the region, the derived LW fluxes at all hours are normalized to the nearest CERES observation of flux. This renormalization is sufficient to reduce the residual regional variance from the narrowband-broadband regression. For points between two CERES measurements, the normalization is linearly scaled inversely by the time difference between the hour in question and the times of the observations.

The renormalization of the broadband LW curve derived from the narrowband radiances to the nearest CERES observation assures that the final diurnal variability assumed in the time interpolation process is directly tied to the measured fluxes. This process also will reduce any errors incurred by variations in the calibration of the narrowband instruments. The narrowband data are used simply to provide extra information concerning meteorological variations between the measurements. As more than one CERES instrument becomes operational, the reliance on the narrowband data to provide the diurnal shape will diminish. With the improved time sampling, the interpolated curves will be dominated by the CERES observed fluxes.

Several studies have been performed to demonstrate the benefits of incorporating narrowband measurements into the averaging process (Harrison et al. 1994). Past studies have shown that the use of techniques such as the half-sine fit used by ERBE over land regions is more effective than linear interpolation in reproducing the LW diurnal variability seen in narrowband measurements (Brooks and Minnis 1984). Studies such as these rely on using 1-hourly GOES data converted to broadband flux using narrowband-broadband regressions as a reference data set. The effects of sampling patterns and the relative errors inherent to various interpolation schemes can be evaluated by sampling this reference set and comparing the results of the interpolation with the reference set.

Unfortunately, in order to show an improvement in interpolation using method 2, it is necessary to have three independent data sets: the broadband measurements, the narrowband time series, and an additional broadband reference data set. Since the GOES data are used in the averaging process, it is improper to use GOES as the reference data set. In addition, there is no 1-hourly global broadband data set to use as the truth.

This problem is overcome by using ERBE data from two different satellites, ERBS and NOAA-9, as two independent data sets. Observations from one satellite are interpolated to the observation times of the other using four different techniques (denoted as techniques a–d). Technique (a) is the ERBE-like combination of linear and half-sine interpolation of method 1. The geostationary-data-enhanced technique described above is performed in three ways. The first, (b), uses 1-hourly GOES data as a best-case test. The second approach, (c), uses the 3-hourly time sampling that is most likely to be available during CERES processing. Finally, in method (d), ERBE measurements are predicted simply using the 3-hourly narrowband measurements converted to broadband using the regression fit, but without the normalization to ERBE to account for regional variations. This method is included to demonstrate the necessity of continually anchoring the narrowband-derived fluxes to the measurements in order to produce the most accurate time-averaged fluxes possible.

A comparison of two of these techniques, (a) and (c), is displayed in figure 7.1-3 for an ERBE 2.5° region over New Mexico during the first 15 days of July 1985. The top curve shows the ERBE-like technique (a), and the bottom curve is the normalized 3-hourly narrowband shapes technique (c). In both figures, ERBS observations of TOA LW flux are displayed as solid squares and NOAA-9 observations are open circles. The interpolation techniques were applied to the NOAA-9 data in order to predict the ERBS observations. Both techniques do a good job on days with adequate sampling and constant cloudiness such as days 6–8 and 10–12. However, the ERBE TSA severely misses several nighttime points during the first three days of the period, as well as daytime points on days 6 and 14. Method (c), however, does a much improved job of filling in the fluxes in the hours between the observations. In particular, the predicted daytime fluxes on day 5 and the nighttime fluxes on days 1–4 are closer to the ERBS values. A few ERBS fluxes have been missed because of the 3-hour time resolution of the narrowband data, but, overall, method (c) shows a substantial improvement over method (a).

The results for the four interpolation techniques are summarized in table 7.1-1 for all 2.5° regions between 50°N–45°S latitude and 155°W–55°W longitude during the entire month of July 1985 and between 50°N–45°S latitude and 145°W–45°W longitude during April 1985. The first row of the table contains a comparison of coincident ERBS and NOAA-9 ERBE observations. Data from all regions

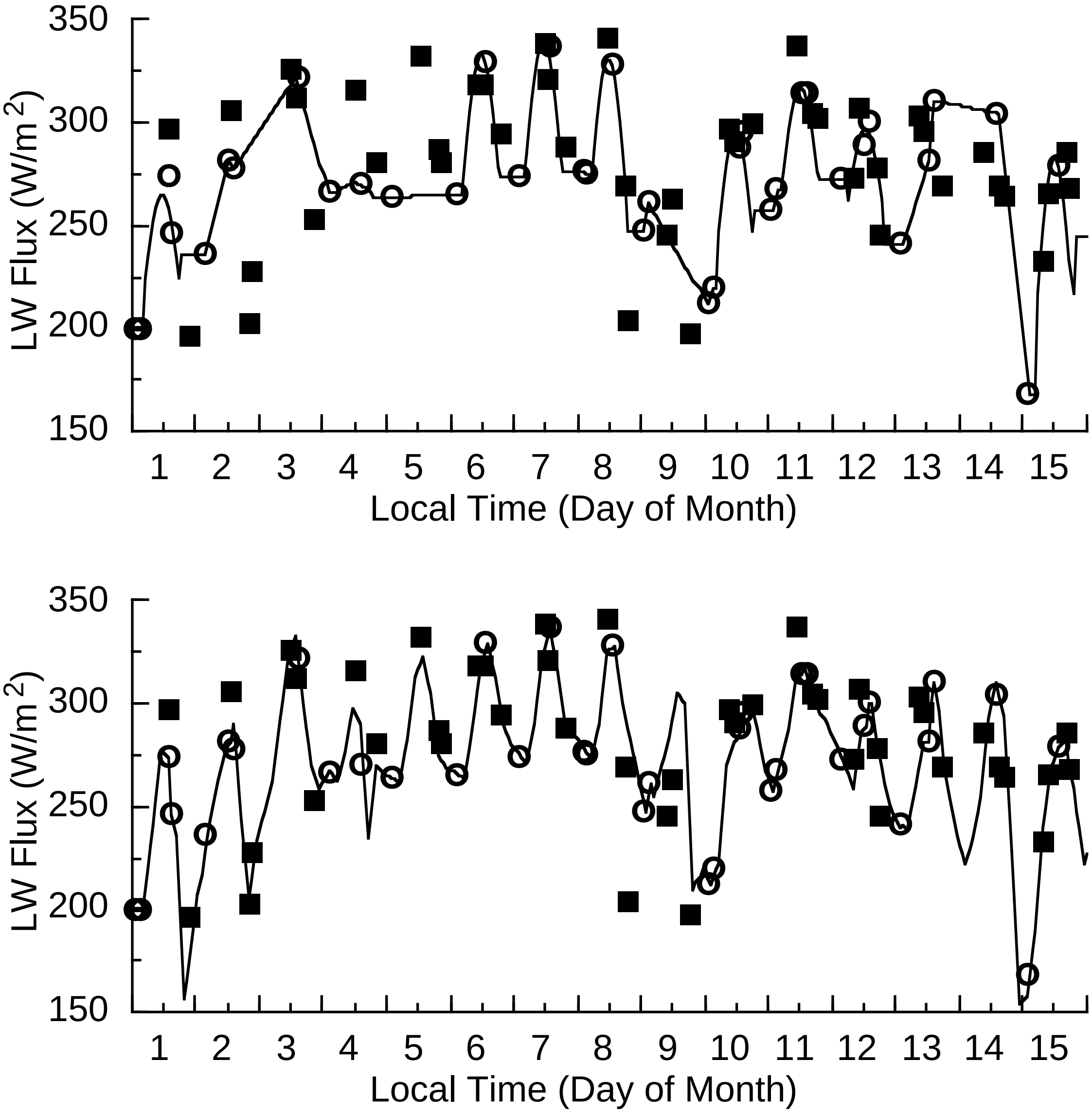

Figure 7.1-3. Time series of ERBE ERBS (■) and NOAA-9 (❍) LW flux observations and interpolated values from July 1985 over New Mexico. The top curve shows the ERBE time interpolated values; the bottom curve shows the geostationary-data-enhanced interpolation.

viewed by both ERBE instruments during the same hour are included. Since this comparison is performed using data averaged in coincident hour boxes, any difference between the two can be due to a combination of temporal and spatial variations within the 2.5° region over one hour as well as miscalibration between the two instruments or errors in the ADM’s used to convert the radiances to fluxes. A 2.4 W-m^{-2} bias and 10.6 W-m^{-2} instantaneous rms error (difference) exists between the two data sets in July. The April data show similar values of -0.1 ± 10.0 W-m^{-2}. An estimate can be made of the magnitude of the errors due to the ADM’s. When the two instruments view the scene with viewing zenith angles within 10° of each other, the rms differences are reduced to 5–6 W-m^{-2} for both months while the biases remain unchanged.

Although the overall biases are small (less than 1% of the mean flux), they are significant to this study. The results of the various time interpolation schemes must be compared with these coincident biases. A perfect time interpolation should not produce a zero bias, but rather should reproduce the bias in the coincident ERBS and NOAA-9 data.

Table 7.1-1. Comparison of LW Flux Time Interpolation Techniques Using ERBE Data From (a) July 1985 and (b) April 1985. Instantaneous Mean and rms Differences (W-m^{-2}) Between NOAA-9 LW Flux Measurements and Fluxes Predicted From ERBS Observations

(a) July 1985	NOAA-9 mean flux	Total error		Time interpolation error	
		Mean	rms	Mean	rms
Coincident data	243.6	2.4	10.6	-	-
a) ERBE TSA	246.5	2.8	16.9	0.4	13.2
b) w/ 1-hourly GOES	246.5	3.1	11.4	0.7	4.2
c) w/ 3-hourly GOES	246.5	2.8	12.0	0.4	5.6
d) Non normalized/3 hr	246.5	2.6	14.4	0.2	9.7

(b) April 1985	NOAA-9 mean flux	Total error		Time interpolation error	
		Mean	rms	Mean	rms
Coincident data	246.6	–0.1	10.0	-	-
a) ERBE TSA	246.2	0.7	15.7	0.8	12.1
b) w/ 1-hourly GOES	246.2	0.8	11.3	0.8	5.3
c) w/ 3-hourly GOES	246.2	0.7	11.8	0.7	6.3
d) Non normalized/3 hr	246.2	0.2	14.9	0.2	11.0

The successive rows of table 7.1-1 show the capability of each interpolation technique to reproduce the NOAA-9 observations by temporally interpolating the ERBS data. The mean LW flux from NOAA-9 is provided in column 1. The next two columns contain the absolute instantaneous mean and rms difference between the observed NOAA-9 flux and the flux predicted for that hour by interpolating the ERBS observations. Estimates of the mean and rms error from the time interpolation processes have also been included in columns 4 and 5. The rms due to time interpolation is calculated assuming that the time interpolation error is independent of the rms difference between coincident ERBS and NOAA-9 measurements. It is calculated as:

$$rms_{ti}^2 = rms_T^2 - rms_o^2 \tag{7.1-3}$$

where rms_T is the total rms from the technique, rms_{ti} is the rms of the time interpolation technique, and rms_o is the rms from comparison of coincident ERBS and NOAA-9 observations. The mean time interpolation error is simply the difference of the total mean error and the mean difference in the coincident fluxes.

It is apparent that the lowest rms errors are obtained using narrowband data with 1-hour temporal resolution. However, there is only a slight (1–2 W-m^{-2}) degradation in the rms error when 3-hourly data are used. There is, however, a substantial improvement in the time interpolation error using the GOES data over the ERBE time averaging scheme. The rms error due to time interpolation decreases from 13.2 W-m^{-2} to only 5.6 W-m^{-2} for the July data and from 12.1 W-m^{-2} to 6.3 W-m^{-2} for April. In addition, the mean bias is less than 1 W-m^{-2} for all cases.

Clearly, the renormalization process is necessary for accurate temporal interpolation. Method (d) simply used the narrowband-broadband correlations to produce the LW flux time series from the GOES data. The instantaneous time interpolation rms error is increased from 5.6 W-m^{-2} to 9.7 W-m^{-2} in July and from 6.3 W-m^{-2} to 11.0 W-m^{-2} in April. The latter error is only a minimal improvement over the ERBE-like method (a). Through renormalization, the time series of LW flux is accurately tied to the original observations. Region-to-region variations in the narrowband-broadband correlations and temporal variations in the narrowband calibration are properly accounted for.

The statistics presented above from these simulations have related to the errors involved in the prediction of instantaneous fluxes. The changes in the temporal interpolation process being proposed here are mainly for improving these instantaneous estimates of flux. It is crucial that any proposed time interpolation technique does not significantly affect the monthly means. Harrison et al. (1990) demonstrated that ERBE regional monthly mean LW flux estimates are accurate within 1 W-m^{-2} if data from two satellites are used. For July, over the entire GOES region, the ERBE method (a) produces monthly mean flux averaged over all regions of 249.0 W-m^{-2}. For methods (c) and (d), the averages are 248.8 W-m^{-2} and 248.4 W-m^{-2}, respectively. Thus, the enhancements to the interpolation process are not adversely affecting the monthly means. Once again, the anchoring of the LW fluxes to the observations in method (c) produces an improvement over the results of method (d).

Another advantage in the use of narrowband data for the interpolation process is that sampling effects are minimized. This is demonstrated by examining the difference in regional monthly mean fluxes calculated using the two ERBE instruments. The polar-orbiting NOAA-9 satellite produces ERBE sampling near 0230 and 1430 local time throughout the month. The local time of observations from the precessing ERBS satellite slowly changes during the month. The region-to-region rms difference between the monthly mean estimates from the two satellites is a measure of independence of the interpolation to sampling effects. For April, when the mean difference between the two data sets is nearly zero, the regional rms difference in monthly mean is 2.4 W-m^{-2} for method (a) and 1.7 W-m^{-2} for method (c). As expected, the incorporation of the time series of narrowband data increased the accuracy of filling in flux values for times between measurements.

Since the lowest interpolation errors are associated with the method that involves 1-hourly narrowband data, any changes to the other techniques that better simulate the 1-hourly narrowband time series from the 3-hourly data should also improve broadband interpolation. Therefore, additional simulations can be performed solely in the narrowband to see which technique best recreates the 1-hourly data set. For these future studies, the complete GOES data set will be used as a reference. Interpolation errors from these studies can only be interpreted as relative errors; the total error is a combination of the errors in simulating the 1-hourly set from the 3-hourly plus the errors in interpolating broadband fluxes from the 1-hourly data.

Future simulations will also use data from December 1986, which is the only month to have three ERBE scanning instruments operating simultaneously. These data can be used to study the advantages of a two-satellite system by using data from the two sun-synchronous ERBE satellites to predict the ERBS observations.

7.1.2.6. Time interpolation of clear-sky TOA LW flux. The ERBE-like averaging technique does not yield clear-sky flux estimates for all hours of the month. The relative scarcity of clear-sky flux estimates derived from ERBE data necessitated the use of monthly-hourly fits instead of continuous interpolation. Since much of the CERES effort is geared toward studying the effects of clouds on the Earth's radiation budget, there will be a significant improvement in the quality of clear-sky data. The misclassification of clear scenes as partly cloudy will no longer be a problem.

Because of these improvements to the CERES clear-sky data set, time interpolation of clear-sky LW flux is performed in a manner identical to the total-sky product. The lack of geostationary data is not serious in the case of clear-sky modeling. The main information provided by the narrowband data is changes in meteorology and cloudiness. For clear-skies, the idealized ERBE models work well and will be used in release 1.

One consideration for the input to the radiative transfer calculations to be performed on the synoptic maps is that clear-sky TOA LW flux is necessary at each synoptic time. Unfortunately, there may be no clear-sky measurements within a day of the desired time. In these cases, clear-sky fits from the nearest day with data will be used.

7.1.2.7. Time interpolation of total-sky TOA SW flux. The decision not to use auxiliary data to assist in the time interpolation of ERBE data not only affected the LW flux means, but also caused similar deficiencies in the SW interpolation process. Between the times of ERBE observations, an assumption of constant or linearly varying cloud conditions was made for all interpolations. This, of course, can lead to biases in the data, particularly in the case of a single satellite-borne instrument measuring SW flux only once each day. Monthly-hourly SW flux estimates for areas with persistent diurnal variations of clouds such as tropical cumulus or coastal stratocumulus regions can have significant errors (Minnis and Harrison 1984). As is the case with LW flux, method 1 for interpolating SW flux is analogous to the ERBE-like interpolation process and method 2 incorporates narrowband geostationary data to provide information concerning changing meteorological conditions between CERES measurements.

The averaging of SW data is not as straightforward as LW data. Unlike the LW flux case, the SW flux interpolation process is heavily dependent upon models. First, anisotropic effects must be accounted for using bidirectional reflectance models. Secondly, whenever averaging data spatially or temporally, all of the data must be adjusted to a common solar zenith using ADM's. For release 1, the ERBE ADM's will be used. The ADM's provide a description of the variation of broadband albedo with changing solar zenith angle. As long as cloud conditions remain constant, SW flux can be temporally interpolated accurately. For regions with diurnal variations in cloudiness, information concerning the variation in cloud conditions must also be available to temporally interpolate TOA SW flux properly.

As stated above, method 1 for SW flux is based upon the ERBE-like SW flux interpolation process described in subsystem 3. Separate means of albedo are stored in the angular model scene class cloud data structure along with scene fraction for each ADM class. Each ADM class albedo is interpolated to the synoptic time using the related ADM. The scene fractions are linearly interpolated to the synoptic time and then used to combine the individual albedos into a single total scene albedo. The SW flux is then computed by multiplying the total albedo by the incident solar flux for that time. The chief difference with the ERBE-like process is that a varying surface type is allowed within a CERES region, whereas ERBE assumes that the surface scene is constant for the month. Thus only four possible ADM classes are used in ERBE, but a single CERES region could possibly include all twelve. This change should not increase time interpolation error and, in fact, should produce a more accurate selection of ADM's.

The introduction of narrowband data into the SW flux interpolation process is more complicated than for the LW. In addition to the problem of simulating broadband fluxes from narrowband measurements as is done with the LW, the narrowband SW radiances must also be converted into fluxes using the proper ADM's. However, the improvement in temporal interpolation derived from the increased information concerning meteorology changes outweighs the narrowband-broadband flux calculation errors. Variations in cloudiness have a much greater impact on the SW. A change from a 100% clear scene to 100% overcast may result in a decrease in LW flux of 20–30%, but total-scene albedo may increase by 400–500%. Thus, the increased knowledge gained from the geostationary data concerning changes in clouds can be crucial to improving time interpolation.

The first step in SW method 2 is the time interpolation of the CERES cloud properties as described in section 7.1.2.4. Once the angular model scene class cloud data are interpolated to each synoptic time, the narrowband radiances are converted to narrowband albedos using the CERES ADM's.

$$\alpha_{nb} = \frac{(\pi I_{nb} / S_v \cos\theta_o)}{\left(\sum_{i=1}^{12} R_i \alpha_i f_i / \sum_{i=1}^{12} \alpha_i f_i i \right)} \tag{7.1-4}$$

where α_{nb} is the narrowband albedo, I_{nb} is the mean narrowband SW radiance within the CERES region, S_v is the Earth-Sun distance-corrected narrowband solar constant (which has a nominal value of 526.9 W-m^{-2}sr$^{-1}\mu$m^{-1}), and α_i, f_i, and R_i are the CERES albedo, scene fraction, and bidirectional anisotropic factor for ADM class *i*. interpolated to the synoptic time. Note that these albedos, α_i, are only initial estimates used solely for more accurately weighting the mean anisotropic factor necessary for the calculation of the total albedo. The CERES broadband anisotropic factors are used in this calculation. Doelling et al. (1990) showed that the use of ERBE broadband anisotropic factors in the calculation of albedos from GOES measurements did not degrade the regressions between GOES and ERBE albedos.

The narrowband albedos are converted to estimates of broadband albedos using regressions of the form used by Doelling et al. (1990):

$$\alpha_{bb} = b_0 + b_1\alpha_{nb} + b_2\alpha_{nb}^2 + b_3\ln(\sec(\theta_0)) \tag{7.1-5}$$

where α_{nb} is the narrowband albedo, α_{bb} is the broadband albedo, and θ_o is the solar zenith angle at the center of the region at the synoptic time. Separate regressions are performed for ocean and land regions.

A time series of broadband albedos calculated from narrowband measurements in the above manner can still contain significant errors (see Doelling et al. 1990; Briegleb and Ramanathan 1982). Doelling et al. found that regressions of the form of 7.1-5 have rms regression errors in excess of 14%. In addition, strong region-to-region variations in the relationship exist. The truest measurements of broadband SW flux are derived from broadband instruments such as CERES. A time series constructed from narrowband measurements can only be used as a guide for accounting for changes in cloud conditions between the CERES observation times. As with the use of narrowband data in the LW flux interpolation process, it is imperative that the narrowband data not dominate the averaging process. Therefore, the time series must be normalized to the CERES broadband observations.

The accuracy of this interpolation technique was tested in a fashion similar to the LW technique. ERBE measurements from ERBS were used to predict SW flux values measured from NOAA-9 using three techniques. The first (a) is the ERBE technique. The other techniques employ narrowband SW radiances from GOES. The difference between the techniques is in the cloud data used to select the ADM's necessary to convert the narrowband radiances into fluxes. The interpolation is first done using cloud amount, and cloud and clear reflectances derived from the narrowband data using the hybrid bispectral threshold method (Minnis et al. 1987). The results from this technique represent best case examples and are labeled (b) and (c) when applied to 1-hourly and 3-hourly GOES data, respectively. The next two techniques, (d) and (e), use linearly interpolated ERBE cloud amounts and albedos to select the proper anisotropic factor. Technique (d) uses 1-hourly GOES data; technique (e) uses 3-hourly data. These methods are closer to the technique that will be used in release 1. A final method (f) is identical to method (e), but does not include the re-normalization of the narrowband-derived fluxes to the nearest observation.

The results are shown in table 7.1-2. As is the case with the LW flux, there is a significant bias between coincident ERBS and NOAA-9 measurements. For July, the instantaneous mean difference is 5.2 W-m^{-2}, with a 36.5 W-m^{-2} rms. For April, the values are 5.1 ±39.1 W-m^{-2}. These differences are much larger than the corresponding values associated with the LW flux. This is due to the greater dependence on ADM's for deriving SW flux from the observations. When the coincident comparison is limited to times when both instruments are viewing within 20° of nadir, the mean bias in July is −1.4 W-m^{-2} and the rms difference falls to only 13.1 W-m^{-2}, which is of the same magnitude as the longwave. Unfortunately, the additional errors associated with model selection hamper some of the comparisons in the simulations. Since the mean differences of even coincident data are strongly angle dependent, it is difficult to determine the absolute accuracy of the averaging techniques. However, the relative effectiveness of the methods can be measured by comparing the rms errors. Thus, analysis of the simulations will stress a comparison of the instantaneous rms errors, not the biases.

Table 7.1-2. Comparison of SW Flux Time Interpolation Techniques Using ERBE Data From (a) July 1985 and (b) April 1985. Instantaneous Mean and rms Differences (W-m^{-2}) Between NOAA-9 LW Flux Measurements and Fluxes Predicted From ERBS Observations.

(a) July 1985	NOAA-9 mean flux	Total error		Time interpolation error	
		Mean	rms	Mean	rms
Coincident data	259.4	5.2	36.2	-	-
Scaled coincident data	228.5	4.6	32.2	-	-
a) ERBE TSA	228.5	0.0	53.8	–4.6	43.1
b) w/ 1-hourly GOES + GOES clouds	228.5	–1.0	35.1	–5.6	14.1
c) w/ 3-hourly GOES + GOES clouds	228.5	–0.8	36.0	–5.4	16.2
d) w/ 1-hourly GOES + ERBE clouds	228.5	6.2	39.5	1.6	22.9
e) w/ 3-hourly GOES + ERBE clouds	228.5	5.9	39.6	1.4	23.1
f) Nonnormalized 3-hr + ERBE clouds	228.5	7.1	42.5	2.5	27.8

(b) April 1985	NOAA-9 mean flux	Total error		Time interpolation error	
		Mean	rms	Mean	rms
Coincident data	251.0	5.1	39.1	-	-
Scaled coincident data	233.3	4.7	36.3	-	-
a) ERBE TSA	233.3	1.7	55.1	–3.0	41.4
b) w/ 1-hourly GOES + GOES clouds	233.3	5.7	37.1	1.0	7.5
c) w/ 3-hourly GOES + GOES clouds	233.3	3.4	38.5	–1.3	12.7
d) w/ 1-hourly GOES + ERBE clouds	233.3	5.2	39.9	0.4	16.5
e) w/ 3-hourly GOES + ERBE clouds	233.3	3.2	42.4	–1.5	21.8
f) Nonnormalized 3-hr + ERBE clouds	233.3	3.1	44.9	–1.6	26.4

The mean and rms errors due to time interpolation are calculated in a slightly different fashion than that used with the LW flux simulations. As can be seen in table 7.1-2, the mean SW flux for the coincident data is 20–30 W-m^{-2} greater than the mean fluxes used in the time interpolation. There are fewer (~7000) coincident data points as compared with the ~35000 NOAA-9 measurements that can be predicted from ERBS data. The difference in the mean fluxes occurs because these coincident data occur at a lower average solar zenith angle. To accommodate this difference, the rms errors from the coincident data (rms_o from equation 7.1-3) are first linearly scaled by the ratio of the mean fluxes before being subtracted from the total rms errors. These scaled values, which are used to calculate the time interpolation error, are shown in the second row of tables 7.1-2.

The addition of narrowband data into the process results in a significant decrease in the interpolation rms errors. As explained above, the ERBE time interpolation technique necessarily assumes constant cloudiness over each day for which there is only one time of observation. By introducing information concerning the temporal variation in cloudiness through the addition of narrowband data, the time interpolation error has been reduced from 43.1 W-m^{-2} to less than 28 W-m^{-2} in all cases (b)–(f) for the July data. The reasons for this increased accuracy can be seen in figure 7.1-4 which shows three days of SW albedo measured by ERBE during July 1985 in the same region as in figure 7.1-3. The ERBS observations are shown as black squares. The NOAA-9 observations are open circles. Also shown are the results of interpolations using the NOAA-9 data and the ERBE time interpolation technique (a) and the 3-hourly geostationary data technique (e). During the first two days, the cloudiness remained constant throughout the day and the two techniques produce similar results. On the third day, however, there was apparently a shift in cloudiness between the times of observation by ERBS and NOAA-9. The ERBE time interpolation technique severely overestimates the albedo over most of the day. The GOES data, however, provide the means for correctly modeling the albedo on that day.

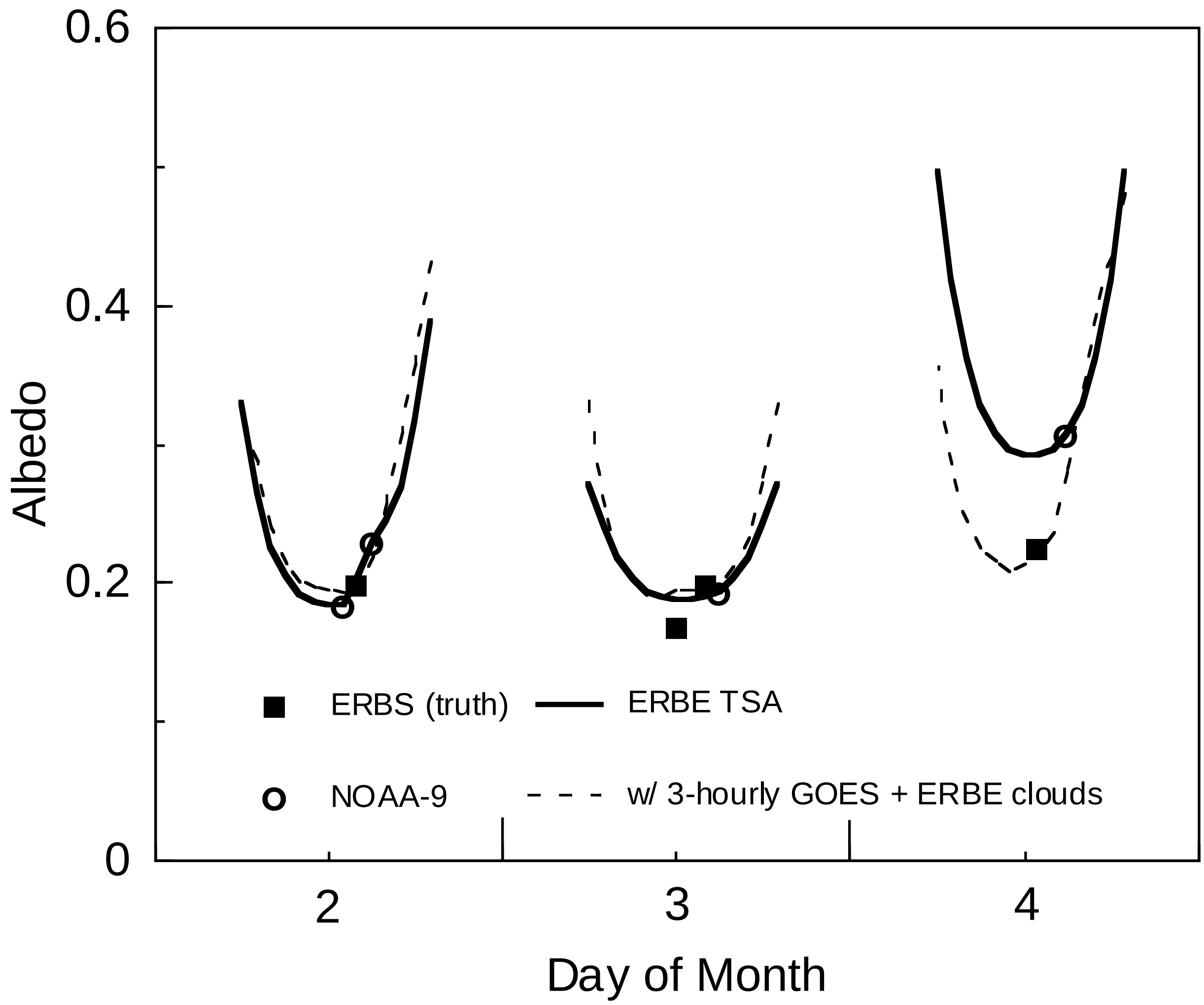

Figure 7.1-4. Time series of ERBE ERBS (■) and NOAA-9 (❍) SW albedo observations and interpolated values from July 1985 over New Mexico. The solid curve shows the ERBE time interpolated values; the dashed curve shows the geostationary-data-enhanced interpolation.

The technique currently proposed for release 1 is method (e). This method is a definite improvement over the ERBE technique, reducing the rms time interpolation error from 43.1 W-m^{-2} to 23.1 W-m^{-2} in July and from 41.4 W-m^{-2} to 21.8 W-m^{-2} in April. The bias errors also show improvement. As expected, the mean rms error associated with using 1-hourly data in method (d) shows a slight improvement over using 3-hourly data. However, this improvement is small compared to the advantages of data volume reduction if 3-hourly data are used instead. Furthermore, for generating SW flux estimates for synoptic maps, the difference between the 1-hourly and 3-hourly data is not significant. Since the fluxes will be derived at times of geostationary observations, the errors should be closer to the 1-hourly estimates shown here.

As is the case with LW flux data, the renormalization of the SW flux estimates to the nearest observation is important. The rms errors increase by 4–5 W-m^{-2} when this renormalization is not included in method (f).

An additional improvement is seen if cloud information is derived at the times of geostationary measurements. As stated above, errors from improper selection of SW ADM’s can be quite large.

Increasing the accuracy of cloud parameters should, therefore, decrease errors in the narrowband-broadband conversion of the GOES data. For methods (d), (e), and (f), cloud fraction estimates are derived for each hour by linearly interpolating between ERBE observations. Cloud fractions derived directly from the narrowband data should be more accurate since time interpolation of cloud fraction is no longer necessary.

The results of using this improved cloud information are shown as methods (b) and (c) for 1-hourly and 3-hourly GOES data, respectively. For the 3-hourly case, rms interpolation errors decrease by 7–9 W-m^{-2} from method (e) which uses the ERBE cloud information. Part of this error is due to the linear interpolation of cloud fractions, but some of the error is due to incorrect ERBE scene identification. This latter error should be greatly diminished because of the improved cloud data from CERES. Thus, the improvement of method (c) over method (e) will not be as great for CERES. This method is not planned in release 1, but will be studied for possible addition to later releases.

These proposed changes in the temporal interpolation process are aimed at improving instantaneous estimates of flux. It is important to ensure that the estimates of monthly mean flux are not adversely affected. ERBE produced regional monthly mean SW flux estimates to within 3 W-m^{-2} (Harrison et al. 1990). For July, the ERBE method (a) produces monthly mean flux averaged over all regions of 95.1 W-m^{-2}. For methods (e) and (f), the averages are 95.5 W-m^{-2} and 95.6 W-m^{-2}, respectively. Thus, the enhancements to the interpolation process are not adversely affecting the monthly means. Once again, anchoring the SW fluxes to the observations in method (e) produces an improvement over the results of method (f).

From the results of these simulations, it is concluded that the introduction of geostationary data represents a significant improvement to the ERBE time interpolation technique, and will, therefore, be included into the CERES algorithm. The technique, method (e) will be used whenever narrowband data are available. The ERBE-like method (a) will be used for regions and times with no narrowband data.

7.1.2.8. Time interpolation of clear-sky TOA SW flux. As is the case with the clear-sky LW flux, there should be a more accurate assessment of the occurrence of clear-sky SW data with CERES than with ERBE. The CERES data are interpolated using the clear-sky ADM’s appropriate to the regional surface type. The lack of geostationary data is not serious in the case of clear-sky modeling. The main information provided by the narrowband data is the changes in meteorology and cloudiness. For clear-skies, the CERES directional models should work well for time interpolation. Geostationary data could only be used in the processing of clear-sky data if cloud properties such as separate total-sky and clear-sky narrowband radiances are derived from the narrowband measurements. This is not planned for release 1. Simulations are underway to evaluate the relative merits of the two averaging methods for clear-sky parameters. If the ERBE-like method is sufficient, then method 2 time interpolation will not be performed for clear-sky SW.

7.1.2.9. Time interpolation of window radiances. The window channel interpolation should be straightforward. This measurement is made in the same spectral region as the infrared measurement from the geostationary satellites. Therefore, the geostationary LW radiance time series can be used in a manner similar to the technique employed to produce the time series of LW flux. The narrowband-broadband regressions will not be used, but the geostationary radiances will be normalized to the CERES measurements in order to correct for any differences in the spectral intervals or the calibration of the instruments.

7.1.2.10. Algorithm core summary

7.1.2.10.1. Input data summary list. The chief input to the computation of synoptic maps is the gridded CERES SW and LW TOA fluxes and cloud information provided by the FSW data product. These data contain spatial averages of 1 hour of CERES measurements on a 1.25° equal-area grid. The relevant parameters from FSW which are used in the averaging process are the total-sky LW and SW TOA fluxes, the clear-sky TOA LW and SW fluxes, and the CERES-derived cloud information. Geostationary satellite-derived radiances will be provided by the GEO data product. Additional data needed to perform this process include solar declination and the current ADM's. A detailed description of the input products is in appendix A.

7.1.2.10.2. Output data summary list. This process produces a global map of TOA total-sky LW and SW flux, TOA clear-sky LW and SW flux, TOA window radiances, and cloud parameters valid at 0, 3, 6, ..., 21 GMT for each day of the month. These synoptic results are used as inputs to computing synoptic maps of vertical radiation fields.

7.1.3. Implementation Issues for Temporal Interpolation

7.1.3.1. Strategic concerns. Major strategic concerns for this subsystem involve the availability and suitability of geostationary data. The first question concerns the timeliness of the data. If the ISCCP DX product is to be used, then there will almost certainly be a delay in obtaining the data since ISCCP will have to calculate the cloud parameters. It is expected that B3 data will be available with only a 1-month delay (William Rossow, private communication).

In addition to time constraints on receiving the data, there is also a problem with data gaps in the ISCCP products. The INSAT data are often not available, which creates a lack of geostationary data over 20% of the globe. Also, some ISCCP products do not include SW data for solar zenith angles greater than 72.5°. This restriction severely limits the effectiveness of using these data in the SW interpolation process. This problem can be alleviated if the radiances are still available even if ISCCP cloud parameters cannot be produced. Whenever geostationary data are not available or are inadequate, data from the polar orbiting satellites, which provide four observations per day, will be used. If no narrowband data are available, the TOA fluxes derived from method 1, the ERBE-like technique, will be used.

Another consideration is the effect on derived cloud properties of increased viewing zenith angle. This effect has been noted by several authors (see Minnis 1989). Studies are being performed to determine if the error in interpolation increases when the viewing zenith angle of the geostationary data increases. If this is the case, then a viewing zenith angle limit may be imposed on these data.

The simulations of time interpolation for total-sky SW flux demonstrated that an additional small increase in interpolation accuracy can be gained if cloud properties are obtained at the times of geostationary measurements. If ISCCP DX data are available, estimates of cloud amount, cloud type, and possibly optical depth will accompany each ISCCP pixel and will, thus, provide a picture of changing cloud conditions every 3 hours. If the ISCCP cloud data are not reliable or available, another source for cloud data exists. The ISCCP radiances could be analyzed at the synoptic times using a limited subset of the CERES cloud analysis algorithm. This method would require a great deal more computation, but may provide the most consistent cloud parameters for the synoptic maps. Further simulations are being performed to study the utility and advantage of producing and using these additional cloud data for total-sky interpolation.

Cloud properties derived at the times of observation can also assist in the interpolation of clear-sky SW and LW fluxes. Clear-sky geostationary radiances could be used to construct a clear-sky flux time series that could be normalized to CERES clear-sky measurements and applied in the same manner as the total-sky time series. This may be the greatest advantage in deriving geostationary cloud products. There may be large data gaps in the clear-sky flux records from CERES, as was the case with ERBE. The synoptic modeling process, however, requires a TOA clear-sky LW and SW flux at each synoptic time. Without the additional cloud information from the narrowband data, assumptions of persistence from the nearest day with data will have to be made. This is a greater problem in the LW than the SW, since the SW clear-sky albedo should not vary rapidly with time. The data gaps in both the clear-sky LW and SW will be handled in one of three ways:

1. The diurnal variation of clear-sky flux for days with no data will be modeled by interpolating between the diurnal curves of the two nearest days with data.
2. A monthly mean diurnal model will be constructed from days with data. This model will be applied to all days with no data.
3. The assumption of regional independence will be waived and clear data from surrounding regions with similar surface types will be used.

Studies are planned to assess the effects of clear-sky data gaps on the input to the synoptic radiative flux calculations.

Another aspect of the problem with data gaps is that decisions must be made concerning whether to restrict the time interval over which temporal interpolation is performed. ERBE interpolated TOA flux to all hours of the month if there was at least one observation during that month. For CERES, particularly for the synoptic product, there may be restrictions imposed based on simulation results. Since the rms errors of interpolation increase with the length of the time interval, at some point the error will exceed acceptable limits. If such restrictions are incorporated, then flux estimates will not be made in regions without adequate time sampling.

The regressions that are to be used to produce broadband simulated fluxes from the narrowband measurements will have to be derived monthly. Separate, global regressions for ocean and land will be used initially. It has been demonstrated that for the simulations performed in this study, the effects of regional variations in these regressions can be minimized by the normalization of the LW and SW flux time series to the CERES measurements. If this normalization proves to be inadequate during the operational data analysis, then regional or climate-regime specific fits may be required each month using coincident CERES and geostationary data.

The simulations described above demonstrated that the linear interpolation of clouds does not seriously diminish the accuracy of the temporal interpolation of SW flux. However, since the clouds are linearly interpolated while the TOA fluxes include some information from the geostationary data concerning the changes in cloudiness, there will be instances when the clouds and TOA conditions will not be consistent. It is expected that most of this inconsistency will be removed during the recalculation of atmospheric fluxes. Several studies are planned to estimate the errors associated with this cloud property interpolation technique. Cloud properties derived from 1-hourly GOES data using the Hybrid Bispectral Threshold Method (Minnis et al. 1987) will be sampled and interpolated to calculate the errors.

Another study to be performed is a calculation of the errors induced from using the sub-sampled geostationary data supplied by the ISCCP B3 product. The simulations discussed in this section used regional mean GOES radiances computed from 8-km resolution data. These data will be sub-sampled to simulate the 32-km resolution of the B3 product and an assessment will be made of the magnitude of error by performing the simulations again using the sub-sampled data. If the additional errors are significant, consideration will have to be given to obtaining the higher spatial resolution data for the CERES processing.

For release 1, the 12 ERBE LW and SW ADM’s will be used. CERES will create an extensive set of directional and bidirectional models that are applicable to specific combinations of cloud type, surface type, and possibly cloud optical depth which will be incorporated into release 3. The methods for including these models into the time interpolation process will be studied.

The narrowband LW ADM used in equation 7.1-2 was developed by Minnis et al. (1991) using theoretical calculations and is scene ID independent. New, expanded narrowband ADM’s may be developed. Additionally, the simulations will be performed using the ERBE broadband ADM's in place of the narrowband model. If no degradation in the results occurs, the ERBE ADM's will be used.

7.1.3.2. Scientific implementation issues

7.1.3.2.1. Calibration. There are two primary calibration considerations for this subsystem. The first is the narrowband-broadband correlations for both SW and LW. This was addressed above in section 7.1.3.1. The second consideration is the calibration of the narrowband radiances for each of the geostationary satellites. If the data source for these data is the ISCCP, the data will have already been calibrated. If the data are not previously calibrated, then procedures will be developed for this purpose. However, the proposed averaging method incorporates safeguards to properly account for both long-term drifts and shorter time scale variations in instrument calibration. Long-term variations in the stability of the geostationary sensors will not present problems to the averaging process since the narrowband-broadband correlations used during the averaging will be recomputed for each sensor for each month of data. Shorter-term variations (of less than 1 month) will also be largely eliminated by the continuous renormalization of the simulated broadband data to the closest CERES observation.

7.1.3.2.2. Validation. In addition to the previously discussed ongoing efforts to test the time-interpolated data, several validation studies are planned to determine the uncertainties in the interpolated cloud properties and surface and TOA fluxes. The new series of the GOES satellites will have 4-km resolution data available every half hour at wavelengths comparable to the VIRS and the Advanced Very High Resolution Radiometer (AVHRR). The CERES cloud analysis algorithms will be applied to selected intervals of data taken by the new GOES to derive a high temporal resolution data set of cloud properties and narrowband-based fluxes. Sampling studies using the time interpolation algorithms will be conducted using the GOES results as the reference case. These validation efforts will be used to quantify the errors introduced in the time interpolation process and to develop improved techniques.

Other validation studies will utilize long-term data sets taken during field programs. The Atmospheric Radiation Measurement (ARM) project plans to measure the surface radiation budget continuously at a minimum of three locations including sites in the central U.S., the tropical Pacific, and the Arctic. The temporal and spatial scales of these instrumented sites are compatible with the CERES regional grid. Unmanned Aerospace Vehicles (UAV's) are also planned as part of ARM. The basic instrument package includes both broadband longwave and shortwave flux radiometers. The UAV's are capable of flying at stratospheric altitudes during missions lasting up to a week. They can be programmed to cover areas as large as the CERES regions. These platforms provide an ideal, calibrated source to validate the time interpolation results over limited but significantly different areas. Other instruments on these UAV's may be used to derive coincident cloud properties. Other field programs including the First ISCCP Regional Experiment (FIRE), SHEBA, and components of the Global Energy and Water Cycle Experiment (GEWEX) may also provide high-temporal resolution data sets that can be used to validate the CERES products.

A comprehensive CERES validation plan encompassing results from all of the Subsystems is currently being developed. The plan is expected to build on the successes of the ERBE approach.

7.2. Compute Surface and Atmospheric Fluxes at Synoptic Times

The CERES Data Management System calculates the full column of the SARB at synoptic times. This process produces a set of archival radiative fluxes at the surface, TOA, and at various atmospheric levels. The SARB calculations are based on the cloud and meteorological inputs that have been interpolated to synoptic times. The radiation calculated at the TOA is compared to the TOA fluxes that are generated at synoptic times as described in section 7.1. If necessary, the cloud and meteorological parameters that are used as inputs to the radiation calculations are tuned, as in subsystem 5, to balance the satellite-based synoptic TOA fluxes. This tuning process produces a set of adjustments to the synoptic cloud and meteorological data, as well as the SARB at synoptic times.

Because this section so closely follows subsystem 5, which describes the SARB calculations and the tuning of the cloud and meteorological variables at the instantaneous ERBE or CERES footprint scale, this section has been kept brief. Subsystem 5 contains a more detailed treatment and a scientific discussion.

7.2.1. Synoptic Data for Input to Radiative Transfer Calculations

The cloud, meteorological, and TOA fluxes which have been estimated for synoptic times by process 7.1 are used to calculate the radiative fluxes through the atmospheric column. The release 1 algorithm for the calculation of these fluxes is analogous to the algorithm in section 5.4.1., and will be executed in a manner similar to that described in section 5.4.2.

The meteorological input is based on an interpolated or analyzed sounding at 38 vertical levels on the 1.25° equal-area grid. Cloud properties available for the calculation are described in section 5.1.2.4. For up to four distinct pressure categories (low, lower middle, upper middle, and high), we use the mean cloud areas, heights of tops and bottoms, cloud liquid water path (LWP) or ice water path (IWP), cloud particle size and phase, and the infrared emittance. Section 7.1.2.4. describes the interpolation of the cloud properties derived from CERES cloud imager retrievals using a cloud area weighting for all cloud properties in the four pressure categories (except for cloud area itself). The initial surface albedo is interpolated from the CERES retrievals, with an adjustment for solar zenith angle.

7.2.2. Initial Calculation of Synoptic Radiative Fluxes

Subsystem 5 describes two SARB retrieval algorithms, FL and HCW, which are used independently. FL is used to produce archival results for release 1, and HCW generates informal results that are used diagnostically. These algorithms are used to calculate clear-sky TOA fluxes (clear sky is always calculated and archived for diagnostic purposes, even if the region is overcast) and TOA fluxes for each of the synoptic cloud conditions. These initial radiative transfer calculations are archived at only the surface and TOA for (1) clear sky and (2) the estimated total-sky condition for the region.

After the initial clear- and total-sky calculations are performed, the TOA total-sky model results for the region are compared to the CERES averages for that region. Then, if the modeled and CERES fluxes differ, tuning of the input variables is attempted as described in section 5.4.2.3. All possible tuning variables such as cloud fraction, optical depth, or cloud height, and atmospheric variables used to adjust the clear-sky flux such as precipitable water and surface albedo are considered to determine which will best tune the modeled fluxes to the observed fluxes. The chosen variables are then placed into the Lagrange multiplier technique of section 5.4.1. to determine the necessary adjustment for each. The radiation transfer models are rerun with the adjusted input variables and the new radiation budget is archived, along with the adjusted input variables. These tuned fluxes are saved at the surface, 500 hpa, the tropopause, and the TOA for both clear-sky and total-sky conditions. Fluxes at other levels are stored informally in release 1.

7.2.3. Strategic Concerns

Subsystem 5 contains a scientific discussion of problems relating to the calculation of the SARB, and strategic concerns are highlighted in section 5.5. One outstanding concern for the production of fluxes and adjusted cloud and meteorological data at synoptic times, is the limitation posed in the synoptic calculations at the large scale of the 1.25° region. The averaging of input data or radiative calculations generally introduces errors at any scale. An opportunity exists to investigate the errors at this scale, by studies with the CRS (subsystem 5) and FSW (subsystem 6) outputs. CRS contains clouds and calculated radiative fluxes at the CERES footprint scale. Those footprint scale cloud properties can be averaged in FSW with the same assumptions used to generate synoptic clouds and fluxes. By performing a synoptic-like calculation with the hourly data in the FSW grid, results can be compared with the standard FSW clouds and fluxes, to learn if a bias is introduced by the synoptic-like spatial averaging process itself.

A second strategic concern, particular to the synoptic flux calculations, is the accuracy of the temporal interpolation. This will be addressed in studies using ISCCP cloud properties at synoptic times and comparing to CERES properties in release 1. The basic assumption in synoptic averaging and tuning is that the TOA fluxes are more accurately interpolated (or estimated from operational satellite data) than cloud properties, which are to be tuned. A comparison of CERES interpolated clouds (adjusted and unadjusted) will provide some insight on this for further releases.

The CERES SARB calculations will be performed on a 3-hourly basis for the synoptic flux computation. Raw averages of 3-hourly fluxes are not adequate for determining the daily mean SW fluxes at the surface and within the atmosphere because of the diurnal course of the Sun. Algorithms for mapping the 3-hourly synoptic fluxes to astronomically consistent daily averaged surface and atmospheric fluxes will be developed using temporally intensive calculations.

7.3. References

Barkstrom, B. R. 1984: The Earth Radiation Budget Experiment (ERBE). *Bull. American Meteorol. Soc.*, vol. 65, pp. 1170–1185.

Barkstrom, Bruce R.; Harrison, Edwin F.; and Lee, Robert B., III 1990: Earth Radiation Budget Experiment—Preliminary Seasonal Results. *EOS*, vol. 71, pp. 279, 299, 304, and 305.

Barkstrom, B. R.; and Smith, G. L. 1986: The Earth Radiation Budget Experiment—Science and Implementation. *Rev. Geophys.*, vol. 24, pp. 379–390.

Briegleb, B.; and Ramanathan, V. 1982: Spectral and Diurnal Variations in Clear Sky Planetary Albedo. *J. Appl. Meteorol.*, vol. 21, pp. 1160–1171.

Brooks, D. R.; and Minnis, P. 1984: Simulation of the Earth's Monthly Average Regional Radiation Balance Derived From Satellite Measurements. *J. Climat. & Appl. Meteorol.*, vol. 23, pp. 392–403.

Brooks, D. R.; Harrison, E. F.; Minnis, P.; Suttles, J. T.; and Kandel, R. S. 1986: Development of Algorithms for Understanding the Temporal and Spatial Variability of the Earth's Radiation Balance. *Rev. Geophys.*, vol. 24, pp. 422–438.

Desbois, Michel; Kayiranga, Theoneste; and Gnamien, Brigitte 1989: Diurnal Cycle of Convective Cloudiness Over Tropical Africa Observed From Meteosat—Geographic Characterization and Interannual Variations. *Annales Geophys.*, vol. 7, pp. 395–404.

Doelling, David R.; Young, David F.; Arduini, Robert F.; Minnis, Patrick; Harrison, Edwin F.; and Suttles, J. T. 1990: On the Role of Satellite-Measured Narrowband Radiances for Computing the Earth's Radiation Balance. *Seventh Conference on Atmospheric Radiation—Preprints*, American Meteorol. Soc., pp. 155–160.

Garand, Louis 1988: Automated Recognition of Oceanic Cloud Patterns. I—Methodology and Application to Cloud Climatology. *J. Climat.*, vol. 1, pp. 20–39.

Harrison, E. F.; Young, D. F.; Minnis, P.; Wielicki, B. A.; Doelling, D. R.; and Gibson, G. G. 1994: Temporal Sampling Analysis for the Clouds and the Earth's Radiant Energy System (CERES) Experiment for Satellite Missions in the Late 1990's. *Seventh Conference on Satellite Meteorology and Oceanography*, pp. 520–523.

Harrison, Edwin F.; Brooks, David R.; Minnis, Patrick; Wielicki, Bruce A.; and Staylor, W. Frank 1988: First Estimates of the Diurnal Variation of Longwave Radiation From the Multiple-Satellite Earth Radiation Budget Experiment (ERBE). *Bull. American Meteorol. Soc.*, vol. 69, pp. 1144–1151.

Harrison, E. F.; Minnis, P.; Barkstrom, B. R.; Ramanathan, V.; and Cess, R. D. 1992: Seasonal Variation of Cloud Radiative Forcing Derived From the Earth Radiation Budget Experiment. *J. Geophys. Res.*, vol. 95, pp. 18687–18703.

Minnis, Patrick 1989: Viewing Zenith Angle Dependence of Cloudiness Determined From Coincident GOES East and GOES West Data. *J. Geophys. Res.*, vol. 94, pp. 2303–2320.

Minnis, P.; and Harrison, E. F. 1984: Diurnal Variability of Regional Cloud and Clear-Sky Radiative Parameters Derived From GOES Data. III—November 1978 Radiative Parameters. *J. Climat. & Appl. Meteorol.*, vol. 23, pp. 1033–1051.

Minnis, Patrick; Harrison, Edwin F.; and Gibson, Gary G. 1987: Cloud Cover Over the Equatorial Eastern Pacific Derived From July 1983 International Satellite Cloud Climatology Project Data Using a Hybrid Bispectral Threshold Method. *J. Geophys. Res.*, vol. 92, pp. 4051–4073.

Minnis, Patrick; Harrison, Edwin F.; and Young, David F. 1991: Examination of the Relationship Between Outgoing Infrared Window and Total Longwave Fluxes Using Satellite Data. *J. Climat.*, vol. 4, pp. 1114–1133.

Suttles, J. T.; Green, R. N.; Minnis, P.; Smith, G. L.; Staylor, W. F.; Wielicki, B. A.; Walker, I. J.; Young, D. F.; Taylor, V. R.; and Stowe, L. L. 1988: *Angular Radiation Models for Earth-Atmosphere System. Volume 1—Shortwave Radiation.* NASA RP-1184.

Suttles, J. T.; Green, R. N.; Smith, G. L.; Wielicki, B. A.; Walker, I. J.; Taylor, V. R.; and Stowe, L. L. 1988: *Angular Radiation Models for Earth-Atmosphere System. Volume 2—Longwave Radiation*. NASA RP-1184.

Wielicki, Bruce A.; and Barkstrom, Bruce R. 1991: Clouds and the Earth's Radiant Energy System (CERES)—An Earth Observing system Experiment. S*econd Symposium on Global Change Studies—Preprints,* American Meteorol. Soc., pp. 11–16.

Appendix A

Input Data Products

Merge Satellites, Time Interpolate, Compute Fluxes (Subsystem 7.0)

This appendix describes the data products which are used by the algorithms in this subsystem. Table A-1 below summarizes these products, listing the CERES and EOSDIS product codes or abbreviations, a short product name, the product type, the production frequency, and volume estimates for each individual product as well as a complete data month of production. The product types are defined as follows:

Archival products:	Assumed to be permanently stored by EOSDIS
Internal products:	Temporary storage by EOSDIS (days to years)
Ancillary products:	Non-CERES data needed to interpret measurements

The following pages describe each product. An introductory page provides an overall description of the product and specifies the temporal and spatial coverage. The table which follows the introductory page briefly describes every parameter which is contained in the product. Each product may be thought of as metadata followed by data records. The metadata (or header data) is not well-defined yet and is included mainly as a placeholder. The description of parameters which are present in each data record includes parameter number (a unique number for each distinct parameter), units, dynamic range, the number of elements per record, an estimate of the number of bits required to represent each parameter, and an element number (a unique number for each instance of every parameter). A summary at the bottom of each table shows the current estimated sizes of metadata, each data record, and the total data product. A more detailed description of each data product will be contained in a user's guide to be published before the first CERES launch.

Table A-1. Input Products Summary

Product code						Monthly
CERES	EOSDIS	Name	Type	Frequency	Size, MB	size, MB
ASTR	CER34	Atmospheric structures	archival	1/hour	10.5	7797
FSW	CER05	Hourly gridded single satellite fluxes and clouds	archival	1/hour	4.2	3105
GEO	GEO	ISCCP radiances	ancillary	8/day	3.8	927

Atmospheric Structures (ASTR)

The CERES archival product, atmospheric structures (ASTR), is produced by the CERES Regrid Humidity and Temperature Subsystem. Each ASTR file contains meteorological data for one hour, and is used by several of the CERES subsystems. Data on the ASTR are derived from several data sources external to the CERES system, such as NMC, MODIS, SAGE, and various other meteorological satellites. These data arrive anywhere from four times daily to once a month. These data are also horizontally and vertically organized differently from what the CERES system requires. The Regrid Humidity and Temperature Subsystem interpolates these data temporally, horizontally, and vertically to conform with CERES processing requirements.

The ASTR contains

- Surface temperature and pressure
- Vertical profiles for up to 38 internal atmospheric levels of temperature, humidity, pressure, and geopotential height
- Column precipitable water
- Vertical ozone profiles for 26 (of the 38) internal atmospheric levels
- Column ozone

- Total column aerosol
- Stratospheric aerosol

The 38 internal atmospheric levels, in hPa, as requested by the CERES Clouds and SARB working groups are:

Surface	925	775	550	275	125	5
Surface - 10	900	750	500	250	100	1
Surface - 20	875	725	450	225	70	
1000	850	700	400	200	50	
975	825	650	350	175	30	
950	800	600	300	150	10	

Level: 3
Type: Archival
Frequency: 1/hour

Portion of Globe Covered
File: Global
Record: 1.25-deg equal area region

Time Interval Covered
File: 1 hour
Record: 1 hour

Portion of Atmosphere Covered
File: Surface and internal

Table A-2. Atmospheric Structures (ASTR)

Description	Parameter Number	Units	Range	Elements/ Record	Bits/ Elem	Elem Num
Meta Data						
Header				1	320	
Regional Data						
Region Number	1	N/A	1..26542	1	16	1
Surface Data						
Surface Temperature	2	K	175..375	1	16	2
Surface Pressure	3	hPa	1100..400	1	16	3
Flag, Source Surface Data	4	N/A	TBD	1	16	4
Temperature and Humidity Profiles						
Geopotential Height Profiles	5	km	0..50	38	16	5
Pressure Profiles	6	hPa	1100..0	38	16	43
Temperature Profiles	7	K	175..375	38	16	81
Humidity Profiles	8	N/A	0..100	38	16	119
Flag, Source Temp. and Humidity Profiles	9	N/A	TBD	1	16	157
Column Precipitable Water						
Precipitable Water	10	cm	0.001..8.000	1	16	158
Precipitable Water, std	11	cm	TBD	1	16	159
Flag, Source Column Precipitable Water	12	N/A	TBD	1	16	160
Ozone Profile Data						
Ozone Profiles	13	g kg^{-1}	0.00002..0.02	26	16	161
Flag, Source Ozone Profile Data	14	N/A	TBD	1	16	187
Column Ozone						
Column Ozone	15	du	200..500	1	16	188
Flag, Source Column Ozone	16	N/A	TBD	1	16	189
Total Column Aerosol						
Aerosol Mass Loading, Total Column	17	g m^{-2}	TBD	1	16	190
Flag, Source Aerosol Mass Loading, Total Column	18	N/A	TBD	1	16	191
Optical Depth, Total Column	19	N/A	0.0..2.0	1	16	192
Flag, Source Optical Depth, Total Column	20	N/A	TBD	1	16	193
Asymmetry Factor, Total Column	21	N/A	0.0..1.0	1	16	194
Flag, Source Asymmetry Factor, Total Column	22	N/A	TBD	1	16	195
Single Scattering Albedo, Total Column	23	N/A	0.0..1.0	1	16	196
Flag, Source Single Scattering Albedo, Total Column	24	N/A	TBD	1	16	197
Effective Particle Size, Total Column	25	µm	0.0..20.0	1	16	198
Flag, Source Effective Particle Size, Total Column	26	N/A	TBD	1	16	199
Mean Aerosol Layer Temperature, Total Column	27	K	150..280	1	16	200
Flag, Source Mean Aerosol Layer Temperature, Total Column	28	N/A	TBD	1	16	201
Stratospheric Aerosol						
Optical Depth, Stratosphere	29	N/A	0.0..0.5	1	16	202
Asymmetry Factor, Stratosphere	30	N/A	0.0..1.0	1	16	203
Single Scattering Albedo, Stratosphere	31	N/A	0.0..1.0	1	16	204
Effective Particle Size, Stratosphere	32	µm	0.0..10.0	1	16	205
Mean Aerosol Layer Temperature, Stratosphere	33	K	150..280	1	16	206
Flag, Source Stratospheric Aerosol	34	N/A	TBD	1	16	207

Total Meta Bits/File:	320
Total Data Bits/Record:	3312
Total Records/File:	26542
Total Data Bits/File:	87907104
Total Bits/File:	87907424

Hourly Gridded Single Satellite Fluxes and Clouds (FSW)

The hourly gridded single satellite fluxes and clouds (FSW) archival data product contains hourly single satellite flux and cloud parameters averaged over 1.25 degree regions. Input to the FSW subsystem is the single satellite CERES footprint, radiative fluxes and clouds (CRS) archival data product. Each FSW covers a single hour swath from a single CERES instrument mounted on one satellite. The product has a product header and multiple records. Each record contains spatially averaged data for an individual region.

The major categories of data output on the FSW are

- Region data
- Total sky radiative fluxes at TOA, surface, and atmospheric levels
- Clear sky radiative fluxes at TOA, surface, and atmospheric levels
- Cloud overlap conditions
- Cloud category properties
- Column-averaged cloud properties
- Angular model scene classes
- Surface only data
- Adjustment parameters

FSW is an archival product generated on an hourly basis. Initially at the launch of the TRMM spacecraft, this product will be produced in validation mode once every 3 months, or for 4 data months a year. During the first 18 months after the launch of TRMM, the CERES Science Team will derive a production quality set of angular distribution models, which are needed to produce the shortwave (SW) and longwave (LW) instantaneous fluxes. Eighteen months after the launch of TRMM, this product will be archived and will contain SW and LW fluxes at the tropopause and at the 500 hPa pressure level, in addition to fluxes at TOA and at the surface. Thirty-six months after the launch of TRMM, this archived product will contain SW and LW fluxes at 26 standard pressure levels.

Level: 3
Type: Archival
Frequency: 1/hour

Portion of Globe Covered
File: Gridded satellite swath
Record: 1.25-degree equal-area regions

Time Interval Covered
File: Hour
Record: N/A

Portion of Atmosphere Covered
File: TOA, surface and atmospheric pressure levels

Table A-3. Hourly Gridded Single Satellite Fluxes and Clouds (FSW)

Description	Parameter Number	Units	Range	Elements/ Record	Bits/ Elem	Elem Num
FSW						
FSW_File_Header						
CERES data product code		N/A	N/A	1	16	
Spacecraft name		N/A	N/A	1	16	
CERES instrument identification code		N/A	N/A	1	16	
Julian Day		Day	2449353 .. 2458500	1	32	
Hour of the day for the FSW product		Hours	1 .. 24	1	16	
Number of regions (records) in the product		N/A	1 .. 2500	1	16	
FSW_Region_Data						
Region number	1	N/A	1 .. 26542	1	16	1
Number of CERES footprints in the region	2	N/A	1 .. 40	1	16	2
Julian Time	3	Day	0.0 .. 1.0	1	32	3
Hour box number for the region	4	N/A	1 .. 744	1	16	4
Precipitable water	5	cm	0.001 .. 8.000	1	16	5
Mean of land type percentage	6	Percent	0.0 .. 100.0	10	16	6
Mean of sea type percentage	7	Percent	0.0 .. 100.0	3	16	16
Mean Sun colatitude	8	Degrees	0.0 .. 180.0	1	16	19
Mean Sun longitude	9	Degrees	0.0 .. 360.0	1	16	20
Mean relative azimuth angle at TOA	10	Degrees	0.0 .. 360.0	1	16	21
Mean cosine of solar zenith angle at TOA	11	N/A	0.0 .. 1.0	1	16	22
Mean spacecraft zenith angle	12	Degrees	0.0 .. 90.0	1	16	23
FSW_Radiative_Flux_Data						
Total_Sky_TOA_Flux_Statistics						
Mean, st dev, and num obs of SW upward flux at TOA	13	$W\text{-}m^{-2}$	0.0 .. 1400.0	3	16	24
Mean, st dev, and num obs of LW upward flux at TOA	14	$W\text{-}m^{-2}$	100.0 .. 500.0	3	16	27
Mean, st dev, and num obs of LW window upward flux at TOA	15	$W\text{-}m^{-2}$	0.0 .. 800.0	3	16	30
Mean, st dev, and num obs of observed - untuned SARB SW flux at TOA	16	$W\text{-}m^{-2}$	0.0 .. 1400.0	3	16	33
Mean, st dev, and num obs of observed - tuned SARB SW flux at TOA	17	$W\text{-}m^{-2}$	0.0 .. 1400.0	3	16	36
Mean, st dev, and num obs of observed - untuned SARB LW flux at TOA	18	$W\text{-}m^{-2}$	0.0 .. 500.0	3	16	39
Mean, st dev, and num obs of observed - tuned SARB LW flux at TOA	19	$W\text{-}m^{-2}$	0.0 .. 500.0	3	16	42
Total_Sky_Surface_Flux_Statistics						
Mean, st dev, and num obs of tuned SW downward sfc flux	20	$W\text{-}m^{-2}$	0.0 .. 1400.0	3	16	45
Mean, st dev, and num obs of tuned SW upward sfc flux	21	$W\text{-}m^{-2}$	0.0 .. 1400.0	3	16	48
Mean, st dev, and num obs of tuned LW downward sfc flux	22	$W\text{-}m^{-2}$	100.0 .. 500.0	3	16	51
Mean, st dev, and num obs of tuned LW upward sfc flux	23	$W\text{-}m^{-2}$	100.0 .. 500.0	3	16	54
Mean, st dev, and num obs of tuned - untuned SW downward sfc flux	24	$W\text{-}m^{-2}$	0.0 .. 1400.0	3	16	57
Mean, st dev, and num obs of tuned - untuned SW upward sfc flux	25	$W\text{-}m^{-2}$	0.0 .. 1400.0	3	16	60
Mean, std, and num obs of tuned - untuned LW downward sfc flux	26	$W\text{-}m^{-2}$	0.0 .. 500.0	3	16	63
Mean, st dev, and num obs of tuned - untuned LW upward sfc flux	27	$W\text{-}m^{-2}$	0.0 .. 500.0	3	16	66
Total_Sky_Atmospheric_Flux_Statistics						
(Atmospheric levels are tropopause and 500 hPa)						
Mean, st dev, and num obs of tuned SW downward flux at atm levels	28	$W\text{-}m^{-2}$	0.0 .. 1400.0	6	16	69
Mean, st dev, and num obs of tuned SW upward flux at atm levels	29	$W\text{-}m^{-2}$	0.0 .. 1400.0	6	16	75
Mean, st dev, and num obs of tuned LW downward flux at atm levels	30	$W\text{-}m^{-2}$	100.0 .. 500.0	6	16	81
Mean, st dev, and num obs of tuned LW upward flux at atm levels	31	$W\text{-}m^{-2}$	100.0 .. 500.0	6	16	87
FSW_Clear_Sky_Fluxes						
Clear_Sky_TOA_Flux_Statistics						
Mean, st dev, and num obs of SW upward flux at TOA	32	$W\text{-}m^{-2}$	0.0 .. 1400.0	3	16	93
Mean, st dev, and num obs of LW upward flux at TOA	33	$W\text{-}m^{-2}$	100.0 .. 500.0	3	16	96
Mean, st dev, and num obs of LW window upward flux at TOA	34	$W\text{-}m^{-2}$	0.0 .. 800.0	3	16	99
Mean, st dev, and num obs of observed - untuned SARB SW flux at TOA	35	$W\text{-}m^{-2}$	0.0 .. 1400.0	3	16	102
Mean, st dev, and num obs of observed - tuned SARB SW flux at TOA	36	$W\text{-}m^{-2}$	0.0 .. 1400.0	3	16	105
Mean, st dev, and num obs of observed - untuned SARB LW flux at TOA	37	$W\text{-}m^{-2}$	0.0 .. 500.0	3	16	108
Mean, st dev, and num obs of observed - tuned SARB LW flux at TOA	38	$W\text{-}m^{-2}$	0.0 .. 500.0	3	16	111

Table A-3. Continued

Description	Parameter Number	Units	Range	Elements/ Record	Bits/ Elem	Elem Num
Clear_Sky_Surface_Flux_Statistics						
Mean, st dev, and num obs of tuned SW downward sfc flux	39	$W\text{-}m^{-2}$	0.0 .. 1400.0	3	16	114
Mean, st dev, and num obs of tuned SW upward sfc flux	40	$W\text{-}m^{-2}$	0.0 .. 1400.0	3	16	117
Mean, st dev, and num obs of tuned LW downward sfc flux	41	$W\text{-}m^{-2}$	100.0 .. 500.0	3	16	120
Mean, st dev, and num obs of tuned LW upward sfc flux	42	$W\text{-}m^{-2}$	100.0 .. 500.0	3	16	123
Mean, st dev, and num obs of tuned - untuned SW downward sfc flux	43	$W\text{-}m^{-2}$	0.0 .. 1400.0	3	16	126
Mean, st dev, and num obs of tuned - untuned SW upward sfc flux	44	$W\text{-}m^{-2}$	100.0 .. 500.0	3	16	132
Mean, st dev, and num obs of tuned - untuned LW upward sfc flux	46	$W\text{-}m^{-2}$	100.0 .. 500.0	3	16	135
Clear_Sky_Atmospheric_Flux_Statistics						
(Atmospheric levels are tropopause and 500 hPa)						
Mean, st dev, and num obs of tuned SW upward flux at atm levels	47	$W\text{-}m^{-2}$	0.0 .. 1400.0	6	16	138
Mean, st dev, and num obs of tuned SW downward flux at atm levels	48	$W\text{-}m^{-2}$	0.0 .. 1400.0	6	16	144
Mean, st dev, and num obs of tuned LW upward fluxes at atm levels	49	$W\text{-}m^{-2}$	100.0 .. 500.0	6	16	150
Mean, st dev, and num obs of tuned LW downward flux at atm levels	50	$W\text{-}m^{-2}$	100.0 .. 500.0	6	16	156
FSW_Cloud_Data						
FSW_Cloud_Overlap_Conditions is Array[11] of:						
(Cloud overlap conditions are clear, low (L), lower middle (LM),						
upper middle (UM), high (H), H/UM, H/LM, H/L, UM/LM, and Lm/L)						
Fractional area for each of 11 conditions	51	Fraction	0.0 .. 1.0	11	16	162
FSW_Cloud_Category_Properties						
(Cloud categories are High, Uppler Middle, Lower Middle, and Low)						
Number of cloud categories with data	52	N/A	0 .. 4	1	16	173
FSW_Cloud_Properties						
Cloud Area Fractions for overcast, broken, and total clouds	53	Fraction	0.0 .. 1.0	12	16	174
Mean, st dev, and num obs of effective pressure	54	hPa	0.0 .. 1100.0	12	16	186
Mean, st dev, and num obs of effective temperature	55	K	100.0 .. 350.0	12	16	198
Mean, st dev, and num obs of effective altitude	56	km	0.0 .. 20.0	12	16	210
Mean, st dev, and num obs of cloud top pressure	57	hPa	0.0 .. 1100.0	12	16	222
Mean, st dev, and num obs of cloud bottom pressure	58	hPa	0.0 .. 1100.0	12	16	234
Mean, st dev, and num obs of particle phase	59	Fraction	0.0 .. 1.0	12	16	246
Mean, st dev, and num obs of liquid water path	60	$g\ m^{-2}$	0.01 .. 1000.0	12	16	258
Mean, st dev, and num obs of ice water path	61	$g\ m^{-2}$	0.01 .. 1000.0	12	16	270
Mean, st dev, and num obs of liquid particle radius	62	µm	0.0 .. 1000.0	12	16	282
Mean, st dev, and num obs of ice particle radius	63	µm	0.0 .. 100.0	12	16	294
Mean, st dev, and num obs of visible optical depth	64	Dimensionless	0.0 .. 50.0	12	16	306
Mean, st dev, and num obs of infrared emissivity	65	Dimensionless	0.0 .. 2.0	12	16	318
Mean, st dev, and num obs of vertical aspect ratio	66	Dimensionless	TBD	12	16	330
Mean, st dev, and num obs of adj. infrared emissivity	67	Dimensionless	0.0 .. 2.0	12	16	342
Mean, st dev, and num obs of adj. fractional area	68	Fraction	0.0 .. 1.0	12	16	354
Mean, st dev, and num obs of adj. effective temperature	69	K	0.0 .. 250.0	12	16	366
Mean, st dev, and num obs of adj. visible optical depth	70	Dimensionless	0.0 .. 400.0	12	16	378
Visible Opt Depth (day) / Infrared Emissivity (night) percentiles	71	Dimensionless	0.0 .. 50.0	52	16	390
FSW_Weighted_Column_Average_Cloud_Properties is Array[5] of:						
(Cloud weightings are SW, LW TOA, LW Surface,						
liquid water path, and ice water path)						
FSW_Cloud_Properties						
Cloud Area Fractions for overcast, broken, and total clouds	72	Fraction	0.0 .. 1.0	15	16	442
Mean, st dev, and num obs of effective pressure	73	hPa	0.0 .. 1100.0	15	16	457
Mean, st dev, and num obs of effective temperature	74	K	100.0 .. 350.0	15	16	472
Mean, st dev, and num obs of effective altitude	75	km	0.0 .. 20.0	15	16	487
Mean, st dev, and num obs of cloud top pressure	76	hPa	0.0 .. 1100.0	15	16	502
Mean, st dev, and num obs of cloud bottom pressure	77	hPa	0.0 .. 1100.0	15	16	517
Mean, st dev, and num obs of particle phase	78	Fraction	0.0 .. 1.0	15	16	532

Table A-3. Concluded

Description	Parameter Number	Units	Range	Elements/ Record	Bits/ Elem	Elem Num
Mean, st dev, and num obs of liquid water path	79	g m^{-2}	0.01 .. 1000.0	15	16	547
Mean, st dev, and num obs of ice water path	80	g m^{-2}	0.01 .. 1000.0	15	16	562
Mean, st dev, and num obs of liquid particle radius	81	µm	0.0 .. 1000.0	15	16	577
Mean, st dev, and num obs of ice particle radius	82	µm	0.0 .. 100.0	15	16	592
Mean, st dev, and num obs of visible optical depth	83	Dimensionless	0.0 .. 50.0	15	16	607
Mean, st dev, and num obs of infrared emissivity	84	Dimensionless	0.0 .. 2.0	15	16	622
Mean, st dev, and num obs of vertical aspect ratio	85	Dimensionless	TBD	15	16	637
Mean, st dev, and num obs of adj. infrared emissivity	86	Dimensionless	0.0 .. 2.0	15	16	652
Mean, st dev, and num obs of adj. fractional area	87	Fraction	0.0 .. 1.0	15	16	667
Mean, st dev, and num obs of adj. effective temperature	88	K	0.0 .. 250.0	15	16	682
Mean, st dev, and num obs of adj. visible optical depth	89	Dimensionless	0.0 .. 400.0	15	16	697
Visible Opt Depth (day) / Infrared Emissivity (night) percentiles	90	Dimensionless	0.0 .. 50.0	65	16	712
Angular_Model_Scene_Type_Parameters						
Fractional area coverage	91	Fraction	0.0 .. 1.0	12	16	777
Mean and standard deviation of albedo	92	Dimensionless	0.0 .. 1.0	24	16	789
Mean and standard deviation of incident solar flux	93	W-h m^{-2}	TBD	24	16	813
Mean and standard deviation of LW flux	94	W-m^{-2}	0.0 .. 400.0	24	16	837
FSW_Surface_Only_Data						
Photosynthetically active radiation	95	W-m^{-2}	0.0 .. 780.0	1	16	861
Direct/Diffuse Ratio	96	N/A	0.0 .. 30.0	1	16	862
FSW_Adjustment_Parameter_Statistics						
Mean and std dev of adjusted precipitable water for clear skies	97	cm	0.001 .. 8.000	2	16	863
Mean and st dev of adjusted precipitable water for total skies	98	cm	0.001 .. 8.000	2	16	865
Mean and standard deviation of adjusted surface albedo	99	Dimensionless	0.0 .. 1.0	2	16	867
Mean and standard deviation of adjusted aerosol optical depth	100	Dimensionless	0.0 .. 2.0	2	16	869
Mean and std dev of adjusted skin temp. for clear skies	101	K	TBD	2	16	871
Mean and std of skin temp. adjustment for total skies	102	K	TBD	2	16	873
Total Meta Bits/File:	112					
Total Data Bits/Record:	14000					
Total Records/File:	2500					
Total Data Bits/File:	35000000					
Total Bits/File:	35000112					

ISCCP Radiances (GEO)

The International Satellite Cloud Climatology Project (ISCCP) produces B3 radiances which are used for filling in unsampled portions of the globe during a particular one-hour interval. The ISCCP B3 radiances are well-enough defined that we do not need to make a further composite data structure to reformat them. In addition, these radiances are part of the LaRC DAAC archival responsibility.

The ISCCP B3 radiances consist of a window channel radiance (near 10.8 micrometers) and a visible channel radiance (near 0.68 micrometers) obtained from up to five geostationary satellites, as well as some data from the equivalent channels of the AVHRR and HIRS instruments on the operational satellites. The radiances from each geostationary imager are sampled at about 32-km resolution and every three hours. Where a geostationary data source is not available (over India, primarily), the AVHRR data are processed into an equivalent format.

Each geostationary satellite has a Sector Processing Center (SPC) that samples and formats the radiances. When they finish their work, the SPC sends the sampled and formatted radiance pairs to the global processing center (GPC), where the radiances are normalized and reformatted into archival form. Because each SPC follows its own schedule, the global radiance sets may not be available on a schedule that is appropriate for CERES operations; the CERES project will use the ISCCP DX radiance data as an alternate source.

The GEO radiances contain two basic kinds of information:

1. Visible (near 0.68 micrometers) and window (near 10.8 micrometers) radiances sampled at 32-km spacing
2. Earth location information

These radiances have been normalized to a common set of locations on the Earth and corrected for gain drifts, insofar as possible.

GEO is an external input data product retrieved from the EOSDIS DAAC at LaRC. GEO will be recycled by the CERES project when all single spacecraft data and all combinations of spacecraft data have been processed for a given month.

Level: 1B
Type: Ancillary
Frequency: 8/day

Time Interval Covered
File: Monthly
Record: 8/day

Portion of Globe Covered
File: Entire globe
Record: 2.5 equal area regions

Portion of Atmosphere Covered
File: TOA

Table A-4. ISCCP Radiances (GEO)

Description	Parameter Number	Units	Range	Elements/ Record	Bits/ Elem	Elem Num
GEO						
Image_ID_Rec is Array[1] of:						
Image_ID_Iteration_Rec						
GEO_Image_ID						
Data year	1	N/A	N/A	1	32	1
Record sequence number within image	2	N/A	1-1	1	32	2
Julian day of data	3	day	N/A	1	32	3
Image sequence number	4	N/A	TBD	1	32	4
Nominal GMT	5	hhmmss	N/A	1	32	5
ISCCP sector processing center identifier	6	N/A	N/A	1	64	6
GEO_Channel_Data						
Number of active channels in image	7	N/A	1-5	1	32	7
ID_Chan is Array[5] of:						
Channel Identifiers	8	N/A	TBD	5	32	8
Noise is Array[5] of:						
Noise estimates for channel	9	count	0-255	5	32	13
Available is Array[5] of:						
Channel availability flag	10	N/A	TBD	5	32	18
Chan_Desc is Array[5] of:						
Channel descriptive information	11	N/A	N/A	5	32	23
Satellite identifier	12	N/A	N/A	1	64	28
Number of data records in image	13	N/A	40-110	1	32	29
Codes_Satellite is Array[7] of:						
Satellite and channel ID code numbers	14	N/A	N/A	7	32	30
GEO_ScanLine_Data						
Number of scan lines in image	15	N/A	400-550	1	32	37
Number of pixels per scan line	16	N/A	TBD	1	32	38
Year and Julian day of first scan line	17	day	N/A	1	32	39
Year and Julian day of last scan line	18	day	N/A	1	32	40
Percentage of bad scan lines in image	19	percent	0.0 - 100.0	1	32	41
Scaling_Info is Array[10] of:						
Scale factor to convert latitude to degrees, other scaling info	20	N/A	TBD	10	32	42
Point_Subsatell is Array[4] of:						
Subsatellite latitude/longitude point information	21	TBD	TBD	4	32	52
Day/Night Flag	22	N/A	TBD	1	32	56
Calibration flag for visible channel	23	N/A	TBD	1	32	57
Fill is Array[643] of:						
Spare Words	24	N/A	N/A	643	32	58
Calibration flag for infrared channel	25	N/A	TBD	1	32	701
Location_Grid_Rec is Array[1] of:						
Location_Grid						
Record sequence number within image	26	N/A	1-1	1	32	702
Image sequence number	27	N/A	TBD	1	32	703
Num_Pixels is Array[648] of:						
Number of image pixels in each 10 degree cell	28	N/A	TBD	648	32	704
Calibration_Tables is Array[5] of:						
Calibration/Normalization tables for each channel	29	TBD	TBD	1	58080	1352
Radiance_Data is Array[110] of:						
Radiance_Data_Rec						
Scan_Line_Rec is Array[550] of:						
Scan_Line_Data_Rec						
Scan line information	30	TBD	TBD	550	288	1353
Navigation range	31	TBD	TBD	550	128	1903
Data range code	32	N/A	TBD	550	64	2453

Table A-4. Concluded

Description	Parameter Number	Units	Range	Elements/ Record	Bits/ Elem	Elem Num
Radiance Data Values	33	TBD	TBD	550	32	3003
Record identification in image	34	TBD	TBD	1	288	3553
Total Meta Bits/File:	0					
Total Data Bits/Record:	22496					
Total Records/File:	1					
Total Data Bits/File:	22496					
Total Data Bits/Record:	20800					
Total Records/File:	1					
Total Data Bits/File:	20800					
Total Data Bits/Record:	58080					
Total Records/File:	5					
Total Data Bits/File:	290400					
Total Data Bits/Record:	281888					
Total Records/File:	110					
Total Data Bits/File:	31007680					
Total Bits/File:	31341376					

Appendix B

Output Data Products

Merge Satellites, Time Interpolate, Compute Fluxes (Subsystem 7.0)

This appendix describes the data products which are produced by the algorithms in this subsystem. Table B-1 below summarizes these products, listing the CERES and EOSDIS product codes or abbreviations, a short product name, the product category, the production frequency, and volume estimates for each individual product as well as a complete data month of production. The product categories are defined as follows:

Archival products: Assumed to be permanently stored by EOSDIS
Internal products: Temporary storage by EOSDIS (days to years)

The following pages describe each product. An introductory page provides an overall description of the product and specifies the temporal and spatial coverage. The table which follows the introductory page briefly describes every parameter which is contained in the product. Each product may be thought of as metadata followed by data records. The metadata (or header data) is not well-defined yet and is included mainly as a placeholder. The description of parameters which are present in each data record includes parameter number (a unique number for each distinct parameter), units, dynamic range, the number of elements per record, an estimate of the number of bits required to represent each parameter, and an element number (a unique number for each instance of every parameter). A summary at the bottom of each table shows the current estimated size of metadata, each data record, and the total data product. A more detailed description of each data product will be contained in a user's guide to be published before the first CERES launch.

Table B-1. Output Products Summary

Product code		Name	Type	Frequency	Size, MB	Monthly size, MB
CERES	EOSDIS					
SYN	CER07	Synoptic radiative fluxes and clouds	archival	Every 3 hours	32.9	8161

Synoptic Radiative Fluxes and Clouds (SYN)

The CERES archival product, synoptic radiative fluxes and clouds (SYN), is produced by the CERES Merge Satellites, Time Interpolate, Compute Fluxes Subsystem. Each SYN file contains regional longwave and shortwave radiative fluxes for the surface, internal atmosphere and TOA. The data are synoptically computed at 3-hour intervals on a 1.25-deg equal area ISCCP-type grid, and are based on measurements from multiple EOS CERES instruments. In addition to being an archival product, the SYN is used by the CERES subsystem, Compute Regional, Zonal and Global Averages.

The SYN contains synoptically averaged

- Regional data
- Observed CERES TOA data for clear-sky and total-sky
- Cloud category properties for four (low, lower middle, upper middle and high) cloud layers
- Column averaged cloud properties for five (TOA SW, TOA LW, SFC LW, LWC and IWC) weighting schemes
- Overlap data for eleven (clear, low (L), lower middle (LM), upper middle (UM), high (H),
- H/UM, H/LM, H/L, UM/LM, UM/L, LM/L) cloud overlap conditions
- Angular model scene classes for 12 ERBE scene types
- Atmospheric flux profile for both clear-sky and total-sky at the surface, 500 hPa, the tropopause and the TOA

- Flux adjustments (tuned-untuned) for clear-sky and total-sky at the surface and TOA
- Surface-only data
- Adjustment parameters for clear skies
- Adjustment parameters for L, LM, UM, and H cloud layers

Level: 3
Type: Archival
Frequency: Every 3 hours

Time Interval Covered
File: 3 hours
Record: 3 hours

Portion of Globe Covered
File: Global
Record: 1.25-deg equal-area region

Portion of Atmosphere Covered
File: Surface, internal and TOA

Table B-2. Synoptic Radiative Fluxes and Clouds (SYN)

Description	Parameter Number	Units	Range	Elements/ Record	Bits/ Elem	Elem Num
Meta Data						
SYN Header FIle		N/A		1	380	
Regional Data						
Julian Day	1	day	2449353..2458500	1	32	1
Julian Time	2	day	0..1	1	32	2
Region number	3	N/A	1..26542	1	16	3
Hour-box region number	4	N/A	1..744	1	16	4
Surface altitude	5	km	-12..10	1	16	5
Surface land area	6	percent	0..100	10	16	6
Surface sea area	7	percent	0..100	3	16	16
Precipitable water	8	cm	0.001..8.000	1	16	19
Observed CERES TOA Data for Clear-sky and Total-sky						
CERES TOA SW flux, mean	9	$W\text{-}m^{-2}$	0..1400	2	16	20
CERES TOA SW flux, std	10	$W\text{-}m^{-2}$	TBD	2	16	22
CERES TOA LW flux, mean	11	$W\text{-}m^{-2}$	0..1000	2	16	24
CERES TOA LW flux, std	12	$W\text{-}m^{-2}$	TBD	2	16	26
CERES TOA LW WN flux, mean	13	$W\text{-}m^{-2}$	10..400	2	16	28
CERES TOA LW WN flux, std	14	$W\text{-}m^{-2}$	TBD	2	16	30
Cloud Category Properties for 4 Cloud Layers (Cloud layers are low, lower middle, upper middle and high)						
Cloud layer index	15	N/A	-1..4	4	16	32
Overcast cloud area fraction	16	N/A	0..1	4	16	36
Total cloud area fraction	17	N/A	0..1	4	16	40
Broken cloud area fraction	18	N/A	0..1	4	16	44
Visible optical depth, mean	19	N/A	0..400	4	16	48
Visible optical depth, std	20	N/A	TBD	4	16	52
IR emissivity, mean	21	N/A	0..1	4	16	56
IR emissivity, std	22	N/A	0..1	4	16	60
Cloud liquid water path, mean	23	$g\ m^{-2}$	0.001..10.00	4	16	64
Cloud liquid water path, std	24	$g\ m^{-2}$	TBD	4	16	68
Cloud ice water path, mean	25	$g\ m^{-2}$	0.001..10.00	4	16	72
Cloud ice water path, std	26	$g\ m^{-2}$	TBD	4	16	76
Cloud top pressure, mean	27	hPa	0..1100	4	16	80
Cloud top pressure, std	28	hPa	TBD	4	16	84
Cloud effective pressure, mean	29	hPa	0..1100	4	16	88
Cloud effective pressure, std	30	hPa	TBD	4	16	92
Cloud effective temperature, mean	31	K	100..350	4	16	96
Cloud effective temperature, std	32	K	TBD	4	16	100
Cloud effective height, mean	33	km	0..20	4	16	104
Cloud effective height, std	34	km	TBD	4	16	108
Cloud bottom pressure, mean	35	hPa	0..1100	4	16	112
Cloud bottom pressure, std	36	hPa	TBD	4	16	116
Cloud water particle radius, mean	37	µm	0..200	4	16	120
Cloud water particle radius, std	38	µm	TBD	4	16	124
Cloud ice particle radius, mean	39	µm	0..200	4	16	128
Cloud ice particle radius, std	40	µm	TBD	4	16	132
Cloud particle phase, mean	41	N/A	0..1	4	16	136
Cloud vertical aspect ratio, mean	42	N/A	0..1	4	16	140
Cloud vertical aspect ratio, std	43	N/A	0..1	4	16	144
Visible optical depth/IR emissivity freq dist	44	N/A	0..400	52	16	148

Table B-2. Continued

Description	Parameter Number	Units	Range	Elements/ Record	Bits/ Elem	Elem Num
Column Averaged Cloud Properties for 5 Weighting Schemes (Weighting schemes are TOA SW, TOA LW, SFC LW, LWC and IWC)						
Overcast cloud area fraction	45	N/A	0..1	5	16	200
Total cloud area fraction	46	N/A	0..1	5	16	205
Broken cloud area fraction	47	N/A	0..1	5	16	210
Visible optical depth, mean	48	N/A	0..400	5	16	215
Visible optical depth, std	49	N/A	TBD	5	16	220
IR emissivity, mean	50	N/A	0..1	5	16	225
IR emissivity, std	51	N/A	0..1	5	16	230
Cloud liquid water path, mean	52	g m^{-2}	0.001..10.00	5	16	235
Cloud liquid water path, std	53	g m^{-2}	TBD	5	16	240
Cloud ice water path, mean	54	g m^{-2}	0.001..10.00	5	16	245
Cloud ice water path, std	55	g m^{-2}	TBD	5	16	250
Cloud top pressure, mean	56	hPa	0..1100	5	16	255
Cloud top pressure, std	57	hPa	TBD	5	16	260
Cloud effective pressure, mean	58	hPa	0..1100	5	16	265
Cloud effective pressure, std	59	hPa	TBD	5	16	270
Cloud effective temperature, mean	60	K	100..350	5	16	275
Cloud effective temperature, std	61	K	TBD	5	16	280
Cloud effective height, mean	62	km	0..20	5	16	285
Cloud effective height, std	63	km	TBD	5	16	290
Cloud bottom pressure, mean	64	hPa	0..1100	5	16	295
Cloud bottom pressure, std	65	hPa	TBD	5	16	300
Cloud water particle radius, mean	66	µm	0..200	5	16	305
Cloud water particle radius, std	67	µm	TBD	5	16	310
Cloud ice particle radius, mean	68	µm	0..200	5	16	315
Cloud ice particle radius, std	69	µm	TBD	5	16	320
Cloud particle phase, mean	70	N/A	0..1	5	16	325
Cloud vertical aspect ratio, mean	71	N/A	0..1	5	16	330
Cloud vertical aspect ratio, std	72	N/A	0..1	5	16	335
Visible optical depth/IR emissivity freq dist	73	N/A	0..400	65	16	340
Overlap Data for 11 Cloud Overlap Conditions (Cloud overlap conditions are clear, low (L), lower middle (LM), upper middle (UM), high (H), H/UM, H/LM, H/L, UM/LM, UM/L, and LM/L)						
Total cloud area fraction	74	N/A	0..1	11	16	405
Angular Model Scene Classes for 12 ERBE Scene Types						
Fractional area coverage	75	N/A	0..1	12	16	416
Albedo, mean	76	N/A	0..1	12	16	428
Albedo, std	77	N/A	0..1	12	16	440
Incident solar flux, mean	78	W-m^{-2}	TBD	12	16	452
Incident solar flux, std	79	W-m^{-2}	TBD	12	16	464
Longwave flux, mean	80	W-m^{-2}	TBD	12	16	476
Longwave flux, std	81	W-m^{-2}	TBD	12	16	488
Atmospheric Flux Profile for Clear-sky and Total-sky (Atmospheric layers in profile are surface, 500hPa, tropopause and TOA)						
Number atmospheric layers	82	N/A	0..4	1	16	500
Pressure, atmospheric layer	83	hPa	0..1100	4	16	501
Upward SW, atmospheric layer	84	W-m^{-2}	0..1400	8	16	505
Downward SW, atmospheric layer	85	W-m^{-2}	0..1400	8	16	513
Upward LW, atmospheric layer	86	W-m^{-2}	0..1000	8	16	521
Downward LW, atmospheric layer	87	W-m^{-2}	0..1000	8	16	529
Flux Adjustments (Tuned - Untuned) for Clear-sky and Total-sky at Surface and TOA						
Upward SW, atmospheric layer	88	W-m^{-2}	0..1400	4	16	537
Downward SW, atmospheric layer	89	W-m^{-2}	0..1400	4	16	541
Upward LW, atmospheric layer	90	W-m^{-2}	0..1000	4	16	545
Downward LW, atmospheric layer	91	W-m^{-2}	0..1000	4	16	549

Table B-2. Concluded

Description	Parameter Number	Units	Range	Elements/ Record	Bits/ Elem	Elem Num
Surface-only Data						
Photosynthetically active radiation	92	$W\text{-}m^{-2}$	0..780	1	16	553
DIrect/diffuse ratio	93	N/A	0..30	1	16	554
Adjustment Parameters for Clear Skies						
Adjusted precipitable water, delta	94	cm	0.001..8.000	1	16	555
Adjusted surface albedo, delta	95	N/A	0..1	1	16	556
Adjusted aerosol optical depth, delta	96	N/A	0.0..2.0	1	16	557
Adjusted skin temperature, delta	97	K	TBD	1	16	558
Adjustment Parameters for L, LM, UM and H Cloud Layers						
Adjusted mean visible optical depth, delta	98	N/A	0..400	4	16	559
Adjusted std visible optical depth	99	N/A	TBD	4	16	563
Adjusted mean cloud fractional area, delta	100	N/A	0..1	4	16	567
Adjusted std cloud fractional area	101	N/A	0..1	4	16	571
Adjusted mean cloud IR emissivity, delta	102	N/A	0..1	4	16	575
Adjusted std cloud IR emissivity	103	N/A	0..1	4	16	579
Adjusted mean cloud effective temperature, delta	104	K	0..250	4	16	583
Adjusted std cloud effective temperature	105	K	TBD	4	16	587
Adjusted optical depth/IR emissivity freq dist, delta	106	N/A	0..400	52	16	591

Total Meta Bits/File:	380
Total Data Bits/Record:	10400
Total Records/File:	26542
Total Data Bits/File:	276036800
Total Bits/File:	276037180

Clouds and the Earth's Radiant Energy System (CERES)

Algorithm Theoretical Basis Document

Monthly Regional, Zonal, and Global Radiation Fluxes and Cloud Properties

(Subsystem 8.0)

David F. Young[1]
Edwin F. Harrison[2]
Enakshi Singh[3]

[1]Lockheed Engineering & Sciences Company, Hampton, Virginia 23666
[2]Atmospheric Sciences Division, NASA Langley Research Center, Hampton, Virginia 23681-0001
[3]Science Applications International Corporation (SAIC), Hampton, Virginia 23666

CERES Top Level Data Flow Diagram

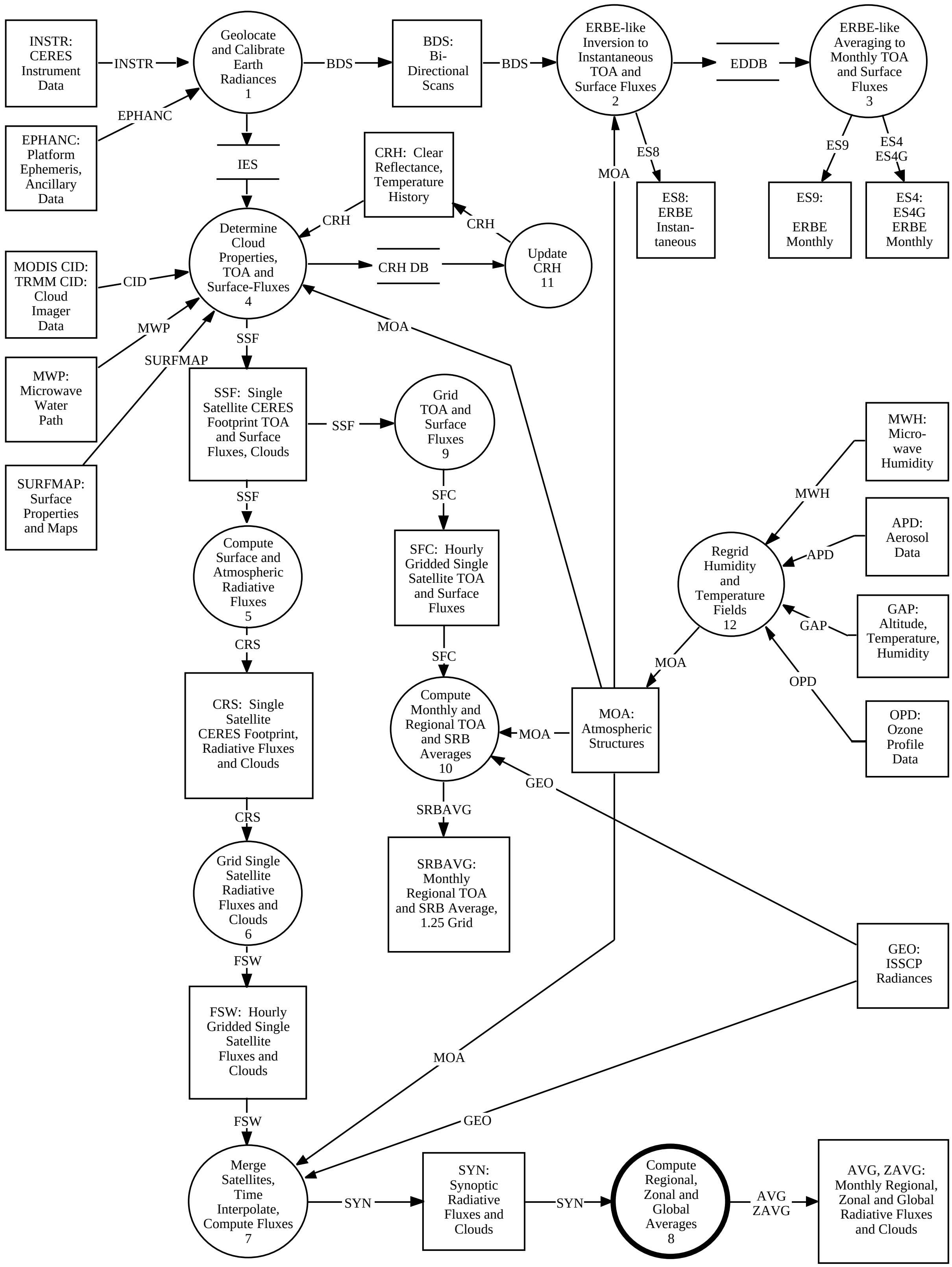

Abstract

The CERES Data Management System produces regional, zonal, and global monthly and monthly-hourly means of the vertical structure of shortwave (SW) and longwave (LW) fluxes and cloud conditions. These means are first calculated on a regional basis from one month of synoptic maps. Regional means are then combined to obtain zonal and global averages.

The input to this subsystem is 1 month of 3-hourly synoptic maps in the form of the SYN data product. This data product contains top-of-the-atmosphere (TOA) LW and SW fluxes, TOA window radiances, upwelling and downwelling SW and LW flux at each standard CERES pressure level, and numerous cloud parameters for each region of the CERES global 1.25° equal-area grid. Both total-sky and clear-sky fluxes are included. A complete description of the input data is provided in appendix A.

This subsystem produces two archived output products. The AVG product contains regional monthly and monthly-hourly means of the vertical structure of SW and LW fluxes and cloud conditions. The ZAVG product contains the same parameters averaged on zonal and global scales. Total-sky and clear-sky fluxes are provided at the TOA, the surface, and at each standard CERES pressure level. Cloud information including SW optical depth, emittance, liquid water path, cloud-top pressure, cloud-bottom pressure, cloud fractional area, cloud droplet radius, and the ice/water phase percentage is provided for each layer bounded by adjacent standard pressure levels. A complete description of the output data is given in appendix B.

The main steps of the monthly averaging process are:

1. *Regionally sort the synoptically-ordered data.*
2. *Linearly average all flux data to produce monthly and monthly-hourly means.*
3. *Average the cloud properties using the proper weighting schemes.*
4. *Combine and average the regional means into zonal and global means.*

8.0. Monthly Regional, Zonal, and Global Radiation Fluxes and Cloud Properties

8.1. Algorithm Description

Zonal and global means are often used by meteorological researchers to study climate. Zonal quantities are useful in studying energy transport. Averaging on large spatial scales minimizes the effects of regional-scale anomalies in studying climate change and global dynamics. Global averages can be compared with other historical data sets derived from different regional scales to detect climate temperature trends and evaluate large-scale climate anomalies such as the effects of major volcanic eruptions.

The first step in the production of monthly means is the organization of the input data. The data are organized as files that each contain synoptic maps of the vertical structure of flux and cloud properties.

A separate data file exists for maps at 0, 3, 6, ..., 21 GMT for each day of the month. Each file contains data organized regionally on the CERES equal-area grid. Sums of data values are maintained for each region and parameter simultaneously. The month of synoptic maps is simply read in sequential order.

The averaging process in this subsystem is extremely straightforward. The temporal interpolation necessary for calculating monthly means has already been performed in subsystem 7, providing a complete data set with uniform time sampling. In addition, the fluxes are also calculated in subsystem 7 at the levels at which they are averaged, so vertical interpolation is not required. Therefore, the monthly means of LW fluxes will be computed by simply averaging the month of synoptic data.

For SW fluxes, special consideration must be made to account for both the constantly changing solar conditions and the change of albedo as a function of solar zenith angle. All SW averages will use the same techniques described in subsystem 3 to correct mean fluxes to more accurately account for the contribution of the total integrated incident solar flux.

Data from each of the four cloud data structures described in subsystem 7 are compiled into monthly means. Monthly means for the cloud category properties and the cloud overlap statistics are averaged linearly using data from the synoptic grids. Monthly means for the angular model scene class data are compiled using only data from times of CERES observations. Column-weighted cloud properties are averaged using the proper weighting schemes as described in subsystem 6.

Since input data are only from 0, 3, 6, ..., 21 GMT, monthly-hourly means are produced for each parameter for only these times. This differs from the monthly-hourly products from SRBAVG which are calculated at all 24 hours based on local, not GMT, time.

Once regional means are computed for all parameters and all regions, these means are combined into zonal and global means. Area weighting factors are used to correct for the slight variation of grid box size with latitude.

8.2. Strategic Concerns

Monthly-hourly averages of LW and SW at the TOA from SRBAVG (the output from subsystem 10) will be compared with the results from averaging the eight synoptic maps to ensure that further interpolation to hourly maps is not required.

Simulations will be performed to determine the effects on the monthly mean SW fluxes of using only 3-hourly synoptic data. Additional time interpolation, similar to that used in the ERBE-like process of subsystem 3 may have to be employed to produce TOA SW flux estimates for all daylight hours before monthly means can be calculated. Studies will be performed to determine the best method for using the TOA SW estimates in an averaging scheme to produce monthly means of surface and atmosphere SW fluxes.

The decision to include additional time interpolation in this Subsystem will also be affected by the handling of data gaps in subsystem 7.1. If restrictions are placed on the maximum time interval over which TOA flux estimates are calculated, then temporal data gaps may exist for some regions. If these gaps are common, then all parameters will be interpolated using the techniques used in subsystem 7.1.

Appendix A

Output Data Products

Compute Regional, Zonal and Global Averages (Subsystem 8.0)

This appendix describes the data products which are used by the algorithms in this subsystem. Table A-1 below summarizes these products, listing the CERES and EOSDIS product codes or abbreviations, a short product name, the product type, the production frequency, and volume estimates for each individual product as well as a complete data month of production. The product types are defined as follows:

Archival products:	Assumed to be permanently stored by EOSDIS
Internal products:	Temporary storage by EOSDIS (days to years)
Ancillary products:	Non-CERES data needed to interpret measurements

The following pages describe each product. An introductory page provides an overall description of the product and specifies the temporal and spatial coverage. The table which follows the introductory page briefly describes every parameter which is contained in the product. Each product may be thought of as metadata followed by data records. The metadata (or header data) is not well-defined yet and is included mainly as a placeholder. The description of parameters which are present in each data record includes parameter number (a unique number for each distinct parameter), units, dynamic range, the number of elements per record, an estimate of the number of bits required to represent each parameter, and an element number (a unique number for each instance of every parameter). A summary at the bottom of each table shows the current estimated sizes of metadata, each data record, and the total data product. A more detailed description of each data product will be contained in a user's guide to be published before the first CERES launch.

Table A-1. Output Products Summary

Product code		Name	Category	Frequency	Size, MB	Monthly size, MB
CERES	EOSDIS					
SYN	CER07	Synoptic radiative fluxes and clouds	archival	Every 3 hours	32.9	8161

Synoptic Radiative Fluxes and Clouds (SYN)

The CERES archival product, synoptic radiative fluxes and clouds (SYN), is produced by the CERES Merge Satellites, Time Interpolate, Compute Fluxes Subsystem. Each SYN file contains regional longwave and shortwave radiative fluxes for the surface, internal atmosphere and TOA. The data are synoptically computed at 3-hour intervals on a 1.25-deg equal area ISCCP-type grid, and are based on measurements from multiple EOS CERES instruments. In addition to being an archival product, the SYN is used by the CERES subsystem, Compute Regional, Zonal and Global Averages.

The SYN contains synoptically averaged

- Regional data
- Observed CERES TOA data for clear-sky and total-sky
- Cloud category properties for four (low, lower middle, upper middle and high) cloud layers
- Column averaged cloud properties for five (TOA SW, TOA LW, SFC LW, LWC and IWC) weighting schemes
- Overlap data for eleven (clear, low (L), lower middle (LM), upper middle (UM), high (H), H/UM, H/LM, H/L, UM/LM, UM/L, LM/L) cloud overlap conditions

- Angular model scene classes for 12 ERBE scene types
- Atmospheric flux profile for both clear-sky and total-sky at the surface, 500 hPa, the tropopause and the TOA
- Flux adjustments (tuned-untuned) for clear-sky and total-sky at the surface and TOA
- Surface-only data
- Adjustment parameters for clear skies
- Adjustment parameters for L, LM, UM, and H cloud layers

Level: 3
Type: Archival
Frequency: Every 3 hours

Portion of Globe Covered
File: Global
Record: 1.25-deg equal-area region

Time Interval Covered
File: 3 hours
Record: 3 hours

Portion of Atmosphere Covered
File: Surface, internal and TOA

Table A-2. Synoptic Radiative Fluxes and Clouds (SYN)

Description	Parameter Number	Units	Range	Elements/ Record	Bits/ Elem	Elem Num
Meta Data						
SYN Header FIle		N/A		1	380	
Regional Data						
Julian Day	1	day	2449353..2458500	1	32	1
Julian Time	2	day	0..1	1	32	2
Region number	3	N/A	1..26542	1	16	3
Hour-box region number	4	N/A	1..744	1	16	4
Surface altitude	5	km	-12..10	1	16	5
Surface land area	6	percent	0..100	10	16	6
Surface sea area	7	percent	0..100	3	16	16
Precipitable water	8	cm	0.001..8.000	1	16	19
Observed CERES TOA Data for Clear-sky and Total-sky						
CERES TOA SW flux, mean	9	$W{\cdot}m^{-2}$	0..1400	2	16	20
CERES TOA SW flux, std	10	$W{\cdot}m^{-2}$	TBD	2	16	22
CERES TOA LW flux, mean	11	$W{\cdot}m^{-2}$	0..1000	2	16	24
CERES TOA LW flux, std	12	$W{\cdot}m^{-2}$	TBD	2	16	26
CERES TOA LW WN flux, mean	13	$W{\cdot}m^{-2}$	10..400	2	16	28
CERES TOA LW WN flux, std	14	$W{\cdot}m^{-2}$	TBD	2	16	30
Cloud Category Properties for 4 Cloud Layers (Cloud layers are low, lower middle, upper middle and high)						
Cloud layer index	15	N/A	-1..4	4	16	32
Overcast cloud area fraction	16	N/A	0..1	4	16	36
Total cloud area fraction	17	N/A	0..1	4	16	40
Broken cloud area fraction	18	N/A	0..1	4	16	44
Visible optical depth, mean	19	N/A	0..400	4	16	48
Visible optical depth, std	20	N/A	TBD	4	16	52
IR emissivity, mean	21	N/A	0..1	4	16	56
IR emissivity, std	22	N/A	0..1	4	16	60
Cloud liquid water path, mean	23	$g\ m^{-2}$	0.001..10.00	4	16	64
Cloud liquid water path, std	24	$g\ m^{-2}$	TBD	4	16	68
Cloud ice water path, mean	25	$g\ m^{-2}$	0.001..10.00	4	16	72
Cloud ice water path, std	26	$g\ m^{-2}$	TBD	4	16	76
Cloud top pressure, mean	27	hPa	0..1100	4	16	80
Cloud top pressure, std	28	hPa	TBD	4	16	84
Cloud effective pressure, mean	29	hPa	0..1100	4	16	88
Cloud effective pressure, std	30	hPa	TBD	4	16	92
Cloud effective temperature, mean	31	K	100..350	4	16	96
Cloud effective temperature, std	32	K	TBD	4	16	100
Cloud effective height, mean	33	km	0..20	4	16	104
Cloud effective height, std	34	km	TBD	4	16	108
Cloud bottom pressure, mean	35	hPa	0..1100	4	16	112
Cloud bottom pressure, std	36	hPa	TBD	4	16	116
Cloud water particle radius, mean	37	µm	0..200	4	16	120
Cloud water particle radius, std	38	µm	TBD	4	16	124
Cloud ice particle radius, mean	39	µm	0..200	4	16	128
Cloud ice particle radius, std	40	µm	TBD	4	16	132
Cloud particle phase, mean	41	N/A	0..1	4	16	136
Cloud vertical aspect ratio, mean	42	N/A	0..1	4	16	140
Cloud vertical aspect ratio, std	43	N/A	0..1	4	16	144
Visible optical depth/IR emissivity freq dist	44	N/A	0..400	52	16	148

Table A-2. Continued

Description	Parameter Number	Units	Range	Elements/ Record	Bits/ Elem	Elem Num
Column Averaged Cloud Properties for 5 Weighting Schemes (Weighting schemes are TOA SW, TOA LW, SFC LW, LWC and IWC)						
Overcast cloud area fraction	45	N/A	0..1	5	16	200
Total cloud area fraction	46	N/A	0..1	5	16	205
Broken cloud area fraction	47	N/A	0..1	5	16	210
Visible optical depth, mean	48	N/A	0..400	5	16	215
Visible optical depth, std	49	N/A	TBD	5	16	220
IR emissivity, mean	50	N/A	0..1	5	16	225
IR emissivity, std	51	N/A	0..1	5	16	230
Cloud liquid water path, mean	52	g m^{-2}	0.001..10.00	5	16	235
Cloud liquid water path, std	53	g m^{-2}	TBD	5	16	240
Cloud ice water path, mean	54	g m^{-2}	0.001..10.00	5	16	245
Cloud ice water path, std	55	g m^{-2}	TBD	5	16	250
Cloud top pressure, mean	56	hPa	0..1100	5	16	255
Cloud top pressure, std	57	hPa	TBD	5	16	260
Cloud effective pressure, mean	58	hPa	0..1100	5	16	265
Cloud effective pressure, std	59	hPa	TBD	5	16	270
Cloud effective temperature, mean	60	K	100..350	5	16	275
Cloud effective temperature, std	61	K	TBD	5	16	280
Cloud effective height, mean	62	km	0..20	5	16	285
Cloud effective height, std	63	km	TBD	5	16	290
Cloud bottom pressure, mean	64	hPa	0..1100	5	16	295
Cloud bottom pressure, std	65	hPa	TBD	5	16	300
Cloud water particle radius, mean	66	μm	0..200	5	16	305
Cloud water particle radius, std	67	μm	TBD	5	16	310
Cloud ice particle radius, mean	68	μm	0..200	5	16	315
Cloud ice particle radius, std	69	μm	TBD	5	16	320
Cloud particle phase, mean	70	N/A	0..1	5	16	325
Cloud vertical aspect ratio, mean	71	N/A	0..1	5	16	330
Cloud vertical aspect ratio, std	72	N/A	0..1	5	16	335
Visible optical depth/IR emissivity freq dist	73	N/A	0..400	65	16	340
Overlap Data for 11 Cloud Overlap Conditions (Cloud overlap conditions are clear, low (L), lower middle (LM), upper middle (UM), high (H), H/UM, H/LM, H/L, UM/LM, UM/L, and LM/L)						
Total cloud area fraction	74	N/A	0..1	11	16	405
Angular Model Scene Classes for 12 ERBE Scene Types						
Fractional area coverage	75	N/A	0..1	12	16	416
Albedo, mean	76	N/A	0..1	12	16	428
Albedo, std	77	N/A	0..1	12	16	440
Incident solar flux, mean	78	W-m^{-2}	TBD	12	16	452
Incident solar flux, std	79	W-m^{-2}	TBD	12	16	464
Longwave flux, mean	80	W-m^{-2}	TBD	12	16	476
Longwave flux, std	81	W-m^{-2}	TBD	12	16	488
Atmospheric Flux Profile for Clear-sky and Total-sky (Atmospheric layers in profile are surface, 500hPa, tropopause and TOA)						
Number atmospheric layers	82	N/A	0..4	1	16	500
Pressure, atmospheric layer	83	hPa	0..1100	4	16	501
Upward SW, atmospheric layer	84	W-m^{-2}	0..1400	8	16	505
Downward SW, atmospheric layer	85	W-m^{-2}	0..1400	8	16	513
Upward LW, atmospheric layer	86	W-m^{-2}	0..1000	8	16	521
Downward LW, atmospheric layer	87	W-m^{-2}	0..1000	8	16	529
Flux Adjustments (Tuned - Untuned) for Clear-sky and Total-sky at Surface and TOA						
Upward SW, atmospheric layer	88	W-m^{-2}	0..1400	4	16	537
Downward SW, atmospheric layer	89	W-m^{-2}	0..1400	4	16	541
Upward LW, atmospheric layer	90	W-m^{-2}	0..1000	4	16	545
Downward LW, atmospheric layer	91	W-m^{-2}	0..1000	4	16	549

Table A-2. Concluded

Description	Parameter Number	Units	Range	Elements/ Record	Bits/ Elem	Elem Num
Surface-only Data						
Photosynthetically active radiation	92	$W\text{-}m^{-2}$	0..780	1	16	553
DIrect/diffuse ratio	93	N/A	0..30	1	16	554
Adjustment Parameters for Clear Skies						
Adjusted precipitable water, delta	94	cm	0.001..8.000	1	16	555
Adjusted surface albedo, delta	95	N/A	0..1	1	16	556
Adjusted aerosol optical depth, delta	96	N/A	0.0..2.0	1	16	557
Adjusted skin temperature, delta	97	K	TBD	1	16	558
Adjustment Parameters for L, LM, UM and H Cloud Layers						
Adjusted mean visible optical depth, delta	98	N/A	0..400	4	16	559
Adjusted std visible optical depth	99	N/A	TBD	4	16	563
Adjusted mean cloud fractional area, delta	100	N/A	0..1	4	16	567
Adjusted std cloud fractional area	101	N/A	0..1	4	16	571
Adjusted mean cloud IR emissivity, delta	102	N/A	0..1	4	16	575
Adjusted std cloud IR emissivity	103	N/A	0..1	4	16	579
Adjusted mean cloud effective temperature, delta	104	K	0..250	4	16	583
Adjusted std cloud effective temperature	105	K	TBD	4	16	587
Adjusted optical depth/IR emissivity freq dist, delta	106	N/A	0..400	52	16	591

Total Meta Bits/File:	380
Total Data Bits/Record:	10400
Total Records/File:	26542
Total Data Bits/File:	276036800
Total Bits/File:	276037180

Appendix B

Output Data Products

Compute Regional, Zonal and Global Averages (Subsystem 8.0)

This appendix describes the data products which are produced by the algorithms in this subsystem. Table B-1 below summarizes these products, listing the CERES and EOSDIS product codes or abbreviations, a short product name, the product type, the production frequency, and volume estimates for each individual product as well as a complete data month of production. The product types are defined as follows:

Archival products:	Assumed to be permanently stored by EOSDIS
Internal products:	Temporary storage by EOSDIS (days to years)

The following pages describe each product. An introductory page provides an overall description of the product and specifies the temporal and spatial coverage. The table which follows the introductory page briefly describes every parameter which is contained in the product. Each product may be thought of as metadata followed by data records. The metadata (or header data) is not well-defined yet and is included mainly as a placeholder. The description of parameters which are present in each data record includes parameter number (a unique number for each distinct parameter), units, dynamic range, the number of elements per record, an estimate of the number of bits required to represent each parameter, and an element number (a unique number for each instance of every parameter). A summary at the bottom of each table shows the current estimated sizes of metadata, each data record, and the total data product. A more detailed description of each data product will be contained in a user's guide to be published before the first CERES launch.

Table B-1. Output Products Summary

Product code		Name	Category	Frequency	Size, MB	Monthly size, MB
CERES	EOSDIS					
AVG	CER08	Monthly regional radiative fluxes and clouds	archival	1/month	364.3	364
ZAVG	CER08	Monthly zonal and global radiative fluxes and clouds	archival	1/month	2.1	2

Monthly Regional Radiative Fluxes and Clouds (AVG)

The AVG product contains a monthly and monthly hourly average of the TOA and surface LW and SW radiative fluxes, together with LW and SW fluxes at standard pressure levels in between. This final product also contains observed cloud and clear-sky properties at the standard 1.25 degree horizontal resolution.

AVG is an archival product produced for each spacecraft and for each combination of spacecraft. Initially at the TRMM launch, this product is produced in a validation mode every 3 months, or for 4 months a year. During these 18 months, the CERES Science Team will derive a production quality set of angular distribution models, which are needed to produce the LW and SW instantaneous fluxes. Eighteen months after the TRMM launch, this product is archived and contains LW and SW fluxes at the tropopause and at 500 hPa pressure levels. Thirty-six months after the TRMM launch, this archived product contains LW and SW fluxes at 18 standard pressure levels. The pressure levels are in addition to fluxes at TOA and at the surface. In addition, the cloud and clear-sky properties are averaged between the 18 pressure levels, resulting in 17 vertical instances of the averaged cloud properties.

The major categories of data on the AVG are

- Regional location data
- Radiative fluxes for both clear-sky and total-sky at TOA
- Cloud category properties for four (low, lower middle, upper middle and high) cloud layers
- Column-averaged cloud properties for five (TOA SW, TOA LW, SFC LW, LWP, and IWP) weighting schemes
- Overlap data for eleven (clear, low (L), lower middle (LM), upper middle (UM), high (H), H/UM, H/LM, H/L, UM/LM, UM/L, LM/L) cloud conditions
- Angular model scene classes
- Adjustment parameters for four cloud layers
- Atmospheric flux profile for clear-sky and total-sky
- Flux adjustments for clear-sky and total-sky
- Surface-only data
- •Adjustment parameters for clear-skies

Level: 3
Type: Archival
Frequency: 1/month

Portion of Globe Covered
File: Entire globe
Record: 1.25 degree regions

Time Interval Covered
File: 1 month
Record: 1 month

Portion of Atmosphere Covered
File: Surface to TOA

Table B-2. Monthly Regional Radiative Fluxes and Clouds (AVG)

Description	Parameter Number	Units	Range	Elements/ Record	Bits/ Elem	Elem Num
AVG						
AVG File Header				1	2048	
Data Avg is Array[26542] of:						
Avg Data						
Location Data						
Region number	1	N/A	1 - 26542	1	16	1
Surface altitude	2	km	-12 - 10	1	16	2
Surface land area	3	percent	0 - 100	10	16	3
Surface sea area	4	percent	0 - 100	3	16	13
Precipitable water	5	cm	0.001 - 8.000	1	16	16
Monthly Data						
Fluxes for 2 Scene Classes is Array[6] of:						
(Scene classes: clear-sky, total-sky)						
SW Flux at TOA: mean, std, num days	6	$W\text{-}m^{-2}$	0.0 - 1400.0	6	16	17
LW flux at TOA: mean, std, num days	7	$W\text{-}m^{-2}$	0.0 - 1000.0	6	16	23
Window flux: mean, std, num days	8	$W\text{-}m^{-2}$	10.0 - 400.0	6	16	29
Cloud Category Properties is Array[4] of:						
(Cloud layers: H,UM,LM, & L)						
Cloud Layer Class	9	N/A	-1 - 4	4	16	35
Cloud Properties is Array[3] of:						
Overcast cloud area fraction	10	N/A	0.0 - 1.0	12	16	39
Total cloud area fraction	11	N/A	0.0 - 1.0	12	16	51
Broken cloud area fraction	12	N/A	0.0 - 1.0	12	16	63
Optical depth: mean, std, num days	13	N/A	0.0 - 400.0	12	16	75
Infrared emissivity: mean, std, num days	14	N/A	0.0 - 1.0	12	16	87
Liquid water path: mean, std, num days	15	$g\ m^{-2}$	0.01 - 1000.0	12	16	99
Ice water path: mean, std, num days	16	$g\ m^{-2}$	0.01 - 1000.0	12	16	111
Cloud top pressure: mean, std, num days	17	hPa	0.0 - 1100.0	12	16	123
Cloud effective pressure: mean, std, num days	18	hPa	TBD	12	16	135
Cloud effective temperature: mean, std, num days	19	K	TBD	12	16	147
Cloud effective height: mean, std, num days	20	km	0.0 - 20.0	12	16	159
Cloud bottom pressure: mean, std, num days	21	hPa	0.0 - 1100.0	12	16	171
Liquid particle radius: mean, std, num days	22	µm	N/A	12	16	183
Ice particle radius: mean, std, num days	23	µm	N/A	12	16	195
Cloud particle phase: mean, std, num days	24	N/A	0 - 1	12	16	207
Cloud vertical aspect ratio: mean, std, num days	25	N/A	TBD	12	16	219
Adjusted effective temperature: mean, std, num days	26	K	TBD	12	16	231
Adjusted optical depth: mean, std, num days	27	N/A	TBD	12	16	243
Adjusted cloud frac area: mean, std, num days	28	percent	0.0 - 100.0	12	16	255
Adjusted IR emissivity: mean, std, num days	29	N/A	TBD	12	16	267
Optical Depth Histogram is Array[13] of:						
Visible optical depth/IR emissivity: freq dist	30	N/A	TBD	156	16	279
Column Averaged Cloud Properties is Array[15] of:						
(Five weightings: TOA SW,TOA LW,SFC LW,LWP, & IWP)						
Overcast cloud area fraction	31	N/A	0.0 - 1.0	15	16	435
Total cloud area fraction	32	N/A	0.0 - 1.0	15	16	450
Broken cloud area fraction	33	N/A	0.0 - 1.0	15	16	465
Optical depth: mean, std, num days	34	N/A	0.0 - 50.0	15	16	480

Table B-2. Continued

Description	Parameter Number	Units	Range	Elements/ Record	Bits/ Elem	Elem Num
Infrared emissivity: mean, std, num days	35	N/A	0.0 - 1.0	15	16	495
Liquid water path: mean, std, num days	36	g m^{-2}	0.001 - 10.0	15	16	510
Ice water path: mean, std, num days	37	g m^{-2}	0.001 - 10.0	15	16	525
Cloud top pressure: mean, std, num days	38	hPa	0.0 - 1100.0	15	16	540
Cloud effective pressure: mean, std, num days	39	hPa	0.0 - 1100.0	15	16	555
Cloud effective temperature: mean, std, num days	40	K	100.0 - 350.0	15	16	570
Cloud effective height: mean, std, num days	41	km	0.0 - 20.0	15	16	585
Cloud bottom pressure: mean, std, num days	42	hPa	0.0 - 1100.0	15	16	600
Liquid particle radius: mean, std, num days	43	µm	0.0 - 200.0	15	16	615
Ice particle radius: mean, std, num days	44	µm	0.0 - 200.0	15	16	630
Cloud particle phase: mean, std, num days	45	N/A	0 - 1	15	16	645
Cloud vertical aspect ratio: mean, std, num days	46	N/A	0.0 - 1.0	15	16	660
Adjusted effective temperature: mean, std, num days	47	K	0.0 250.0	15	16	675
Adjusted optical depth: mean, std, num days	48	N/A	0.0 - 400.0	15	16	690
Adjusted cloud frac area: mean, std, num days	49	N/A	0.0 - 1.0	15	16	705
Adjusted IR emissivity: mean, std, num days	50	N/A	0.0 - 1.0	15	16	720
Optical Depth Histogram is Array[13] of:						
Visible optical depth/IR emissivity: freq dist	51	N/A	0.0 - 400.0	195	16	735
Eleven Cloud Overlap Conditions is Array[11] of:						
Area Coverage: regional	52	N/A	0.0 - 1.0	11	16	930
Angular Model Scene Classes is Array[12] of:						
Fractional area coverage	53	N/A	0.0 - 1.0	12	16	941
Albedo: mean, std	54	N/A	0.0 - 1.0	24	16	953
Incident solar flux: mean, std	55	W-m^{-2}	TBD	24	16	977
LW flux: mean, std	56	W-m^{-2}	TBD	24	16	1001
Fluxes levels						
Atmospheric Flux Profile for 2 Scene Classes & 4 Layers						
(Scene classes: clear-sky & total-sky is Array[24] of:						
Layers: sfc,500hPa,tropopause, & TOA)						
Upward SW flux: mean, std, num days	57	W-m^{-2}	0.0 - 1400.0	24	16	1025
Downward SW flux: mean, std, num days	58	W-m^{-2}	0.0 - 1400.0	24	16	1049
Upward LW flux: mean, std, num days	59	W-m^{-2}	0.0 - 1000.0	24	16	1073
Downward LW flux: mean, std, num days	60	W-m^{-2}	0.0 - 1000.0	24	16	1097
Number atmospheric layers	61	N/A	0 - 4	1	16	1121
Pressure, atmospheric layer	62	hPa	0 - 1100	4	16	1122
Flux Adjustments (Tuned-Untuned) for 2 Scene Classes & 2 Layers						
(Scene classes: clear-sky, total-sky is Array[12] of:						
Layers: sfc, TOA)						
Upward SW flux: mean, std, num days	63	W-m^{-2}	0.0 - 1400.0	12	16	1126
Downward SW flux: mean, std, num days	64	W-m^{-2}	0.0 - 1400.0	12	16	1138
Upward LW flux: mean, std, num days	65	W-m^{-2}	0.0 - 1000.0	12	16	1150
Downward LW flux: mean, std, num days	66	W-m^{-2}	0.0 - 1000.0	12	16	1162
Surface Only Data						
Photosynthetically active radiation	67	W-m^{-2}	0.0 - 780.0	1	16	1174
Direct/Diffuse ratio at surface: mean	68	N/A	0.0 - 30.0	1	16	1175
Adjustment Parameters						
Adjusted precipitable water: mean	69	cm	0.001 - 8.000	1	16	1176
Adjusted surface albedo: mean	70	N/A	0 - 1	1	16	1177

Table B-2. Continued

Description	Parameter Number	Units	Range	Elements/ Record	Bits/ Elem	Elem Num
Adjusted aerosol optical depth: mean	71	N/A	0.0 - 2.0	1	16	1178
Adjusted skin temperature: mean	72	K	TBD	1	16	1179
Monthly Hourly Data is Array[8] of:						
Eight hours						
Fluxes for 2 Scene Classes MH is Array[6] of:						
(Scene classes: clear-sky, total-sky)						
SW flux at TOA: mean, std, num hrs	73	$W\text{-}m^{-2}$	0.0 - 1400.0	48	16	1180
LW flux at TOA: mean, std, num hrs	74	$W\text{-}m^{-2}$	0.0 - 1000.0	48	16	1228
Window flux: mean, std, num hrs	75	$W\text{-}m^{-2}$	10.0 - 400.0	48	16	1276
Column Averaged Cloud Properties MH is Array[15] of:						
(Five weightings: TOA SW,TOA LW,SFC LW,LWP, & IWP)						
Overcast cld area fraction	76	N/A	0.0 - 1.0	120	16	1324
Total cloud area fraction	77	N/A	0.0 - 1.0	120	16	1444
Broken cloud area fraction	78	N/A	0.0 - 1.0	120	16	1564
Visible optical depth: mean, std, num hrs	79	N/A	0.0 - 400.0	120	16	1684
Infrared emissivity: mean, std, num hrs	80	N/A	0.0 - 1.0	120	16	1804
Cloud liquid water path: mean, std, num hrs	81	$g\ m^{-2}$	0.001 - 10.0	120	16	1924
Cloud ice water path: mean, std, num hrs	82	$g\ m^{-2}$	0.001 - 10.0	120	16	2044
Cloud top pressure: mean, std, num hrs	83	hPa	0.0 - 1100.0	120	16	2164
Cloud effective pressure: mean, std, num hrs	84	hPa	0.0 - 11.00	120	16	2284
Cloud effective temperature: mean, std, num hrs	85	K	100.0 - 250.0	120	16	2404
Cloud effective height: mean, std, num hrs	86	km	0.0 - 20.0	120	16	2524
Cloud bottom pressure: mean, std, num hrs	87	hPa	0.0 - 1100.0	120	16	2644
Cloud liquid particle radius: mean, std, num hrs	88	µm	0.0 - 200.0	120	16	2764
Cloud ice particle radius: mean, std, num hrs	89	µm	0.0 - 200.0	120	16	2884
Cloud particle phase: mean, std, num hrs	90	N/A	0.0 - 1.0	120	16	3004
Cloud vertical aspect ratio: mean, std, num hrs	91	N/A	0.0 - 1.0	120	16	3124
Adjusted cloud effective temperature: mean, std, num hrs	92	K	0.0 - 250.0	120	16	3244
Adjusted optical depth: mean, std, num hrs	93	N/A	0.0 - 400.0	120	16	3364
Adjusted cloud IR emissivity: mean, std, num hrs	94	N/A	0.0 - 1.0	120	16	3484
Adjusted cloud fractional area: mean, std, num hrs	95	N/A	0.0 - 1.0	120	16	3604
Optical Depth Histogram MH is Array[13] of:						
Visible optical depth/IR emissivity, freq dist	96	N/A	0.0 - 400.0	1560	16	3724
Angular Model Scene Classes MH is Array[12] of:						
Fractional area coverage	97	N/A	0.0 - 1.0	96	16	5284
Albedo: mean, std	98	N/A	0.0 - 1.0	192	16	5380
Incident solar flux: mean, std	99	$W\text{-}m^{-2}$	TBD	192	16	5572
LW flux: mean, std	100	$W\text{-}m^{-2}$	TBD	192	16	5764
Fluxes levels MH						
Atmospheric Flux Profile for 2 Scene Classes & 4 Layers						
(Scene classes: clear-sky, total-sky is Array[24] of:						
Layers: sfc,500hPa,tropopause, & TOA)						
Upward SW flux: mean, std, num hrs	101	$W\text{-}m^{-2}$	0.0 - 1400.0	192	16	5956
Downward SW flux: mean, std, num hrs	102	$W\text{-}m^{-2}$	0.0 - 1400.0	192	16	6148
Upward LW flux: mean, std, num hrs	103	$W\text{-}m^{-2}$	0.0 - 1000.0	192	16	6340
Downward LW flux: mean, std, num hrs	104	$W\text{-}m^{-2}$	0.0 - 1000.0	192	16	6532

Table B-2. Concluded

Description	Parameter Number	Units	Range	Elements/ Record	Bits/ Elem	Elem Num
Number atmospheric layers	105	N/A	0 - 4	8	16	6724
Pressure, atmospheric layer	106	hPa	0 - 1100	32	16	6732
Flux Adjustments (Tuned - Untuned) for 2 Scene Classes & 2 Layers						
(Scene classes: clear-sky & total-sky is Array[12] of:						
Layers: sfc, TOA)						
Upward SW flux: mean, std, num hrs	107	$W\text{-}m^{-2}$	0.0 - 1400.0	96	16	6764
Downward SW flux: mean, std, num hrs	108	$W\text{-}m^{-2}$	0.0 - 1400.0	96	16	6860
Upward LW flux: mean, std, num hrs	109	$W\text{-}m^{-2}$	0.0 - 1000.0	96	16	6956
Downward LW flux: mean, std, num hrs	110	$W\text{-}m^{-2}$	0.0 - 1000.0	96	16	7052
Surface Only Data MH						
Photosynthetically active radiation	111	$W\text{-}m^{-2}$	0.0 - 780.0	8	16	7148
Direct/Diffuse ratio at surface: mean	112	N/A	0.0 - 30.0	8	16	7156
Adjustment Parameters MH						
Adjusted precipitable water: mean	113	cm	0.001 - 8.000	8	16	7164
Adjusted surface albedo: mean	114	N/A	0 - 1	8	16	7172
Adjusted aerosol optical depth: mean	115	N/A	0.0 - 2.0	8	16	7180
Adjusted skin temperature: mean	116	K	TBD	8	16	7188
Total Meta Bits/File:	2048					
Total Data Bits/Record:	115120					
Total Records/File:	26542					
Total Data Bits/File:	3055515040					
Total Bits/File:	3055517088					

Monthly Zonal and Global Radiative Fluxes and Clouds (ZAVG)

The ZAVG product is a summary of the zonal and global averages of the radiative fluxes and cloud properties, probably most suitable for inclusion in the EOSDIS IMS as a browse product. This product is the CERES equivalent to the zonal averages and global averages in the ERBE S-4 product.

ZAVG is an archival product produced by the TISA subsystem for each spacecraft and for each combination of spacecraft. Initially at the TRMM launch, this product is produced in a validation mode every 3 months, or for 4 months a year. During these 18 months, the CERES Science Team will derive a production quality set of angular distribution models, which are needed to produce the LW and SW instantaneous fluxes. Eighteen months after the TRMM launch, this product is archived and contains LW and SW fluxes at the tropopause and at 500 hPa pressure levels. Thirty-six months after the TRMM launch, this archived product contains LW and SW fluxes at 18 standard pressure levels. The pressure levels are in addition to fluxes at TOA and at the surface. In addition, the cloud and clear-sky properties are averaged between the 18 pressure levels, resulting in 17 vertical instances of the averaged cloud properties. ZAVG contains one record of monthly and monthly hourly averages for each of the 144 latitudinal zones and one record of global averages.

The major categories of data on the ZAVG are

- Regional location data
- Radiative fluxes for both clear-sky and total-sky at TOA
- Cloud category properties for four (low, lower middle, upper middle and high) cloud layers
- Column-averaged cloud properties for five (TOA SW, TOA LW, SFC LW, LWP, and IWP) weighting schemes
- Overlap data for eleven (clear, low (L), lower middle (LM), upper middle (UM), high (H), H/UM, H/LM, H/L, UM/LM, UM/L, LM/L) cloud conditions
- Angular model scene classes
- Adjustment parameters for four cloud layers
- Atmospheric flux profile for clear-sky and total-sky
- Flux adjustments for clear-sky and total-sky
- Surface-only data
- Adjustment parameters for clear-skies

Level: 3
Type: Archival
Frequency: 1/month

Time Interval Covered
File: 1 month
Record: 1 month

Portion of Globe Covered
File: Entire globe
Record: Zonal and global

Portion of Atmosphere Covered
File: Surface to TOA

Table B-3. Monthly Zonal and Global Radiative Fluxes and Clouds (ZAVG)

Description	Parameter Number	Units	Range	Elements/ Record	Bits/ Elem	Elem Num
ZAVG						
AVG File Header				1	2048	
Data Zavg is Array[145] of:						
ZAVG Zonal and Global Averages						
Location Data Zon						
Zone number	1	N/A	1 - 145	1	16	1
Surface altitude	2	km	-12 - 10	1	16	2
Surface land area	3	percent	0 - 100	10	16	3
Surface sea area	4	percent	0 - 100	3	16	13
Precipitable water	5	cm	0.001 - 8.000	1	16	16
Monthly Zonal and Global Data						
Fluxes Zonal for 2 Scene Classes is Array[6]] of:						
(Scene Classes: clear-sky total-sky)						
SW flux at TOA: mean, std, num days	6	W-m^{-2}	0.0 - 1400.0	6	16	17
LW flux at TOA: mean, std, num days	7	W-m^{-2}	0.0 - 1400.0	6	16	20
Window flux: mean, std, num days	8	W-m^{-2}	10.0 - 400.0	6	16	23
Cloud Category Properties Zonal is Array[4] of:						
(Cloud Layers: H,UM,LM, & L)						
Cloud layer class	9	N/A	-1 - 4	4	16	26
Cloud Properties Zonal is Array[3] of:						
Overcast cloud area fraction	10	N/A	0.0 - 1.0	12	16	30
Total cloud area fraction	11	N/A	0.0 - 1.0	12	16	42
Broken cloud area fraction	12	N/A	0.0 - 1.0	12	16	54
Visible optical depth: mean, std, num days	13	N/A	0.0 - 400.0	12	16	66
Infrared emissivity: mean, std, num days	14	N/A	0.0 - 1.0	12	16	78
Cloud liquid water path: mean, std, num days	15	g m^{-2}	0.001 - 10.0	12	16	90
Cloud ice water path: mean, std, num days	16	g m^{-2}	0.001 - 10.0	12	16	102
Cloud top pressure: mean, std, num days	17	hPa	0.0 - 1100.0	12	16	114
Cloud effective pressure: mean, std, num days	18	hPa	0.0 - 11.0	12	16	126
Cloud effective temperature: mean, std, num days	19	K	100.0 - 350.0	12	16	138
Cloud effective height: mean, std, num days	20	km	0.0 - 20.0	12	16	150
Cloud bottom pressure: mean, std, num days	21	hPa	0.0 - 1100.0	12	16	162
Cloud liquid particle radius: mean, std, num days	22	µm	0.0 - 200.0	12	16	174
Cloud ice particle radius: mean, std, num days	23	µm	0.0 - 200.0	12	16	186
Cloud particle phase: mean, std, num days	24	N/A	0 - 1	12	16	198
Cloud vertical aspect ratio: mean, std, num days	25	N/A	0.0 - 1.0	12	16	210
Zonal Optical Depth Histogram is Array[13] of:						
Visible optical depth/IR emissivity, freq dist	26	N/A	0.0 - 400.0	156	16	222
Column Averaged Cloud Properties ZAVG is Array[15] of:						
(Five weightings: TOA SW,TOA LW,SFC LW,LWP, & IWP)						
Overcast cloud area fraction	27	N/A	0.0 - 1.0	15	16	378
Total cloud area fraction	28	N/A	0.0 - 1.0	15	16	393
Broken cloud area fraction	29	N/A	0.0 - 1.0	15	16	408
Visible optical depth: mean, std, num days	30	N/A	0.0 - 400.0	15	16	423
Infrared emissivity: mean, std, num days	31	N/A	0.0 - 1.0	15	16	438
Cloud liquid water path: mean, std, num days	32	g m^{-2}	0.001 - 10.0	15	16	453
Cloud ice water path: mean, std, num days	33	g m^{-2}	0.001 - 10.0	15	16	468

Table B-3. Continued

Description	Parameter Number	Units	Range	Elements/ Record	Bits/ Elem	Elem Num
Cloud top pressure: mean, std, num days	34	hPa	0.0 - 1100.0	15	16	483
Cloud effective pressure: mean, std, num days	35	hPa	0.0 - 1100.0	15	16	498
Cloud effective temperature: mean, std, num days	36	K	100.0 - 350.0	15	16	513
Cloud effective height: mean, std, num days	37	km	0.0 - 20.0	15	16	528
Cloud bottom pressure: mean, std, num days	38	hPa	0.0 - 1100.0	15	16	543
Cloud liquid particle radius: mean, std, num days	39	µm	0.0 - 200.0	15	16	558
Cloud ice particle radius: mean, std, num days	40	µm	0.0 - 200.0	15	16	573
Cloud particle phase: mean, std, num days	41	N/A	0.0 - 1.0	15	16	588
Cloud vertical aspect ratio: mean, std, num days	42	N/A	0.0 - 1.0	15	16	603
Zonal Optical Depth Histogram is Array[13] of:						
Visible optical depth/IR emissivity, freq dist	43	N/A	0.0 - 400.0	195	16	618
Eleven Cloud Overlap Conditions Zonal is Array[11] of:						
Area coverage	44	N/A	0.0 - 1.0	11	16	813
Angular Model Scene Classes is Array[12] of:						
Fractional area coverage	45	N/A	0.0 - 1.0	12	16	824
Albedo: mean, std	46	N/A	0.0 - 1.0	24	16	836
Incident solar flux: mean, std	47	$W\text{-}m^{-2}$	TBD	24	16	860
LW flux: mean, std	48	$W\text{-}m^{-2}$	TBD	24	16	884
Adjustment Parameters for 4 Cloud Layers Zonal						
Adjusted cloud effective temperature: mean, std, num days	49	K	0.0 - 250.0	12	16	908
Adjusted optical depth: mean, std, num days	50	N/A	0.0 - 400.0	12	16	909
Adjusted cloud fractional area: mean, std, num days	51	N/A	0.0 - 1.0	12	16	910
Adjusted cloud IR emissivity: mean, std, num days	52	N/A	0.0 - 1.0	12	16	911
Zonal Optical Depth Histogram Cloud Layer is Array[13] of:						
Visible optical depth/IR emissivity, freq dist	53	N/A	0.0 - 400.0	52	16	912
Fluxes-levels Zonal						
Atmospheric Flux Profile for 2 Scene Classes & 4 Layers						
(Scene classes, clear-sky, total-sky is Array[24] of:						
Layers:sfc,500 hPa, tropopause, & TOA)						
Number atmospheric layers	54	N/A	0 - 4	1	16	925
Pressure, atmospheric layer	55	hPa	0 - 1100	4	16	926
Upward SW flux: mean, std, num days	56	$W\text{-}m^{-2}$	0.0 - 1400.0	24	16	930
Downward SW flux: mean, std, num days	57	$W\text{-}m^{-2}$	0.0 - 1400.0	24	16	954
Upward LW flux: mean, std, num days	58	$W\text{-}m^{-2}$	0.0 - 1000.0	24	16	978
Downward LW flux: mean, std, num days	59	$W\text{-}m^{-2}$	0.0 - 1000.0	24	16	1002
Flux, Adjustments (Tuned - Untuned) for 2 Scene Classes & 2 Layers						
(Scene classes: clear-sky, total sky is Array[12] of:						
Layers: sfc, TOA)						
Upward SW flux; mean, std, num days	60	$W\text{-}m^{-2}$	0.0 - 1400.0	12	16	1026
Downward SW flux: mean, std, num days	61	$W\text{-}m^{-2}$	0.0 - 1400.0	12	16	1038
Upward LW flux: mean, std, num days	62	$W\text{-}m^{-2}$	0.0 - 1000.0	12	16	1050
Downward LW flux: mean, std, num days	63	$W\text{-}m^{-2}$	0.0 - 1000.0	12	16	1062
Surface only Data Zonal						
Photosynthetically active radiation	64	$W\text{-}m^{-2}$	0.0 - 780.0	1	16	1074
Direct/Diffuse ratio	65	N/A	0.0 - 30.0	1	16	1075
Adjustment Parameters for Clear-sky Zonal						

Table B-3. Continued

Description	Parameter Number	Units	Range	Elements/ Record	Bits/ Elem	Elem Num
Adjusted precipitable water: mean	66	cm	0.001 - 8.000	1	16	1076
Adjusted surface albedo: mean	67	N/A	0 - 1	1	16	1077
Adjusted aerosol optical depth: mean	68	N/A	0.0 - 2.0	1	16	1078
Adjusted skin temperature: mean	69	K	TBD	1	16	1079
Monthly Hourly Zonal and Global Data is Array[8] of:						
Eight hours						
Fluxes for 2 Scene Classes Zonal MH is Array[6] of:						
(Scene classes: clear-sky, total-sky)						
SW flux at TOA: mean, std, num hrs	70	$W\text{-}m^{-2}$	0.0 - 1400.0	48	16	1080
LW flux at TOA: mean, std, num hrs	71	$W\text{-}m^{-2}$	0.0 - 1000.0	48	16	1104
Window flux: mean, std, num hrs	72	$W\text{-}m^{-2}$	10.0 - 400.0	48	16	1128
Column Averaged Cloud Properties Zonal MH is Array[15] of:						
(Five weightings: TOA SW,TOA LW,SFC LW,LWP,&IWP)						
Overcast cloud area fraction	73	N/A	0.0 - 1.0	120	16	1152
Total cloud area fraction	74	N/A	0.0 - 1.0	120	16	1272
Broken cloud area fraction	75	N/A	0.0 - 1.0	120	16	1392
Visible optical depth: mean, std, num hrs	76	N/A	0.0 - 400.0	120	16	1512
Infrared emissivity: mean, std, num hrs	77	N/A	0.0 - 1.0	120	16	1632
Cloud liquid water path: mean, std, num hrs	78	$g\ cm^{-2}$	0.001 - 10.0	120	16	1752
Cloud ice water path: mean, std, num hrs	79	$g\ cm^{-2}$	0.001 - 10.0	120	16	1872
Cloud top pressure: mean, std, num hrs	80	hPa	0.0 - 1100.0	120	16	1992
Cloud effective pressure: mean, std, num hrs	81	hPa	0.0 - 1100.0	120	16	2112
Cloud effective temperature: mean, std, num hrs	82	K	100.0 - 350.0	120	16	2232
Cloud effective height: mean, std, num hrs	83	km	0.0 - 20.0	120	16	2352
Cloud bottom pressure: mean, std, num hrs	84	hPa	0.0 - 1100.0	120	16	2472
Cloud liquid particle radius: mean, std, num hrs	85	TBD	0.0 - 200.0	120	16	2592
Cloud ice particle radius: mean, std, num hrs	86	TBD	0.0 - 200.0	120	16	2712
Cloud particle phase: mean, std, num hrs	87	N/A	0 - 1	120	16	2832
Cloud vertical aspect ratio: mean, std, num hrs	88	N/A	0.0 - 1.0	120	16	2952
Zonal Optical Depth Histogram MH is Array[13] of:						
Visible optical depth/IR emissivity, freq dist	89	N/A	0.0 - 400.0	1560	16	3072
Angular Model Scene Classes is Array[12] of:						
Fractional area coverage	90	N/A	0.0 - 1.0	96	16	4632
Albedo: mean, std	91	N/A	0.0 - 1.0	192	16	4728
Incident solar flux: mean, std	92	$W\text{-}m^{-2}$	TBD	192	16	4920
LW flux: mean, std	93	$W\text{-}m^{-2}$	TBD	192	16	5112
Adjustment Parameters for 4 Cloud Layers, Zonal MH						
Adjusted cloud effective temperature: mean, std, num days	94	K	0.0 - 250.0	12	16	5304
Adjusted optical depth: mean, std, num days	95	N/A	0.0 - 400.0	12	16	5312
Adjusted cloud fractional area: mean, std, num days	96	N/A	0.0 - 1.0	12	16	5320
Adjusted cloud IR emissivity: mean, std, num days	97	N/A	0.0 - 1.0	12	16	5328
Zonal Optical Depth Histogram Cloud Class MH is Array[13] of:						
Visible optical depth/IR emissivity, freq dist	98	N/A	0.0 - 400.0	104	16	5336
Fluxes levels, Zonal MH						
Atmospheric Flux Profile for 2 Scene Classes & 4 Layers, MH						

Table B-3. Concluded

Description	Parameter Number	Units	Range	Elements/ Record	Bits/ Elem	Elem Num
(Scene Classes: clear-sky, total-sky is Array[24] of:						
Layers: sfc,500 hPa, tropopause, & TOA)						
Number atmospheric layers	99	N/A	0 - 4	8	16	5440
Pressure, atmospheric layer	100	hPa	0 - 1100	32	16	5448
Upward SW flux: mean, std, num hrs	101	$W\text{-}m^{-2}$	0.0 - 1400.0	192	16	5480
Downward SW flux: mean, std, num hrs	102	$W\text{-}m^{-2}$	0.0 - 1400.0	192	16	5672
Upward LW flux: mean, std, num hrs	103	$W\text{-}m^{-2}$	0.0 - 1000.0	192	16	5864
Downward LW flux: mean, std, num hrs	104	$W\text{-}m^{-2}$	0.0 - 1000.0	192	16	6056
Flux Adjustments (Tuned - Untuned) for 2 Scene Classes & 2 Layers, MH						
(Scene classes: clear-sky, total-sky is Array[12] of:						
Layers: sfc & TOA)						
Upward SW flux: mean, std, num hrs	105	$W\text{-}m^{-2}$	0.0 - 1400.0	96	16	6248
Downward SW flux: mean, std, num hrs	106	$W\text{-}m^{-2}$	0.0 - 1400.0	96	16	6344
Upward LW flux: mean, std, num hrs	107	$W\text{-}m^{-2}$	0.0 - 1000.0	96	16	6440
Downward LW flux: mean, std, num hrs	108	$W\text{-}m^{-2}$	0.0 - 1000.0	96	16	6536
Surface only Data Zonal MH						
Photsynthetically active radiation	109	$W\text{-}m^{-2}$	**0.0 - 780.0**	**8**	**16**	**6632**
Direct/Diffuse ratio	110	N/A	0.0 - 30.0	8	16	6640
Adjustment Parameters Zonal MH						
Adjusted precipitable water: mean	111	cm	0.001 - 8.000	8	16	6648
Adjusted surface albedo: mean	112	N/A	0 - 1	8	16	6656
Adjusted aerosol optical depth: mean	113	N/A	0.0 - 2.0	8	16	6664
Adjusted skin temperature: mean	114	K	TBD	8	16	6672
Total Meta Bits/File:	2048					
Total Data Bits/Record:	120112					
Total Records/File:	145					
Total Data Bits/File:	**1741620**					
Total Bits/File:	17418288					

Clouds and the Earth's Radiant Energy System (CERES)

Algorithm Theoretical Basis Document

Grid TOA and Surface Fluxes for Instantaneous Surface Product

(Subsystem 9.0)

G. Louis Smith[1]
Kathryn A. Bush[2]
F. E. Martino III[2]
Rajeeb Hazra[3]
Natividad Manalo-Smith[4]
David Rutan[4]

[1]Atmospheric Sciences Division, NASA Langley Research Center, Hampton, Virginia 23681-0001
[2]Science Applications International Corporation (SAIC), Hampton, Virginia 23666
[3]Oregon State University, Corvallis, Oregon
[4]Analytical Services & Materials, Inc., Hampton, Virginia 23666

Abstract

Subsystem 9 provides the transformation from instrument-referenced data to spatially averaged data. The gridding and spatial averaging subsystems perform two major functions. The first is to assign CERES footprints to the proper gridded regions. This assignment is based on the colatitude and longitude of the CERES footprint field of view at the top of the atmosphere. The second major function is to perform spatial averaging of the various radiative fluxes and column-averaged cloud properties over each region. This subsystem uses the SSF archival product from Subsystem 4.0 for input. A CERES footprint is assigned to the appropriate region of an ISCCP-like equal-area grid with 1.25^o resolution in latitude. Fluxes and column-averaged cloud properties are spatially averaged over each region on an hourly basis. Subsystem 9.0 outputs the SFC archival data product, which includes radiative fluxes at the top of the atmosphere and the surface, column-averaged cloud properties, and angular model scene classes. After passing through this subsystem, the CERES data lose their traceability to specific CERES measurements.

9.0. Grid Top of Atmosphere and Surface Fluxes

9.1. Introduction

Gridding and averaging over regions for fluxes and other quantities is perfomed by Subsystems 6.0 and 9.0. Subsystem 9.0 (SFC) performs these functions for fluxes at the top of the atmosphere and at the surface, and for column-averaged cloud properties. Input to the SFC subsystem is the SSF product (see Appendix A), and output is the SFC product (see Appendix B). Surface fluxes that are gridded and averaged in this subsystem have been calculated in Subsystem 4.0 from simple empirical algorithms, rather than from radiative transfer models, as is the case in Subsystem 6.0. The rationale and procedures for gridding and averaging are the same as for Subsystem 6.0, which grids and spatially averages the output of Subsystem 5.0 Details of the averaging algorithms are presented in the ATBD for Subsystem 6.0.

Appendix A

Input Data Products

Grid TOA and Surface Fluxes (Subsystem 9.0)

This appendix describes the data products which are produced by the algorithms in this subsystem. Table A-1 below summarizes these products, listing the CERES and EOSDIS product codes or abbreviations, a short product name, the product type, the production frequency, and volume estimates for each individual product as well as a complete data month of production. The product types are defined as follows:

Archival products:	Assumed to be permanently stored by EOSDIS
Internal products:	Temporary storage by EOSDIS (days to years)
Ancillary products:	Non-CERES data needed to interpret measurements

The following pages describe each product. An introductory page provides an overall description of the product and specifies the temporal and spatial coverage. The table which follows the introductory page briefly describes every parameter which is contained in the product. Each product may be thought of as metadata followed by data records. The metadata (or header data) is not well-defined yet and is included mainly as a placeholder. The description of parameters which are present in each data record includes parameter number (a unique number for each distinct parameter), units, dynamic range, the number of elements per record, an estimate of the number of bits required to represent each parameter, and an element number (a unique number for each instance of every parameter). A summary at the bottom of each table shows the current estimated sizes for metadata, each data record, and the total data product. A more detailed description of each data product will be contained in a user's guide to be published before the first CERES launch.

Table A-1. Input Products Summary

Product code		Name	Type	Frequency	Size, MB	Monthly size, MB
CERES	EOSDIS					
SSF	CER11	Single satellite footprint TOA and surface fluxes, clouds	archival	1/hour	154.0	114576

Single Satellite Footprint, TOA and Sfc Flux, Clouds (SSF)

The single satellite flux and cloud swaths (SSF) is produced from the cloud identification, inversion, and surface processing for CERES. Each SSF covers a single hour swath from a single CERES instrument mounted on one satellite. The product has a product header and multiple records of approximately 125 parameters or 315 elements for each pixel.

The major categories of data output on the SSF are

- CERES footprint geometry and CERES viewing angles
- CERES footprint radiance and flux (TOA and Surface)
- CERES footprint cloud statistics and imager viewing angles
- CERES footprint clear area statistics
- CERES footprint cloudy area statistics for each of four cloud height categories
  - Visible optical depth (mean and standard deviation)
  - Infrared emissivity (mean and standard deviation)
  - Liquid water path (mean and standard deviation)
  - Ice water path (mean and standard deviation)
  - Cloud top pressure (mean and standard deviation)
  - Cloud effective pressure (mean and standard deviation)
  - Cloud effective temperature (mean and standard deviation)
  - Cloud effective height (mean and standard deviation)
  - Cloud bottom pressure (mean and standard deviation)
  - Water particle radius (mean and standard deviation)
  - Ice particle radius (mean and standard deviation)
  - Particle phase (mean and standard deviation)
  - Vertical aspect ratio (mean and standard deviation)
  - Visible optical depth/IR emissivity (13 percentiles)
- CERES footprint cloud overlap conditions (11 conditions)

The SSF is an archival product that will be run daily in validation mode starting with the TRMM launch until sufficient data have been collected and analyzed to produce a production quality set of CERES angular distrubution models (ADM). It is estimated that at TRMM launch plus 18 months, the SSF product will be produced on a routine basis and will be archived within EOSDIS for distribution. The inversion process will be rerun starting from the TRMM launch and a new SSF produced, in which case, only the TOA fluxes and surface parameters will be replaced in the inversion rerun process. If the cloud algorithms are rerun, the SSF product itself will be input into the cloud identification process in order to retrieve the CERES radiance and location data input data needed.

Level: 2
Type: Archival
Frequency: 1/hour

Portion of Globe Covered
File: Satellite swath
Record: One footprint

Time Interval Covered
File: 1 hour
Record: 1/100 second

Portion of Atmosphere Covered
File: Surface to TOA

Table A-2. Single Satellite Footprint, TOA and Sfc Flux, Clouds (SSF)

Description	Parameter Number	Units	Range	Elements/ Record	Bits/ Elem	Elem Num
SSF						
SSF_Header						
Julian Day at Hour Start		day	2449353..2458500	1	32	
Julian Time at Hour Start		day	0..1	1	32	
Character name of satellite		N/A		1	16	
Number of orbits		N/A	TBD	1	16	
Name of high resolution imager instrument		N/A	N/A	1	16	
Number of footprints in IES product		count	1..245475	1	32	
Number of imager channels used		N/A	1 .. 11	1	16	
WavLen_Array is Array[11] of:						
Central wavelengths of imager channels		µm	0.4 .. 15.0	11	16	
SSF_Record is Array[245475] of:						
SSF_Footprints						
Footprint_Geometry						
Time_and_Position						
Time of observation	1	day	0..1	1	32	1
Earth-Sun distance	2	AU	0.98 .. 1.02	1	16	2
Radius of satellite from center of Earth at observation	3	km	6000..8000	1	32	3
Colatitude of satellite at observation	4	deg	0..180	1	16	4
Longitude of satellite at observation	5	deg	0..360	1	16	5
Colatitude of Sun at observation	6	deg	0..180	1	16	6
Longitude of Sun at observation	7	deg	0..360	1	16	7
Colatitude of CERES FOV at TOA	8	deg	0..180	1	16	8
Longitude of CERES FOV at TOA	9	deg	0..360	1	16	9
Colatitude of CERES FOV at surface	10	deg	0..180	1	16	10
Longitude of CERES FOV at surface	11	deg	0..360	1	16	11
Scan sample number	12	N/A	1..660	1	16	12
Cone angle of CERES FOV at satellite	13	deg	0..180	1	16	13
Clock angle of CERES FOV at satellite wrt inertial velocity	14	deg	0..180	1	16	14
Rate of change of cone angle	15	deg sec^{-1}	-100..100	1	16	15
Rate of change of clock angle	16	deg sec^{-1}	-10..10	1	16	16
Along-track angle of CERES FOV at TOA	17	deg	0..360	1	16	17
Cross-track angle of CERES FOV at TOA	18	deg	-90..90	1	16	18
X component of satellite inertial velocity	19	km sec^{-1}	-10..10	1	16	19
Y component of satellite inertial velocity	20	km sec^{-1}	-10..10	1	16	20
Z component of satellite inertial velocity	21	km sec^{-1}	-10..10	1	16	21
CERES_Viewing_Angles						
CERES viewing zenith at TOA	22	deg	0..90	1	16	22
CERES solar zenith at TOA	23	deg	0..180	1	16	23
CERES relative azimuth at TOA	24	deg	0..360	1	16	24
CERES viewing azimuth at TOA wrt North	25	deg	0..360	1	16	25
Surface_Map_Parameters						
Mean altitude of surface above sea level	26	km	-12 .. 10	1	16	26
LandTyps is Array[10] of:						
Area fraction of land types in percent	27	N/A	0 .. 100	10	16	27
SeaTyps is Array[3] of:						
Area fraction of sea types in percent	28	N/A	0 .. 100	3	16	37
Scene_Type						
CERES clear sky or full sky indicator	29	N/A	N/A	1	16	40
CERES scene type for Inversion process	30	N/A	0 .. 200	1	16	41
Footprint_Radiation						
CERES_Filtered_Radiances						

Table A-2. Continued

Description	Parameter Number	Units	Range	Elements/ Record	Bits/ Elem	Elem Num
CERES total filtered radiance, upwards	31	$W\text{-}m^{-2}\ sr^{-1}$	0..700	1	16	42
CERES shortwave filtered radiance, upwards	32	$W\text{-}m^{-2}\ sr^{-1}$	-10..510	1	16	43
CERES window filtered radiance, upwards	33	$W\text{-}m^{-2}\ sr^{-1}$	0..50	1	16	44
Quality flag for total radiance value	34	N/A	N/A	1	16	45
Quality flag for SW radiance value	35	N/A	N/A	1	16	46
Quality flag for window radiance value	36	N/A	N/A	1	16	47
CERES_Unfiltered_Radiances						
CERES shortwave radiance, upwards	37	$W\text{-}m^{-2}sr^{-1}$	-10..510	1	16	48
CERES longwave radiance, upwards	38	$W\text{-}m^{-2}sr^{-1}$	0..200	1	16	49
CERES window radiance, upwards	39	$W\text{-}m^{-2}sr^{-1}$	0..50	1	16	50
TOA_and_Surface_Flux						
CERES shortwave flux at TOA, upwards	40	$W\text{-}m^{-2}$	0..1400	1	16	51
CERES longwave flux at TOA, upwards	41	$W\text{-}m^{-2}$	0..500	1	16	52
CERES window flux at TOA, upwards	42	$W\text{-}m^{-2}$	10..400	1	16	53
CERES shortwave flux at surface, downwards	43	$W\text{-}m^{-2}$	0..1400	1	16	54
CERES longwave flux at surface, downwards	44	$W\text{-}m^{-2}$	0..500	1	16	55
CERES net shortwave flux at surface	45	$W\text{-}m^{-2}$	0..1400	1	16	56
CERES net longwave flux at surface	46	$W\text{-}m^{-2}$	0..500	1	16	57
CERES surface emissivity	47	N/A	0..1	1	16	58
Photosynthetically active radiation at surface	48	$W\ m^{-2}$	0..780	1	16	59
Direct/Diffuse ratio at the surface	49	TBD	0..30	1	16	60
Full_Footprint_Area						
Mean imager viewing zenith over CERES FOV	50	deg	0 .. 90	1	16	61
Mean imager relative aziumth angle over CERES FOV	51	deg	0 .. 360	1	16	62
Number of cloud height categories	52	N/A	-1 .. 4	1	16	63
Number of imager pixels in CERES FOV	53	N/A	0 .. 9000	1	16	64
BDRF_Image is Array[11] of:						
Bidirectional reflectance or brightness temperature	54	TBD	TBD	11	16	65
Precipitable water	55	cm	0.001 .. 8	1	16	76
5th percentile of 0.6 μm imager radiances over CERES FOV	56	$W\text{-}m^{-2}sr^{-1}\mu m^{-1}$	TBD	1	16	77
Mean of 0.6 μm imager radiances over CERES FOV	57	$W\text{-}m^{-2}sr^{-1}\mu m^{-1}$	TBD	1	16	78
95th percentile of 0.6 μm imager radiances over CERES FOV	58	$W\text{-}m^{-2}sr^{-1}\mu m^{-1}$	TBD	1	16	79
5th percentile of 3.7 μm imager radiances over CERES FOV	59	$W\text{-}m^{-2}sr^{-1}\mu m^{-1}$	TBD	1	16	80
Mean of the 3.7 μm imager radiances over CERES FOV	60	$W\text{-}m^{-2}sr^{-1}\mu m^{-1}$	TBD	1	16	81
95th percentile of 3.7 μm imager radiances over CERES FOV	61	$W\text{-}m^{-2}sr^{-1}\mu m^{-1}$	TBD	1	16	82
5th percentile of 11 μm imager radiances over CERES FOV	62	$W\text{-}m^{-2}sr^{-1}\mu m^{-1}$	TBD	1	16	83
Mean of the 11 μm imager radiances over CERES FOV	63	$W\text{-}m^{-2}sr^{-1}\mu m^{-1}$	TBD	1	16	84
95th percentile of 11 μm imager radiances over CERES FOV	64	$W\text{-}m^{-2}sr^{-1}\mu m^{-1}$	TBD	1	16	85
Notes on general procedures	65	N/A	TBD	1	16	86
Texture algorithm flag	66	N/A	TBD	1	16	87
Multi-level cloud algorithm flag	67	N/A	TBD	1	16	88
Spatial coherence algorithm flag	68	N/A	TBD	1	16	89
Infrared sounder algorithm flag	69	N/A	TBD	1	16	90
Threshhold algorithm flag	70	N/A	TBD	1	16	91
Visible optical depth algorithm flag	71	N/A	TBD	1	16	92
Infrared emissivity algorithm flag	72	N/A	TBD	1	16	93
Cloud particle size algorithm flag	73	N/A	TBD	1	16	94
Cloud water path algorithm flag	74	N/A	TBD	1	16	95
Clear_Footprint_Area						
Mean of 0.6 μm imager radiances over clear area	75	$W\text{-}m^{-2}sr^{-1}\mu m^{-1}$	TBD	1	16	96
Stddev of the 0.6 μm imager radiances over clear area	76	$W\text{-}m^{-2}sr^{-1}\mu m^{-1}$	TBD	1	16	97
Mean of the 3.7 μm imager radiances over clear area	77	$W\text{-}m^{-2}sr^{-1}\mu m^{-1}$	TBD	1	16	98
Stddev of 3.7 μm imager radiances over clear area	78	$W\text{-}m^{-2}sr^{-1}\mu m^{-1}$	TBD	1	16	99
Mean of the 11 μm imager radiances over clear area	79	$W\text{-}m^{-2}sr^{-1}\mu m^{-1}$	TBD	1	16	100
Stddev of the 11 μm imager radiances over clear area	80	$W\text{-}m^{-2}sr^{-1}\mu m^{-1}$	TBD	1	16	101
Stratospheric aerosol visible optical depth in clear area	81	N/A	0 .. 0.5	1	16	102
Stratospheric aerosol effective radius in clear area	82	μm	0 .. 10	1	16	103

Table A-2. Concluded

Description	Parameter Number	Units	Range	Elements/ Record	Bits/ Elem	Elem Num
Total aerosol visible optical depth in clear area	83	N/A	0 .. 2	1	16	104
Total aerosol effective radius in clear area	84	μm	0 .. 20	1	16	105
Cloudy_Footprint_Area is Array[4] of:						
Cloud_Cat_Arrays						
Number of imager pixels for cloud category	85	N/A	0 .. 9000	4	16	106
Number of overcast pixels for cloud category	86	N/A	0 .. 9000	4	16	110
Cloud category weighted area fraction	87	N/A	0 .. 1	4	16	114
Cloud category weighted overcast fraction	88	N/A	0 .. 1	4	16	118
Cloud category weighted broken fraction	89	N/A	0 .. 1	4	16	122
Mean of 0.6μm imager radiances for cloud category	90	W-m^{-2}sr$^{-1}\mu$m^{-1}	TBD	4	16	126
Stddev of 0.6μm imager radiance for cloud category	91	W-m^{-2}sr$^{-1}\mu$m^{-1}	TBD	4	16	130
Mean of 3.7μm imager radiances for cloud category	92	W-m^{-2}sr$^{-1}\mu$m^{-1}	TBD	4	16	134
Stddev of 3.7μm imager radiances for cloud category	93	W-m^{-2}sr$^{-1}\mu$m^{-1}	TBD	4	16	138
Mean of 11μm imager radiances for cloud category	94	W-m^{-2}sr$^{-1}\mu$m^{-1}	TBD	4	16	142
Stddev of 11μm imager radiances for cloud category	95	W-m^{-2}sr$^{-1}\mu$m^{-1}	TBD	4	16	146
Mean cloud visible optical depth for cloud category	96	N/A	0 .. 400	4	16	150
Stddev of visible optical depth for cloud category	97	N/A	TBD	4	16	154
Mean cloud infrared emissivity for cloud category	98	N/A	0 .. 1	4	16	158
Stddev of cloud infrared emissivity for cloud category	99	N/A	TBD	4	16	162
Mean liquid water path for cloud category	100	kg m^{-2}	TBD	4	16	166
Stddev of liquid water path for cloud category	101	kg m^{-2}	TBD	4	16	170
Mean ice water path for cloud category	102	kg m^{-2}	TBD	4	16	174
Stdev of ice water path for cloud category	103	kg m^{-2}	TBD	4	16	178
Mean cloud top pressure for cloud category	104	hPa	0 .. 1100	4	16	182
Stddev of cloud top pressure for cloud category	105	hPa	TBD	4	16	186
Mean cloud effective pressure for cloud category	106	hPa	0 .. 1100	4	16	190
Stddev of cloud effective pressure for cloud category	107	hPa	TBD	4	16	194
Mean cloud effective temperature for cloud category	108	K	100 .. 350	4	16	198
Stddev of cloud effective temperature for cloud category	109	K	TBD	4	16	202
Mean cloud effective height for cloud category	110	km	0 .. 20	4	16	206
Stddev of cloud effective height for cloud category	111	km	TBD	4	16210	
Mean cloud bottom pressure for cloud category	112	hPa	0 .. 1100	4	16214	
Stddev of cloud bottom pressure for cloud category	113	hPa	TBD	4	16218	
Mean water particle radius for cloud category	114	TBD	TBD	4	16222	
Stddev of water particle radius for cloud category	115	TBD	TBD	4	16226	
Mean ice particle radius for cloud category	116	TBD	TBD	4	16230	
Stddev of ice particle radius for cloud category	117	TBD	TBD	4	16234	
Mean cloud particle phase for cloud category	118	N/A	0 .. 1	4	16238	
Stddev of cloud particle phase for cloud category	119	N/A	0 .. 1	4	16242	
Mean vertical aspect ratio for cloud category	120	N/A	0 .. 1	4	16246	
Stddev of vertical aspect ratio for cloud category	121	N/A	TBD	4	16250	
Optical_Depth_Percentile is Array[13] of:						
Percentiles of visible optical depth/IR emissivity for cloud category	122	N/A	TBD	52	16254	
Overlap_Footprint_Area is Array[11] of:						
Overlap_Conditions						
Number of imager pixels for overlap condition	123	N/A	0 .. 9000	11	16306	
Overlap condition weighted area fraction	124	N/A	0 .. 1	11	16317	

Total Meta Bits/File:	336
Total Data Bits/Record:	5264
Total Records/File:	245475
Total Data Bits/File:	1292180400
Total Bits/File :	1292180736

Appendix B

Output Data Products

Grid TOA and Surface Fluxes (Subsystem 9.0)

This appendix describes the data products which are produced by the algorithms in this subsystem. Table B-1 below summarizes these products, listing the CERES and EOSDIS product codes or abbreviations, a short product name, the product type, the production frequency, and volume estimates for each individual product as well as a complete data month of production. The product types are defined as follows:

Archival products:	Assumed to be permanently stored by EOSDIS
Internal products:	Temporary storage by EOSDIS (days to years)

The following pages describe each product. An introductory page provides an overall description of the product and specifies the temporal and spatial coverage. The table which follows the introductory page briefly describes every parameter which is contained in the product. Each product may be thought of as metadata followed by data records. The metadata (or header data) is not well-defined yet and is included mainly as a placeholder. The description of parameters which are present in each data record includes parameter number (a unique number for each distinct parameter), units, dynamic range, the number of elements per record, an estimate of the number of bits required to represent each parameter, and an element number (a unique number for each instance of every parameter). A summary at the bottom of each table shows the current estimated sizes for metadata, each data record, and the total data product. A more detailed description of each data product will be contained in a user's guide to be published before the first CERES launch.

Table B-1. Output Products Summary

Product code		Name	Type	Frequency	Size, MB	Monthly size, MB
CERES	EOSDIS					
SFC	CER12	Hourly gridded single satellite TOA and surface fluxes	archival	1/hour	2.1	1563

Hourly Gridded Single Satellite TOA and Surface Fluxes (SFC)

The hourly gridded single satellite fluxes and clouds (SFC) archival data product contains hourly single satellite flux and cloud parameters averaged over 1.25 degree regions. Input to the SFC subsystem is the single satellite CERES footprint TOA and surface fluxes, clouds (SSF) archival data product. Each SFC covers a single hour swath from a single CERES instrument mounted on one satellite. The product has a product header and multiple records. Each record contains spatially averaged data for an individual region.

The major categories of data output on the SFC are

- Region data
- Total sky radiative fluxes at TOA and surface
- Clear sky radiative fluxes at TOA and surface
- Column-averaged cloud properties
- Angular model scene classes
- Surface only data

Level: 3
Type: Archival
Frequency: 1/hour

Portion of Globe Covered
File: Gridded satellite swath
Record: 1.25-degree equal-area region

Time Interval Covered
File: Hour
Record: N/A

Portion of Atmosphere Covered
File: TOA and surface

Table B-2. Hourly Gridded Single Satellite TOA and Surface Fluxes (SFC)

Description	Parameter Number	Units	Range	Elements/ Record	Bits/ Elem	Elem Num
SFC						
SFC_File_Header						
CERES data product code		N/A	N/A	1	16	
Spacecraft name		N/A	N/A	1	16	
CERES instrument identification code		N/A	N/A	1	16	
Julian Day		Day	2449353 .. 2458500	1	16	
Hour of the day for the SFC product		Hours	1 .. 24	1	16	
Number of regions (records) in the product		N/A	1 .. 2500	1	16	
SFC_Regionally_Averaged_Data is Array[2500] of:						
Regional_Parameters						
SFC_Region_Data						
Region number	1	N/A	1 .. 26542	1	16	1
Number of CERES footprints in the region	2	N/A	1 .. 40	1	16	2
Julian Time	3	Day	0.0 .. 1.0	1	16	3
Hour box number for the region	4	N/A	1 .. 744	1	16	4
Regional_Geographic_Scene_Type						
SFC_Land_Type is Array[10] of:						
Mean of land type percentage	5	Percent	0.0 .. 100.0	10	16	5
SFC_Sea_Type is Array[3] of:						
Mean of sea type percentage	6	Percent	0.0 .. 100.0	3	16	15
Geometry_Data						
Mean Sun colatitude	7	Degrees	0.0 .. 180.0	1	16	18
Mean Sun longitude	8	Degrees	0.0 .. 360.0	1	16	19
Mean relative azimuth angle at TOA	9	Degrees	0.0 .. 360.0	1	16	20
Mean cosine of solar zenith angle at TOA	10	N/A	0.0 .. 1.0	1	16	21
Mean spacecraft zenith angle	11	Degrees	0.0 .. 90.0	1	16	22
SFC_Radiative_Flux_Data						
SFC_Total_Sky_Fluxes						
Total_Sky_TOA_Fluxes_Array is Array[3] of:						
Total_Sky_TOA_Flux_Statistics						
Mean, st dev, and num obs of SW upward flux at TOA	12	$W\text{-}m^{-2}$	0.0 .. 1400.0	3	16	23
Mean, st dev, and num obs of LW upward flux at TOA	13	$W\text{-}m^{-2}$	100.0 .. 500.0	3	16	26
Mean, st dev, and num obs of LW window upward flux at TOA	14	$W\text{-}m^{-2}$	0.0 .. 800.0	3	16	29
Total_Sky_Surface_Fluxes_Array is Array[3] of:						
Total_Sky_Surface_Flux_Statistics						
Mean, st dev, and num obs of SW net flux at surface	15	$W\text{-}m^{-2}$	0.0 .. 1400.0	3	16	32
Mean, st dev, and num obs of SW downward flux at surface	16	$W\text{-}m^{-2}$	0.0 .. 1400.0	3	16	35
Mean, st dev, and num obs of LW net flux at surface	17	$W\text{-}m^{-2}$	100.0 .. 500.0	3	16	38
Mean, st dev, and num obs of LW downward flux at surface	18	$W\text{-}m^{-2}$	100.0 .. 500.0	3	16	41
SFC_Clear_Sky_Fluxes						
Clear_Sky_TOA_Fluxes_Array is Array[3] of:						
Clear_Sky_TOA_Flux_Statistics						
Mean, st dev, and num obs of SW upward flux at TOA	19	$W\text{-}m^{-2}$	0.0 .. 1400.0	3	16	44
Mean, st dev, and num obs of LW upward flux at TOA	20	$W\text{-}m^{-2}$	100.0 .. 500.0	3	16	47
Mean, st dev, and num obs of LW window upward flux at TOA	21	$W\text{-}m^{-2}$	0.0 .. 800.0	3	16	50
Clear_Sky_Surface_Fluxes_Array is Array[3] of:						
Clear_Sky_Surface_Flux_Statistics						
Mean, st dev, and num obs of SW net flux at surface	22	$W\text{-}m^{-2}$	0.0 .. 1400.0	3	16	53
Mean, st dev, and num obs of SW downward flux at surface	23	$W\text{-}m^{-2}$	0.0 .. 1400.0	3	16	56
Mean, st dev, and num obs of LW net flux at surface	24	$W\text{-}m^{-2}$	100.0 .. 500.0	3	16	59
Mean, st dev, and num obs of LW downward flux at surface	25	$W\text{-}m^{-2}$	100.0 .. 500.0	3	16	62

Table B-2. Concluded

Description	Parameter Number	Units	Range	Elements/ Record	Bits/ Elem	Elem Num
SFC_Weighted_Column_Average_Cloud_Properties is Array[5] of:						
(Cloud weightings are SW, LW TOA, LW Surface, liquid water path, and ice water path)						
SFC_Cloud_Properties						
Cloud_Area_Fractions_Array is Array[3] of:						
Cloud Area Fractions	26	Fraction	0.0 - 1.0	15	16	65
SFC_Cloud_Properties_Array is Array[3] of:						
SFC_Cloud_Property_Parameters						
Mean, st dev, and num obs of effective pressure	27	hPa	TBD	15	16	80
Mean, st dev, and num obs of effective temperature	28	K	TBD	15	16	95
Mean, st dev, and num obs of effective altitude	29	km	0.0 - 20.0	15	16	110
Mean, st dev, and num obs of cloud top pressure	30	hPa	0.0 - 1100.0	15	16	125
Mean, st dev, and num obs of cloud bottom pressure	31	hPa	0.0 - 1100.0	15	16	140
Mean, st dev, and num obs of particle phase	32	Fraction	0.0 - 1.0	15	16	155
Mean, st dev, and num obs of liquid water path	33	kg cm^{-2}	0.01 - 1000.0	15	16	170
Mean, st dev, and num obs of ice water path	34	kg cm^{-2}	0.01 - 1000.0	15	16	185
Mean, st dev, and num obs of liquid particle radius	35	µm	0.0 - 1000.0	15	16	200
Mean, st dev, and num obs of ice particle readius	36	µm	0.0 - 100.0	15	16	215
Mean, st dev, and num obs of visible optical depth	37	Dimensionless	0.0 - 50.0	15	16	230
Mean, st dev, and num obs of infrared emissivity	38	Dimensionless	0.0 - 2.0	15	16	245
Mean, st dev, and num obs of vertical aspect ratio	39	Dimensionless	TBD	15	16	260
Percentiles_Visible_Opt_Depth_Array is Array[13] of:						
VIS Opt Depth (day) / Infrared Emissivity (night) percentiles	40	Dimensionless	0.0 - 50.0	65	16	275
SFC_Angular_Model_Scene_Types is Array[12] of:						
Angular_Model_Scene_Type_Parameters						
Fractional area coverage	41	Fraction	0.0 .. 1.0	12	16	340
Albedos_Statistics is Array[2] of:						
Mean and standard deviation of albedo	42	Dimensionless	0.0 .. 1.0	24	16	352
Incident_Solar_Flux_Statistics is Array[2] of:						
Mean and standard deviation of incident solar flux	43	W-h m^{-2}	TBD	24	16	376
LW_Flux_Statistics is Array[2] of:						
Mean and standard deviation of LW flux	44	W-m^{-2}	0.0 .. 400.0	24	16	400
SFC_Surface_Only_Data						
Photosynthetically active radiation	45	W-m^{-2}	0.0 .. 780.0	1	16	424
Direct/Diffuse Ratio	46	Dimensionless	0.0 .. 30.0	1	16	425
Total Meta Bits/File:	96					
Total Data Bits/Record:	6800					
Total Records/File:	2500					
Total Data Bits/File:	17000000					
Total Bits/File:	17000096					

vtClouds and the Earth's Radiant Energy System (CERES)

Algorithm Theoretical Basis Document

Monthly Regional TOA and Surface Radiation Budget

(Subsystem 10.0)

Edwin F. Harrison[1]

David F. Young[2]

Patrick Minnis[1]

Gary G. Gibson[2]

Robert D. Cess[3]

V. Ramanathan[4]

Timothy D. Murray[5]

D. Jill Travers[5]

[1]Atmospheric Sciences Division, NASA Langley Research Center, Hampton, Virginia 23681-0001

[2]Lockheed Engineering & Sciences Company, Hampton, Virginia 23666

[3]Laboratory for Planetary and Atmospheric Research Light Engineering Building, Room 169, State University of New York at Stony Brook, Stony Brook, New York 11794

[4]Scripps Institution of Oceanography & California Space Institute, University of California at San Diego, Mail Code 0221, La Jolla, California 92093

[5]Science Applications International Corporation (SAIC), Hampton, Virginia 23666

CERES Top Level Data Flow Diagram

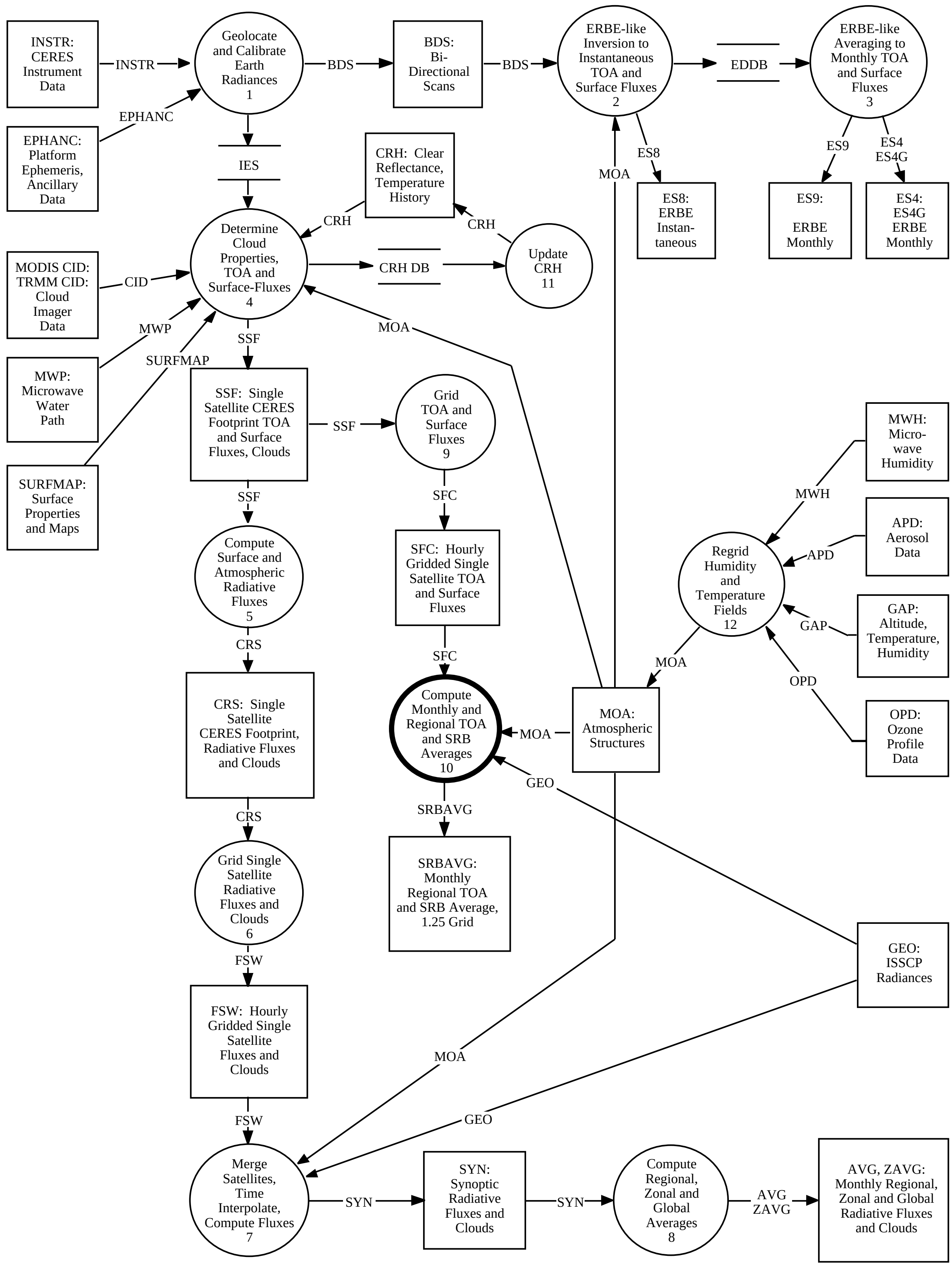

Abstract

The CERES Data Management System computes averages of top-of-atmosphere (TOA) shortwave (SW) and longwave (LW) flux on regional, zonal, and global spatial scales. Separate regional averages are computed using the two methods discussed in subsystem 7. TOA flux estimates from both of the methods are used to produce estimates of surface flux at all temporal and spatial scales using the TOA-to-surface flux parameterization schemes for SW and LW described in subsystem 4.6.

The temporal interpolation process uses the gridded CERES SW and LW TOA fluxes and cloud information provided by the SFC data product. The SFC data contain spatial averages of one hour of CERES measurements on a 1.25° equal-area grid. Geostationary satellite-derived radiances are provided by the GEO data product. Additional input data include directional models of albedo, solar declination, and the coefficients necessary to produce surface flux estimates (see appendix A).

The TSA process produces monthly-hourly and monthly means of TOA and surface SW and LW flux on regional, zonal, and global spatial scales. Separate estimates are calculated for clear-sky and total-sky fluxes. In addition, means are computed and output using two different averaging techniques (see appendix B).

Temporal interpolation is accomplished by the two methods presented in subsection 7: (1) the ERBE-like method and (2) the geostationary data enhancement method. Using the hours with observations from the SFC product, time series of TOA total-sky and clear-sky fluxes are constructed for all hours of the month for each region.

Parameterization schemes are used to estimate surface fluxes from TOA data for all hours with TOA fluxes. Monthly and monthly-hourly means are calculated from the interpolated fluxes. The TOA and surface LW and SW fluxes are averaged on zonal and global scales.

10.0. Monthly Regional TOA and Surface Radiation Budget

10.1. Algorithm Description

10.1.1. Introduction

The goal of the CERES experiment is to accurately determine the components of the Earth's radiation budget and cloud parameters on regional, zonal, and global spatial scales. CERES will produce a large data set of highly accurate measurements of regional-scale incoming and outgoing radiant energy over the Earth. These measurements must be properly averaged in space and time. In addition, variations in Earth's climate can only be detected using stable, long-term global data sets. In order to accomplish the dual goals of a stable, long-term data set and averages produced using the most accurate techniques available, CERES will produce regional, zonal, and global means by both the ERBE-like technique and the geostationary data enhancement method (see subsection 7).

The ERBE-like interpolation (method 1) is used to provide a consistent data set for long-term climate studies. The results of this subsystem incorporate the improved CERES scene identification and angular distribution models (ADM's). The monthly averages from method 1 can be compared to similar results from the ERBE-like processing (subsystem 3) to evaluate the effect of these improvements on both TOA and surface fluxes. An output product based on using the geostationary-data-enhanced interpolation technique (method 2) is also included. The use of geostationary data in the interpolation process significantly improves the accuracy of the diurnal modeling. This not only provides the best possible monthly averages, but also yields accurate hourly fluxes for use in detailed regional studies of radiation and clouds and for CERES Interdisciplinary Studies. The geostationary-data-enhanced interpolation technique depends on the availability of geostationary or polar orbiting narrowband radiance measurements. Data gaps due to satellite failures or spatial sampling patterns may pose problems when studying climate data on a global scale. method 1 provides a consistent data set which can be used to evaluate zonal and global results from method 2. For regions where geostationary data are not available, only method 1 will be used.

A complete description of the methods used to produce the time series of TOA fluxes is included in subsystem 7. The major departure from the methods described there concerns the times to which the fluxes will be interpolated. The primary goal of the temporal interpolation described in subsystem 7 is to produce accurate estimates of cloud properties and TOA fluxes at specific synoptic times. For this subsystem, fluxes will be interpolated to all local hours of the month in order to produce a complete time series. In the following subsections, only the differences from the methods used in subsystem 7 will be described.

10.1.2. Sorting and Merging of Gridded Observations

This process is essentially identical to subsystem 7. The input data are derived from the SFC data product instead of the FSW. The other difference is that the data are sorted in terms of local time rather than GMT.

10.1.3. Regridding of Geostationary Data

This process is identical to subsystem 7.

10.1.4. Time Interpolation of Cloud Properties

The SFC data product contains fewer cloud data structures than the FSW. This subsystem will retain only the column-averaged cloud data (summarized in subsystem 6) and the Angular Model Scene Class data. The data in both of these structures are linearly interpolated to all local hours of the month, as described in subsystem 7. The complete time series of column-averaged data is used to compute monthly and monthly-hourly means. Monthly means of the Angular Model Scene Class data will be computed using only data from the times of CERES observations.

10.1.5. Time Interpolation of Total-Sky LW Flux

The temporal interpolation of method 1 is identical to the technique described in subsystem 7. For method 2, all hours between the times of CERES observations must be filled with LW flux values. In order to accomplish this, the time series from the narrowband data is linearly interpolated between the synoptic times. This complete time series is then normalized to the CERES LW fluxes at the times of observation.

10.1.6. Time Interpolation of Clear-Sky LW Flux

Only the ERBE-like process of method 1 is performed on clear-sky LW flux data. The half-sine fits and linear interpolation of method 1 model the clear-sky LW flux well when there is adequate sampling. No attempt will be made to produce clear-sky flux estimates at every hour. For all surface types, a fit is performed only during days with at least one daytime measurement and at least one nighttime measurement before and after the day. The monthly means will be computed only from these days. If this technique produces too many regions with no monthly clear averages, then a single diurnal model will be fit to monthly-hourly means of the data, as is done in the ERBE-like processing (subsystem 3).

10.1.7. Time Interpolation of Total-Sky SW Flux

The albedos and scene fractions for each Angular Model Scene Class are used in method 1 to select ADM’s to interpolate the data to hours between the observations (see subsystems 3 and 7). For method 2, these data are also used to select anisotropic factors used in the conversion of narrowband SW radiances into fluxes. A complete time series of simulated broadband fluxes is produced from the synoptic geostationary data using directional models selected using the interpolated angular model scene class data. An estimate of SW flux is then made for all daylight hours of all days within a region that contain at least one CERES observation by normalizing the time series of albedo produced from the geostationary data to the CERES observations. Only the days with observations will be used in the calculation of monthly mean fluxes.

10.1.8. Time Interpolation of Clear-Sky SW Flux

Only the ERBE-like process of method 1 is performed on clear-sky SW flux data. Once again, only days with at least one clear-sky flux measurement are modeled and used in the computation of monthly means.

10.1.9. Time Interpolation of Window Radiance

This interpolation will be performed in the same manner as described in subsystem 7.

10.1.10. Surface SW and LW fluxes

An independent set of parameterized models has been developed for the calculation of LW and SW surface fluxes from the time series of TOA fluxes. These models are discussed in subsystem 4.6. The procedure used to incorporate these models into the averaging process begins with the modeling of the TOA fluxes as explained above. For every hour in which a TOA flux is calculated, the TOA-to-surface parameterization models are used to determine a corresponding surface flux. Monthly, monthly-hourly, and daily means will be computed in the same manner as used for the TOA flux.

10.1.11. Computation of Monthly and Monthly-Hourly Means

Unlike subsection 7, days with no clear-sky flux measurements are not modeled or used, and data used in monthly and monthly-hourly means are limited to data from days in which there is at least one CERES observation.

10.1.12. Computation of Zonal and Global Means

Zonal and global means of CERES 1.25 gridded TOA and surface LW and SW fluxes are calculated in the same manner as used with ERBE data (see subsystem 3). Area weighting factors are applied to account for the small differences in the areas of regions in different latitude zones.

10.2. Implementation Issues

10.2.1. Strategic Concerns

Many of the strategic concerns of this subsystem are identical with those discussed in subsystem 7.1 and are not repeated here.

Currently, there is no adopted method for producing total-sky surface LW flux from TOA flux. It is expected that a method will be available by the time of release 1. Any atmospheric data necessary for this parameterization must be obtained from either the ASTR atmospheric data set or from a combination of CERES and ISCCP cloud properties.

The output product does not contain daily means of fluxes, as in the ERBE-like product. The size of the SRBAVG data product is quite large compared with the ES9 ERBE-like product (see appendix B). The addition of daily means would increase the output product size. The needs of the Science Team and potential users will be assessed to see if daily means are required.

Appendix A

Input Data Products

Compute Monthly and Regional TOA and SRB Averages (Subsystem 10.0)

This appendix describes the data products which are used by the algorithms in this subsystem. Table A-1 below summarizes these products, listing the CERES and EOSDIS product codes or abbreviations, a short product name, the product type, the production frequency, and volume estimates for each individual product as well as a complete data month of production. The product types are defined as follows:

Archival products:	Assumed to be permanently stored by EOSDIS
Internal products:	Temporary storage by EOSDIS (days to years)
Ancillary products:	Non-CERES data needed to interpret measurements

The following pages describe each product. An introductory page provides an overall description of the product and specifies the temporal and spatial coverage. The table which follows the introductory page briefly describes every parameter which is contained in the product. Each product may be thought of as metadata followed by data records. The metadata (or header data) is not well-defined yet and is included mainly as a placeholder. The description of parameters which are present in each data record includes parameter number (a unique number for each distinct parameter), units, dynamic range, the number of elements per record, an estimate of the number of bits required to represent each parameter, and an element number (a unique number for each instance of every parameter). A summary at the bottom of each table shows the current estimated sizes of metadata, each data record, and the total data product. A more detailed description of each data product will be contained in a user's guide to be published before the first CERES launch.

Table A-1. Input Products Summary

Product code		Name	Type	Frequency	Size, MB	Monthly size, MB
CERES	EOSDIS					
ASTR	CER34	Atmospheric structures	archival	1/hour	10.5	7797
GEO	GEO	ISCCP radiances	ancillary	8/day	3.8	927
SFC	CER12	Hourly gridded single satellite TOA and surface fluxes	archival	1/hour	2.1	1563

Atmospheric Structures (ASTR)

The CERES archival product, atmospheric structures (ASTR), is produced by the CERES Regrid Humidity and Temperature Subsystem. Each ASTR file contains meteorological data for one hour, and is used by several of the CERES subsystems. Data on the ASTR are derived from several data sources external to the CERES system, such as NMC, MODIS, SAGE, and various other meteorological satellites. These data arrive anywhere from four times daily to once a month. These data are also horizontally and vertically organized differently from what the CERES system requires. The Regrid Humidity and Temperature Subsystem interpolates these data temporally, horizontally, and vertically to conform with CERES processing requirements.

The ASTR contains

- Surface temperature and pressure
- Vertical profiles for up to 38 internal atmospheric levels of temperature, humidity, pressure, and geopotential height
- Column precipitable water

- Vertical ozone profiles for 26 (of the 38) internal atmospheric levels
- Column ozone
- Total column aerosol
- Stratospheric aerosol

The 38 internal atmospheric levels, in hPa, as requested by the CERES Clouds and SARB working groups are

Surface	925	775	550	275	125	5
Surface - 10	900	750	500	250	100	1
Surface - 20	875	725	450	225	70	
1000	850	700	400	200	50	
975	825	650	350	175	30	
950	800	600	300	150	10	

Level: 3
Type: Archival
Frequency: 1/hour

Portion of Globe Covered
File: Global
Record: 1.25-deg equal area region

Time Interval Covered
File: 1 hour
Record: 1 hour

Portion of Atmosphere Covered
File: Surface and internal

Table A-2. Atmospheric Structures (ASTR)

Description	Parameter Number	Units	Range	Elements/ Record	Bits/ Elem	Elem Num
Meta Data						
Header				1	320	
Regional Data						
Region Number	1	N/A	1..26542	1	16	1
Surface Data						
Surface Temperature	2	K	175..375	1	16	2
Surface Pressure	3	hPa	1100..400	1	16	3
Flag, Source Surface Data	4	N/A	TBD	1	16	4
Temperature and Humidity Profiles						
Geopotential Height Profiles	5	km	0..50	38	16	5
Pressure Profiles	6	hPa	1100..0	38	16	43
Temperature Profiles	7	K	175..375	38	16	81
Humidity Profiles	8	N/A	0..100	38	16	119
Flag, Source Temp. and Humidity Profiles	9	N/A	TBD	1	16	157
Column Precipitable Water						
Precipitable Water	10	cm	0.001..8.000	1	16	158
Precipitable Water, std	11	cm	TBD	1	16	159
Flag, Source Column Precipitable Water	12	N/A	TBD	1	16	160
Ozone Profile Data						
Ozone Profiles	13	$g\ kg^{-1}$	0.00002..0.02	26	16	161
Flag, Source Ozone Profile Data	14	N/A	TBD	1	16	187
Column Ozone						
Column Ozone	15	du	200..500	1	16	188
Flag, Source Column Ozone	16	N/A	TBD	1	16	189

Table A-2. Concluded

Description	Parameter Number	Units	Range	Elements/ Record	Bits/ Elem	Elem Num
Total Column Aerosol						
Aerosol Mass Loading, Total Column	17	g m^{-2}	TBD	1	16	190
Flag, Source Aerosol Mass Loading, Total Column	18	N/A	TBD	1	16	191
Optical Depth, Total Column	19	N/A	0.0..2.0	1	16	192
Flag, Source Optical Depth, Total Column	20	N/A	TBD	1	16	193
Asymmetry Factor, Total Column	21	N/A	0.0..1.0	1	16	194
Flag, Source Asymmetry Factor, Total Column	22	N/A	TBD	1	16	195
Single Scattering Albedo, Total Column	23	N/A	0.0..1.0	1	16	196
Flag, Source Single Scattering Albedo, Total Column	24	N/A	TBD	1	16	197
Effective Particle Size, Total Column	25	µm	0.0..20.0	1	16	198
Flag, Source Effective Particle Size, Total Column	26	N/A	TBD	1	16	199
Mean Aerosol Layer Temperature, Total Column	27	K	150..280	1	16	200
Flag, Source Mean Aerosol Layer Temperature, Total Column	28	N/A	TBD	1	16	201
Stratospheric Aerosol						
Optical Depth, Stratosphere	29	N/A	0.0..0.5	1	16	202
Asymmetry Factor, Stratosphere	30	N/A	0.0..1.0	1	16	203
Single Scattering Albedo, Stratosphere	31	N/A	0.0..1.0	1	16	204
Effective Particle Size, Stratosphere	32	µm	0.0..10.0	1	16	205
Mean Aerosol Layer Temperature, Stratosphere	33	K	150..280	1	16	206
Flag, Source Stratospheric Aerosol	34	N/A	TBD	1	16	207

Total Meta Bits/File:	320
Total Data Bits/Record:	3312
Total Records/File:	26542
Total Data Bits/File:	87907104
Total Bits/File:	87907424
ISCCP Radiances (GEO)	

ISCCP Radiances (GEO)

The International Satellite Cloud Climatology Project (ISCCP) produces B3 radiances which are used for filling in unsampled portions of the globe during a particular one-hour interval. The ISCCP B3 radiances are well-enough defined that we do not need to make a further composite data structure to reformat them. In addition, these radiances are part of the LaRC DAAC archival responsibility.

The ISCCP B3 radiances consist of a window channel radiance (near 10.8 micrometers) and a visible channel radiance (near 0.68 micrometers) obtained from up to five geostationary satellites, as well as some data from the equivalent channels of the AVHRR and HIRS instruments on the operational satellites. The radiances from each geostationary imager are sampled at about 32 km resolution and every three hours. Where a geostationary data source is not available (over India, primarily), the AVHRR data are processed into an equivalent format.

Each geostationary satellite has a sector processing center (SPC) that samples and formats the radiances. When they finish their work, the SPC sends the sampled and formatted radiance pairs to the global processing center (GPC), where the radiances are normalized and reformatted into archival form. Because each SPC follows its own schedule, the global radiance sets may not be available on a schedule that is appropriate for CERES operations. The CERES project will use the ISCCP DX radiance data as an alternate source.

The GEO radiances contain two basic kinds of information:

1. Visible (near 0.68 micrometers) and window (near 10.8 micrometers) radiances sampled at 32 km spacing
2. Earth location information

These radiances have been normalized to a common set of locations on the Earth and corrected for gain drifts, insofar as possible.

GEO is an external input data product retrieved from the EOSDIS DAAC at LaRC. GEO will be recycled by the CERES project when all single spacecraft data and all combinations of spacecraft data have been processed for a given month.

Level: 1B
Type: Ancillary
Frequency: 8/day

Time Interval Covered
File: Monthly
Record: 8/day

Portion of Globe Covered
File: Entire globe
Record: 2.5 equal area regions

Portion of Atmosphere Covered
File: TOA

Table A-3. ISCCP Radiances (GEO)

Description	Parameter Number	Units	Range	Elements/ Record	Bits/ Elem	Elem Num
GEO						
Image_ID_Rec is Array[1] of:						
Image_ID_Iteration_Rec						
GEO_Image_ID						
Data year	1	N/A	N/A	1	32	1
Record sequence number within image	2	N/A	1-1	1	32	2
Julian day of data	3	day	N/A	1	32	3
Image sequence number	4	N/A	TBD	1	32	4
Nominal GMT	5	hhmmss	N/A	1	32	5
ISCCP sector processing center identifier	6	N/A	N/A	1	64	6
GEO_Channel_Data						
Number of active channels in image	7	N/A	1-5	1	32	7
ID_Chan is Array[5] of:						
Channel Identifiers	8	N/A	TBD	5	32	8
Noise is Array[5] of:						
Noise estimates for channel	9	count	0-255	5	32	13
Available is Array[5] of:						
Channel availability flag	10	N/A	TBD	5	32	18
Chan_Desc is Array[5] of:						
Channel descriptive information	11	N/A	N/A	5	32	23
Satellite identifier	12	N/A	N/A	1	64	28
Number of data records in image	13	N/A	40-110	1	32	29
Codes_Satellite is Array[7] of:						
Satellite and channel ID code numbers	14	N/A	N/A	7	32	30
GEO_ScanLine_Data						
Number of scan lines in image	15	N/A	400-550	1	32	37
Number of pixels per scan line	16	N/A	TBD	1	32	38
Year and Julian day of first scan line	17	day	N/A	1	32	39
Year and Julian day of last scan line	18	day	N/A	1	32	40
Percentage of bad scan lines in image	19	percent	0.0 - 100.0	1	32	41
Scaling_Info is Array[10] of:						
Scale factor to convert latitude to degrees, other scaling info	20	N/A	TBD	10	32	42
Point_Subsatell is Array[4] of:						
Subsatellite latitude/longitude point information	21	TBD	TBD	4	32	52
Day/Night Flag	22	N/A	TBD	1	32	56
Calibration flag for visible channel	23	N/A	TBD	1	32	57
Fill is Array[643] of:						
Spare Words	24	N/A	N/A	643	32	58
Calibration flag for infrared channel	25	N/A	TBD	1	32	701

Table A-3. Concluded

Description	Parameter Number	Units	Range	Elements/ Record	Bits/ Elem	Elem Num
Location_Grid_Rec is Array[1] of:						
Location_Grid						
Record sequence number within image	26	N/A	1-1	1	32	702
Image sequence number	27	N/A	TBD	1	32	703
Num_Pixels is Array[648] of:						
Number of image pixels in each 10 degree cell	28	N/A	TBD	648	32	704
Calibration_Tables is Array[5] of:						
Calibration/Normalization tables for each channel	29	TBD	TBD	1	58080	1352
Radiance_Data is Array[110] of:						
Radiance_Data_Rec						
Scan_Line_Rec is Array[550] of:						
Scan_Line_Data_Rec						
Scan line information	30	TBD	TBD	550	288	1353
Navigation range	31	TBD	TBD	550	128	1903
Data range code	32	N/A	TBD	550	64	2453
Radiance Data Values	33	TBD	TBD	550	32	3003
Record identification in image	34	TBD	TBD	1	288	3553
Total Meta Bits/File:	0					
Total Data Bits/Record:	22496					
Total Records/File:	1					
Total Data Bits/File:	22496					
Total Data Bits/Record:	20800					
Total Records/File:	1					
Total Data Bits/File:	20800					
Total Data Bits/Record:	58080					
Total Records/File:	5					
Total Data Bits/File:	290400					
Total Data Bits/Record:	281888					
Total Records/File:	110					
Total Data Bits/File:	31007680					
Total Bits/File:	31341376					
Hourly Gridded Single Satellite TOA and Surface Fluxes (SFC)						

Hourly Gridded Single Satellite TOA and Surface Fluxes (SFC)

The hourly gridded single satellite fluxes and clouds (SFC) archival data product contains hourly single satellite flux and cloud parameters averaged over 1.25 degree regions. Input to the SFC subsystem is the single satellite CERES footprint TOA and surface fluxes, clouds (SSF) archival data product. Each SFC covers a single hour swath from a single CERES instrument mounted on one satellite. The product has a product header and multiple records. Each record contains spatially averaged data for an individual region.

The major categories of data output on the SFC are

- Region data
- Total sky radiative fluxes at TOA and surface

- Clear sky radiative fluxes at TOA and surface
- Column-averaged cloud properties
- Angular model scene classes
- Surface only data

Level: 3
Type: Archival
Frequency: 1/hour

Time Interval Covered
File: Hour
Record: N/A

Portion of Globe Covered
File: Gridded satellite swath
Record: 1.25-degree equal-area region

Portion of Atmosphere Covered
File: TOA and surface

Table A-4. Hourly Gridded Single Satellite TOA and Surface Fluxes (SFC)

Description	Parameter Number	Units	Range	Elements/ Record	Bits/ Elem	Elem Num
SFC						
SFC_File_Header						
CERES data product code		N/A	N/A	1	16	
Spacecraft name		N/A	N/A	1	16	
CERES instrument identification code		N/A	N/A	1	16	
Julian Day		Day	2449353 .. 2458500	1	16	
Hour of the day for the SFC product		Hours	1 .. 24	1	16	
Number of regions (records) in the product		N/A	1 .. 2500	1	16	
SFC_Regionally_Averaged_Data is Array[2500] of:						
Regional_Parameters						
SFC_Region_Data						
Region number	1	N/A	1 .. 26542	1	16	1
Number of CERES footprints in the region	2	N/A	1 .. 40	1	16	2
Julian Time	3	Day	0.0 .. 1.0	1	16	3
Hour box number for the region	4	N/A	1 .. 744	1	16	4
Regional_Geographic_Scene_Type						
SFC_Land_Type is Array[10] of:						
Mean of land type percentage	5	Percent	0.0 .. 100.0	10	16	5
SFC_Sea_Type is Array[3] of:						
Mean of sea type percentage	6	Percent	0.0 .. 100.0	3	16	15
Geometry_Data						
Mean Sun colatitude	7	Degrees	0.0 .. 180.0	1	16	18
Mean Sun longitude	8	Degrees	0.0 .. 360.0	1	16	19
Mean relative azimuth angle at TOA	9	Degrees	0.0 .. 360.0	1	16	20
Mean cosine of solar zenith angle at TOA	10	N/A	0.0 .. 1.0	1	16	21
Mean spacecraft zenith angle	11	Degrees	0.0 .. 90.0	1	16	22
SFC_Radiative_Flux_Data						
SFC_Total_Sky_Fluxes						
Total_Sky_TOA_Fluxes_Array is Array[3] of:						
Total_Sky_TOA_Flux_Statistics						
Mean, st dev, and num obs of SW upward flux at TOA	12	$W\text{-}m^{-2}$	0.0 .. 1400.0	3	16	23
Mean, st dev, and num obs of LW upward flux at TOA	13	$W\text{-}m^{-2}$	100.0 .. 500.0	3	16	26
Mean, st dev, and num obs of LW window upward flux at TOA	14	$W\text{-}m^{-2}$	0.0 .. 800.0	3	16	29
Total_Sky_Surface_Fluxes_Array is Array[3] of:						
Total_Sky_Surface_Flux_Statistics						
Mean, st dev, and num obs of SW net flux at surface	15	$W\text{-}m^{-2}$	0.0 .. 1400.0	3	16	32
Mean, st dev, and num obs of SW downward flux at surface	16	$W\text{-}m^{-2}$	0.0 .. 1400.0	3	16	35
Mean, st dev, and num obs of LW net flux at surface	17	$W\text{-}m^{-2}$	100.0 .. 500.0	3	16	38
Mean, st dev, and num obs of LW downward flux at surface	18	$W\text{-}m^{-2}$	100.0 .. 500.0	3	16	41

Table A-4. Concluded

Description	Parameter Number	Units	Range	Elements/ Record	Bits/ Elem	Elem Num
SFC_Clear_Sky_Fluxes						
Clear_Sky_TOA_Fluxes_Array is Array[3] of:						
Clear_Sky_TOA_Flux_Statistics						
Mean, st dev, and num obs of SW upward flux at TOA	19	$W\text{-}m^{-2}$	0.0 .. 1400.0	3	16	44
Mean, st dev, and num obs of LW upward flux at TOA	20	$W\text{-}m^{-2}$	100.0 .. 500.0	3	16	47
Mean, st dev, and num obs of LW window upward flux at TOA	21	$W\text{-}m^{-2}$	0.0 .. 800.0	3	16	50
Clear_Sky_Surface_Fluxes_Array is Array[3] of:						
Clear_Sky_Surface_Flux_Statistics						
Mean, st dev, and num obs of SW net flux at surface	22	$W\text{-}m^{-2}$	0.0 .. 1400.0	3	16	53
Mean, st dev, and num obs of SW downward flux at surface	23	$W\text{-}m^{-2}$	0.0 .. 1400.0	3	16	56
Mean, st dev, and num obs of LW net flux at surface	24	$W\text{-}m^{-2}$	100.0 .. 500.0	3	16	59
Mean, st dev, and num obs of LW downward flux at surface	25	$W\text{-}m^{-2}$	100.0 .. 500.0	3	16	62
SFC_Weighted_Column_Average_Cloud_Properties is Array[5] of:						
(Cloud weightings are SW, LW TOA, LW Surface, liquid water path, and ice water path)						
SFC_Cloud_Properties						
Cloud_Area_Fractions_Array is Array[3] of:						
Cloud Area Fractions	26	Fraction	0.0 - 1.0	15	16	65
SFC_Cloud_Properties_Array is Array[3] of:						
SFC_Cloud_Property_Parameters						
Mean, st dev, and num obs of effective pressure	27	hPa	TBD	15	16	80
Mean, st dev, and num obs of effective temperature	28	K	TBD	15	16	95
Mean, st dev, and num obs of effective altitude	29	km	0.0 - 20.0	15	16	110
Mean, st dev, and num obs of cloud top pressure	30	hPa	0.0 - 1100.0	15	16	125
Mean, st dev, and num obs of cloud bottom pressure	31	hPa	0.0 - 1100.0	15	16	140
Mean, st dev, and num obs of particle phase	32	Fraction	0.0 - 1.0	15	16	155
Mean, st dev, and num obs of liquid water path	33	$kg\ cm^{-2}$	0.01 - 1000.0	15	16	170
Mean, st dev, and num obs of ice water path	34	$kg\ cm^{-2}$	0.01 - 1000.0	15	16	185
Mean, st dev, and num obs of liquid particle radius	35	µm	0.0 - 1000.0	15	16	200
Mean, st dev, and num obs of ice particle readius	36	µm	0.0 - 100.0	15	16	215
Mean, st dev, and num obs of visible optical depth	37	Dimensionless	0.0 - 50.0	15	16	230
Mean, st dev, and num obs of infrared emissivity	38	Dimensionless	0.0 - 2.0	15	16	245
Mean, st dev, and num obs of vertical aspect ratio	39	Dimensionless	TBD	15	16	260
Percentiles_Visible_Opt_Depth_Array is Array[13] of:						
VIS Opt Depth (day) / Infrared Emissivity (night) percentiles	40	Dimensionless	0.0 - 50.0	65	16	275
SFC_Angular_Model_Scene_Types is Array[12] of:						
Angular_Model_Scene_Type_Parameters						
Fractional area coverage	41	Fraction	0.0 .. 1.0	12	16	340
Albedos_Statistics is Array[2] of:						
Mean and standard deviation of albedo	42	Dimensionless	0.0 .. 1.0	24	16	352
Incident_Solar_Flux_Statistics is Array[2] of:						
Mean and standard deviation of incident solar flux	43	$W\text{-}h\ m^{-2}$	TBD	24	16	376
LW_Flux_Statistics is Array[2] of:						
Mean and standard deviation of LW flux	44	$W\text{-}m^{-2}$	0.0 .. 400.0	24	16	400
SFC_Surface_Only_Data						
Photosynthetically active radiation	45	$W\text{-}m^{-2}$	0.0 .. 780.0	1	16	424
Direct/Diffuse Ratio	46	Dimensionless	0.0 .. 30.0	1	16	425
Total Meta Bits/File:	96					
Total Data Bits/Record:	6800					
Total Records/File:	2500					
Total Data Bits/File:	17000000					

Appendix B

Output Data Products

Compute Monthly and Regional TOA and SRB Averages (Subsystem 10.0)

This appendix describes the data products which are produced by the algorithms in this subsystem. Table B-1 below summarizes these products, listing the CERES and EOSDIS product codes or abbreviations, a short product name, the product type, the production frequency, and volume estimates for each individual product as well as a complete data month of production. The product types are defined as follows:

Archival products: Assumed to be permanently stored by EOSDIS
Internal products: Temporary storage by EOSDIS (days to years)

The following pages describe each product. An introductory page provides an overall description of the product and specifies the temporal and spatial coverage. The table which follows the introductory page briefly describes every parameter which is contained in the product. Each product may be thought of as metadata followed by data records. The metadata (or header data) is not well-defined yet and is included mainly as a placeholder. The description of parameters which are present in each data record includes parameter number (a unique number for each distinct parameter), units, dynamic range, the number of elements per record, an estimate of the number of bits required to represent each parameter, and an element number (a unique number for each instance of every parameter). A summary at the bottom of each table shows the current estimated sizes of metadata, each data record, and the total data product. A more detailed description of each data product will be contained in a user's guide to be published before the first CERES launch.

Table B-1. Output Products Summary

Product code		Name	Type	Frequency	Size, MB	Monthly size, MB
CERES	EOSDIS					
SRBAVG	CER06	Monthly TOA and SRB averages	archival	1/month	564.4	564

Monthly TOA and SRB Averages (SRBAVG)

The SRBAVG product contains monthly and monthly hourly regional, zonal, and global averages of the TOA and surface LW and SW fluxes and the observed cloud conditions for each 1.25 degree equal-area region. This product differs from the AVG product in three ways. First, the surface fluxes have been calculated from the TOA fluxes using parameterizations provided by the science team, instead of using the models provided by the SARB subsystem. Secondly, no flux fields are calculated at levels between TOA and the surface. Lastly, the regional fluxes are calculated using two methods.

SRBAVG is an archival product produced by subsystem 10. There is one produced for each spacecraft and one for each combination. At the TRMM launch, this product will be produced in a validation mode for the first 18 months. During these 18 months, the CERES Science Team will derive a production quality set of angular distribution models which are needed to produce the LW and SW instantaneous fluxes.

SRBAVG is composed of the following structures:

On a Regional, Zonal, and Global Basis:
- Location data
- Total Sky radiative fluxes at TOA and surface
- Clear Sky radiative fluxes at TOA and surface
- Column-Averaged Cloud properties for five weighting schemes:
  - (TOA SW, TOA LW, SFC LW, LWP and IWP)
- Angular model scene types

Level: 3
Type: Archival
Frequency: 1/month

Time Interval Covered
File: Month
Record: Month

Portion of Globe Covered
File: Entire globe
Record: 1.25 degree regions

Portion of Atmosphere Covered
File: Surface and TOA

Table B-2. Monthly TOA and SRB Averages (SRBAVG)

Description	Parameter Number	Units	Range	Elements/ Record	Bits/ Elem	Elem Num
SRBAVG						
SRBAVG File Header				1	2048	
SRBAVG_Data is Array[26687] of:						
SRBAVG_Location_Data						
Region Number	1	N/A	1 - 26542	1	16	1
SRBAVG_Geographic_Type						
Histogram of geographic land type for region	2	N/A	TBD	10	16	2
Histogram of geographic sea type for region	3	N/A	TBD	3	16	12
SRBAVG_Calculation_Methods is Array[2] of:						
SRBAVG_Mnth_Fluxes is Array[3] of:						
TOA_Total_Sky						
Mean, st dev, and num obs of SW flux	4	$W\text{-}m^{-2}$	0.0 - 800.0	6	16	15
Mean, st dev, and num obs of LW flux	5	$W\text{-}m^{-2}$	0.0 - 400.0	6	16	21
Mean, st dev, and num obs of Wn flux	6	$W\text{-}m^{-2}$	0.0 - 800.0	6	16	27
Sfc_Down_Total_Sky						
Mean, st dev, and num obs of SW flux	7	$W\text{-}m^{-2}$	0.0 - 800.0	6	16	33
Mean, st dev, and num obs of LW flux	8	$W\text{-}m^{-2}$	0.0 - 400.0	6	16	39
Sfc_Net_Total_Sky						
Mean, st dev, and num obs of SW flux	9	$W\text{-}m^{-2}$	0.0 - 800.0	6	16	45
Mean, st dev, and num obs of LW flux	10	$W\text{-}m^{-2}$	0.0 - 400.0	6	16	51
TOA_Clear_Sky						
Mean, st dev, and num obs of SW flux	11	$W\text{-}m^{-2}$	0.0 - 800.0	6	16	57
Mean, st dev, and num obs of LW flux	12	$W\text{-}m^{-2}$	0.0 - 400.0	6	16	63
Mean, st dev, and num obs of Wn flux	13	$W\text{-}m^{-2}$	0.0 - 800.0	6	16	69
Sfc_Down_Clear_Sky						
Mean, st dev, and num obs of SW flux	14	$W\text{-}m^{-2}$	0.0 - 800.0	6	16	75
Mean, st dev, and num obs of LW flux	15	$W\text{-}m^{-2}$	0.0 - 400.0	6	16	81
Sfc_Net_Clear_Sky						
Mean, st dev, and num obs of SW flux	16	$W\text{-}m^{-2}$	0.0 - 800.0	6	16	87
Mean, st dev, and num obs of LW flux	17	$W\text{-}m^{-2}$	0.0 - 400.0	6	16	93
SRBAVG_Mnth_Hr_Fluxes is Array[24] of:						
SRBAVG_Mnth_Fluxes is Array[3] of:						
TOA_Total_Sky						
Mean, st dev, and num obs of SW flux	18	$W\text{-}m^{-2}$	0.0 - 800.0	144	16	99
Mean, st dev, and num obs of LW flux	19	$W\text{-}m^{-2}$	0.0 - 400.0	144	16	243
Mean, st dev, and num obs of Wn flux	20	$W\text{-}m^{-2}$	0.0 - 800.0	144	16	387
Sfc_Down_Total_Sky						
Mean, st dev, and num obs of SW flux	21	$W\text{-}m^{-2}$	0.0 - 800.0	144	16	531
Mean, st dev, and num obs of LW flux	22	$W\text{-}m^{-2}$	0.0 - 400.0	144	16	675
Sfc_Net_Total_Sky						
Mean, st dev, and num obs of SW flux	23	$W\text{-}m^{-2}$	0.0 - 800.0	144	16	819
Mean, st dev, and num obs of LW flux	24	$W\text{-}m^{-2}$	0.0 - 400.0	144	16	963
TOA_Clear_Sky						
Mean, st dev, and num obs of SW flux	25	$W\text{-}m^{-2}$	0.0 - 800.0	144	16	1107
Mean, st dev, and num obs of LW flux	26	$W\text{-}m^{-2}$	0.0 - 400.0	144	16	1251
Mean, st dev, and num obs of Wn flux	27	$W\text{-}m^{-2}$	0.0 - 800.0	144	16	1395

Table B-2. Continued

Description	Parameter Number	Units	Range	Elements/ Record	Bits/ Elem	Elem Num
Sfc_Down_Clear_Sky						
Mean, st dev, and num obs of SW flux	28	W-m^{-2}	0.0 - 800.0	144	16	1539
Mean, st dev, and num obs of LW flux	29	W-m^{-2}	0.0 - 400.0	144	16	1683
Sfc_Net_Clear_Sky						
Mean, st dev, and num obs of SW flux	30	W-m^{-2}	0.0 - 800.0	144	16	1827
Mean, st dev, and num obs of LW flux	31	W-m^{-2}	0.0 - 400.0	144	16	1971
SRBAVG_Mnth_Cloud_Properties						
SRBAVG_Angular_Model_Scene_Types is Array[12] of:						
Fractional area coverage	32	fraction	0.0 - 1.0	12	16	2115
Mean and st dev of albedo	33	N/A	0.0 - 1.0	24	16	2127
Mean and st dev of incident solar flux	34	W-h m^{-2}	TBD	24	16	2151
Mean and st dev of longwave flux	35	W-m^{-2}	0.0 - 400.0	24	16	2175
SRBAVG_Weighted_Cloud_Properties is Array[5] of:						
Cloud Area Fractions	36	N/A	0.0 - 1.0	15	16	2199
VIS Opt Depth (day) / Infrared Emissivity (night) percentiles	37	N/A	0.0 - 50.0	65	16	2214
SRBAVG_Column_Averaged_Properties_Data is Array[3] of:						
Mean, st dev, and num obs of effective pressure	38	hPa	TBD	15	16	2279
Mean, st dev, and num obs of effective temperature	39	K	TBD	15	16	2294
Mean, st dev, and num obs of effective altitude	40	km	0.0 - 20.0	15	16	2309
Mean, st dev, and num obs of particle phase	41	fraction	0.0 - 1.0	15	16	2324
Mean, st dev, and num obs of cloud top pressure	42	hPa	0.0 - 1100.0	15	16	2339
Mean, st dev, and num obs of cloud bottom pressure	43	hPa	0.0 - 1100.0	15	16	2354
Mean, st dev, and num obs of liquid water path	44	kg cm^{-2}	0.01 - 1000.0	15	16	2369
Mean, st dev, and num obs of ice water path	45	kg cm^{-2}	0.01 - 1000.0	15	16	2384
Mean, st dev, and num obs of liquid partical radius	46	µm	0.0 - 1000.0	15	16	2399
Mean, st dev, and num obs of ice particle radius	47	µm	0.0 - 100.0	15	16	2414
Mean, st dev, and num obs of infrared emissivity	48	N/A	0.0 - 2.0	15	16	2429
Mean, st dev, and num obs of vertical aspect ratio	49	N/A	TBD	15	16	2444
Mean, st dev, and num obs of VIS optical depth	50	N/A	0.0 - 50.0	15	16	2459
SRBAVG_Mnth_Hr_Cloud_Properties is Array[24] of:						
SRBAVG_Mnth_Cloud_Properties						
SRBAVG_Angular_Model_Scene_Types is Array[12] of:						
Fractional area coverage	51	fraction	0.0 - 1.0	288	16	2474
Mean and st dev of albedo	52	N/A	0.0 - 1.0	576	16	2762
Mean and st dev of incident solar flux	53	W-h m^{-2}	TBD	576	16	3338
Mean and st dev of longwave flux	54	W-m^{-2}	0.0 - 400.0	576	16	3914
SRBAVG_Weighted_Cloud_Properties is Array[5] of:						
Cloud Area Fractions	55	N/A	0.0 - 1.0	360	16	4490
VIS Opt Depth (day) / Infrared Emissivity (night) percentiles	56	N/A	0.0 - 50.0	1560	16	4850
SRBAVG_Column_Averaged_Properties_Data is Array[3] of:						
Mean, st dev, and num obs of effective pressure	57	hPa	TBD	360	16	6410
Mean, st dev, and num obs of effective temperature	58	K	TBD	360	16	6770
Mean, st dev, and num obs of effective altitude	59	km	0.0 - 20.0	360	16	7130
Mean, st dev, and num obs of particle phase	60	fraction	0.0 - 1.0	360	16	7490
Mean, st dev, and num obs of cloud top pressure	61	hPa	0.0 - 1100.0	360	16	7850
Mean, st dev, and num obs of cloud bottom pressure	62	hPa	0.0 - 1100.0	360	16	8210
Mean, st dev, and num obs of liquid water path	63	kg cm^{-2}	0.01 - 1000.0	360	16	8570
Mean, st dev, and num obs of ice water path	64	kg cm^{-2}	0.01 - 1000.0	360	16	8930
Mean, st dev, and num obs of liquid partical radius	65	µm	0.0 - 1000.0	360	16	9290
Mean, st dev, and num obs of ice particle radius	66	µm	0.0 - 100.0	360	16	9650
Mean, st dev, and num obs of infrared emissivity	67	N/A	0.0 - 2.0	360	16	10010
Mean, st dev, and num obs of vertical aspect ratio	68	N/A	TBD	360	16	10370
Mean, st dev, and num obs of VIS optical depth	69	N/A	0.0 - 50.0	360	16	10730

Table B-2. Concluded

Description	Parameter Number	Units	Range	Elements/ Record	Bits/ Elem	Elem Num
Total Meta Bits/File:	2048					
Total Data Bits/Record:	177424					
Total Records/File:	26687					
Total Data Bits/File:	4734914288					
Total Bits/File:	4734916336					

Clouds and the Earth's Radiant Energy System (CERES)

Algorithm Theoretical Basis Document

Update Clear Reflectance, Temperature History (CHR)

(Subsystem 11.0)

Cloud Working Group Chair

B. A. Wielicki[1]

Inversion Working Group Chair

R. N. Green[1]

Data Management Team

C. J. Tolson[2]
A. Fan[2]

[1]Atmospheric Sciences Division, NASA Langley Research Center, Hampton, Virginia 23681-0001
[2]Science Applications International Corporation (SAIC), Hampton, Virginia 23666

CERES Top Level Data Flow Diagram

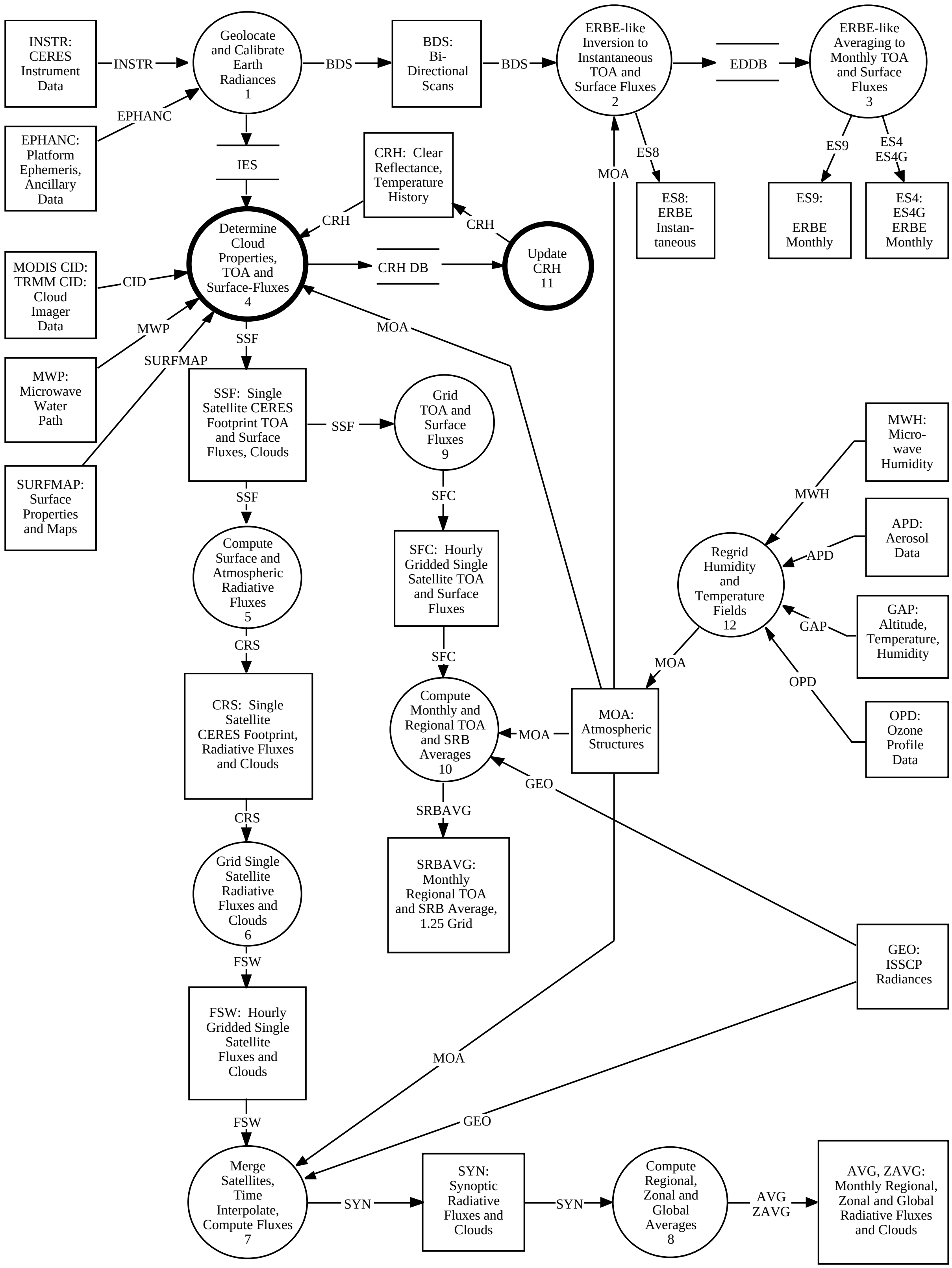

The text for the technical discussion for this subsystem is a part of subsystem 4.1, Overview of Cloud Retrieval and Radiative Flux Inversion. However, to maintain consistency with the CERES Top Level Data Flow Diagram, the data products catalogs have been retained in this location (see appendixes A and B).

Appendix A

Input Data Products

Update CRH (Subsystem 11.0)

This appendix describes the data products which are used by the algorithms in this subsystem. Table A-1 below summarizes these products, listing the CERES and EOSDIS product codes or abbreviations, a short product name, the product type, the production frequency, and volume estimates for each individual product as well as a complete data month of production. The product types are defined as follows:

Archival products:	Assumed to be permanently stored by EOSDIS
Internal products:	Temporary storage by EOSDIS (days to years)
Ancillary products:	Non-CERES data needed to interpret measurements

The following pages describe each product. An introductory page provides an overall description of the product and specifies the temporal and spatial coverage. The table which follows the introductory page briefly describes every parameter which is contained in the product. Each product may be thought of as metadata followed by data records. The metadata (or header data) is not well-defined yet and is included mainly as a placeholder. The description of parameters which are present in each data record includes parameter number (a unique number for each distinct parameter), units, dynamic range, the number of elements per record, an estimate of the number of bits required to represent each parameter, and an element number (a unique number for each instance of every parameter). A summary at the bottom of each table shows the current estimated sizes of metadata, each data record, and the total data product. A more detailed description of each data product will be contained in a user's guide to be published before the first CERES launch.

Table A-1. Input Products Summary

Product code						Monthly
CERES	EOSDIS	Name	Type	Frequency	Size, MB	size, MB
CRH_DB	none	Clear reflectance history	archival	Every 10 days	91.1	91

Clear Reflectance History (CRH_DB)

The clear reflectance/temperature history (CRH) data are organized on a global equal-area grid that is approximately 10 km by 10 km. The data coverage is 24 hours, and is updated twice a day if clear-sky condition exist for the particular grid cell. The data product consists of a product header followed by fixed-length records organized according to the grid pattern. The parameters are derived from cloud imager measurements by subsystem 4. The CRH_DB product is the same structure for both MODIS values and VIRS values. There is a source indication on the header record.

The CRH_DB is used in subsystem 11 to update the CRH archival product about every 10 days. The CRH product retains clear-sky information for the life of the mission, whereas the CRH_DB contains only the most recent 10 day clear-sky data.

Level: 3
Type: Internal
Frequency: Every 10 days

Portion of Globe Covered
File: Entire globe
Record: 10 km by 10 km grid

Time Interval Covered
File: 10 days
Record: 2/day

Portion of Atmosphere Covered
File: Surface reference

Table A-2. Clear Reflectance History (CRH_DB)

Description	Parameter Number	Units	Range	Elements/ Record	Bits/ Elem	Elem Num
CRH_DB						
CRH header record		N/A	N/A	1	2048	
Record_CRH_DB is Array[4341600] of:						
Grid_CRH_DB						
Day of observation	1	day	Mission Life	1	32	1
Time of observation	2	day	0..1	1	32	2
Visible albedo for collimated, overhead sun illumination	3	N/A	0 .. 1	1	16	3
Temperature derived from 3.7 µm imager channel	4	K	TBD	1	16	4
Temperature derived from 11 µm imager channel	5	K	TBD	1	16	5
Solar zenith angle from imager	6	deg	0 .. 90	1	16	6
Mean imager viewing zenith over CERES FOV	7	deg	0 .. 90	1	16	7
Mean imager relative aziumth angle over CERES FOV	8	deg	0 .. 360	1	16	8
Narrowband ADM Type	9	N/A	TBD	1	16	9

Total Meta Bits/File:	2048
Total Data Bits/Record:	176
Total Records/File:	4341600
Total Data Bits/File:	764121600
Total Bits/File :	764123648

Appendix B

Output Data Products

Update CRH (Subsystem 11.0)

This appendix describes the data products which are produced by the algorithms in this subsystem. Table B-1 below summarizes these products, listing the CERES and EOSDIS product codes or abbreviations, a short product name, the product type, the production frequency, and volume estimates for each individual product as well as a complete data month of production. The product types are defined as follows:

Archival products:	Assumed to be permanently stored by EOSDIS
Internal products:	Temporary storage by EOSDIS (days to years)

The following pages describe each product. An introductory page provides an overall description of the product and specifies the temporal and spatial coverage. The table which follows the introductory page briefly describes every parameter which is contained in the product. Each product may be thought of as metadata followed by data records. The metadata (or header data) is not well-defined yet and is included mainly as a placeholder. The description of parameters which are present in each data record includes parameter number (a unique number for each distinct parameter), units, dynamic range, the number of elements per record, an estimate of the number of bits required to represent each parameter, and an element number (a unique number for each instance of every parameter). A summary at the bottom of each table shows the current estimated sizes for metadata, each data record, and the total data product. A more detailed description of each data product will be contained in a user's guide to be published before the first CERES launch.

Table B-1. Output Products Summary

Product code		Name	Type	Frequency	Size, MB	Monthly size, MB
CERES	EOSDIS					
CRH	CER24	Clear reflectance history	archival	Every 10 days	91.1	282

Clear Reflectance History (CRH)

The clear reflectance/temperature history (CRH) data are organized on a global equal-area grid that is approximately 10 km by 10 km. The data coverage is 24 hours, and is updated every 10 days from the clear reflectance/temperature history database (CRH_DB). The CRH_DB has the same structure as CRH, and is updated twice a day if clear-sky conditions exist for the particular grid cell. The data product consists of a product header followed by fixed-length records organized according to the grid pattern. Each record has

- Visible albedo
- Temperature
- Viewing angles

The parameters are derived from cloud imager measurements by subsystem 4. The CRH product is the same structure for both MODIS values and VIRS values. There is a source indication on the header record. The CRH is archived so that the CERES Investigation will have access to any particular day throughout the life of the mission and it is needed for reprocessing.

Level: 3
Type: Archival
Frequency: Every 10 days

Portion of Globe Covered
File: Entire globe
Record: 10 km by 10 km grid

Time Interval Covered
File: Life of mission
Record: Every 10 days

Portion of Atmosphere Covered
File: Surface reference

Table B-2. Clear Reflectance History (CRH)

Description	Parameter Number	Units	Range	Elements/ Record	Bits/ Elem	Elem Num
CRH						
CRH header record		N/A	N/A	1	2048	
Record_CRH is Array[4341600] of:						
Grid_CRH						
Day of observation	1	day	Mission Life	1	32	1
Time of observation	2	day	0..1	1	32	2
Visible albedo for collimated, overhead sun illumination	3	N/A	0 .. 1	1	16	3
Temperature derived from 3.7 µm imager channel	4	K	TBD	1	16	4
Temperature derived from 11 µm imager channel	5	K	TBD	1	16	5
Solar zenith angle from imager	6	deg	0 .. 90	1	16	6
Mean imager viewing zenith over CERES FOV	7	deg	0 .. 90	1	16	7
Mean imager relative aziumth angle over CERES FOV	8	deg	0 .. 360	1	16	8
Narrowband ADM Type	9	N/A	TBD	1	16	9

Total Meta Bits/File:	2048
Total Data Bits/Record:	176
Total Records/File:	4341600
Total Data Bits/File:	764121600
Total Bits/File :	764123648

Clouds and the Earth's Radiant Energy System (CERES)

Algorithm Theoretical Basis Document

Regrid Humidity and Temperature Fields

(Subsystem 12.0)

Shashi K. Gupta[1]
Anne C. Wilber[1]
Nancy A. Ritchey[1]
Wayne L. Darnell[2]
Fred G. Rose[1]
Thomas P. Charlock[2]

[1]Analytical Services & Materials, Inc., Hampton, Virginia 23666
[2]NASA Langley Research Center, Hampton, Virginia 23681-0001

Abstract

This subsystem describes interpolation procedures used to convert meteorological fields obtained from diverse outside sources to spatial and temporal resolution required by various other CERES subsystems. The inputs for this subsystem come from many different sources on many different grids, though mainly from the NMC analysis products. The outputs consist of the same meteorological fields as the inputs, but at a uniform spatial and temporal resolution necessary to meet the requirements of the other processing subsystems. Interpolation procedures are used for all meteorological fields but the details of the procedure vary depending on the nature of the field and the resolution of the input data.

12.0. Regrid Humidity and Temperature Fields

12.1. Introduction

Meteorological and other atmospheric parameters such as surface temperature and pressure, profiles of geopotential height, temperature, humidity, and ozone and column burdens of water vapor, ozone, and aerosols are essential ancillary inputs to the various CERES processing subsystems, such as inversion, cloud analysis, ERBE-like inversion, and SARB analysis. These ancillary data can only be assembled from a variety of outside sources. Originating from diverse sources, these data do not conform to a common spatial and temporal grid system. The primary purpose of this subsystem is to put these ancillary data fields on an ISCCP-type 1.25° equal-area grid (see Subsystem 6.0) and 1-hourly time resolution. Each set can then be used for processing the hourly segments of satellite data.

12.2. Data Sources

The bulk of the inputs for this subsystem; namely, the surface temperature and pressure, and profiles of temperature and humidity are available from operational NMC products. However, the currently available NMC products have coarser resolution, both spatially and temporally, than is desirable for the purposes of CERES project. For some parameters, the coverage in one or more domains is inadequate. For example, standard NMC products are currently available only twice/day (00Z and 12Z), and the temperature profiles extend only to 50 hPa. Planned enhancements of the operational NMC products, e.g., availability at four synoptic times (00Z, 06Z, 12Z, 18Z), and extending the temperature profile up to 0.4 hPa will remedy some of the above shortcomings. Water vapor burden over the oceans from SSM/I on the DMSP satellites will be used to quality check and supplement the NMC humidity data. Also, the high-quality assimilated products from the 4-Dimensional Data Assimilation (4-DDA) are expected to be available in the EOS time period. The 4-DDA data are expected to be on a $1° \times 1°$ grid at 50 to 56 levels, and with 1-hourly time resolution. Ozone burden of the atmosphere is currently available from the TOVS on NOAA's operational Sun-synchronous satellites, and nadir-viewing SBUV-2 provide a coarse vertical distribution of stratospheric ozone. Aerosol column loading is being obtained at NOAA on a weekly-average basis over the oceans from AVHRR radiances (see Rao et al. 1989). Profiles of stratospheric aerosols can be obtained from the climatologies developed from SAGE data. In the EOS time period, column burdens of water vapor, ozone, and aerosols will all be available concurrently from MODIS-N.

The output from this subsystem consists of surface temperature and pressure, temperature profile at 34 levels up to 1 hPa, humidity profiles at 22 levels up to 300 hPa, and profiles of ozone and aerosol parameters separately for troposphere and stratosphere. Horizontally, these fields are generated for a 1.25° equal-area ISCCP-type grid. Temporally, they are produced every hour so that each set may be used for processing hourly segments of satellite data.

12.3. Technical Basis

The processing in this subsystem involves interpolation in three domains. The first interpolation is in the horizontal domain to project the available fields (generally on a 2.5° latitude × 2.5° longitude grid) onto the desired 1.25° equal-area ISCCP-type grid. The second interpolation is temporal to obtain hourly fields from the 12-hourly or 6-hourly fields available. The third interpolation is in the vertical, where temperature, humidity, and ozone profiles are desired at many more levels than are available in the input data.

Horizontal interpolation of most parameters will be simple bilinear in latitude and longitude. However, linear interpolation of relative humidity in the horizontal has the potential for creation or destruction of water mass spuriously when there are large horizontal variations of surface temperature. Therefore, horizontal interpolation of humidity will be done linearly in terms of specific humidity.

Temporal interpolations for most of the parameters are also linear. Availability of inputs twice daily is generally inadequate to capture the diurnal variability, but four times daily would be adequate. During the EOS period, meteorological fields will be available from 4-DDA with 1-hourly time resolution. This will permit the development and use of detailed diurnal models.

Vertical interpolation of temperature is accomplished using the equation

$$T_x = T_1 + ((T_1 - T_2)/\ln(P_1/P_2))*\ln(P_x/P_1) \qquad (1)$$

because pressure changes logrithmically while temperature changes linearly with height (see Darnell et al. 1983). In the above equation, T_x is the temperature at the desired pressure level P_x, which lies between P_1 and P_2 ($P_1 > P_2$). An illustration of results obtained from Equation (1) for a ISCCP temperature profile with inversion near the surface is shown in Figure 1. Vertical interpolation of moisture will be linear in relative humidity. Vertical distribution of ozone will be obtained by using the column burdens available from SBUV-2 and TOVS, and distributing it vertically in accordance with the climatological profiles. These profiles are seasonally and latitudinally dependent.

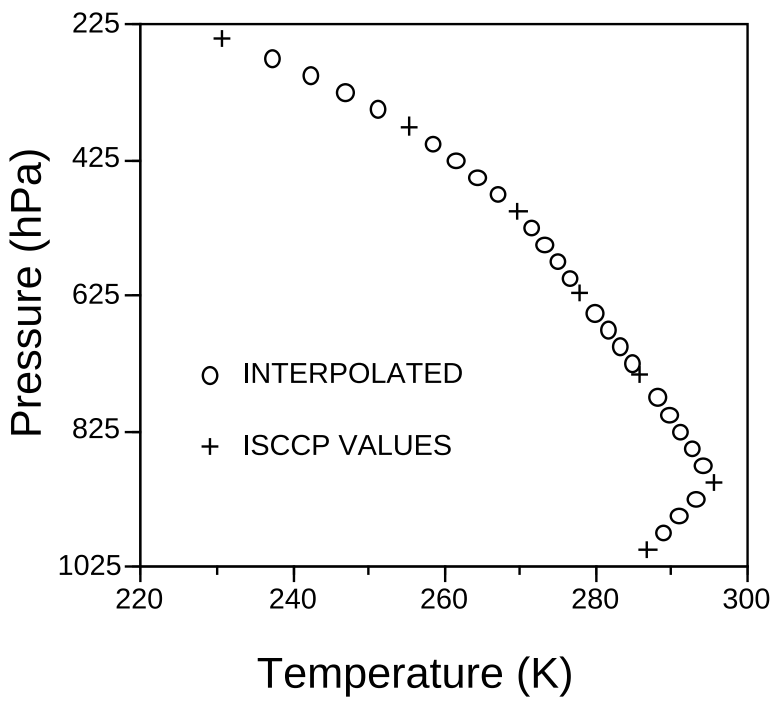

Figure 1. Results of interpolation obtained from Equation (1) for an ISCCP temperature profile with inversion near the surface.

12.4. Accuracy/Error Analysis

Errors incurred in vertical interpolation of the profiles of temperature and humidity are expected to be small (±0.5 K and 2%, respectively) because the input profiles are well defined and constrain the output profiles. Errors introduced in bilinear interpolation for regridding are also expected to be of similar magnitudes. Errors due to temporal interpolation may be considerably larger, if NMC inputs are available only twice daily. When NMC inputs are available four times daily, thus defining the diurnal cycle much better, temporal interpolation errors should also decrease significantly (±1 K and ±5%, respectively). Accuracy of ozone burden from TOVS and SBUV-2 is believed to be about 5–7% (15–20 Dobson units). Uncertainties in aerosol retrievals are believed to be much greater: up to 30% absolute and about 10% relative.

12.5. Strategic Concerns and Remedies

Important concerns at this time are the following: (1) the operational NMC products may not be available four times daily as expected, and (2) the special NMC data covering the 50 hPa to 1 hPa region may not be available routinely. Both of these situations will adversely affect the quality of the meteorological inputs to the inversion processes of the various subsystems using these data, and consequently the quality of the final CERES products. If NMC operational products turn out to be inadequate in temporal resolution and/or vertical coverage as indicated above, appropriate datasets would be obtained from the ECMWF. Operational ECMWF analyses are available four times daily. Of course, during the EOS period, meteorological fields will also be available from 4-DDA, and will have high spatial and temporal resolution.

A common problem with operational datasets and satellite datasets (both of which are used as sources here) is the occurrence of gaps in the data. Fill values (–999. is a common choice) are frequently substituted in the data streams where real data are missing. Use of such numbers in the interpolation schemes has the potential to corrupt the parameter values in adjacent locations also. To avoid this condition, the input parameters will be checked against carefully chosen limits. When an input parameter is found to lie outside the limits, attempts will be made to generate a value for it by interpolation between nearest neighbors in space and/or time. When missing parameters cannot be filled by interpolation, attempts are made to fill them with appropriate climatological data. Only when a consistent set of parameters cannot be generated for any location or time with either of the above methods, that data segment will be rejected, and will be flagged as unavailable in the output stream.

12.6. References

Darnell, W. L.; Gupta, S. K.; and Staylor, W. F. 1983: Downward Longwave Radiation at the Surface From Satellite Measurements. *J. Climat. & Appl. Meteorol.*, vol. 22, pp. 1956–1960.

Nagaraja Rao, C. R.; Stowe, L. L.; and McClain, E. P. 1989: Remote Sensing of Aerosols Over the Oceans Using AVHRR Data—Theory, Practice, and Applications. *Int. J. Remote Sens.*, vol. 10, pp. 743–749.

Appendix A

Input Data Products

Regrid Humidity and Temperature Fields (Subsystem 12.0)

This appendix describes the data products which are produced by the algorithms in this subsystem. Table A-1 below summarizes these products, listing the CERES and EOSDIS product codes or abbreviations, a short product name, the product type, the production frequency, and volume estimates for each individual product as well as a complete data month of production. The product types are defined as follows:

Archival products:	Assumed to be permanently stored by EOSDIS
Internal products:	Temporary storage by EOSDIS (days to years)
Ancillary products:	Non-CERES data needed to interpret measurements

The following pages describe each product. An introductory page provides an overall description of the product and specifies the temporal and spatial coverage. The table which follows the introductory page briefly describes every parameter which is contained in the product. Each product may be thought of as metadata followed by data records. The metadata (or header data) is not well-defined yet and is included mainly as a placeholder. The description of parameters which are present in each data record includes parameter number (a unique number for each distinct parameter), units, dynamic range, the number of elements per record, an estimate of the number of bits required to represent each parameter, and an element number (a unique number for each instance of every parameter). A summary at the bottom of each table shows the current estimated sizes for metadata, each data record, and the total data product. A more detailed description of each data product will be contained in a user's guide to be published before the first CERES launch.

Table A-1. Input Products Summary

Product code						
CERES	EOSDIS	Name	Type	Frequency	Size, MB	Monthly size, MB
APD	CER31	Aerosol data	ancillary	Daily to monthly	TBD	TBD
GAP	CER30	Altitude, temperature, humidity	ancillary	Every 6 hours	TBD	TBD
MWH	CER32	Microwave humidity	ancillary	Daily	TBD	TBD
OPD	CER33	Ozone profile data	ancillary	Daily to monthly	TBD	TBD

Aerosol Data (APD)

The external ancillary data product, aerosol data (APD), is input to the CERES Regrid Humidity and Temperature Subsystem. The APD is the source of both total column aerosol data and stratospheric aerosol data. The total column aerosol data may be derived daily from the MODIS instrument for the EOS-AM and EOS-PM platforms, while for TRMM the total column aerosol data may be derived from weekly AVHRR data. AVHRR data may also be used for the EOS-AM and EOS-PM platforms. The stratospheric aerosol data may be derived monthly from either concurrent SAGE data or a climatology based on SAGE data. MODIS data will have a horizontal resolution of either 50 km × 50 km or 5 km × 5 km for ocean, and 50 km × 50 km for nondesert land. AVHRR data have a horizontal resolution of one-deg longitude by 1 deg latitude, while the SAGE data have a horizontal resolution of 10° longitude by 10° latitude. MISR may be used as a backup source. It will provide full global coverage every 10–15 days. The Regrid Humidity and Temperature Subsystem interpolates these data temporally, horizontally and vertically to conform with CERES processing requirements.

Level: 3
Type: Ancillary
Frequency: Daily, weekly and monthly

Portion of Globe Covered
File: Global
Record: 1.25-deg equal-area region

Time Interval Covered
File: 1 day for MODIS
1 week for AVHRR,
1 month for SAGE,
Record: 1 day for MODIS,
1 week for AVHRR,
1 month for SAGE

Portion of Atmosphere Covered
File: Total column and stratosphere

Altitude, Temperature, Humidity (GAP)

The external ancillary data product, altitude, temperature, humidity (GAP), is input to the CERES Regrid Humidity and Temperature Subsystem. The GAP contains vertical profiles of temperature, humidity, pressure, and geopotential height, along with surface temperature and pressure. These data will be available every six hours from NMC on a 1.25-deg equal-area grid. Data from ECMWF may be used should data from NMC not be available. The Regrid Humidity and Temperature Subsystem interpolates these data temporally, horizontally and vertically to conform with CERES processing requirements.

Level: 3
Type: Ancillary
Frequency: Every 6 hours

Portion of Globe Covered
File: Global
Record:1.25-degequal-arearegion

Time Interval Covered
File: Every 6 hours
Record: Every 6 hours

Portion of Atmosphere Covered
File: Surface, internal atmosphere, TOA

Microwave Humidity (MWH)

The external ancillary data product, microwave humidity (MWH), is input to the CERES Regrid Humidity and Temperature Subsystem. The MWH is the source of the column precipitable water vapor burden as measured by a microwave instrument. These data may be derived daily from the SSM/I instrument, which has a horizontal resolution of 16 km × 23 km. The Regrid Humidity and Temperature Subsystem interpolates these data temporally, horizontally and vertically to conform with CERES processing requirements.

Level: 3
Type: Ancillary
Frequency: Daily

Portion of Globe Covered
File: Global
Record: 16 km × 23 km

Time Interval Covered
File: Daily
Record: Daily

Portion of Atmosphere Covered
File: Total column

Ozone Profile Data (OPD)

The external ancillary data product, ozone profile data (OPD), is input to the CERES Regrid Humidity and Temperature Subsystem. The OPD is the source of both total column ozone data and stratospheric ozone data. The total column ozone data may be derived daily from the TOMS instrument. The stratospheric ozone data may be derived monthly from either concurrent SAGE data or a climatology based on SAGE data, or weekly from SBUV-2. TOMS data are horizontally organized according to a 1.25 deg $\times$ 1.25 deg equal angle grid. SAGE and SBUV-2 data are horizontally organized according to a 10 deg longitude by 10 deg latitude grid. The Regrid Humidity and Temperature Subsystem interpolates these data temporally, horizontally and vertically to conform with CERES processing requirements.

Level: 3
Type: Ancillary
Frequency: Daily, weekly and monthly

Time Interval Covered
File: 1 day for TOMS,
1 week for SBUV-2,
1 month for SAGE,
Record: 1 day for TOMS,
1 week for SBUV-2,
1 month for SAGE

Portion of Globe Covered
File: Global
Record: 1.25-deg equal-area region

Portion of Atmosphere Covered
File: Total column and stratosphere

Appendix B

Output Data Products

Regrid Humidity and Temperature Fields (Subsystem 12.0)

This appendix describes the data products which are produced by the algorithms in this subsystem. Table B-1 below summarizes these products, listing the CERES and EOSDIS product codes or abbreviations, a short product name, the product type, the production frequency, and volume estimates for each individual product as well as a complete data month of production. The product types are defined as follows:

Archival products:	Assumed to be permanently stored by EOSDIS
Internal products:	Temporary storage by EOSDIS (days to years)

The following pages describe each product. An introductory page provides an overall description of the product and specifies the temporal and spatial coverage. The table which follows the introductory page briefly describes every parameter which is contained in the product. Each product may be thought of as metadata followed by data records. The metadata (or header data) is not well-defined yet and is included mainly as a placeholder. The description of parameters which are present in each data record includes parameter number (a unique number for each distinct parameter), units, dynamic range, the number of elements per record, an estimate of the number of bits required to represent each parameter, and an element number (a unique number for each instance of every parameter). A summary at the bottom of each table shows the current estimated sizes for metadata, each data record, and the total data product. A more detailed description of each data product will be contained in a user's guide to be published before the first CERES launch.

Table B-1. Output Products Summary

Product code		Name	Type	Frequency	Size, MB	Monthly size, MB
CERES	EOSDIS					
MOA	CER34	Meteorology, Ozone, and Aerosol	archival	1/hour	10.5	7797

Meteorology, Ozone, and Aerosol (MOA)

The CERES archival product, meteorology, ozone, and aerosol (MOA), is produced by the CERES Regrid Humidity and Temperature Subsystem. Each MOA file contains meteorological data for one hour, and is used by several of the CERES subsystems. Data on the MOA are derived from several data sources external to the CERES system, such as NMC, MODIS, SAGE, and various other meteorological satellites. These data arrive anywhere from four times daily to once a month. These data are also horizontally and vertically organized differently from what the CERES system requires. The Regrid Humidity and Temperature Subsystem interpolates these data temporally, horizontally, and vertically to conform with CERES processing requirements.

The MOA contains

- Surface temperature and pressure
- Vertical profiles for up to 38 internal atmospheric levels of temperature, humidity, pressure, and geopotential height
- Column precipitable water
- Vertical ozone profiles for 26 (of the 38) internal atmospheric levels
- Column ozone
- Total column aerosol
- Stratospheric aerosol

The 38 internal atmospheric levels, in hPa, as requested by the CERES clouds and SARB working groups are:

Surface	925	775	550	275	125	5
Surface–10	900	750	500	250	100	1
Surface–20	875	725	450	225	70	
1000	850	700	400	200	50	
975	825	650	350	175	30	
950	800	600	300	150	10	

Level: 3
Type: Archival
Frequency: 1/hour

Time Interval Covered
File: 1 hour
Record: 1 hour

Portion of Globe Covered
File: Global
Record: 1.25-deg equal area region

Portion of Atmosphere Covered
File: Surface and internal

Table B-2. Meteorology, Ozone, and Aerosol (MOA)

Description	Parameter Number	Units	Range	Elements/ Record	Bits/ Elem	Elem Num
Meta Data						
Header				1	320	
Regional Data						
Region Number	1	N/A	1..26542	1	16	1
Surface Data						
Surface Temperature	2	K	175..375	1	16	2
Surface Pressure	3	hPa	1100..400	1	16	3
Flag, Source Surface Data	4	N/A	TBD	1	16	4
Temperature and Humidity Profiles						
Geopotential Height Profiles	5	km	0..50	38	16	5
Pressure Profiles	6	hPa	1100..0	38	16	43
Temperature Profiles	7	K	175..375	38	16	81
Humidity Profiles	8	N/A	0..100	38	16	119
Flag, Source Temp. and Humidity Profiles	9	N/A	TBD	1	16	157
Column Precipitable Water						
Precipitable Water	10	cm	0.001..8.000	1	16	158
Precipitable Water, std	11	cm	TBD	1	16	159
Flag, Source Column Precipitable Water	12	N/A	TBD	1	16	160
Ozone Profile Data						
Ozone Profiles	13	g kg^{-1}	0.00002..0.02	26	16	161
Flag, Source Ozone Profile Data	14	N/A	TBD	1	16	187
Column Ozone						
Column Ozone	15	du	200..500	1	16	188
Flag, Source Column Ozone	16	N/A	TBD	1	16	189
Total Column Aerosol						
Aerosol Mass Loading, Total Column	17	g m^{-2}	TBD	1	16	190
Flag, Source Aerosol Mass Loading, Total Column	18	N/A	TBD	1	16	191
Optical Depth, Total Column	19	N/A	0.0..2.0	1	16	192
Flag, Source Optical Depth, Total Column	20	N/A	TBD	1	16	193
Asymmetry Factor, Total Column	21	N/A	0.0..1.0	1	16	194
Flag, Source Asymmetry Factor, Total Column	22	N/A	TBD	1	16	195

Table B-2. Concluded

Description	Parameter Number	Units	Range	Elements/ Record	Bits/ Elem	Elem Num
Single Scattering Albedo, Total Column	23	N/A	0.0..1.0	1	16	196
Flag, Source Single Scattering Albedo, Total Column	24	N/A	TBD	1	16	197
Effective Particle Size, Total Column	25	µm	0.0..20.0	1	16	198
Flag, Source Effective Particle Size, Total Column	26	N/A	TBD	1	16	199
Mean Aerosol Layer Temperature, Total Column	27	K	150..280	1	16	200
Flag, Source Mean Aerosol Layer Temperature, Total Column	28	N/A	TBD	1	16	201
Stratospheric Aerosol						
Optical Depth, Stratosphere	29	N/A	0.0..0.5	1	16	202
Asymmetry Factor, Stratosphere	30	N/A	0.0..1.0	1	16	203
Single Scattering Albedo, Stratosphere	31	N/A	0.0..1.0	1	16	204
Effective Particle Size, Stratosphere	32	µm	0.0..10.0	1	16	205
Mean Aerosol Layer Temperature, Stratosphere	33	K	150..280	1	16	206
Flag, Source Stratospheric Aerosol	34	N/A	TBD	1	16	207

Total Meta Bits/File:	320
Total Data Bits/Record:	3312
Total Records/File:	26542
Total Data Bits/File:	87907104
Total Bits/File:	87907424

REPORT DOCUMENTATION PAGE	*Form Approved* *OMB No. 0704-0188*

1. AGENCY USE ONLY *(Leave blank)*	2. REPORT DATE	3. REPORT TYPE AND DATES COVERED
	December 1995	Reference Publication

4. TITLE AND SUBTITLE
Clouds and the Earth's Radiant Energy System (CERES) Algorithm Theoretical Basis Document. *Volume IV—Determination of Surface and Atmosphere Fluxes and Temporally and Spatially Averaged Products (Subsystems 5–12)*

5. FUNDING NUMBERS
WU 148-65-41-01

6. AUTHOR(S)
CERES Science Team

7. PERFORMING ORGANIZATION NAME(S) AND ADDRESS(ES)
NASA Langley Research Center
Hampton, VA 23681-0001

8. PERFORMING ORGANIZATION REPORT NUMBER
L-17523

9. SPONSORING/MONITORING AGENCY NAME(S) AND ADDRESS(ES)
National Aeronautics and Space Administration
Washington, DC 20546-0001

10. SPONSORING/MONITORING AGENCY REPORT NUMBER
NASA RP-1376, Volume IV

11. SUPPLEMENTARY NOTES

12a. DISTRIBUTION/AVAILABILITY STATEMENT
Unclassified–Unlimited
Subject Category 47
Availability: NASA CASI (301) 621-0390

12b. DISTRIBUTION CODE

13. ABSTRACT *(Maximum 200 words)*
The theoretical bases for the Release 1 algorithms that will be used to process satellite data for investigation of the Clouds and the Earth's Radiant Energy System (CERES) are described. The architecture for software implementation of the methodologies is outlined. Volume IV details the advanced CERES techniques for computing surface and atmospheric radiative fluxes (using the coincident CERES cloud property and top-of-the-atmosphere (TOA) flux products) and for averaging the cloud properties and TOA, atmospheric, and surface radiative fluxes over various temporal and spatial scales. CERES attempts to match the observed TOA fluxes with radiative transfer calculations that use as input the CERES cloud products and NOAA National Meteorological Center analyses of temperature and humidity. Slight adjustments in the cloud products are made to obtain agreement of the calculated and observed TOA fluxes. The computed products include shortwave and longwave fluxes from the surface to the TOA. The CERES instantaneous products are averaged on a 1.25° latitude-longitude grid, then interpolated to produce global, synoptic maps to TOA fluxes and cloud properties by using 3-hourly, normalized radiances from geostationary meteorological satellites. Surface and atmospheric fluxes are computed by using these interpolated quantities. Clear-sky and total fluxes and cloud properties are then averaged over various scales.

14. SUBJECT TERMS
Earth Observing System; Clouds and the Earth's Radiant Energy System; Earth radiation budget; Clouds satellite measurements; Surface radiation; Atmospheric radiative divergence

15. NUMBER OF PAGES
189

16. PRICE CODE
A09

17. SECURITY CLASSIFICATION OF REPORT	18. SECURITY CLASSIFICATION OF THIS PAGE	19. SECURITY CLASSIFICATION OF ABSTRACT	20. LIMITATION OF ABSTRACT
Unclassified	Unclassified	Unclassified	

NSN 7540-01-280-5500

Standard Form 298 (Rev. 2-89)
Prescribed by ANSI Std. Z39-18
298-102